FOSSIL ENERGY

DOE/BC/14881-5
(DE94000142)

IMPROVING RESERVOIR CONFORMANCE USING GELLED POLYMER SYSTEMS

Annual Report for the Reporting Period
September 25, 1992 to September 24, 1993

By
Don W. Green
G. Paul Willhite

August 1994

Performed Under Contract No. DE-AC22-92BC14881

The University of Kansas
Lawrence, Kansas

Bartlesville Project Office
U. S. DEPARTMENT OF ENERGY
Bartlesville, Oklahoma

DOE/BC/14881-5
Distribution Category UC-122

Improving Reservoir Conformance Using Gelled Polymer Systems

Annual Report for the Reporting Period
September 25, 1992 to September 24, 1993

by
Don W. Green
G. Paul Willhite

August 1994

Work Performed Under Contract No. DE-AC22-92BC14881

Prepared for
U.S. Department of Energy
Assistant Secretary for Fossil Energy

Jerry F. Casteel, Project Manager
Bartlesville Project Office
P.O. Box 1398
Bartlesville, OK 74005

Prepared by
The University of Kansas
Lawrence, Kansas

Abstract

The general objectives of the research program are to (1) identify and develop gelled polymer systems which have potential to improve reservoir conformance of fluid displacement processes, (2) determine the performance of these systems in bulk and in porous media, and (3) develop methods to predict their performance in field applications. The research focuses on three types of gel systems--an aqueous polysaccharide (KUSPI) that gels as a function of pH, polyacrylamide or xanthan crosslinked by Cr(III) and a polyacrylamide-aluminum citrate system. Work to date has focused primarily on development of a database, selection of systems, and work to characterize the gel/polymer physical properties and kinetics. The use of ester hydrolysis to control the rate of pH change of a gel system has been investigated and this approach to gel-time control shows promise. Extensive kinetic data were taken on the uptake of Cr(III) oligomers by polyacrylamide. A model was developed which describes very well the monomer uptake rates. The model described the dimer uptake data less well and the trimer uptake data poorly. Studies of the flow and gelation in rock materials have been initiated. A mathematical model of rock-fluid interaction during flow of high pH solutions has been developed.

Executive Summary

OBJECTIVES

The general objectives of this research program are to 1) identify and develop gelled polymers systems which have potential to improve reservoir conformance of fluid displacement processes, 2) to determine the performance of these systems in bulk and in porous media, and 3) to develop methods to predict the capability of these systems to recover oil from petroleum reservoirs.

The research focuses on three types of gel systems- an aqueous polysaccharide (KUSP1) system that gels as a function of pH, a chromium-based system where polyacrylamide and xanthan are crosslinked by Cr(III) and an organic crosslinked system. Development of the KUSP1 system and evaluation and identification of a suitable organic crosslinked system will be done.

The laboratory research is directed at the fundamental understanding of the physics and chemistry of the gelation process in bulk form and in porous media. This knowledge will be used to develop conceptual and mathematical models of the gelation process. Mathematical models will then be extended to predict the performance of gelled polymer treatments in oil reservoirs.

The project is divided into five major tasks. These are:

- Development and Selection of Gelled Polymer Systems
- Physical and Chemical Characterization of Gel Systems
- Flow and Gelation in Rock Materials
- Mathematical Modeling of Gel Systems
- Sponsor International Forums on Gelled Polymer Treatments

SUMMARY OF PROGRESS

Development and Selection of Gelled Polymer Systems

Research activities were focused on development of the KUSP1 polysaccharide and derivatives and selection of an organic crosslinked system for further studies.

Development of KUSP1. KUSP1 is an unbranched (1→3)-D-glucan which is produced by bacterial activity in a simple medium containing an excess of glucose as the carbon and energy source and is deposited as a capsule surrounding the bacterium. The polymer is separated from the capsule by dissolution in 1N NaOH. KUSP1 forms a gel when the pH is reduced to the vicinity of 10.8. The polymer is insoluble in water and organic solvents. The polymer is not toxic.

Research during the first year of the project was initiated in three areas. A study was completed to determine the possibility that the polysaccharide reacts with the alkali and is altered by the extraction process. Extraction of KUSP1 with dimethylsulfoxide (DMSO) yields a polysaccharide with characteristics slightly different from alkali extracted polymer. Both form hydrogels when the pH is decreased. Hydrogels from the DSMO extracted polymer contain more water and are less rigid. The DMSO extracted polysaccharide is more resistance to acid hydrolysis.

Derivatives of KUSP1 were prepared in an attempt to improve water solubility. Carboxymethyl esters of KUSP1 were prepared by treatment of the polysaccharide dissolved in alkali with chloroacetic acid and will be evaluated in subsequent tests. The degree of polymerization can be controlled according to growth conditions. The capability of the KUSP1 hydrogel to hold water is diminished by exopolysaccharide synthesized at late stages of the culture. Techniques to purify KUSP1 are under development. Scaleup of the production of polymer is being studied in a 16 liter air-lift fermentor.

Other Gel Systems. An objective of the research program is to study an organic gel system. A database was developed containing 29 gel systems. Criteria for selection of an organic gel system were defined. Four criteria evolved from this process. They are: 1) environmental acceptance; 2) gel times on the order of several days to months; 3) wide temperature range with a minimum temperature of 25°C; 4) wide pH range that encompassed pH values between 6 and 8; and 5) cost.

Two systems were selected for initial screening experiments. A crosslinked polymer system using organic compounds that contain at least two positively charged nitrogen atoms as the crosslinker will be studied. Examples of the crosslinker are salts of diamines, including alkylene diamines such as propylene diamine. Toxicity remains a significant concern regarding the use of these gels. Because of environmental concerns associated with organic crosslinking systems, our search for gelling systems was expanded to consider low toxicity systems such as those which use aluminum ion as the crosslinker.

Physical and Chemical Characterization of Gel Systems

Rheological Studies. The first phase in rheological studies of gelation was completed. In this phase, methods to monitor gelation as a function of time using rheological measurements were developed. Experimental techniques were developed to determine the storage modulus as a function of time during gelation using oscillatory rheometry. These include, sample preparation techniques, control of evaporation during long gelation runs and identifying conditions necessary for acquisition of credible data. Reproducibility was determined for a Cr(III)-polyacrylamide system under oscillatory shear. All measurements were made using a Weissenberg R-19 Rheogoniometer or a Bohlin Controlled Stress Rheometer.

After establishing that reproducible data could be obtained, the principal variable studied was the effect of frequency of oscillation on the gelation. A Cr(III)-polyacrylamide system containing 7,500 ppm polymer and 100 ppm Cr(III) in a solution containing 2% sodium chloride was used in all studies. The storage moduli of gels prepared at a specified frequency were a strong function of frequency of oscillation (from 0.01 Hz to 1.0 Hz) at all stages of the gelling process. Thus, the frequency of measurement must be considered in relating the storage modulus to gel structure.

All gelation experiments showed an initial dependence of the rate of change of the storage modulus with frequency of oscillation. The maximum slope of the storage modulus-versus-time curve did not depend on the frequency of gelation. The gel time based on the equivalence of storage modulus and loss modulus increased as the frequency of oscillation increased. For the system studied, the gel did not attain an equilibrium value of the storage modulus even after 5 days of observation. Definition of gel point continues to be ambiguous in describing gel systems.

During screening experiments, the gelation of polyacrylamide-Cr(III) systems was observed to vary with the anion present in the system as well as the concentration of the anion. A series of gelation experiments was completed in which the effects of nitrate, perchlorate, chloride, sulfate and acetate anions

on the rate of gelation were determined using rheological measurements. A single polymer concentration (9,000 ppm) was used in these experiments with two Cr(III) concentrations. The time of gelation for the five systems studied is ordered as follows: $NO_3^- < ClO_4^- < Cl^- < SO_4^- < OAc^-$.

The dependence of gelation on anion concentration was examined by preparing solutions at salt concentrations ranging from 0.00 M to 1.0 M. Initial results show that gelation time for the nitrate systems decreases with increase in salt concentration. The perchlorate system has a maximum gelation time between 0.1 M and 1.0 M salt concentration followed by a decrease in gelation time with a corresponding decrease in salt concentration. In the chloride system, gelation time increases with increasing salt concentration. Addition of acetate anion appears to inhibit gel formation in the pH range studied.

Kinetic Studies (Chromium Oligomers). Chromium(III) is a commonly used crosslinking agent for polyacrylamide and polysaccharide. The chromium(III) used in some of these systems is present as monomeric Cr(III) when added to the polymer solution. The gelation process is sensitive to pH and it is known that oligomers of Cr(III) form as the pH increases. The gelation process is visualized as a two-step process in which the Cr(III) reacts with the polymer in what is termed the uptake reaction. This is followed by a gelation reaction where crosslinks are formed between polymer chains containing Cr(III).

A research program was completed to determine and compare the uptake and gelation rates of the Cr(III) monomer, dimer and trimer with partially hydrolyzed polyacrylamide. The three species of Cr(III) were separated by ion chromatography. Oligomer uptake was measured by separating unreacted chromium from the gel solution using a dialysis technique. Relative rates of gelation were determined from rheological measurements of the change of storage modulus with time.

Data were obtained for uptake and gelation in the pH range of 4 to 5, Cr(III) concentrations of 8-30 ppm and polymer concentrations of 4,000 - 20,000 ppm. Uptake and gelation rates increased with increasing oligomer size, oligomer concentration and pH. Uptake rate also increased with polymer concentration. In general, gelation reactions closely followed the uptake of oligomers by the polyacrylamide. Comparison of uptake results with other data indicated that the uptake rates were affected by the salt type and concentration.

A kinetic model was developed to describe the uptake rates for monomer at pH 4 and 5. The monomer data were well described by the model. The dimer data were less well described and the trimer data were not fit well at all by the model. A number of possibilities were examined to explain the lack of fit for the dimer and trimer.

Kinetic Studies (Gelation of KUSP1 by Ester Hydrolysis). The gelation of KUSP1 occurs when the pH of the alkaline solution is reduced from 13 to the vicinity of 10.8. Reduction of pH can be accomplished by adding an ester to the alkaline solution. During the first year of the project, esters were examined to identify a candidate which would be soluble in the alkaline solution containing KUSP1 and would hydrolyze at a slow enough rate to gel the polymer in a time period of several days. This would permit gelation of KUSP1 in porous rock after placement.

A commercially available ester that met these criteria was not found. However, the ester *ethylbenzoate-2-sulfonic acid* (EBSA) was easily prepared. Experimental data showed that the gelation of KUSP1 could be controlled by ester hydrolysis. Gel times on the order of days(at room temperature) were obtained. Gel times can be controlled by selection of the concentrations of the polymer and the ester.

Insights into the gelation of KUSP1 were obtained from analysis of the experimental data. Rheological data indicated that the polymer developed structure and aggregates as the pH of the solution was lowered from initial values to pH of approximately 10.8. In some runs, gelation was characterized by the appearance of a plateau in the pH profile at pH 10.8. The pH remained constant for a period of time, indicating that the gelation process consumed hydrogen ions at the rate that they were being generated by the hydrolysis of the ester.

Unfortunately, the cost of *ethylbenzoate-2-sulfonic acid* appears to be prohibitive for use in field treatments. A less expensive ester will be sought.

Flow and Gelation in Rock Materials

In Situ Gelation of KUSP1 by CO_2. Gelation of alkaline solutions of KUSP1 in beakers can be accomplished by bubbling carbon dioxide gas into the solution. In this process, CO_2 dissolves in the aqueous solution and reacts with water to form an acidic species which lowers the pH. Preliminary experiments were completed to determine if CO_2 would gel KUSP1 under flow conditions in sandpacks. These experiments were conducted at low pressures and at about 25°C. They were intended to be the precursor to experiments conducted using supercritical CO_2.

Initial gelation experiments were conducted in short sandpacks (30.2 cm). Two experiments were completed. In the first experiment CO_2 was injected continuously into a sandpack saturated by KUSP1 solution at a pH of 13.5. Initial permeability of the sandpack was 3,600 md. Uniform permeability reduction to an average permeability of 45 md was observed in this experiment.

In the second experiment, alternate slugs of KUSP1 polymer solution and CO_2 were injected. Substantial permeability reduction was observed, but most of the reduction was limited to the front section of the sandpack.

Equipment is being assembled to conduct flow experiments in Berea cores with CO_2 at supercritical conditions. The objective will be to determine the applicability of KUSP1 gel system for permeability modification treatments during miscible-CO_2 floods.

Mathematical Modeling of Gel Systems

The gelation of many polymer systems is a strong function of solution pH. Fluid-rock interactions play an important role in determining the pH behavior of solutions injected into reservoirs. For example, in some porous rocks there may be sufficient fluid-rock interaction to cause gelation of an alkaline solution of KUSP1. Modeling efforts during the first year were focused on the important forms of fluid-rock interactions in reservoir sands with the objective of mathematically modeling their effects on the solution pH. The research conducted in this period was limited to a simplified system consisting of the injection of high pH NaCl solutions in sandstone cores containing silica.

The initial steps in this project involved simulation of flooding experiments with high pH brine solutions using UTCHEM, a widely applied chemical flooding simulator. Comparison with experimental data revealed that the kinetics of dissolution is important in many situations of practical interest. UTCHEM was developed by assuming equilibrium exists between all species and does not account for the kinetics of dissolution.

A kinetic model describing silica dissolution reaction was developed which is generally valid for all time frames. Based on sodium/hydrogen equilibria and silica dissolution kinetics, a new mathematical model was developed for describing core flood experiments. This model describes the effects of flow rate and core length in terms of the Damkohler Group. By varying the value of the Damkohler Group it is possible to scale the effects of silica dissolution from laboratory-scale conditions to field-scale conditions. A mathematical criterion was developed for checking the validity of the local equilibrium assumption.

The model was used to study sodium/hydrogen ion-exchange in simulated core floods. Concentration profiles show formation of two distinct fronts which move through the porous medium, a salinity wave and an ion-exchange wave. The predictions are in agreement with data in the literature, although the data available are limited.

Sponsor International Forums on Gelled Polymer Treatments

The objective of this task was to conduct an international meeting which would focus on conformance improvement through application of gelled polymer technology. Subsequent to funding of this proposal, the Society of Petroleum Engineers scheduled a forum on Improvements in Conformance Technology during the 1993 Forum Series under the leadership of Bob Sydansk, Marathon Oil Company. We decided to focus our efforts for the 1992-93 Year on supporting this forum which was held at Snowmass, CO, August 8-13, 1993. G. Paul Willhite was a member of the Planning Committee for this forum. C. Stanley McCool attended the forum and made a presentation. Response of the participants was quite favorable.

Improving Reservoir Conformance Using Gelled Polymer Systems

TABLE OF CONTENTS

List of Figures

List of Tables

Chapter 1

Introduction

Principal Investigators: D.W. Green, G.P. Willhite, C.S. McCool, S. Vossoughi, M.J. Michnick

The application of techniques to improve volumetric displacement efficiency in petroleum reservoir displacement processes has proven to be effective. Such techniques are commonly referred to as reservoir conformance or in situ permeability modification processes. The investigation of gelled polymer systems which are applicable or potentially applicable for this purpose is the focus of this research project.

The gel systems being studies are: 1) KUSP1, a biopolymer developed at the University of Kansas which gels upon lowering of pH; 2) polyacrylamide or polysaccharide crosslinked by Cr(III); and 3) polyacrylamide crosslinked by aluminum to form gel aggregates rather than a bulk gel.

These systems are being studied using a variety of approaches. These approaches include: a) rheological measurements; b) chemical characterization and kinetics; c) flow experiments in sandpacks and rock core material; and d) mathematical modelling. Results of the first year of the project are described in Chapters 2 — 9.

Chapter 2

Development of the KUSP1 Polysaccharide and Derivatives

Principal Investigator: Clarence S. Buller
Graduate Research Assistant: Ping Chen

INTRODUCTION AND OBJECTIVES

Growth of *Cellulomonas flavigena* in a simple medium containing an excess of glucose as the carbon and energy source results in the production of a large amount of a polysaccharide that is deposited as a capsule surrounding the bacterium. Suspension of the encapsulated cells in 1 N NaOH results in the dissolution of that polysaccharide. Neutralization of the alkaline extract, with CO_2, acid, or by dialysis, results in the formation of a polysaccharide hydrogel. The polysaccharide, which has been named KUSP1, is an unbranched (1→3)-β-D-glucan. KUPS1 is insoluble in H_2O and organic solvents. It dissolves in alkali, concentrated formic acid and phosphoric acid, and in dimethylsulfoxide (DMSO).

The first goal is to find out if the polysaccharide that comprises the capsule of *Cellulomonas flavigena* is chemically modified by the alkali used for its extraction. (1→3)-β-D-Glucans are specifically stained by water soluble aniline blue (Nakanishi et al., 1974, 1976). Although encapsulated *C. flavigena* cells contain a large amount of the (1→3)-β-D-glucans (up to 80% of their dry weight), they are not stained by the dye. The KUPS1 that can be precipitated from alkaline extracts of such cells, however, is readily stained by aniline blue. This raises the possibility that the NaOH used in the extraction alters the polysaccharide. One possibility is that prior to its extraction into alkali, the polysaccharide contains ester groups that are labile to the alkaline extraction process.

The versatility of polysaccharide polymers often can be increased by derivatization of the various functional groups. As an example, the industrial applications of cellulose have been widely expanded by the formation of various ethers and esters of cellulose. The second objective of this study is to determine if chemical modification of KUPS1 can also increase its versatility and suitability of permeability modification. Cellulose and KUPS1 both are water insoluble homoglucans, and many of the techniques developed for cellulose modification can be expected to be applicable to KUPS1.

It has been reported that the degree of polymerization (DP) of curdlan, a (1→3)-β-D-glucan produced by *Alkaligenes faecalis*, varies according to the growth conditions (Sasaki and Sugino, 1984). As the length of the incubation time of the culture was increased, the degree of polymerization of the (1→3)-β-D-glucan tended to decrease, and the thermogelability of the curdlan also decreased. When DP was less than 113, curdlan was not geleable. Good gels formed if the DP of curdlan was 170 or greater.

Exopolysaccharides that are produced by microorganisms frequently have polydispersity, i.e., they have variations in the degree of polymerization (DP). The relationship of the polydispersity of KUPS1 to the quality of the hydrogel formed by it cannot conveniently and reliably be established because KUSP1 is not soluble in water. A third objective of this study, therefore, is to identify conditions that affect the quality of the hydrogel. It has become clear that the quality of the KUSP1 hydrogel, ie. its ability to hold

water, is diminished with exopolysaccharide synthesized at late stages of the culture. This, in part, may be due to production of extracellular (1→3)-β-D-endoglucanase enzymes that can randomly hydrolyze the polysaccharide. We have begun to characterize such enzymes, with the intent of determining how their activity can be regulated, with the possible consequence of improving the quality of the hydrogels.

EXPERIMENTAL METHODS

Effect of Alkali Used in Extraction

A comparison was made of the polysaccharides extracted into two solvents, DMSO and NaOH. *Cellulomonas flavigena* was grown under conditions leading to polysaccharide synthesis and the formation of extracellular capsules. After collecting the cells by centrifugation of the cultures, equivalent amounts of precipitated cells were extracted with either dimethylsulfoxide (DMSO) or 1.0 N NaOH. KUPS1 is soluble in DMSO, and extraction of encapsulated cells by this solvent is not expected to result in ester hydrolysis. KUSP1 extracted into this solvent therefore would be representative of the **intracellular** form of the polysaccharide. After resuspension in DMSO, the residual bacterial cells were removed by centrifugation and the polysaccharide was precipitated from the solvent by the addition of isopropanol. The precipitate was collected by centrifugation, washed extensively with water, and then dried by lyophilization. KUPS1 was recovered from cell free alkaline extracts of *C. flavigena* by neutralization of the solvent, followed by extensive H_2O washing of the precipitate.

Periodate oxidation of polysaccharides is a valuable analytical technique that has been used in the structural characterization and monosaccharide sequence determination of polysaccharides. Carbohydrate residues containing glycol groups (vicinal hydroxyls) are oxidized to dialdehydes. If the residues contain hydroxyl groups on three adjacent carbons, formic acid may also be produced. In (1→3)-β-D-glucans, only the reducing end would contain vicinal hydroxyl groups, and therefore attempts have been made to use this method to determine the degree of polymerization (Harada et al., 1968). However, because of the water insolubility of KUSP1, we found that the periodate oxidation method was not reliable. Accordingly, the number of reducing ends in KUPS1 was determined by modifying the colorimetric arsenomolybdate method described by Nelson (1944). The reagents for the Nelson colorimetric assay were made up as originally described (Nelson, 1944). The test polysaccharides and glucose standards, however, were prepared in DMSO. Absorbency at 600 nm was recorded. Glucose standard curves, in DMSO, were linear in the range of 0-0.56 mmoles of glucose.

Chemical Modification of KUSP1

The formation of O-carboxymethyl-KUSP1 was accomplished by a modification of the method developed by Green (1963) for preparation of O-carboxymethylcellulose. The acidic ether of KUPS1 was prepared by the interaction of alkaline-KUSP1 and chloroacetic acid (Table 2.1). The process is effected with an excess of NaOH, so that the sodium salt of carboxymethyl-KUSP1 is obtained. By-products in the process are sodium chloride, sodium glycolate, and excess alkali. Since the final reaction mixture contains a water-soluble product, neutralization of the excess alkali is best done with a mixture of alcohol and acid. Washing will then remove the salts present, and the O-carboxymethyl-KUSP1 will be left. O-Carboxymethyl-KUSP1 can be further purified by washing with aqueous ethanol or methanol. It can also be precipitated from aqueous solution by acidification and addition of ethanol.

Table 2.1: Procedure for the Generation of Carboxymethyl-KUPS1

5 Grams of purified KUPS1

↓

Make slurry in 135 ml of isopropyl alcohol
(Stir for 30 min at room temp.)

↓

Slowly (over a period of 1 hour) add 13.6 ml of 7.5 M NaOH
(Stir for 90 minutes)

↓

Slowly (over period of 30 min.) add 6 gm of chloroacetic acid
(Stir for 150 minutes)

↓

Centrifuge (2,000 x g, 5 min.)

↓

Precipitate

↓

Dissolve in 150 ml H_2O

↓

Neutralize with acetic acid

↓

Add 250 ml methanol

↓

Centrifuge (2,000 x g, 5 min.)

↓

Precipitate

↓

Wash with mixture containing 500 ml 80% aqueous methanol
+ 250 ml of ethanol

↓

Centrifuge (2,000 x g, 5 min.)

↓

Precipitate

↓

Wash with 1,000 ml of 80% ethanol

↓

Centrifuge (2,000 x g, 5 min.)

↓

Precipitate (Carboxymethyl-KUPS1)

Conditions that Affect Gel Quality

The steps in the purification of (1→3)-β-D-glucanases from cultures of *C. flaviginea* grown in media in which KUSP1 is the only carbon and energy source are shown in Table 2.2. Such enzymes are synthesized because the organisms are able to utilize the polysaccharide as an energy storage mechanism (Voepel and Buller, 1990). The hydrolytic enzymes can be precipitated by treatment of culture supernatants with ammonium sulfate, to 70% saturation, followed by ion-exchange chromatography. Purification of such enzymes will allow determination of how their activity can be regulated, and thereby possibly improve the quality of the hydrogel produced.

Table 2.2: Purification of (1→3)-β-D-Glucanase

Cellulomonas flavigena grown in CM9 medium containing (1→3)-β-D-glucan, at a concentration of 0.5%, as the carbon and energy source. Culture was incubated for 48 hrs, with aeration, at 30°C.

↓

Culture centrifuged at 8,000 x g, 30 min.

↓

Supernatant is cell free and does not contain insoluble (1→3)-β-D-glucan.

↓

Add $(NH_4)_2SO_4$ to 70% saturation, then centrifuge to collect precipitated protein.

↓

Add 20 mM Tris buffer (pH 7) to precipitated protein. Not all of the precipitate dissolves. Dialyze against 20 mM Tris buffer, pH 7.

↓

Centrifuge to remove insoluble protein. Add supernatant, which contains yellow pigment, to DEAE anion exchange column.

↓

Elute with salt gradient (0 - 1 M) in 20 mM Tris buffer, pH 7.

↓

Dialyze eluate and lyophilize.

↓

Dissolve dry residue in 20 mM Tris buffer, pH 7, and apply to gel filtration (Sephadex 100) column.

↓

Elute with 20 mM Tris buffer, pH 7.

↓

Assay fractions for glucanase activity.

↓

Pool active fractions and fractionate by polyacrylamide gel electrophoresis.

RESULTS AND DISCUSSION

Effect of Alkali

The extraction of KUSP1 by treatment of encapsulated *Cellulomonas flavigena* with dimethylsulfoxide yields a polysaccharide with characteristics slightly different from alkali extracted polymer (Table 2.3). Both form hydrogels, but that formed from DMSO extracted polymer is less rigid and holds more water than the hydrogel formed from alkali extracted KUSP1. A further difference is that the DMSO extracted polysaccharide is more resistant to acid hydrolysis.

Table 2.3: Characteristics of DMSO- and NaOH Soluble Polysaccharide

	KUPS1 (Alkali Extracted)	DMSO Extracted Polysaccharide
Hydrogel composition	97% H_2O	93% H_2O
Protein content[a]	0.5%	0.5%
Phosphate content[b]	None detected	None detected
Thermal gelation[c]	Yes	No
Aniline blue staining[d]	Yes	Yes

[a] BCA protein assay (Pierce Kit No. 23225)
[b] Ames, 1966
[c] Harada, 1968
[d] Nakanishi, 1974, 1976

The average degree of polymerization (DP) of KUSP1, as estimated colorimetrically by the measurement of reducing ends, was 511 (range 487-544). The same procedure with curdlan gave an average DP of 525 (478-570). Curdlan is an extracellular, unbranched (1→3)-β-D-glucan that is synthesized and excreted by *Alkaligenes faecalis* (Harada et al., 1968).

Chemical Modification of KUSP1

Carboxymethyl ethers of KUSP1 have been prepared and are being characterized. Such derivatives are more water soluble than KUSP1. The degree of substitution (DS) expected to obtain under the indicated conditions is 1. The rheological properties of O-carboxymethyl-KUPS1 have not yet been determined.

Gel Quality

The (1→3)-β-D-glucanases have been partially purified. At this time polyacrylamide gel electrophoresis indicates the presence of two major proteins and one minor protein band in the Sephadex 100 gel filtrates.

Progress has been made in the scale-up of polymer production. Scale up of the production process by use of 16 liter air-lift fermentor initially resulted in poor yields of polymer, and the gels formed by the KUSP1 produced were not as rigid as those from KUSP1 from smaller cultures. This difference apparently was a consequence of the difficulty in providing adequate aeration. Inadequate aeration causes an increase in accumulation of acid in the *Cellulomonas flavigena* cultures, with a concomitant decrease in yield of KUSP1. A method for adequate control of culture pH has been developed.

REFERENCES

Ames, B. N. 1966. Assays of inorganic phosphate, total phosphate, and phosphatases, pp. 115-118. In E. F. Neufeld and V. Ginsburg (eds.), Methods in Enzymology Vol. VIII. Academic Press, New York.

Buller, C. S., and K. C. Voepel. 1990. Production and purification of an extracellular polyglucan produced by *Cellulomonas flavigena*. J. Ind. Microbiol. 5:139-146.

Green, J. W. 1963. O-Carboxymethylcellulose., pp. 322-327. In R. L. Whistler, J. W. Green, and J. N. BeMiller, (eds.) Methods in Carbohydrate Chemistry, Vol III. Academic Press.

Harada, T., A. Misaki, and H. Saito. 1968. Curdlan: A bacterial gel-forming β-1,3-glucan. Arch. Biochem. Biophys. **124**: 292-298.

Nakanishi, I, K. Kimura, S. Kusui, and E. Yamazaki. 1974. Complex formation of gel-forming bacterial (1→3)-β-D-glucans (curdlan type polysaccharides) with dyes in aqueous solution. Carbohyd. Res. **32**: 47-52.

Nakanishi, I., K. Kimura, T. Suzuki, M. Ishikawa, I. Banno, T. Sakane, and T. Harada. 1976. Demonstration of curdlan-type polysaccharide and some other β-1,3-glucan in microorganisms with aniline blue. J. Gen. Appl. Microbiol. **22**: 1-11.

Sasaki, S., and T. Sugino. 1984. Carboxymethylated Derivatives of β-1→3-Glucan. United States Patent 4,454,315

Voepel, K. C., and C. S. Buller. 1990. Formation of an extracellular energy reserve by *Cellulomonas flavigena*. J. Ind. Microbiol. **5**: 131-138.

C. S. Buller and K. C. Voepel. 1990. Production and purification of an extracellular polyglucan produced by *Cellulomonas flavigena*. J. Ind. Microbiol. 5:139-146.

Chapter 3

Database Development and Selection of (Organic) Crosslinking System to be Investigated

Principal Investigators: Don Green, Paul Willhite and Stan McCool
Graduate Research Assistant: Ashok Fichadia

INTRODUCTION

Fundamental studies on the gelation of three gel systems were proposed for this research program. Two systems, Cr(III)-polyacrylamide and KUSP1 polysaccharide, were selected initially and the third system was to be selected after examination of the literature and completion of screening experiments. This chapter reports work conducted on selection of the third gel system.

A literature search was conducted to identify gelled polymer systems that have applicability for permeability modification treatments. A database was constructed that displays key technical information of the gel systems. Criteria were defined for the selection of a system. Screening experiments were conducted with candidate systems to determine bulk gelation characteristics. The result of this process was the selection of the aluminum-crosslinked polyacrylamide system.

RESULTS AND DISCUSSION

A literature search was conducted to identify gel systems that have been proposed for use in permeability-modification treatments. A database was prepared that contained the entries of temperature range, gel times and pH requirements for application of the gel system. These technical data were obtained from the listed reference. Hazard ratings for each gel system component are also included in the database. The hazard rating, HR, was obtained from "Sax's Dangerous Properties of Industrial Materials." This handbook assigns a relative Hazard Rating (HR) to commonly used industrial materials on the basis of its toxicity using the codes of 1, 2, 3 or D that identifies the level of toxicity or hazard. These codes are described in Table 3.1.

The database is shown in Table 3.2. Twenty-nine gel systems were identified.

Table 3.1 : Hazard Ratings for Entries in Table 3.2.

Hazard Rating	Explanation
1	Indicates that the material is low in toxic, fire, explosive or reactivity hazard. Materials that have LD_{50} (Lethal Dose, 50% kill) between 4,000-40,000 mg/kg or LC_{50} (Lethal Concentration, 50% kill) between 500-5,000 ppm or are combustible or have some reactivity hazard are assigned HR of 1.
2	Indicates that the material is medium in toxic, fire, explosive or reactivity hazard. Materials that have LD_{50} between 400-4,000 mg/kg or LC_{50} between 100-500 ppm or are flammable or reactive or explosive hazard are assigned HR of 2.
3	Indicates that the material is high in toxic, fire, explosive or reactivity hazard. Materials that have LD_{50} less than 400 mg/kg or LC_{50} less than 500 ppm or are explosive or highly flammable or highly reactive are assigned HR of 3.
D	Indicates that the data available is insufficient to indicate a relative rating.
?	Indicates compound not listed in Sax handbook.

Table 3.2 : Database of Gel Systems

Gel System	Reference #'s	Hazard Rating	Temperature Range	Gel Time	pH Requirements
* Sodium Aluminate * Polymer	(1)	2 ?	Room temperatures	Gelling occurs @ pH below 10.0	< 10.0
* Aluminum citrate * Polyacrylamide	(2), (3)	? ?	77°F - 212°F	Few minutes - few days	4.6 - 8.3
* Zirconium IV salt * Hydrophilic Organic Polymer * SO^{4-} & $RCOO^{-}$ anions	(4)	3 ? ?	Room Temperatures	Instantly - 30 seconds	?
* Ferrous salt * Polysaccharide * Sodium chlorate	(5)	3 ? 3	Room Temperatures	Few seconds - few hours	2.0 - 9.0 preferably b/w 3.0 - 7.0
* Organic Ti complex * Organic Polymer * Hydrocarboxylic Acid	(6), (7)	3 ? 3	60°F - 120°F	Few seconds - few hours	3.0 - 4.5
* Resorcinol * Formaldehyde	(8), (9)	3 3	104°F	5-120 hrs	7.0 - 10.0
* Polyacrylamide * Formaldehyde	(10)	? 3	68°F - 392°F preferably b/w 86°F - 194°F	?	8.0 - 10.5 preferably b/w 10.0 - 10.5
* Polyphenol * Formaldehyde * Complexing agent	(11)	? 3 ?	5°F - room temperatures	1 sec - several hours	8.5 - 11.5
* Polyacrylamide * Salicylic Acid * Aldehyde	(12)	? 3 ?	150°F - 300°F	Few hours - few days	?
* Polyvinyl Alcohol * Aldehyde (glyoxal) * Crosslinker (aldehyde)	(13), (14)	3 3 ?	175°F - 257°F	Several hours - several days	2.0 - 5.0
* Biopolymer * Melamine * Formaldehyde	(15)	? 3 3	< 150°F < 75°F if shear	0.5 - 6.0 hours	< 5.5
* Polyacrylamide * Phenol * Formaldehyde	(16)	? 3 3	122°F - 212°F	1 - 10 days	> 7.0

Table 3.2 : Database of Gel Systems (Continued)

Gel System	Reference #'s	Hazard Rating	Temperature Range	Gel Times	pH Requirements
* Aminoalkylated Polyacrylamide * Formaldehyde	(17)	? 3	50°F - 176°F	2 - 10 days	5.5 - 8.5
* Polyacrylamide * Aldehyde * Resorcinol/Catechol * Stabilizers / Buffers	(18)	? ? 3 ?	86°F - 176°F	40 hrs - 12 months	< 7.0
* Polyacrylamide * Ammonium silicate * Gelling agent	(19), (20)	? 3 ?	77°F - 122°F	Few minutes - 20 hours	< 9.0
* Polysilicate ester	(20), (21)	?	Room temperatures	Gels as soon as shear is removed	Acidic / Alkaline (preferred)
* Organic polymer * Organic nitrogen compounds	(22)	? 2	50°F - 200°F	Depends on temperature	4.0 - 13.0
* N-N dialkylacrylamide-Acrylic acid salt copolymer * Polyvalent metal	(23)	3 ?	Till 392°F	Few hours	?
* Polyacrylamide * Guar gum * Chromium acetate	(24)	? 1 3	Low - room temperatures	Instantly - 48 hours	3.0 - 13.0 (6.0 - 13.0 preferred)
* Melamine * Formaldehyde * Salt of sulphurous acid * Modifying agent	(25)	3 3 ? ?	68°F - 248°F	1 - 10 hours	5.0 - 11.0
* Lignosulfonate * Sodium dichromate * Modifier	(26),(27)	? 3 ?	170°F - 500°F	10 - 2,000 hours	Insensitive to pH
* Carboxamide polymer * Hypohalite salt	(28)	? 3	Room temperatures	24 - 49 hours	7.0 - 12.0 (7.5 - 8.5 preferred)
* Cellulose * Various metal ions	(29)	1 3	80°F - 300°F	?	8.0 - 14.0
* Heteropolysaccharide (S-130) * Chromium(III), etc	(30)	3 3	77°F - 302°F	Gels as soon as shear is removed	5.0 - 11.0
* PVA/PV amines * Resorcinol/Catechol * Paraformaldehyde, etc.	(31)	3 3 3	300°F - 450°F	1 day - 10 days	?

Table 3.2 : Database of Gel Systems (Continued)

Gel System	Reference #'s	Hazard Rating	Temperature Range	Gel Times	pH Requirements
* Polyacrylamide * Chromium(III)	(34), (35)	? 3	55°F-260°F	Few minutes - weeks	4.0 - 12.5
* Polyacrylamide * Chromium(VI) redox	(36), (37), (38)	? 3	120°F-180°F	Few hours	5.0 - 7.0
* Xanthan Biopolymer * Chromium(III)	(39), (40)	? 3	Room Temperatures	Few hours - few days	4.5 - 7.0
* KUSP1 Polysaccharide * pH reducing agent/crosslinker	(41), (42)	? ?	90°F-150°F	Instantaneous-few days	< 10.8 if crosslinker is not used

Three criteria were used to select candidate systems for screening experiments. These criteria were:

Minimal toxicity - The selected system was to be less toxic than the widely-used chromium-based systems. The Hazard Rating was used to determine relative toxicity levels. The Hazard Rating of chromium is 3. Systems that contained chemicals with a Hazard Rating of 3 were considered unacceptable.

Potential for in-depth treatments - The selected system was to gel slowly such that the reservoir distant from the well could be treated. This criterion was met if the gel times for the system were on the order of several days.

Reasonable cost - The selected system contained chemicals that were available in bulk quantities and at reasonable costs.

The systems selected for screening experiments were the sodium aluminate-polyacrylamide, aluminum citrate-polyacrylamide and piperazine di-HCl-polyacrylamide. These systems have potential for in-depth treatments, can be prepared at reasonable costs and were the only systems that did not have Hazard Ratings of 3. It is noted that hazard ratings were not listed for several of the systems identified.

Sodium Aluminate - Polyacrylamide System

Sodium aluminate is nonreactive in high pH environments and releases reactive aluminum which crosslinks the polymer upon pH reduction. The gelation reaction does not occur unless the pH drops below a threshold value of approximately 10. Reduction of pH can be accomplished by interactions with reservoir rock and fluids or by introducing a chemical to the system that reacts to produce acid. The acid-producing additive was selected as the method to trigger gelation.

A search was conducted to identify chemicals that had potential to be used as slow-reacting acid-producing agents in aqueous alkali solutions. An additional requirement was that the chemical be available in bulk quantities. Saccharin, mono-ethyl succinate and mono-ethyl phthalate were identified. Experiments were conducted to determine the pH-time behavior of these three chemicals in 0.1 N NaOH solutions at 25 °C. The initial pH of 0.1 N NaOH samples was approximately 12.8 and the time for this value to drop to a value of 10 was used as the basis for approval of a chemical. This time should be on the order of days.

The results of experiments with saccharin were negative. Saccharin did not produce a drop in pH. The time for reaching a pH value of 10 in a sample containing 0.05 M mono-ethyl succinate was 2.7 hours. This time was considered to be too short for application of in-depth treatments.

The pH-time behavior for samples containing mono-ethyl phthalate are shown in Figure 3.1. Times to reach a pH of 10 can be varied between 20 to 144 hours by the selection of a mono-ethyl phthalate concentration between 0.05 and 0.075 M. The use of mono-ethyl phthalate to trigger gelation in sodium aluminate-polyacrylamide system was examined. It was found that when mono-ethyl phthalate was added to the gel system, a precipitate was formed. Attempts to eliminate the precipitation were unsuccessful.

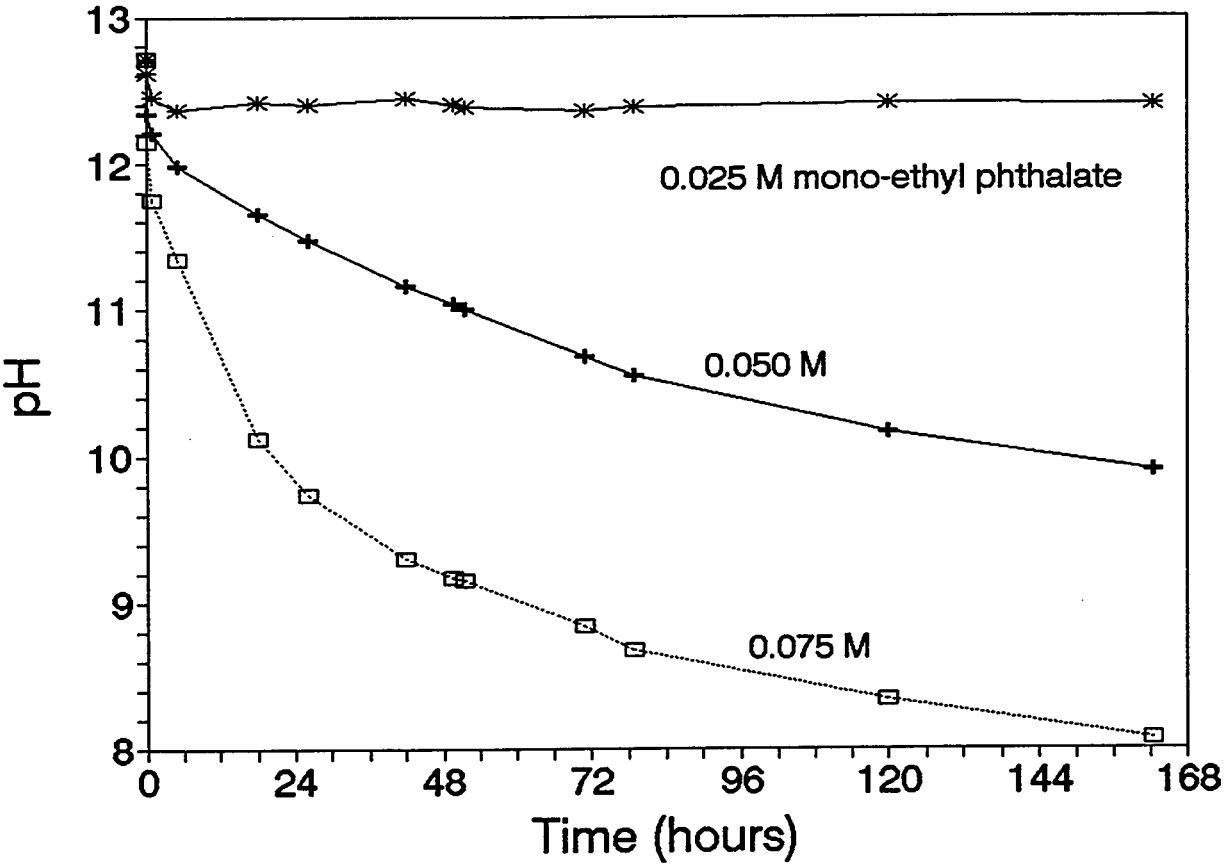

Figure 3.1 pH Reduction by Hydrolysis of mono-ethyl phthalate in 0.1 N NaOH solutions

The sodium-aluminum-polyacrylamide system was not selected for further investigation because of the precipitation problem.

The mono-ethyl phthalate will be investigated for use as a pH control chemical with the KUSP1 polymer described in Chapter 2 and Chapter 7.

Piperazine di-HCl - Polyacrylamide System

Piperazine di-HCl contains two positively charged nitrogen atoms that are capable of forming bonds with reactive groups on polymer chains producing crosslinks and eventually a gel. The patent[22] describing the use of this crosslinker states that these type of molecules will crosslink a variety of polymers including hydrolyzed polyacrylamide although no data were presented using polyacrylamides.

Experiments were conducted to determine bulk gelation times using concentrations of piperazine di-HCl and hydrolyzed polyacrylamide and pH values that were suggested in the original patent. Evidence of gelation was not observed in any of the samples indicating little or no crosslinking of the polyacrylamide by piperazine di-HCl. Testing with other polymers was not pursued.

Aluminum Citrate-Polyacrylamide System

A renewed interest in the aluminum citrate-polyacrylamide system has developed in the oil industry. It is perceived that this system is less toxic than chromium-based systems. Earlier work with the system involved the development of bulk gels through crosslinking of polyacrylamide with aluminum. This system was shown to have problems such as plugging at the injection face, i.e., in-depth treatment was difficult to achieve.[2] More recent applications have involved the development of polymer-gel aggregates which filter and/or adsorb in a porous medium.[33] In-depth treatment with the aggregate system is feasible. This system has proved successful in field trials but the mechanism of permeability reduction is not well understood.

Because of the potential for in-depth treatment and the hazard rating, this system was selected for further study.

SUMMARY

A literature search was conducted to select a gel system for further study. The criteria for selection of a system were low toxicity, potential for in-depth treatment and relatively low cost. Three systems were selected for screening experiments. These were: 1) sodium aluminate-polyacrylamide; 2) piperazine di-HCl-polyacrylamide; and 3) aluminum citrate-polyacrylamide. The screening experiments resulted in elimination of the first two systems and the third system was selected for further study.

REFERENCES

1. Dovan, H.T., and Hutchins R.D., "Development of a New Aluminum-Polymer Gel System for Permeability Adjustment," SPE/DOE 12641, Fourth Symposium on EOR, Tulsa, OK, (April 16-18, 1984).

2. Parmeswar, R and Willhite, G.P., "A Study of the Reduction of Brine Permeability in Berea Sandstone With the Aluminum Citrate Process," *SPE Reservoir Engineering*, (August 1988) p. 959.

3. Podlas, T.J., "Method of Preparing Polymer Gels Using Chelated Aluminum Salt," U.S. Patent 3 839 255, (Oct. 1, 1974).

4. Shu, P. and Wszolek, M., "Zirconium Crosslinked Gel Compositions, Methods of Preparation and Applications in EOR," U.S. Patent 4 676 930 (June 30, 1987).

5. Miller, E.E., and Strydom, P.J., "Crosslinking Water Soluble Polymers with Iron to Form Gels for Use in Subterranean Profile Modification," U.S. Patent 5 065 822 (November 19, 1991).

6. Hodge, R., "Method of Fracturing a Subterranean Formation Using Delayed Crosslinker Compositions Containing Organic Titanium Complexes,", U.S. Patent 4 657 080 (April 14, 1987).

7. Tiner, R., "Method and Compositions for Fracturing Well Formations," U.S. Patent 3 888 312 (June 10, 1975).

8. Chang, P.W., et al., "Enhanced Hydrocarbon Recovery by Permeability Modification with Phenolic Gels," U.S. Patent 4 708 974 (Nov. 24, 1987).

9. Chang, P.W. and Goldman, I.M., "Laboratory Studies and Field Evaluation of a New Gelant for High-Temperature Profile Modification," SPE 14235, presented at the 60th Annual Technical Conference and Exhibition of SPE, Las Vegas, NV, (Sept. 22-25, 1985).

10. Argabright, P.A., "Method of Improving Injectivity Profiles And/Or Vertical Conformance in Heterogenous Formation," U.S. Patent 4 098 337 (July 4, 1978).

11. Whitworth, Tung and Hajto, "Soil Grouting Process and Composition," U.S. Patent 3 884 861 (May 20, 1975).

12. Moradi-Araghi, "Method for Altering High Temperature Subterranean Formation Permeability," U.S. Patent 4 934 456 (June 19, 1990).

13. Marracco, M.L., "Gel for Retarding Water Flow," U.S. Patent 4 498 540 (Feb. 12, 1985).

14. Calif, S.A., "Gel for Retarding Water Flow," U.S. Patent 4 664 194 (May 12, 1987).

15. Mitchell, T., "Organic Crosslinking of Polymers for CO_2 Flooding Profile Control," U.S. Patent 4 793 416 (Dec. 27, 1988).

16. Falk, D.O., "Process for Selectively Plugging Permeable Zones in a Subterranean Formation," U.S. Patent 4 485 875 (Dec. 4, 1984).

17. Fung, F., "Aminoalkylated Polyacrylamide Aldehyde gels, Their Preparation and Use in Oil Recovery," U.S. Patent 4 782 900 (Nov. 08, 1988).

18. Swanson, B., "Gelled Compositions and Well Treatment," U.S. Patent 4 440 228 (April 3, 1984).

19. Norton, C., "Hydrocarbon Recovery Process Using an In-situ Silicate/Polymer," U.S. Patent 4 564 070 (Jan. 14, 1986).

20. Hoskin, D., "Polysilicate esters for Oil Reservoir Permeability Control," U.S. Patent 4 785 883 (Nov. 22, 1988).

21. Hoskin, D., "Polysilicate esters for Oil Reservoir Permeability Control," U.S. Patent 4 660 640 (April 28, 1987).

22. Espenscheid, W., "Crosslinked Polymers for EOR," U.S. Patent 4 613 631 (Sept. 23, 1986).

23. Ryles, R., "High Temperature Profile Modification Agents and Methods for Using Same," U.S. Patent 4 865 129 (Sept. 12, 1989).

24. Falk, D., "Polymer Gelation Process for Oil Recovery Applications," U.S. Patent 4 688 639 (Aug. 25, 1987).

25. Meltz, C., "Aqueous Sulfomethylated Melamine Gel-Forming Compositions," U.S. Patent 4 772 641 (Sept 20, 1988).

26. Felber, B., "Lignosulfonate Gels for Sweep Improvement in Flooding Operations," U.S. Patent 3 897 827 (Aug. 5,1975).

27. Felber, B. and Dauben, D.L., "Method of Using Lignosulfonate Gels for High-Temperature Plugging," U.S. Patent 4 074 757 (Feb. 21, 1978).

28. Kocsis, D., "Method of Controlling the Flow of Liquids Through a Subterranean Formation," U.S. Patent 4 712 617 (Dec. 15, 1987).

29. Wessler, G.A. and Epler, W.N., "Hydroxyl Ethyl Cellulose Complex and Method of Plugging Underground Formations Therewith," U.S. Patent 3 378 070 (April 16, 1968).

30. Paul, J., "Oil Reservoir Permeability Control Using Polymeric Gels," U.S. Patent 4 658 898 (April 21, 1987).

31. Shu, P. and Shu, W., "Composition for Selective Placement of Polymer Gels for Profile Control in Thermal Oil Recovery," U.S. Patent 5,071,890 (Dec. 10, 1991).

32. Richard J. Lewis, Sr., *SAX's Dangerous Properties of Industrial Materials*, 8th Edition, Van Nostrand, Reinhold, NY.

33. Smith, T.E., "The Transition Pressure: A Quick Method for Quantifying Polyacrylamide Gel Strength," SPE 18739, presented at the International Symposium on Oilfield Chemistry, Houston, TX, February 8-10, 1989.

34. Argabright, P.A. and Sydansk, R.D., "Conformance Improvement in a Subterranean Hydrocarbon-Bearing Formation Using a Polymer Gel," U.S. Patent 4 683 949 (Aug. 4, 1987).

35. Sydansk, R.D., "A Newly Developed Chromium(III) Gel Technology," *SPE Reservoir Engineering*, (August, 1990), p. 346.

36. Clampitt, R. L. and Hessert, J.E., "Method for Controlling Formation Permeability," U.S. Patent 3 785 437 (January 15, 1974).

37. McCool, C.S., Green, D.W. and Willhite, G.P., "Permeability Reduction Mechanisms Involved in In-Situ Gelation of a Polyacrylamide/Chromium(VI)/Thiourea System," *SPE Reservoir Engineering*, (February 1991) p. 77.

38. Purkaple, J.D. and Summers, L.E., "Evaluation of Commercial Crosslinked Polyacrylamide Gel Systems for Injection Profile Control Modification," SPE 17331, SPE/DOE Symposium on EOR, OK, (April 17-20, 1988).

39. Phillips, J.C., Miller, J.W., Wernan, W.C., Tate, B.E. and Auerbach, M.H., "A High-Pyruvate Xanthan for EOR," *SPEJ*, (August, 1985) p. 594.

40. Dolan, D.M., "An Experimental Study of the Effects of pH and Shear on the Gelation of a Xanthan-Chromium(III) Solution," Master's Thesis, University of Kansas (1989).

41. Vossoughi, S. and Putz, A., "Application of a Newly Discovered Biopolymer in Enhanced Oil Recovery," TT 93012, 11th Technical Conference and Exhibition of SPE, Trinidad West Indies, (June 23-25, 1993).

42. Vossoughi, S. and Buller, C.S., "Permeability Modification by In-situ Gelation with a Newly Discovered Biopolymer," *SPE Reservoir Engineering*, (November 1991) p. 485.

Chapter 4

Development of Rheological Methods to Monitor Gelation

Principal Investigators: Don W. Green, G. Paul Willhite, C. S. McCool

Graduate Research Assistant: Prashant Khanna

INTRODUCTION

Rheological parameters such as the storage modulus, G', the loss modulus, G'', and the dynamic viscosity, η', are useful to characterize gel systems and provide data on gelation rate. The purpose of the work described in this chapter was to develop the experimental techniques necessary to obtain reliable, reproducible rheological data. The rheometers used for the experimental work were a Bohlin CS rheometer and a Weissenberg R-19 rheogoniometer. The gel system used was polyacrylamide crosslinked with chromium(III).

To obtain credible rheological data, operating parameters must be properly selected and designation of acceptable operating criteria was considered a part of this study. It was determined, based on preliminary experiments, that acquisition of reproducible data required a precise experimental technique for preparation and mixing of the chemicals involved. Development of this technique was also a part of the study.

BACKGROUND

The study of gelation by rheological measurements can be divided into three steps: 1) gel sample preparation; 2) data acquisition; and 3) data analysis. Careful attention to procedures in the Steps 1 and 2 are required in order to obtain reliable and reproducible data for analysis in Step 3. Procedures for sample preparation are described in the Experimental Section. Background information concerning data acquisition, data analysis and polymer aging are addressed here.

Conditions Required for Data Acquisition

Dynamic rheological experiments were used to monitor gelation. This experiment consists of subjecting the sample to sinusoidal shear deformation at low amplitudes of shear stress and strain. The experiment can be run by applying sinusoidal strain and measuring the resultant stress or by applying sinusoidal stress and measuring the strain. Low amplitude shear is required such that the deformation is described by the theory of linear viscoelasticity. That is, the amplitudes of stress and strain are directly proportional and are not a function of the magnitude of either quantity. The range of operation where this type of relatively small deformation occurs is referred to as the *linear viscoelastic region* (LVER). The theory of linear viscoelasticity and the measurement of rheological properties are well documented in the literature[1,2,3,4].

A condition that must be satisfied for the determination of storage modulus and other rheological properties by dynamic measurements is that the deformation be in the LVER. In order to test this

condition, dynamic experiments can be conducted in which measurements are taken over a range of shear strain (or stress) amplitudes that include the amplitude of interest. The deformation is in the LVER if the amplitudes of the shear stresses and strains are proportional. In addition, the computed rheological functions, e.g. the storage modulus, will be independent of the strain (or stress) amplitude when the deformation is in the LVER.

An additional condition on the deformation during dynamic experiments that must be satisfied is *gap loading*. Gap loading occurs when inertial effects are negligible and the shear wave propagating away from the driven surface is immediately reflected from the stationary surface such that every point in the sample moves in phase with the driving surface. If gap loading is not achieved, a complex standing wave field can occur within the sample resulting in incorrect measurements.

A theoretical analysis of the deformation within a sample during dynamic experiments, with respect to wave theory, was conducted by Schrag[5]. He presented equations that can be used to determine deviations in the deformation of the sample caused by reflected shear waves. Deviations in the velocity gradient and in the phase lag between the stress and strain data are calculated as a function of the distance between the platens. We have adopted Schrag's criteria for determining if the data are credible with respect to gap loading. The criteria are that the deviation of the velocity gradient be less than 1% and that the deviation in the phase lag be less than 1° at the position (platen) where the measurements are taken.

The three parameters which influence the gap loading limit are:

- frequency of oscillation
- spacing of gap between the platens
- complex shear modulus, $G^{\star}$, of the sample

The complex shear modulus, $G^{\star}$, incorporates both elastic and viscous components of the material. These components are G' and G'', respectively, and are described later. Increase in these components increases the complex shear modulus which, in turn, increases the gap loading. Gap loading can also be achieved by decreasing the oscillatory frequency or the gap between the platens.

Parameters Measured for Data Analysis

The results of the rheological measurements are presented in terms of the storage modulus, the loss modulus and the dynamic viscosity. The *storage modulus*, G', is a measure of the elasticity of the sample. Initially, the gel system is fluid and the value of the storage modulus is relatively small. As the chemical reactions proceed, the polymers are crosslinked until a 3-dimensional network or gel is formed. The network development results in an increase in the elastic component of the sample. The gelation is thus characterized by the development of the storage modulus with time.

The *loss modulus*, G'', is a measure of the viscous component of the material. Initially, the loss modulus is typically small. As gelation proceeds, the loss modulus increases to a maximum value and then decreases. The *dynamic viscosity*, η', is also a measure of the viscous component of the material and is equal to the loss modulus divided by the frequency of oscillation.

A characteristic of gelation is the relationship between the storage and loss moduli. Initially, the loss modulus is much higher than the storage modulus. After gelation has occurred, the storage modulus is much higher than the loss modulus. Thus, there is a time during the gelation process at which the loss

and storage moduli are equal. This time is termed the G′-G″ crossover point.

Analyses of these types of data have taken different forms. A simple approach has been to define a *gel time* that corresponds to a characteristic of the data. A definition of gel time described in the literature[6] is the G′-G″ crossover. A second definition is the time when the maximum value of the dynamic viscosity occurs[7]. Gel times measured in these ways can be correlated with parameters such as pH, temperature and component concentrations.

Kinetics of the crosslinking reaction have been investigated using dynamic rheological data. Prud'homme *et al.*[8] equated the slopes of the G′- time curves with the crosslink density using the classical theory of rubber elasticity. Maximum rates of reactions (maximum slopes) from experiments conducted at selected component concentrations were used to derive an overall reaction rate expression. Analyses of rheological data provides a convenient method to study kinetics of the gelation process.

Studies indicate that the data used in these analysis methods are dependent on the parameters selected for the rheological measurement. The two parameters that define a dynamic experiment are the frequency of oscillation and the amplitude of either the stress or strain. Winter[9] has shown that the G′-G″ crossover is not a function of the frequency only for systems that exhibit a particular rheological behavior. Lullo *et al.*[10] have shown for gel systems similar to the ones studied here that the time of the G′-G″ crossover was a function of the frequency over the range from 0.21 to 6.4 Hz. They suggest an involved method to determine a "gel time" from the relationship between the G′-G″ crossover time and frequency. An objective of this study is to determine the effect of frequency on the results obtained by the analysis methods described above.

No information on the effect of the strain amplitude (or stress amplitude) on rheological data and the subsequent analyses was found in the literature. It is presumed that most investigators assume that the strain amplitude is sufficiently small such that no effects would be observed. Future studies addressing this topic should be performed.

Polymer Aging

Aqueous polyacrylamide solutions undergo an aging process after preparation. The viscosity of a freshly prepared solution decreases over several days to an equilibrium value. Narkis and Rebhun[11] have proposed that disaggregation of the molecules is occurring during this time period. It is speculated that the rheological data collected during gelation would be affected by the aging process of the polyacrylamide solution used to prepare the gel solution. That is, reproducible data may not be obtained until after the aging process of the stock polymer solution was completed. An objective of this study is to determine the effect of the aging process of polyacrylamide solutions on the rheological data obtained during gelation.

EXPERIMENTAL METHODS

A brief description of the equipment and the experimental procedure is given here. A detailed description of the experimental apparatus and the procedure is presented elsewhere[12,13,14].

A polyacrylamide-chromium(III) gel system was used in this study. The gel solution was prepared from polymer and chromium stock solutions which were first prepared in bulk quantities. The compositions of the gel solution and the stock solutions are given in Table 4.1.

Table 4.1: Compositions of the gel solutions and stock solutions.

Gel solution	7,500 ppm polyacrylamide 100 ppm chromium(III) 2.0% sodium chloride initial pH = 5.0
Polymer solution	1.0% polyacrylamide (PAAm) Aldrich Lot #12 2.66% sodium chloride
Chromium solution	400 ppm chromium(III) (using $CrCl_3 \bullet 6H_2O$)

The procedure for mixing the gel solution from the stock solutions was critical to obtaining reproducible rheological data. Stock solutions were stored in pyrex bottles in a constant temperature bath maintained at 25°C. The required amount of polymer solution was weighed in a glass bottle. The polymer solution was maintained at 25°C by placing the glass bottle in a jacketed beaker. The solution was stirred using a magnetic stir bar and a stir plate until a reasonably-sized vortex could be observed. Addition of the chromium solution was done volumetrically using a graduated syringe. The required volume of the chromium solution was squirted on the shoulder of the vortex to ensure homogeneity of the solution. The pH of the gel solution was measured and adjusted to 5.0 using a 0.1 N sodium hydroxide solution.

The polymer stock solutions were aged by storing them in Erlenmeyer flasks in a cool, dark place. Prior to gel preparation, the required amount of the polymer solution was kept in a water bath maintained at 25°C until the temperature of the polymer solution was 25°C.

Two rheometers were used in the study. Most of the data were obtained on a Weissenberg R-19 using a cone-and-plate geometry that had a diameter of 75 mm and a gap angle of 0.96 degrees. Dynamic experiments on the R-19 were conducted at a strain amplitude of 0.5 and at selected frequencies. Supplemental data were obtained on a Bohlin CS rheometer using cone-and-plate geometries having diameters of 40 mm. Cone angles of 1 and 4 degrees were used and are described by the names *CP 1/40* and *CP 4/40*, respectively. The stress (rather than strain) amplitude is controlled on the Bohlin rheometer. Specification of the stress amplitude is included with data obtained from the Bohlin.

The gel solutions were prepared just prior to loading them on the rheometers. After the samples had been placed on the rheometers, the exposed edges were covered with a thin layer of light mineral oil in order to prevent evaporation. A constant temperature of 25°C was maintained.

RESULTS AND DISCUSSION

Data Acquisition

Considerable attention was given to determining the validity of the rheological data. Since no viscoelastic standards have similar properties of the gel system studied here, experiments using standard oils and polymer solutions were conducted on both the rheometers in order to check the validity of data acquisition.

Viscosities of several standard oils were determined from steady-shear experiments. Ranges of shear rate were determined where accurate data could be obtained for a given viscosity on each rheometer.

Experiments were conducted on polymer solutions at several polymer concentrations. Data obtained on one of the rheometers were within 10% of values determined by the other rheometer. Data examined were steady-shear viscosities as a function of shear rate and loss and storage moduli as functions of oscillatory frequency. These experiments on standard oils and polymer solutions demonstrated the general validity of the rheological measurements.

Experiments were conducted on gel solutions prepared from different sets of stock solutions in order to demonstrate reproducible gel preparation. Figure 4.1 shows the results from the gelation runs depicting the build-up of storage modulus with time. Good reproducibility was obtained for these runs and the storage modulus values were within 4% of the averaged value at the end of nearly 18 hours.

Conditions for Credible Measurements

The selection of proper operating parameters is an important factor in determining the credibility of rheological measurements. The two conditions which were examined are:

- gap loading limit
- linear viscoelasticity

The results obtained for these criteria are presented and credibility of the rheological measurements was justified on the basis of these results.

Gap Loading Limit. Based on the method developed by Schrag[5], calculations were performed for the measurements made on the samples under study. Base-line conditions were determined by performing tests on polymer solutions having concentrations similar to the gel but without the chromium. Since a higher value of the complex modulus, $G^{\star}$, increases the gap loading, thus satisfying the criterion for the base line case ensured that the gap loading limit is satisfied for the entire gelation run. From these calculations it is possible to determine the error introduced in the magnitude of velocity gradient (g/g_c) and the phase lag (Φ).

Results of the calculations performed for the polymer solutions are given in Table 4.2. The data were measured for a 7,500 ppm PAAm, 2.0% NaCl solution on the Weissenberg rheogoniometer and the Bohlin CS rheometer. The geometry used for the Bohlin was *CP 1/40*. The phase angle and complex modulus ($G^{\star}$) are measured for the polymer solution. The other two parameters required for performing the calculations are the frequency of oscillation and the gap between the platens at the edges. Following Schrag's method, a complex set of calculations was performed using these to determine the error involved in measurements. For determining the actual error one must consider the deviation of $|g|/|g_c|$ from 1 and Φ from 0°.

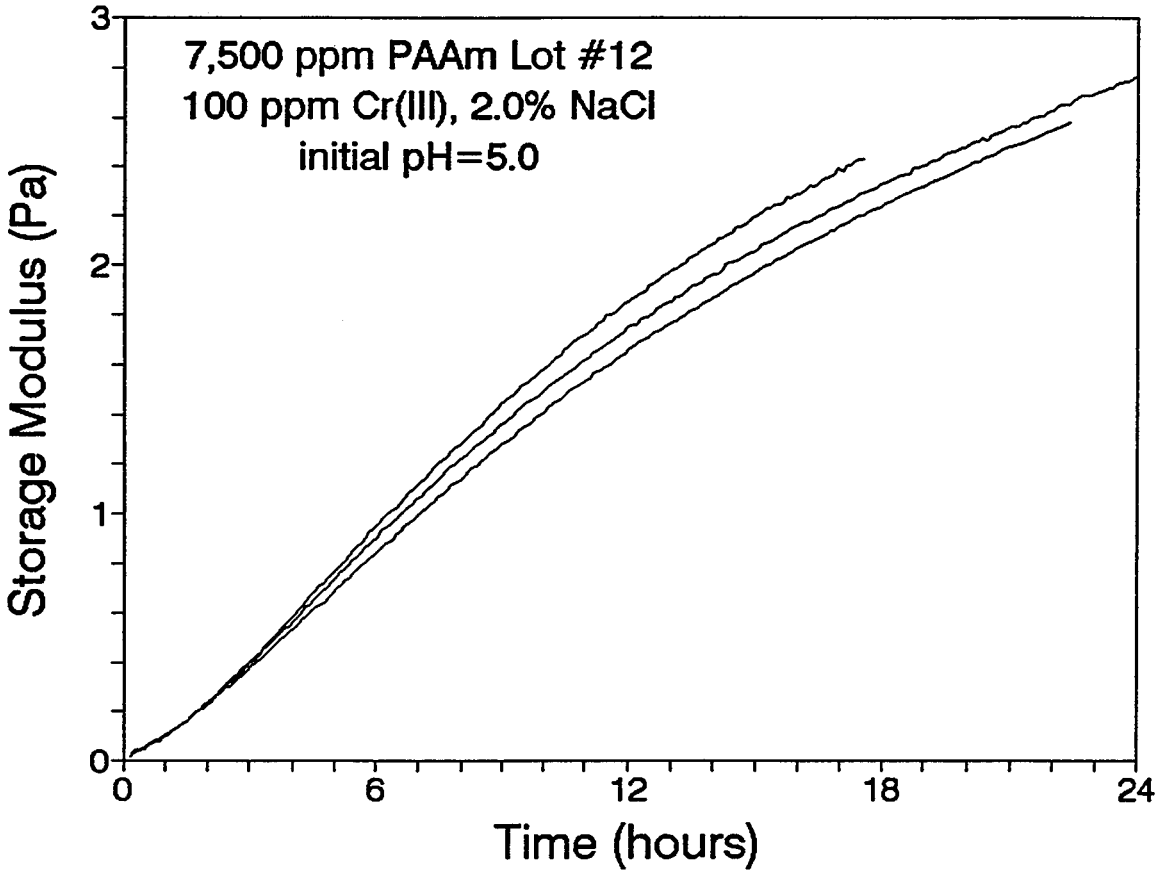

Figure 4.1: Reproducibility of gelation runs under oscillatory shear at a frequency of 1.0 Hz. Each gel sample was prepared from different sets of stock solutions.

Table 4.2: Deviations from the Gap Loading Limit for the Weissenberg rheogoniometer and Bohlin CS rheometer

Phase (degrees) G^* (Pa) Frequency (Hz) Gap (mm)	Weissenberg 83.39 0.151 1.00 0.63		Bohlin CP 1/40 87.01 0.136 1.00 0.35	
x/D	g/g_c	Φ	g/g_c	Φ
0	1.002	-0.977	1.000	-0.337
0.1	1.002	-0.948	1.000	-0.327
0.2	1.002	-0.860	1.000	-0.297
0.3	1.001	-0.713	1.000	-0.246
0.4	1.001	-0.508	1.000	-0.175
0.5	1.001	-0.244	1.000	-0.084
0.6	1.000	-0.079	1.000	0.027
0.7	0.999	0.461	0.999	0.159
0.8	0.998	0.902	0.999	0.311
0.9	0.998	1.402	0.999	0.483
1.0	0.997	1.962	0.999	0.675

The ratio x/D in Table 4.2 corresponds to the dimensionless distance between the platens; x/D = 0 is at the fixed plane and x/D = 1 is at the oscillating plane. The measurements are taken on the fixed plane on the Weissenberg rheogoniometer and, therefore, the region of interest is at x/D = 0. For the Bohlin CS rheometer, the measurements are made on the oscillating plane and thus the region of interest for this machine is at x/D = 1. It can be observed from the table that the error involved in magnitude is less than 1%, whereas the deviation for the phase angle is less than 1 degree at the respective regions of interest. Thus, it can safely concluded from these results that the rheological experiments conducted during this study satisfy the criterion for operation under the gap loading limit.

Linear Viscoelastic Region (LVER). The calculations for all rheological properties are based on the assumption that the sample lies in the LVER. The test for linearity is to check that the computed viscoelastic functions are independent of the magnitude of the stresses and strains applied. The Bohlin CS rheometer allows for running these tests under the option of *Stress Sweep*. Under this mode of operation the stress applied to sample can be varied at a fixed frequency, and the corresponding strains and other viscoelastic functions are computed.

Stress Sweep tests were conducted on polymer solutions and gel samples at intermittent times to ensure that no deviations from the LVER were observed for the entire range of operation. Figure 4.2

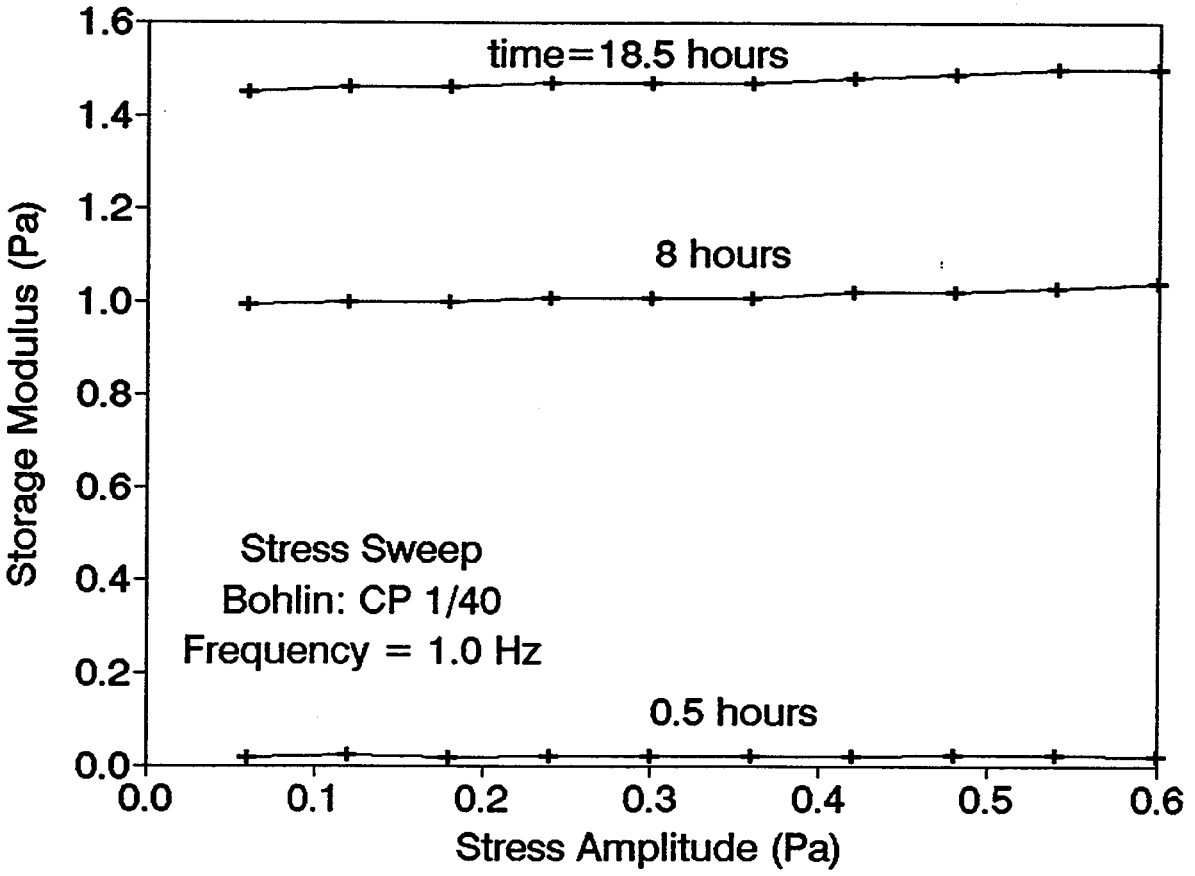

Figure 4.2: Test for LVER for a gel sample showing that the storage modulus is independent of the magnitude of the stress applied. The composition of the gel is given in Table 4.1.

shows the storage modulus as a function of the stresses applied for a gelation experiment. The value of the storage modulus is nearly independent of the magnitude of the stresses applied.

On the basis of the results presented in this section, it can be concluded that for the conditions specific to this study, the conditions for obtaining correct rheological measurements are satisfied.

Effect of Frequency on Gelation

Measurement of rheological properties for a gelling system is normally done by subjecting the sample to a small oscillatory shear. The frequency of oscillation has an upper bound for obtaining correct rheological data, which is determined by the gap loading limit. The principal frequency of oscillation during the course of this study was 1.0 Hz, but the effect of varying the frequency on different gelation measurements has also been investigated. The frequency of oscillation was varied over two decades, from 1.0 Hz to 0.01 Hz. The effect of frequency has been examined with respect to the different definitions of *gel point* given in the literature.

One definition of the *gel point* of a chemically crosslinking system is the instant at which the weight-average molecular weight goes to infinity[9]. As a consequence, the crosslinking polymer undergoes a transition from a liquid to a more solid-like state.

Modulus Crossover as a Measure of Gel Point. It has been cited in the literature that the *gel point* of a crosslinking polymer occurs at the instant at which the storage modulus and the loss modulus, cross each other[6]. The storage modulus (or G′) is representative of the solid or elastic component of the complex modulus, whereas the loss modulus (or G″) represents the liquid or viscous component. At the beginning of the experiment, the loss modulus is orders of magnitude larger than the storage modulus, and the order is reversed after gelation has occurred. Since, the crossover of the two moduli is indicative of a relative transition from a "more" viscous behavior to a "more" elastic behavior, the theory of the crossover point as being the gel point has been widely propagated.

During this study, the crossover point is taken as a relative measure of the *gel point*. Figure 4.3 shows a typical gelation curve for the polyacrylamide and chromium(III) gel system depicting the crossover of the dynamic moduli. The frequency of oscillation for this experiment was 1.0 Hz. The G′-G″ crossover time for this run was found to be 2.8 hours from the time the gel was mixed. Table 4.3 lists the crossover times for gelation experiments at different frequencies.

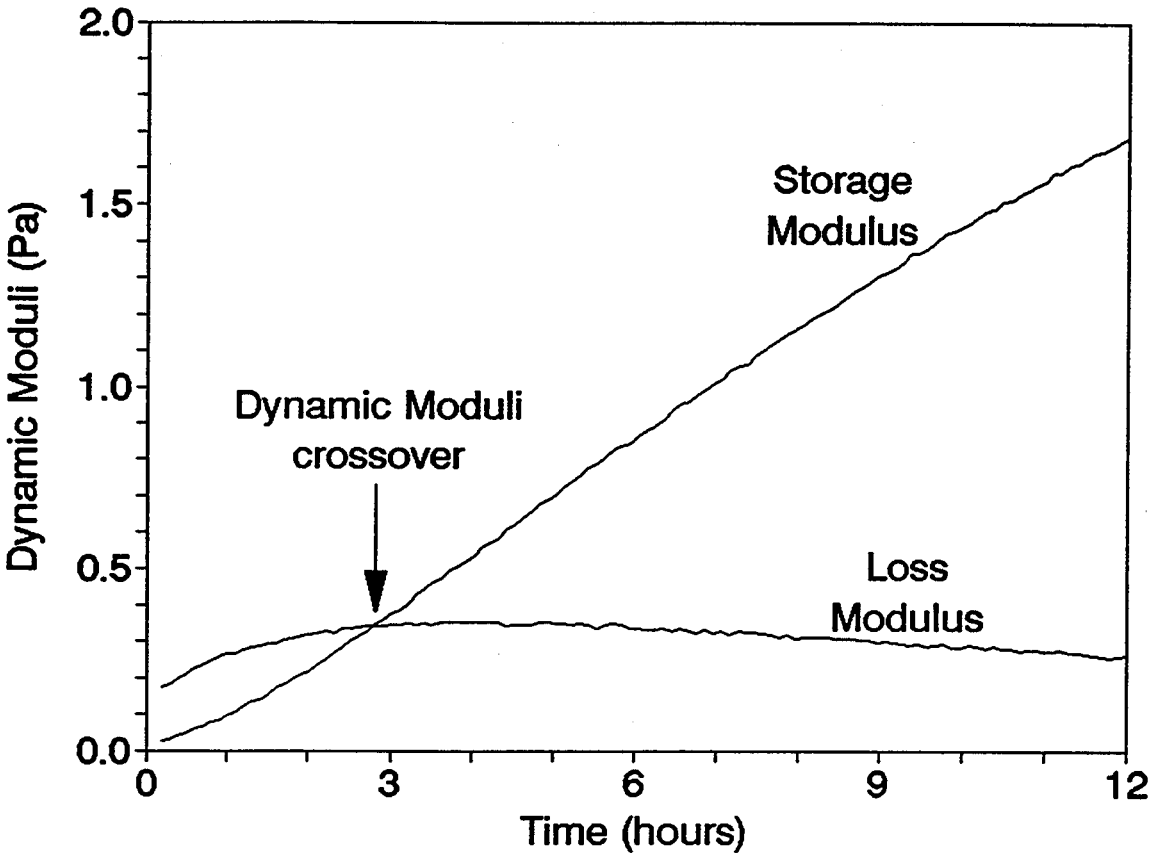

Figure 4.3: A typical gelation run for the polyacrylamide/chromium(III) gel system depicting the crossover of the storage modulus and the loss modulus.

Table 4.3: The crossover time of the dynamic moduli as a function of the frequency of oscillation for the given gel system.

Frequency (Hz)	G′-G″ crossover time (hours)	
	Run No. 1	Run No. 2
1.0	2.82	2.85
0.316	2.31	-
0.1	2.25	2.20
0.01	2.03	2.04

As indicated a decrease in the frequency of oscillation results in a decrease in the crossover time. The same results are plotted on a semi-logarithmic scale in Figure 4.4. A definite trend is seen from the graph over the range of frequency studied. Due to time limitations, experiments could not be performed at intermediate frequencies, thus no correlations were drawn from this data. It was not possible to obtain data at lower frequencies due to the limitations of the experimental apparatus being used. The upper bound of the frequency was restricted by the gap loading limit.

Similar trends have also been observed by Tung and Dynes[6] and Lullo *et al.*[10]. Tung and Dynes examined the viscoelastic behavior for thermosetting resins and have investigated the effect of frequency on the modulus crossover. The frequency for their experiments was varied from 0.1 rad/sec (0.016 Hz) to 100 rad/sec (16 Hz) and the modulus crossover time showed an increase with frequency. Lullo *et al.* worked with Cr^{3+}/polyacrylamide compositions while investigating the same effect. They varied the frequency from 1.3 rad/sec (0.21 Hz) to 30 rad/sec (4.78 Hz) and observed an increase in the crossover time with frequency. Thus, the results obtained from this study are in agreement with similar work reported in the literature.

Peak in Dynamic Viscosity as a Measure of Gel Point. Bhaskar[7] proposed a new definition for the *gel point*. This *gel point* is defined as the point at which the dynamic viscosity exhibits a maximum under zero net shear conditions. The theoretical reasoning for the peak in dynamic viscosity coinciding with the *gel point* is now discussed.

At the beginning of the run, there is little interaction between the polymer molecules in the gelling solution, and the dynamic viscosity is representative of the shear viscosity of the solution. As gelation progresses, the gel clusters become larger, thereby increasing viscous dissipation in the fluid. At the gel point, the clusters reach a critical size, corresponding to the maximum in dynamic viscosity. Beyond this point, a decrease in the dynamic viscosity is observed, as the fluid becomes more elastic and, therefore, more efficient at transmitting the stress to the upper platen.

Figure 4.5 shows the change in dynamic viscosity with time for the polyacrylamide/chromium(III) gel at different frequencies. The peak in dynamic viscosity is observed at about 4 hours. Specific to this system, a few problems are encountered in determining the gel point as defined by the peak in dynamic viscosity. Sometimes the data are rather noisy, especially at lower frequencies (0.1 Hz and 0.01 Hz), and

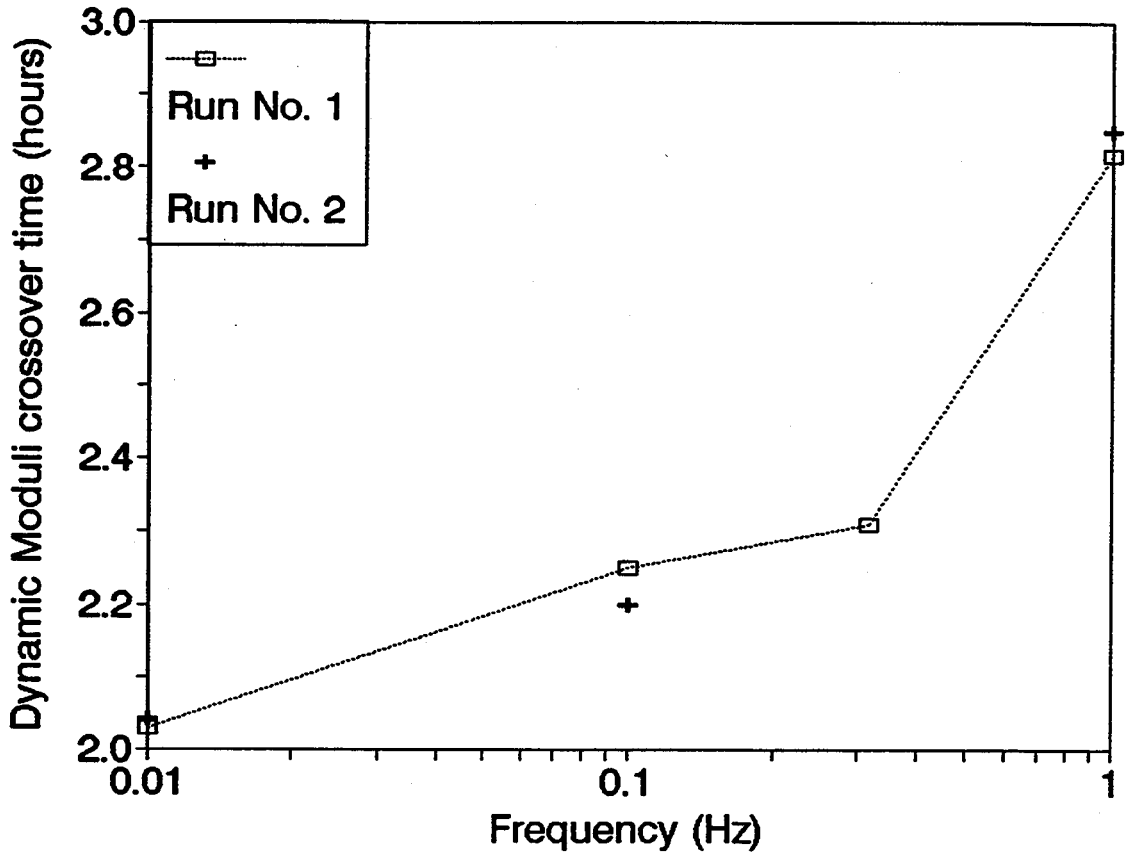

Figure 4.4: The crossover time of the dynamic moduli as a function of the frequency for the polyacrylamide/chromium(III) gel system.

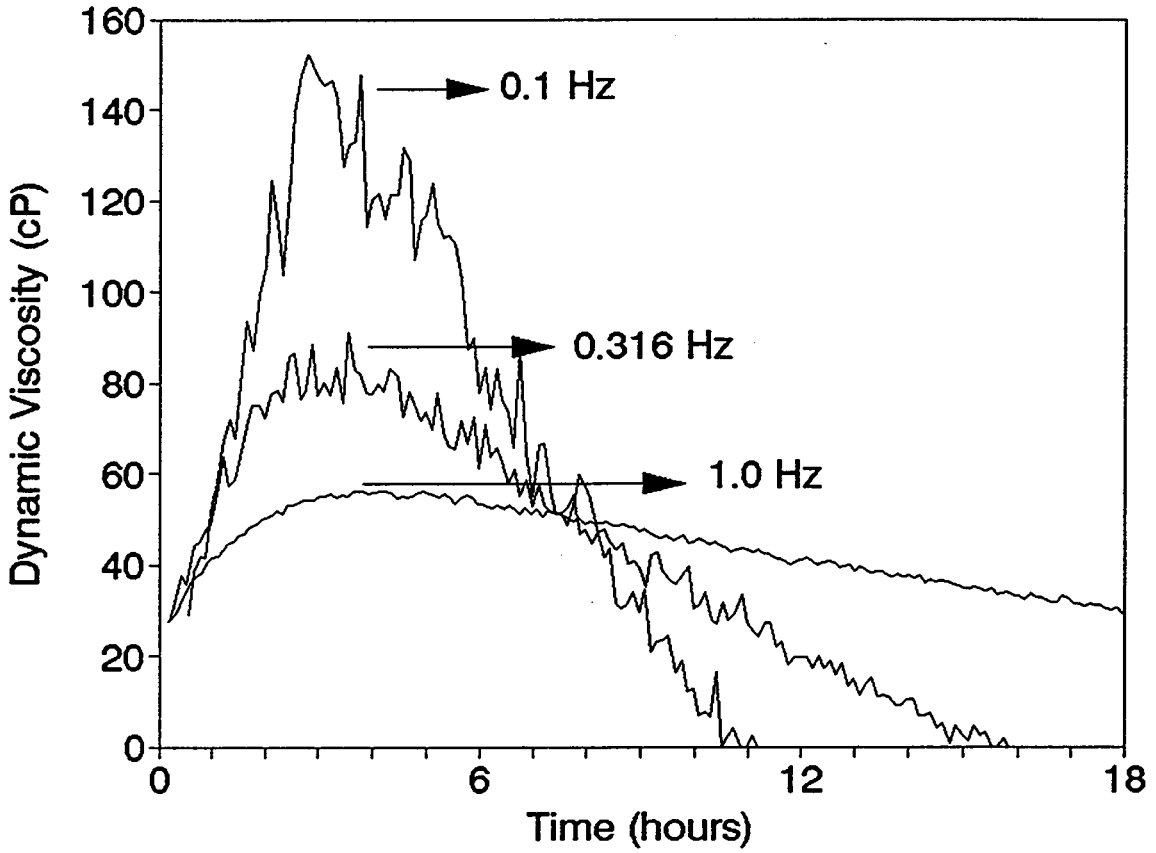

Figure 4.5: A comparison of gelation runs at different frequencies depicting the change in dynamic viscosity with time.

thus it might not be possible to distinguish between the noise and the peak in the viscosity value. Based on this definition of *gel point*, it appears from the figure that the frequency of oscillation does not have an effect on the gel point. However, no conclusions can be drawn because of the noise in the data. According to Bhaskar's definition, the dynamic viscosity is representative of shear viscosity during the initial stages of gelation. It has been postulated that the peak in dynamic viscosity should coincide with the time at which the shear viscosity tends to infinity. During this study no shear viscosity measurements were made, thus it was not possible to supplement the postulate with any data.

Value of Storage Modulus as a Measure of Gel Point. During this study the gelation process was monitored by the build-up of storage modulus with time. The measured storage modulus is a function of frequency for the polymer solutions. At the beginning of the gelation process, the gel solution exhibits behavior similar to the polymer solutions, i.e. a frequency dependent storage modulus. As gelation progresses, the dependence seems to diminish. Figure 4.6 shows a comparison of gelation runs made at different frequencies (the gelation runs shown in this experiment correspond to the same runs for which dynamic viscosity data have been presented in Figure 4.5). It can be observed from the figure that for the initial time period of 2 to 3 hours the values of storage modulus appear to be dependent on the frequency of oscillation. After this initial time period, which is in coherence with the crossover time of the dynamic moduli, the rate of change of the storage modulus with time appears to be constant irrespective of the frequency of oscillation. The effect of frequency on the rate of change of storage modulus with time is discussed in detail in the next section.

Figure 4.7 shows the storage modulus as a function of frequency for a gel solution at intermittent times. The zero time is the time when the gel was mixed. The principal frequency of oscillation for this experiment was 1.0 Hz. The curves indicate a transition from viscous behavior to elastic behavior, where the frequency dependence of the storage modulus appears to diminish. Since the results are shown on a logarithmic scale, they appear a little ambiguous in the sense that the storage modulus at the end of 23 hours is not completely independent of the frequency as apparent from the graph. Figure 4.8 shows a gelation run at a frequency of 1.0 Hz run over a period of 5 days. This run shows that even at the end of 5 days, the storage modulus had not reached an equilibrium value, and was still increasing with time.

Slope of Storage Modulus with Time as a Measure of Gel Point. The time dependence of the storage modulus has been used by Prud'homme *et al.*[8] to analyze the kinetics of the gelation process. He used the kinetic theory of rubber elasticity to determine the rate of gelation from the measured value of the storage modulus. The maximum rate of gelation is determined by measuring the maximum slope of storage modulus with time.

Two methods were used to determine the slope of the G'-time curves. It was initially attempted to determine the slope directly from the storage modulus-versus-time data for a gelation experiment by using a divided-difference formula. The slope data were found to be rather noisy and no meaningful interpretations could be drawn. Thus, it was decided to fit a curve to the gelation data and use the resultant equation to determine the slope by taking its first derivative. A fifth-order polynomial equation was used to fit the gelation curve. Figure 4.9 shows a 5^{th} order polynomial fit for a gelation experiment at a frequency of 1.0 Hz. Only a few selected data points are shown in order to distinguish between the fit and the data points. The equation for the curve was differentiated in order to determine the slope of storage modulus with time. The same procedure was followed for all the frequencies, ranging from 1.0 Hz to 0.01 Hz.

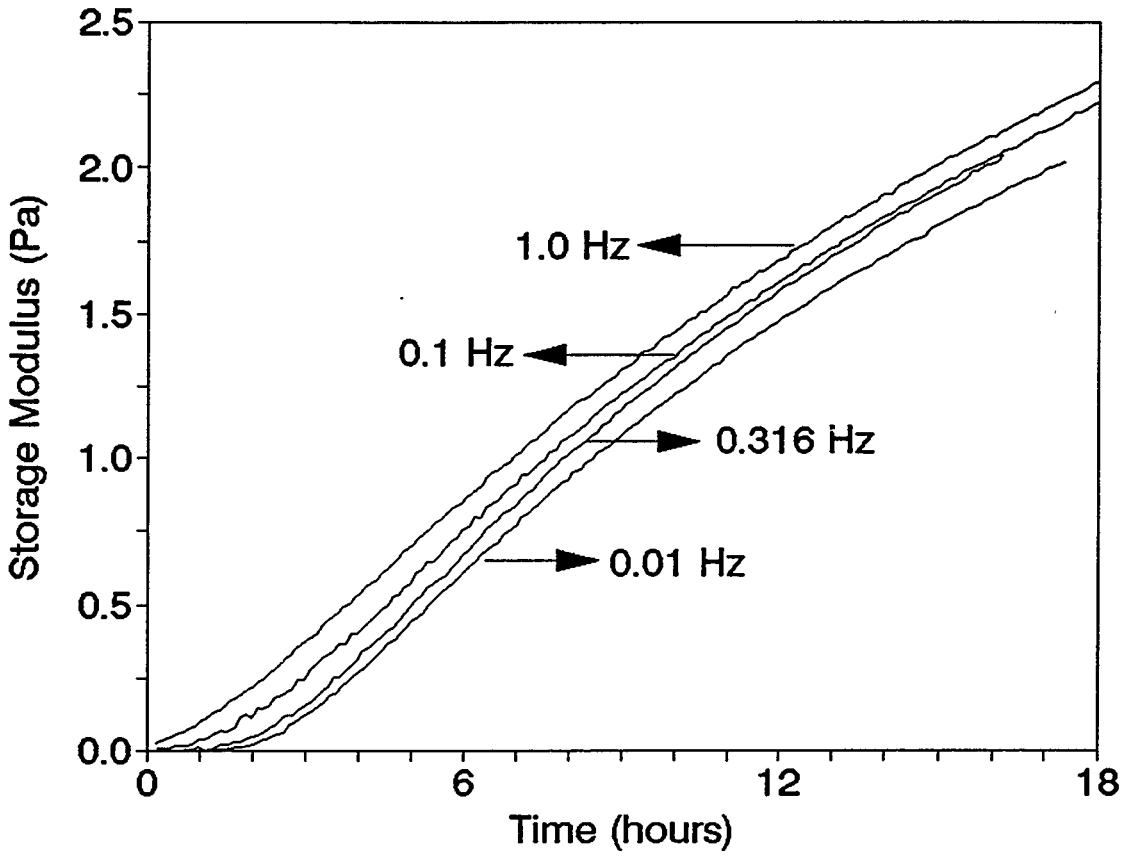

Figure 4.6: A comparison of gelation runs at different frequencies showing the build-up of storage modulus with time.

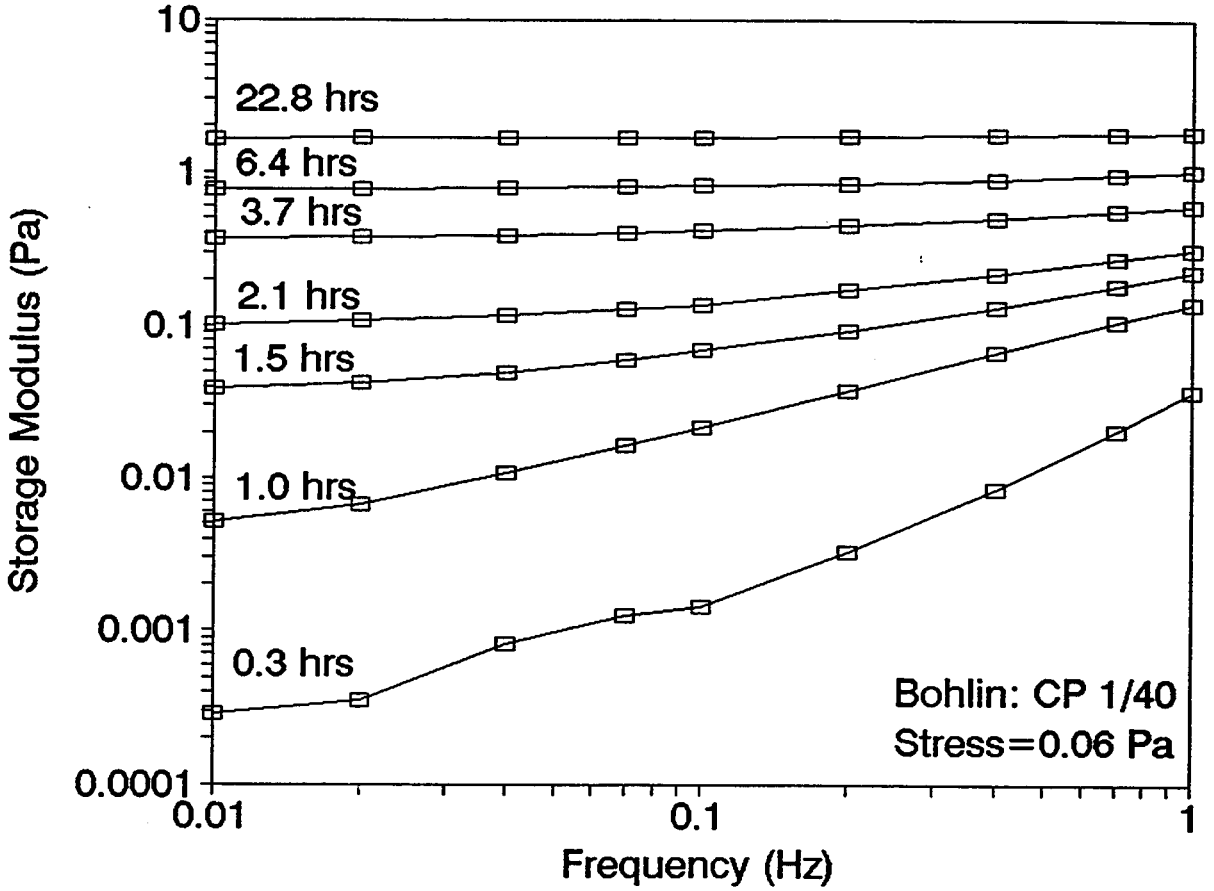

Figure 4.7: Storage modulus as a function of frequency at intermittent times for the gel system on the Bohlin CS rheometer.

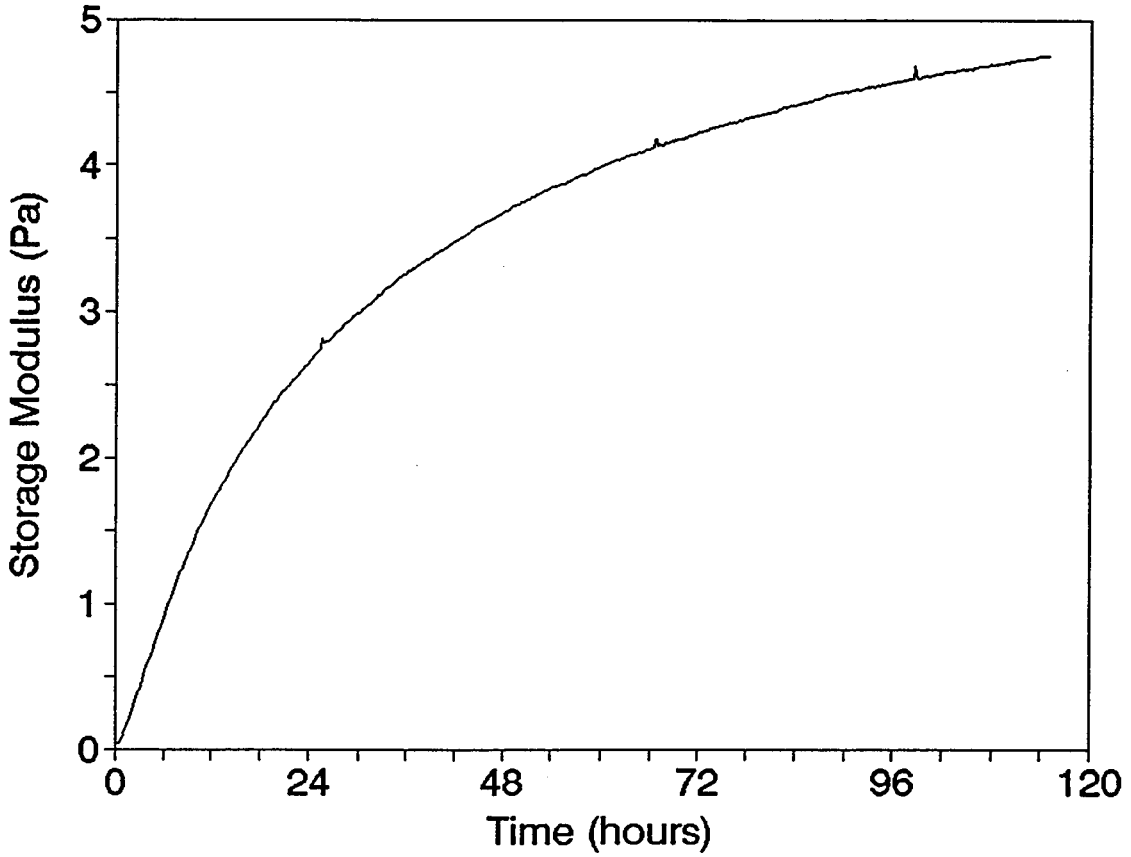

Figure 4.8: A gelation experiment at a frequency of 1.0 Hz run over a period of 5 days.

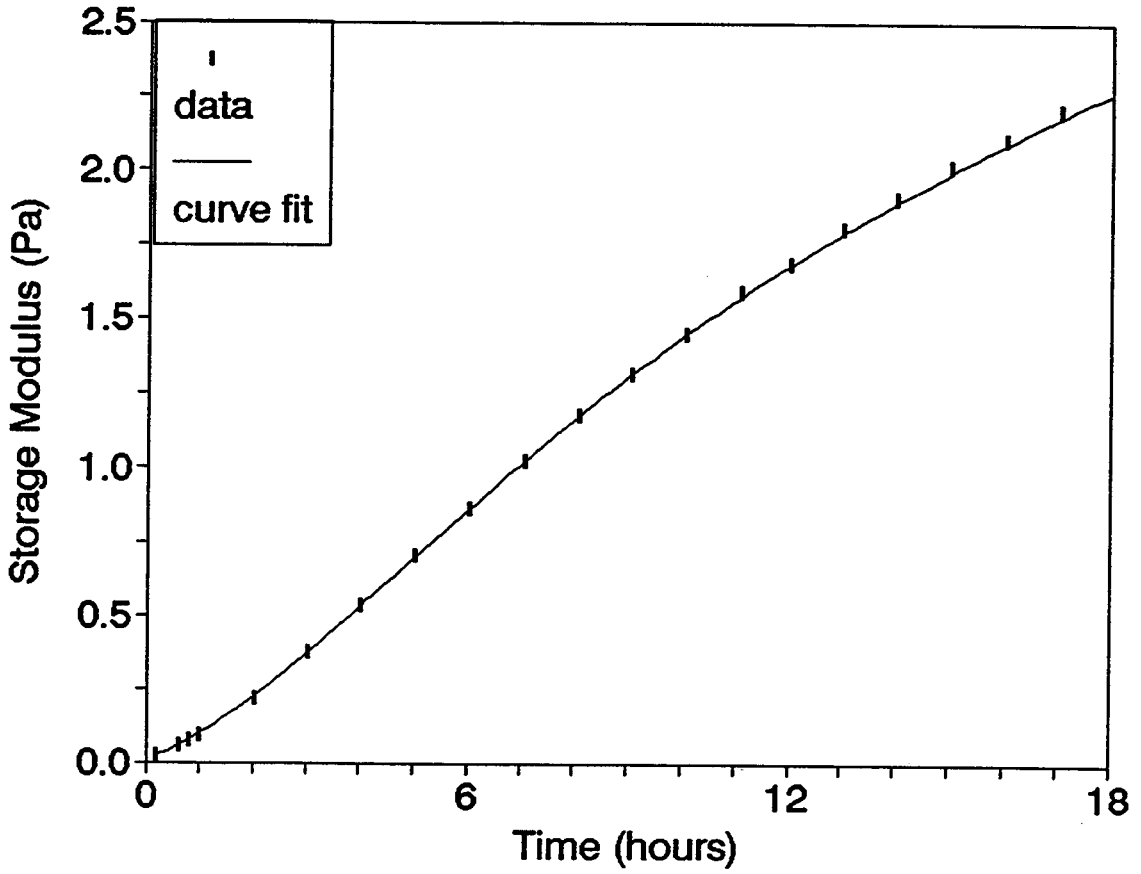

Figure 4.9: A 5th order polynomial fit to the storage modulus versus time curve of a polyacrylamide/chromium(III) gel at a frequency of 1.0 Hz.

Based on the method proposed by Prud'homme *et al.*, the maximum gelation rate is determined from the maximum slope of the storage modulus-versus-time curve. Figure 4.10 shows the comparison of slope and time curves at various frequencies. The maxima for the slope appears to be independent of the frequency of gelation. Table 4.4 lists the maxima for the slope at various frequencies as determined from Figure 4.10.

Table 4.4: The maximum value of the slope for the storage modulus-versus-time curves at various frequencies.

Frequency (Hz)	Maximum value of the slope (Pa/hour)
1.0	0.164
0.316	0.168
0.1	0.181
0.01	0.176

The maximum value of the slope is found to be within 5% of the averaged value for a frequency variation of two decades. On the basis of this method for determination of gelation rate, the frequency of oscillation does not appear to be having an effect. The time required to reach this maxima has been referred to as the "induction period".

Aging of Polymer Solutions

Polyacrylamide dissolved in water undergoes a slow aging process during storage at room temperature. Aging of solution primarily refers to a decrease in viscosity with time until the viscosity reaches a constant value. Narkis and Rebhun[11] have proposed that the disaggregation of entangled polyacrylamide molecules is being completed during aging. A decrease in the viscosity of a polymer solution on standing does not necessarily indicate degradation. The polymer molecules can be twisted internally or the molecules can become entangled during formation of the polymer. The disentanglement of the molecules during storage is reflected in the decrease of the solution viscosity.

Since the chain entanglements are a function of the size and the number of molecules in the solution, the molecular weight and concentration of the dissolved solution are important factors. As the molecular weight increases, there is an increasing probability of a large number of entanglements for the length of the chain. In addition, as the concentration increases, the number of chains in a given volume increases, thereby increasing the likelihood for molecules to become entangled in loops of other molecules. Narkis and Rebhun also found that maintaining a higher temperature did not decrease the aging time for reaching the limiting viscosity value.

The aging effect for the polyacrylamide solutions used in this work was examined. Steady shear and oscillatory shear experiments were performed on polymer solutions in order to study the effect of aging and the time required for the viscoelastic properties of the polymer solution to reach a constant

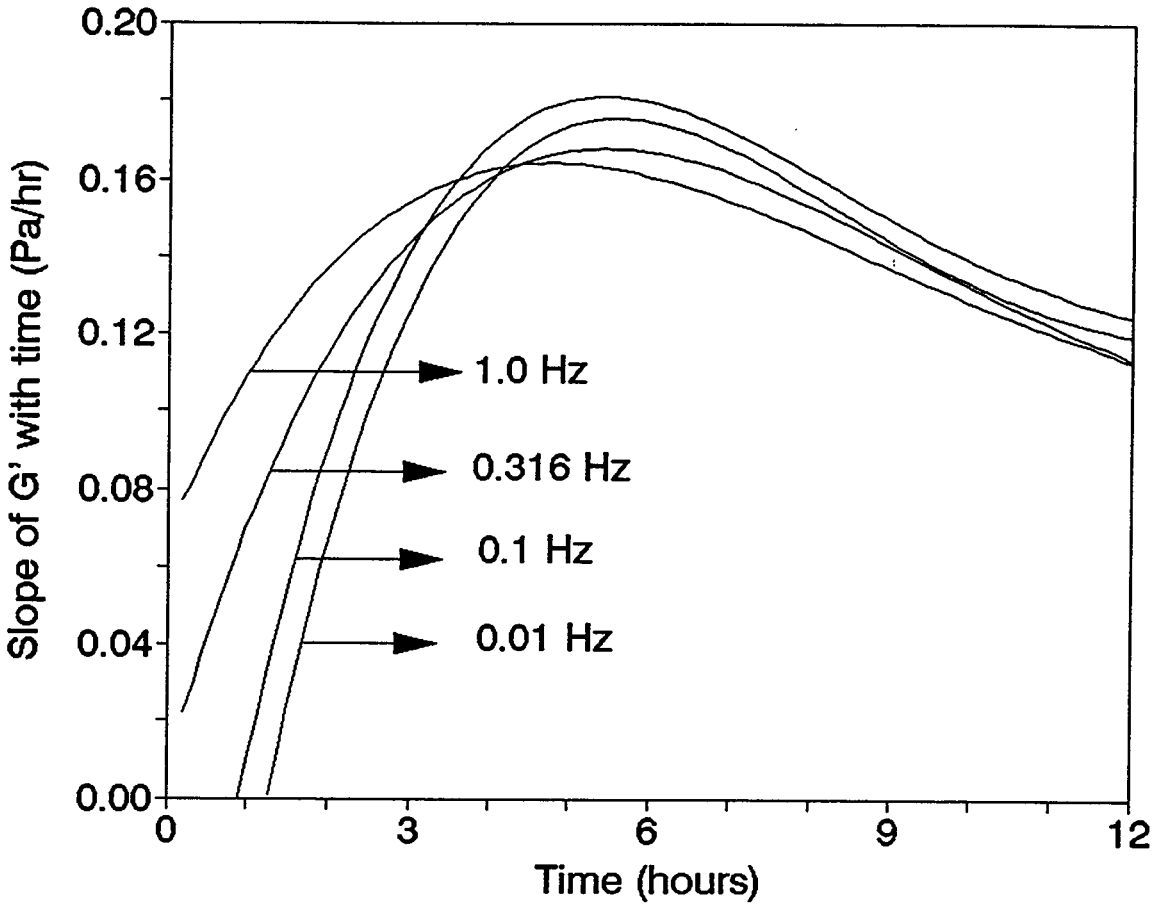

Figure 4.10: A comparison of the gelation rates at different frequencies as determined by the slope of the storage modulus versus time curves.

value. The effect of aging with respect to gelation of polyacrylamide with chromium was also investigated. Gel samples were prepared from polymer solutions of different ages and the build-up of storage modulus with time was monitored for the samples.

Figure 4.11 shows the results of the rheograms (measurement of viscosity as a function of shear rate) on the polymer stock solution. The stock solution had a concentration of 1.0% polyacrylamide and 2.66% NaCl. The days referenced in the graph denote the age of the polymer solution. The viscosity of the solution appears to decrease slightly with time, by about 8% of its initial value, to a constant value. The anomaly in the viscosity data at the lowest shear rate is attributed to the noise due to the limitations of the experimental apparatus being used.

Gel samples were prepared from the polymer stock solution of different ages and the gelation process was monitored. Figure 4.12 shows the results of the few gelation runs performed on the Weissenberg rheogoniometer. The build-up of storage modulus with time was monitored. The days referenced with each run denote the age of the polymer solution. At any fixed time there is a perceivable decrease in the value of the storage modulus with the age of the polymer solution until the solution has been aged for more than 5 days. After 5 days, the storage modulus reaches a near constant value where the gelation curves are identical within experimental error.

Thus, the age of the polymer solutions has an effect on the measured value of the storage modulus during gelation. This effect can be detected until the polymer solution was 5 days old.

CONCLUSIONS

The experimental techniques developed for the preparation of polymer solutions and gel solutions, and for the measurement of their rheological properties gave reproducible measurements.

The conditions necessary for acquisition of credible rheological measurements were satisfied. The two conditions which were examined are linear viscoelasticity and gap loading.

The effect of frequency on gelation was investigated with the following conclusions:

(a) The crossover time of the storage modulus and loss modulus increased as the frequency of oscillation was increased.

(b) The peak observed in dynamic viscosity during a gelation experiment is not a good measure of the "gel time" for the given system.

(c) All the gelation experiments show an initial dependence on the frequency of oscillation. The gel did not attain an equilibrium value for the storage modulus even after 5 days.

(d) The maximum rate of gelation determined from the maximum slope of storage modulus-versus-time curve shows no dependence on the frequency of oscillation.

There was an effect of the polymer solution age on the build-up of storage modulus of the gel solutions until the polymer solution was 5 days old.

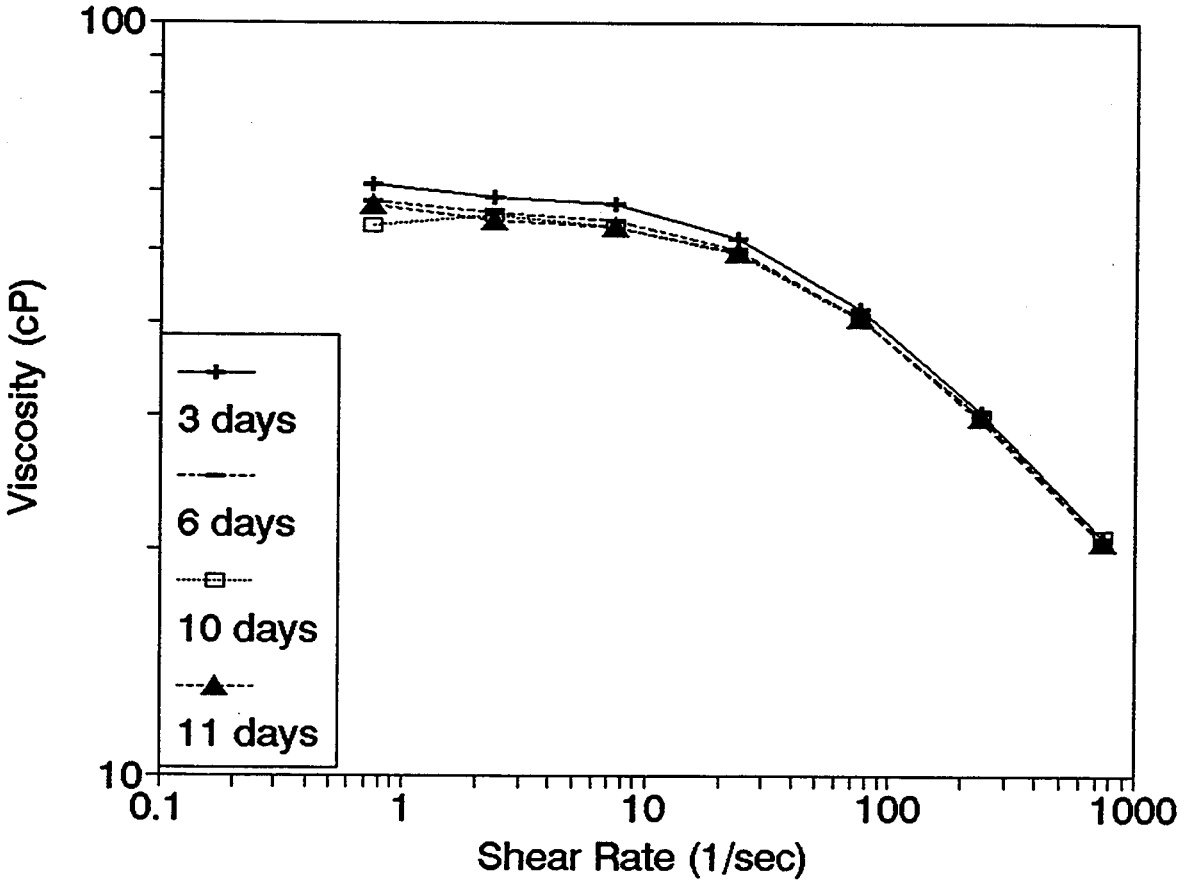

Figure 4.11: Rheograms on 1.0% polyacrylamide, 2.66% sodium chloride solutions to illustrate the effect of polymer aging.

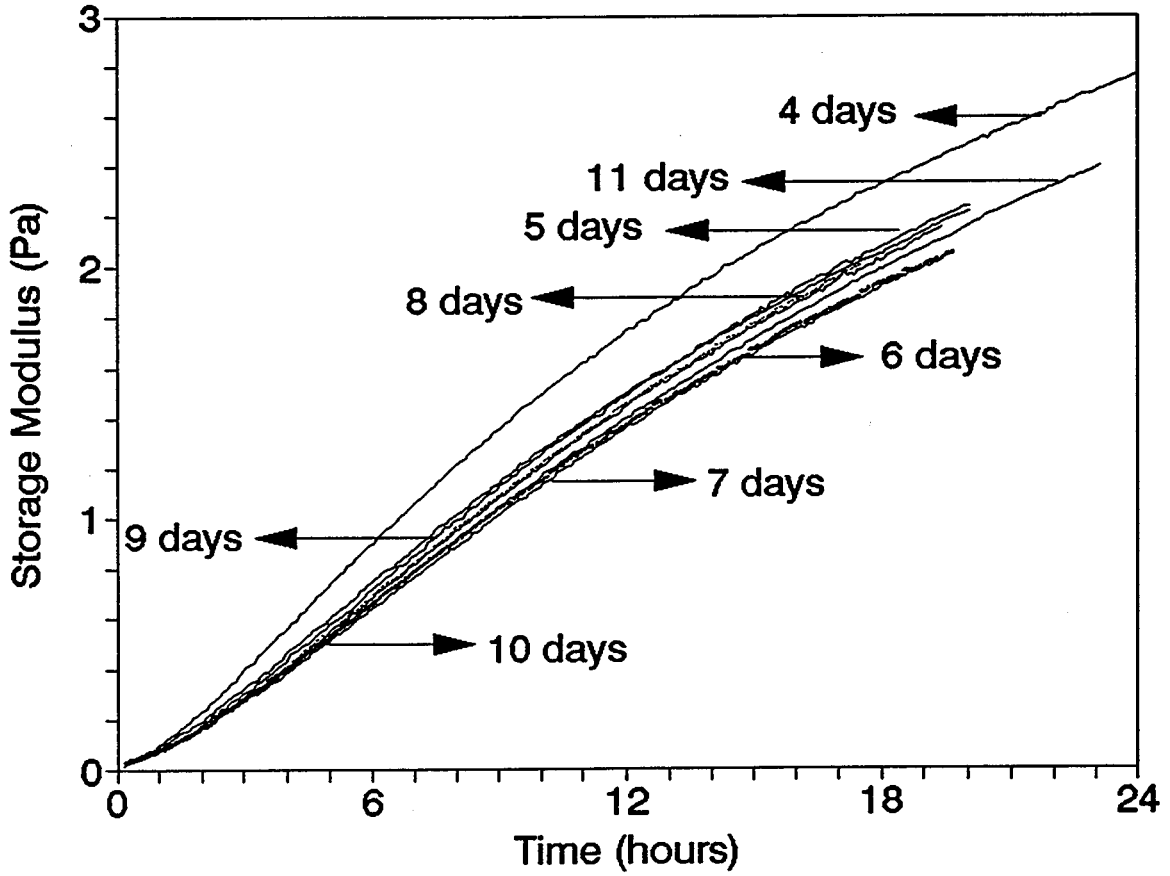

Figure 4.12: Gelation runs for the polyacrylamide/chromium(III) gel system. The days referenced with each run denote the age of the stock solutions.

Chapter 5

Effect of Anions on Gelation of Cr(III)-Polyacrylamide Systems

Principal Investigators: Don W. Green, G. Paul Willhite, Stan McCool, Mike Michnick

Graduate Research Assistant: Mark McGuire

INTRODUCTION AND OBJECTIVES

This work was undertaken to determine the effects of various salt types and concentrations on the gelation of Cr(III)-polyacrylamide systems. Gelation rate was determined by dynamic rheological measurements and shear viscosity measurements. Salt types investigated were nitrate, perchlorate, chloride, and acetate, with sodium being the cation in all cases.

BACKGROUND

A previous study of Cr(III)-polyacrylamide gel systems by Dona (1993) indicated that when a gel solution contains salt, both the salt type and concentration affect the rate of gelation. Since the gel systems under investigation in the current research are to be placed in a reservoir environment in which various salts exist, it was decided to investigate the effect of anion type and concentration on the rate of gelation.

EXPERIMENTAL METHODS

Experimental Parameters

A polymer concentration of 9,000 ppm was chosen. Maintaining the anion type as a constant in the final gel preparation required that the stock Cr(III) solution and PAAm solution be prepared with the same salt type. Na+ was selected as the cation. Mixing procedure was determined to be one of the more crucial factors. A series of procedural steps were established for use with all gel preparations. Table 5.1 summarizes these parameters.

Table 5.1
Constant Factors for Gel Solution Preparation

Polyacrylamide	9,000 ppm
Temperature	25°C
Cation	Na+
Mixing Procedure	(See Appendix C)

The two variables selected for investigation were anion type and concentration. Tables 5.2 and 5.3 display these two parameters and their respective values.

Table 5.2
Anion Species

1.)	Nitrate	(NO_3^-)
2.)	Perchlorate	($ClO4^-$)
3.)	Chloride	(Cl^-)
4.)	Sulfate	(SO_4^{2-})
5.)	Acetate	($C_2H_3O_2^-$)

Table 5.3
Salt Concentration

1.)	1.0 m (molal => moles/Kg Solvent)
2.)	0.1 m
3.)	0.01 m
4.)	0.001 m*
5.)	0.000 m

*Note: This concentration is only included for nitrate system under slow gelation conditions

Five salts were selected to study the effects of anion type. The selection of these salts was based upon use reported in literature and field studies. The five salts chosen were nitrate, perchlorate, chloride, sulfate, and acetate. Four salt concentrations were chosen for analysis. The effects of salt type were evaluated over four-orders of concentration magnitude. The values in Table 5.3 represent the final salt concentration value in the gel solution. This does not take into account the additional amount of anion which would be found in the gel solution as a result of dissociation of the negatively charged molecules on the Cr(III) species.

After a series of preliminary experiments, two additional constraints became apparent. These were the Cr(III) concentration and the final gel pH. For the purposes of simplification, these conditions were grouped together into slow and fast gelation conditions. Table 5.4 illustrates the parameter values for each condition.

Table 5.4
Fast and Slow Factors for Gel Solution Preparation

	Slow	Fast
Cr(III) Concentration	25 ppm	100 ppm
pH	4.5	5.0

Experimental Materials

The polyacrylamide used throughout this work was Aldrich Chemical Company, Inc. poly(acrylamide) Lot #9. Solutions of this polymer were prepared for 12,000 ppm PAAm and a set salt concentration. The solutions were prepared by adding the salt to a known quantity of water which was rapidly stirred with a magnetic stir bar. After the salt had been added and allowed to fully dissolve (each of the salts is readily soluble in water so very little time is required for dissolution), the dry polymer was added to the shoulder of the vortex created by the stirring solution.

Chromium stock solutions were prepared at concentrations of 100 ppm and 400 ppm Cr(III). The 100 ppm Cr(III) concentration corresponds to the slow gelation method and the 400 ppm Cr(III) concentration coincides with the fast gelation conditions. For the purpose of comparison a series of Cr(III) stock solutions were prepared with the appropriate anion type (NO_3^-, ClO_4^-, Cl^-, SO_4^{2-}, and OAc^-). These solutions were prepared at least a week in advance, to allow for chromium hydration.

The gels were made from the polyacrylamide-salt stock solution mixed with the corresponding Cr(III) stock solution containing the appropriate anion. A 3:1 ratio of PAAm:Cr(III) was used for this process. Each gelling sample was prepared by adding the appropriate amount of chromium stock solution by infusion pump controlled syringe addition into an overhead stirred thermal jacketed beaker of polymer solution. While the chromium stock solution was being added a pH electrode was used to monitor the pH and a Fisher automatic titrator was used to add 0.1 M sodium hydroxide as needed to adjust the pH. This resulted in the final values of concentration and pH as seen in Tables 5.1 and 5.4.

Experimental Procedure

Mixing Procedure. The preliminary experiments involved the analysis of two gel preparation techniques. The first procedure required placing a set concentration of salt in the polyacrylamide solution and a similar concentration in the corresponding chromium stock solution. The second procedure involved placing all of the salt in the polyacrylamide solution. When mixed with the chromium stock solution during gel preparation the salt would be dispersed throughout the entire solution. Figure 5.1 illustrates that no significant differences were found between procedures. The later procedure was adopted for all of the proceeding runs.

Gelation Monitoring. Storage modulus measurements were made using a Bohlin Rheometer equipped with a 2-cm diameter cone and plate geometry with a cone angle of 4/40. This machine was operated in constant stress mode for measurement of storage and loss moduli.

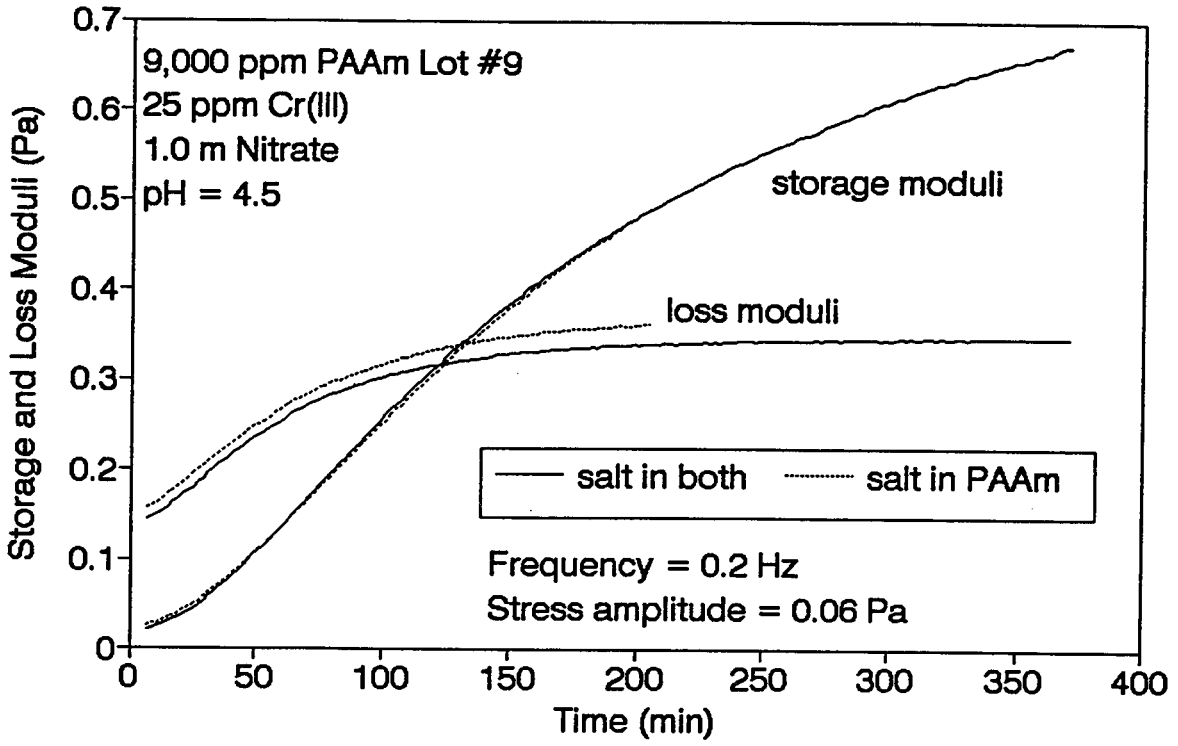

Figure 5.1 Effect of Nitrate Salt Location on Gelation of a Cr(III)-Polyacrylamide System using Slow Method.

Gelling solutions were prepared just prior to loading onto the cone and plate assembly. A calibrated syringe was used to withdraw 1.25 ml of sample from the newly prepared gel solution. This sample was then placed in the center of the stationary lower platen and the upper platen lowered into position. Once loaded, the air-exposed edges of the sample on the Bohlin rheometer were coated with a thin layer of light mineral oil to prevent evaporation. The experiments reported for the Bohlin rheometer were taken at a frequency of 0.2 Hz, and an oscillatory shear stress of 0.06 Pa. The sample was maintained at 25°C throughout the gelation process.

Viscosity measurements were also made using a Brookfield microviscometer model LVT and model LVTDCP. Each machine was maintained at a constant temperature of 25°C by connection to a controlled temperature water bath. Samples were taken from the originally prepared gel solution at periodic time intervals with a 3-ml syringe. These samples were then placed on a Brookfield microviscometer. A 0.5 ml portion was loaded onto the lower removable platen and the apparatus reassembled for measurements. Data were taken over a series of motor settings. These motor settings change the rate at which the upper platen is rotated. This change in rotation speed causes an increase in the shear rate. Thus each motor setting corresponds to a particular steady shear rate. Values for each shear rate were recorded and the sample removed. This data was then plotted on a time vs. shear viscosity curve.

Gel Point Determination

Use of G'=G" Cross-Over Point. It was important to establish a consistent method of determining gelation time. The method chosen for working with the Bohlin rheometer data was the G'=G" cross-over. This is the time at which the storage modulus (G') becomes greater than the loss modulus (G"). In this analysis technique the storage modulus (G') represents the elastic behavior of the solution and the loss modulus (G") represents the viscous behavior. This method was indicated in the literature (Winter, 1987) as an effective method of monitoring gelation.

Use of Viscosity Increase. The method of measuring gelation time chosen for use with the Brookfield microviscometer was the time when viscosity increases to a value above 1,028 cP. This was selected as the time which most nearly represented the point where "viscosity tends to infinity." This method was indicated in the literature (Marrs, 1976) as an effective method of monitoring gelation. Use of this method involved taking periodic viscosity data and plotting this data against the corresponding times at which the data was taken. The resultant graph clearly indicated when the onset of gelation had occurred by this method as seen in Figure 5.2.

Reproducibility of Data

All of the data points shown in each of the gelation time vs. salt concentration graphs represents two reproducible runs at the same set of conditions. Figure 5.3 is an example of two sets of data that were obtained for the Perchlorate system using the fast gelation method as monitored on the Bohlin rheometer. This figure is representative of all of the data presented in this report.

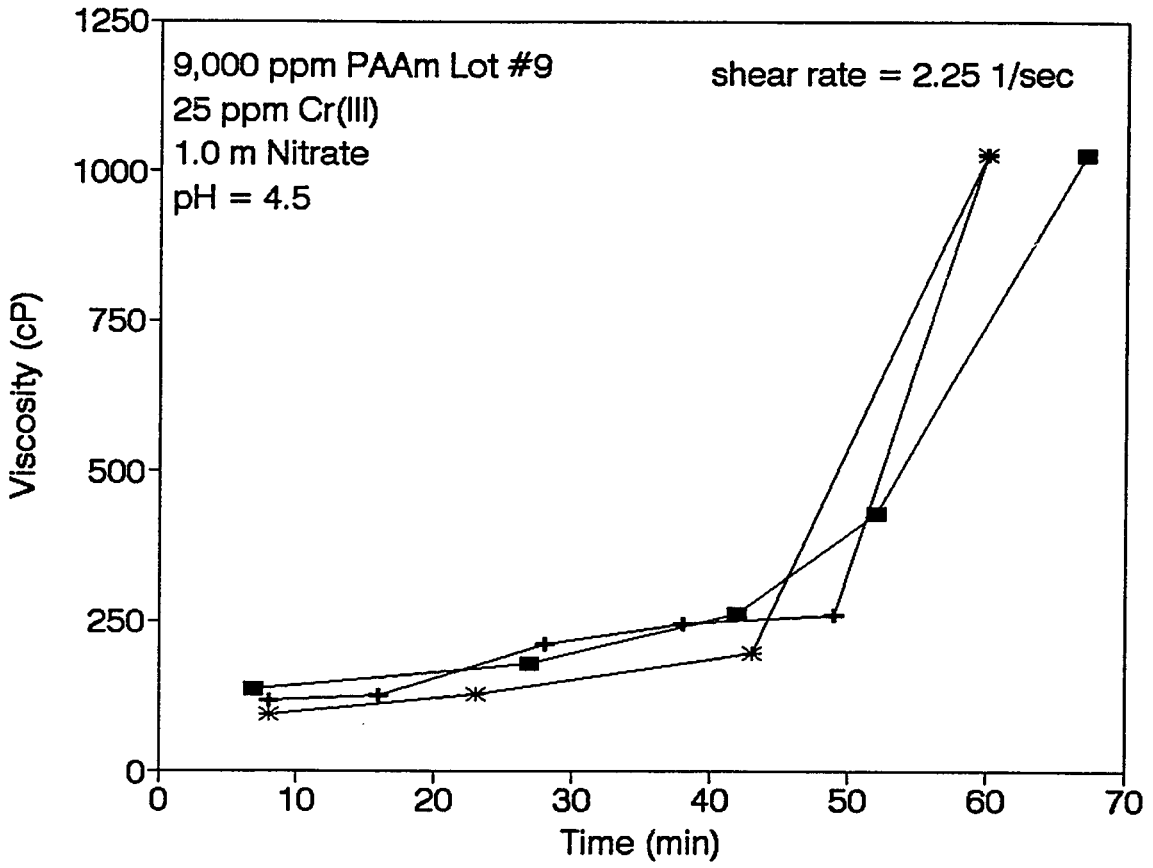

Figure 5.2 Microviscometer Analysis of the Effect of Nitrate Salt on Gelation of Cr(III)-Polyacrylamide Systems using Slow Method.

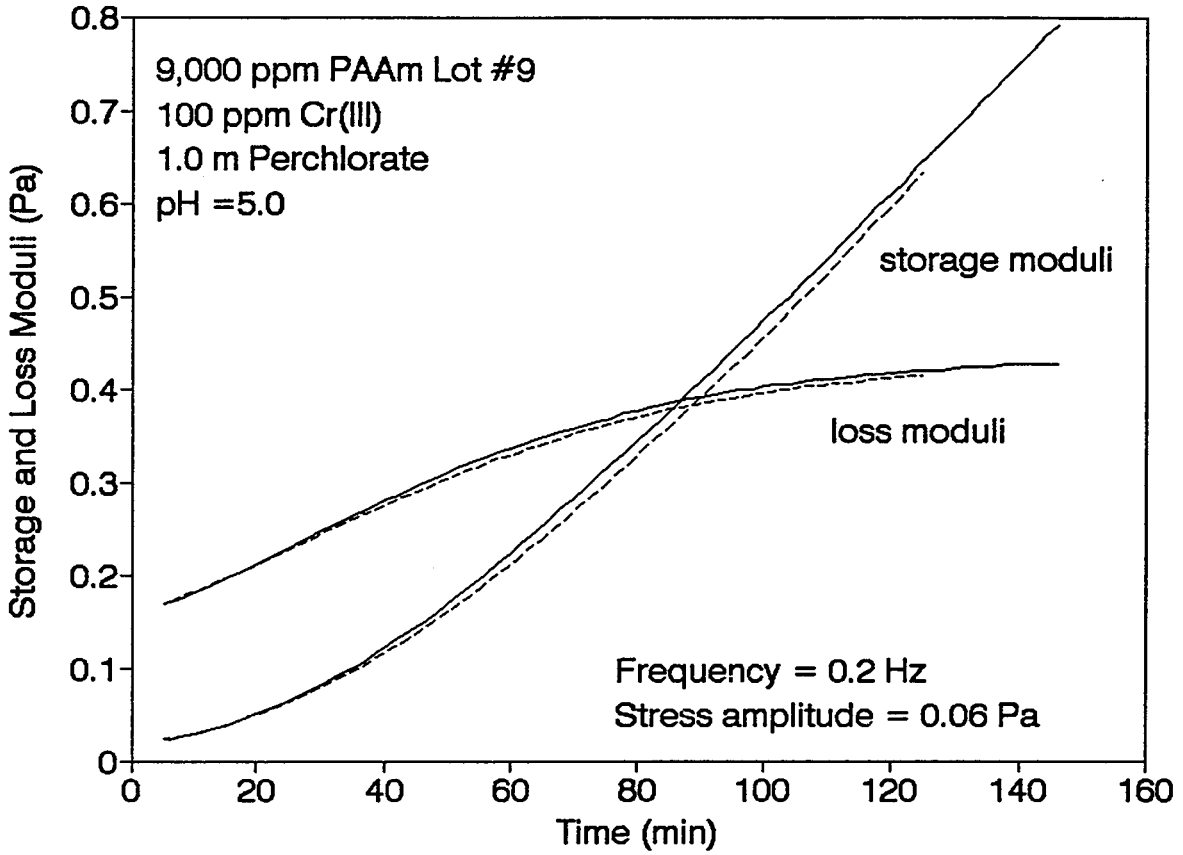

Figure 5.3 Effect of Perchlorate Salt on Gelation of a Cr(III)-Polyacrylamide System using Fast Conditions.

RESULTS AND DISCUSSION

Effect of Salt Type

When comparing each of the systems under the same operating conditions, the nitrate system is by far the fastest gelling system studied. The perchlorate system gels faster than the chloride systems but slower than the nitrate system. The sulfate system is much slower than the chloride system but faster than the Acetate system. The time of gelation for the five systems studied can be characterized as follows: $NO_3^- < ClO_4^- < Cl^- < SO_4^{2-} < OAc^-$.

Nitrate System

The slow method established for the Cr(III)-polyacrylamide system was selected for use with the nitrate system due to the fast rate of gelation. Five salt concentrations (1.0 m, 0.1 m, 0.01 m, 0.001 m, and 0.000 m) were chosen for analysis. The results shown in Figure 5.4 illustrate the lengthening of gelation time caused by the lowering of the nitrate anion concentration. This plot also reveals the nearly linear relationship of gelation time with respect to salt concentration (molal) on a log-log plot for both methods of data analysis.

Perchlorate System

The perchlorate system under the fast gelation conditions yielded gelation within one to two hours. The four salt concentrations chosen for analysis. The results shown in Figure 5.5 suggest that gel time goes through a maximum value somewhere between 1.0 m and 0.1 m salt. This maximum gel time is then followed by a drop off in the gel time with decreasing salt concentration. This is the opposite effect to that seen for the nitrate system.

Chloride System

The data for the chloride system shown in Figure 5.6, were taken for the four salt concentrations chosen for analysis. The results illustrate a similar behavior to that seen in the perchlorate system, with the omission of the maximum value. This trend of decreasing gel times with decreasing salt concentration is an inverse effect to that seen in the nitrate system result.

Sulfate System

Gels have been prepared using the fast method for the sulfate system. Gel formation has taken place with 1.0 m sodium sulfate salt between 12-14 hours by analysis on the Brookfield microviscometer and 17-19 hours on Bohlin Rheometer.

Acetate System

Gels prepared using the slow method have been observed for several months with no sign of gelation taking place using 1.0 m sodium acetate salt. Gels have been prepared for the fast conditions using 1.0 m sodium acetate salt at pH's ranging from 5.0 to 9.5, with no sign of gelation over several weeks. Gels prepared using the fast parameters but with no additional salt added have been observed to gel after 19 hours on the microviscometer. Based upon these results, it appears that the addition of acetate anion inhibits gelation.

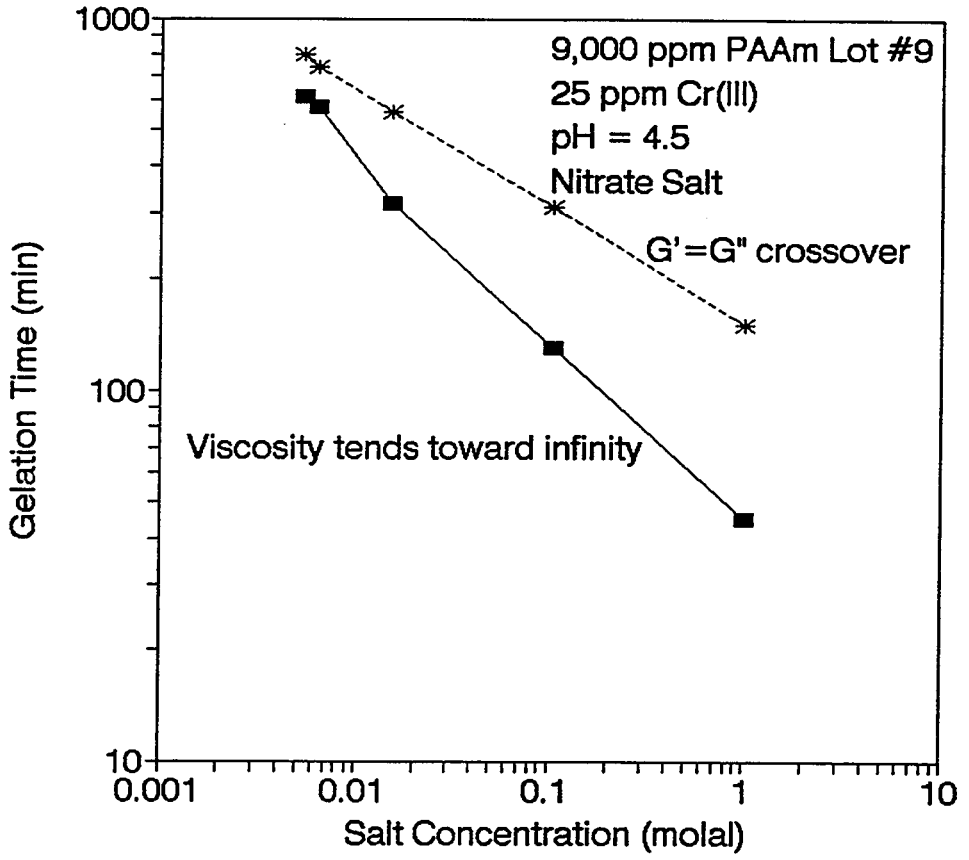

Figure 5.4 Effect of a Nitrate Salt Concentration on the Gelation of a Cr(III)-Polyacrylamide System using Slow Conditions.

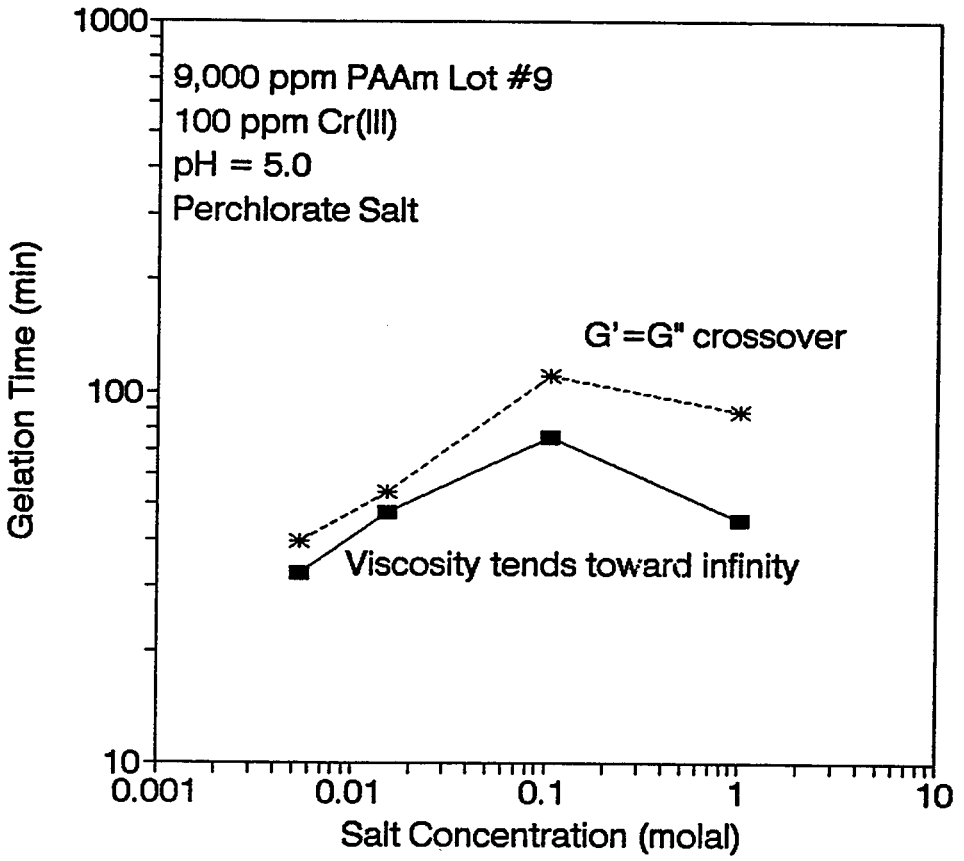

Figure 5.5 Effect of Perchlorate Salt Concentration on the Gelation of a Cr(III)-Polyacrylamide System under Slow Conditions.

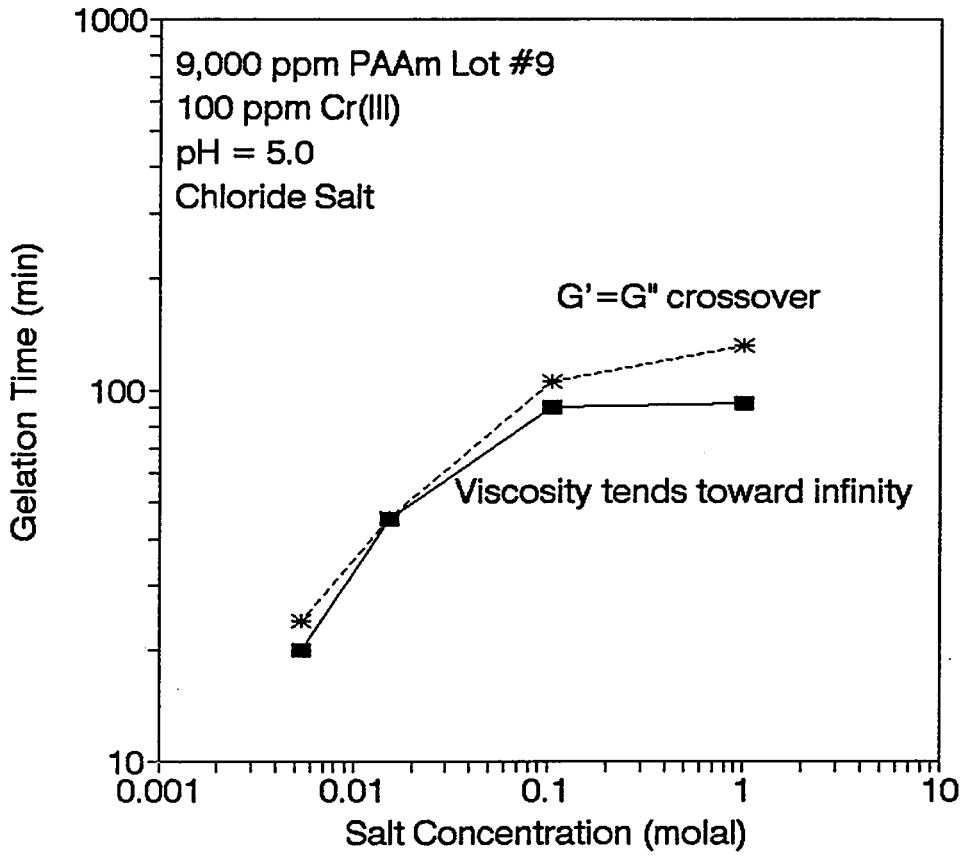

Figure 5.6 Effect of Chloride Salt Concentration on the Gelation of a Cr(III)-Polyacrylamide System under Slow Conditions.

CONCLUSIONS

Both the Brookfield microviscometry data and the Bohlin rheometer data revealed similar trends in gel time as a function of concentration. The oscillatory shear data taken on the Bohlin rheometer indicated slightly longer gelation times than the corresponding steady shear data taken on the microviscometer.

The time of gelation for the five systems studied can be characterized as follows: NO_3^- < ClO_4^- < Cl^- < SO_4^{2-} < OAc^-. The nitrate system is clearly the fastest gelling of the five systems and the acetate system is the slowest.

The nitrate system shows a decrease in gelation time with an increase in salt concentration. The perchlorate system results display a maximum gelation time between 0.1 m and 1.0 m salt concentration followed by a decrease in gelation time with a corresponding decrease in salt concentration. The chloride system results indicate an increase in gelation time with an increase in salt concentration. Addition of the acetate anion appears to inhibit gel formation.

REFERENCES

Dona, C.L.G. "An Experimental Study of the Uptake and Gelation Reactions of Cr(III) Oligomers with Polyacrylamide", Ph.D. Dissertation, University of Kansas (1993).

Khanna, P., "A Study of Rheological Methods to Monitor Gelation of Polyacrylamide/Chromium(III) Gels." M.S. Thesis, University of Kansas (1993).

Winter, H.H.,"Can the Gel Point of a Cross-linking Polymer be Detected by the G'-G" Crossover?," *Polymer Engineering and Science*, Vol. 27, No. 22, December, 1987, pp. 1698-1702.

Marrs, W.M. and Wood, P.D.: "The Gelation and Rupture Properties of Gelatin Gels," *Photographic Gelatin*, (1976), pp. 101-119.

Chapter 6

Kinetics of Cr(III) Oligomers and Polyacrylamide

Principal Investigators: Don W. Green, G. Paul Willhite

Graduate Research Assistant: Carol L. Dona

INTRODUCTION

Cr(III) solutions are commonly used with dilute solutions of polymers with carboxyl side chains to form in situ gels in heterogeneous and/or fractured oil reservoirs to divert displacement fluids from high permeability to lower permeability reservoir zones. A typical gelling solution preparation technique is addition of a monomeric Cr(III) salt solution to a polymer solution, followed by upwards adjustment of the gelling solution pH. Until recently, it was generally assumed that the Cr(III)) remained in monomeric form during the gelation (Hunt, 1987; Bhaskar, 1988). The results of recent studies, however, indicate that under typical gelation conditions, Cr(III) also reacts with itself to form higher molecular weight Cr(III) oligomers (Cr(III) oligomerization) (Rotzinger et al., 1986; Shu, 1988; Stunzi et al.,1989).

The different-sized Cr(III) oligomers potentially present in the Cr(III)-polymer gelling solutions have been shown to have different gelation characteristics. The rates of gelation increase with increasing oligomer size, with the gelation times for the higher molecular weight oligomers being particularly rapid (Shu, 1988; Fei and Mertes, 1991). The pH ranges over which gelation occurs also increase as the size of the oligomer increases (Fei and Mertes, 1989). The amounts of total Cr(III) necessary for gelation generally decrease as the oligomer size increases (Fei and Mertes, 1989).

The broader ranges of gelation times and useable gelling solution pH values obtainable from the different-sized Cr(III) oligomers indicate the possibility of using mixtures of Cr(III) oligomers to perform successful permeability modification treatments over wider ranges of field conditions than those currently possible with the commonly used monomeric Cr(III)-polymer systems. The lower Cr(III) concentrations necessary for gelation with the higher molecular oligomers, the Cr(III) dimer and trimer (Fei and Mertes, 1989), indicate that significantly lower levels of total Cr(III) are possible if higher molecular weight oligomer solutions are used instead of Cr(III) monomeric salt solutions. This factor is important because of potential future environmental limits on the total Cr(III) allowed in subsurface oil-field treatments (Kansas Department of Health and Environment, 1992).

In this chapter, the work which was performed on the characterization of the uptake and gelation reactions of the Cr(III) monomer, dimer, and trimer (Figures 6.1—6.3) with partially-hydrolyzed PAAm (Figure 6.4) is described.

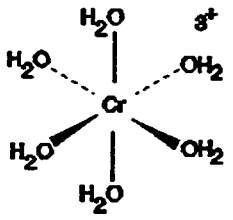

Figure 6.1 Cr(III) monomer.

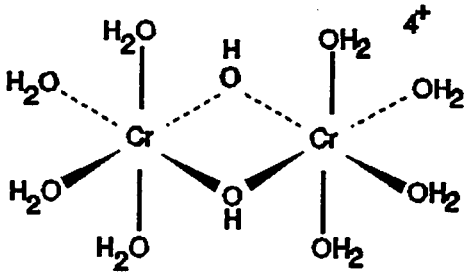

Figure 6.2 Cr(III) dimer.

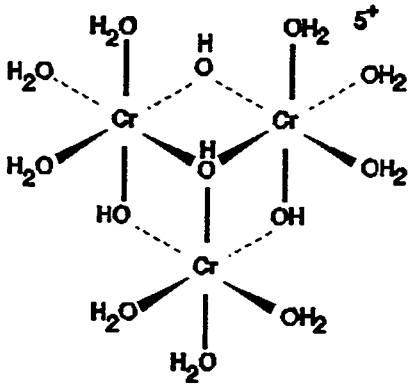

Figure 6.3 Cr(III) trimer.

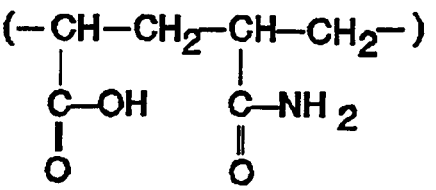

Figure 6.4 Partially hydrolyzed polyacrylamide.

CR(III) OLIGOMER-PAAm GELATION CHEMISTRY

Three chemical reaction processes have been shown to occur in Cr(III)-PAAm gelation systems (Dona, 1993). The first is the reaction of Cr(III) with other Cr(III), termed here Cr(III) oligomerization. For the pH, [Cr(III)], and time ranges commonly used in Cr(III)-PAAm gelation systems, Cr(III) oligomerization has been observed experimentally in the absence of PAAm through the formation of higher molecular weight Cr(III) oligomers (Rotzinger et al., 1986; Besso, 1984; and Stunzi et al. 1989). The second process is the reaction of the free Cr(III) in solution with PAAm, termed here the uptake process. This process has been observed through the disappearance of free Cr(III) from solution by Hunt

(1987) and through measurement of the Cr(III) bound to the PAAm (Montanarri et al. (1992)). The third process, gelation of the PAAm through the reaction of the Cr(III) attached to the PAAm with other PAAm molecules, has been followed visually through changes in gelling solution flow behavior (Fei and Mertes, 1989; Sydansk, 1988; Lockhart, 1991), through changes in gelling solution viscosities (Terry et al., 1981; Billheimer and Parrette, 1956; Jordan et al., 1982; Green et al., 1986; Sydansk, 1988; Githens and Burnham, 1977, Kolnes, 1991), and rheologically through the measurement of storage and loss moduli of the gelling solutions (Prudhomme et al., 1983; Bhaskar, 1988; Montanari et al., 1992; Lockhart, 1991; Dolan, 1989; Winter, 1987).

Assuming that only oligomers of size i exist in solution originally, that no oligomer species of sizes greater than 2i form, and the reactive group on the PAAm molecule is the carboxyl group, Eqns. 6.1—6.7 represent a simplified kinetic description of the processes that are occurring. Two oligomers exist in solution; the original oligomer (Cr_i) and the immediate oligomer product (Cr_{2i}) (Eqn. 6.7). The reactions which result in the uptake of the Cr(III) oligomers by PAAm are expressed in Eqns. 6.1—6.3, where the Cr(III) in solution can either react with an attached Cr(III) molecule (oligomerization) or with a PAAmcarboxyl group. The reactions between Cr(III) molecules attached to the PAAm which result in gelation are also a combination of either oligomerization or Cr(III)-PAAmcarboxyl reactions and are listed in Eqns. 6.4—6.6.

Uptake of the solution Cr(III) oligomers by PAAmcarboxyl or PAAmcarboxylCr_i

$$Cr_i + carboxylPAAm \rightarrow Cr_i carboxylPAAm \quad (6.1$$

$$Cr_{2i} + carboxylPAAm \rightarrow Cr_{2i} carboxylPAAm \quad (6.2$$

$$Cr_i + Cr_i carboxylPAAm \rightarrow Cr_{2i} carboxylPAAm \quad (6.3$$

Gelation by PAAmcarboxyl-attached Cr(III) reacting with PAAmcarboxyl-attached Cr(III) or with PAAmcarboxyl

$$Cr_i carboxyPAAm + Cr_i carboxylPAAm \rightarrow PAAmcarboxylCr_{2i} carboxylPAAm \quad (6.4$$

$$Cr_i carboxylPAAm + PAAmcarboxyl \rightarrow PAAmcarboxylCr_i carboxylPAAm \quad (6.5$$

$$Cr_{2i} carboxylPAAm + PAAmcarboxyl \rightarrow PAAmcarboxylCr_{2i} carboxylPAAm \quad (6.6$$

Oligomerization in solution

$$Cr_i + Cr_i \rightarrow Cr_{2i} \quad (6.7$$

where i=1 (Cr(III) monomer), i=2 (Cr(III) dimer), and i=3 (Cr(III) trimer)

EXPERIMENTAL SYSTEM

Experimental Conditions

Three types of experiments were performed. The first type consisted of experiments which followed the uptake of the free Cr(III) by PAAm in gelling solutions prepared from pure monomer, dimer, or trimer oligomer solutions. The second type was experiments which followed the relative rates of gelation of the same solutions used in the uptake experiments or solutions prepared under similar experimental conditions. The third type was oligomerization experiments which followed the rates of disappearance of the monomer, dimer, and trimer at conditions similar to those used in the uptake and gelation experiments except in the absence of PAAm.

Two sets of experimental conditions were used to characterize the uptake and gelation processes. The first set used 25 ppm Cr(III), PAAm concentrations between 4,400 and 19,800 ppm, 1 M $NaClO_4$, and an initial gelling solution pH value of 4. The second set used 10 ppm Cr(III), 15,000 ppm PAAm, 1 M $NaClO_4$, and a initial solution pH of 5. For both systems, 0.01 M NaOH was used to adjust the pH and a base temperature of 25°C was maintained. These experimental conditions were chosen because they resulted in H^+ and PAAmcarboxyl concentrations which remained approximately constant during the experiments, allowed for adequate mixing of the gelling solutions, produced reasonable gelation times, allowed relatively good accuracy in the Cr(III) concentration measurements, and had relatively low estimated oligomerization rates in the monomer gelling solutions.

The oligomerization experimental conditions were 25-60 ppm Cr(III), 1 M $NaClO_4$, and pH values of 4 and 5. The higher Cr(III) concentrations were used because of the restrictions on the minimum Cr(III) oligomer concentrations which could be measured. As with the uptake and gelation systems, 0.01 N NaOH was used to adjust the pH and a temperature of 25 °C was maintained.

Preparation of the Cr(III) purified oligomer solutions

Stock solutions of chromic perchlorate were prepared by reducing CrO_3 with 30% H_2O_2 in the presence of an excess of perchloric acid, followed by neutralization to pH 3 with $NaHCO_3$. Chromium(II) perchlorate was prepared by passing the chromic perchlorate stock solution through zinc amalgam in a Jones reductor. The Cr(II) solution was oxidized to a mixture of monomer, dimer, trimer, and higher Cr(III) oligomers by bubbling vigorously with O_2 gas for 30 minutes.

The multi-oligomer solution was absorbed onto a Sephadex C-25 ion exchange column. The Cr(III) monomer, dimer, and trimer were successively eluted by solutions of sodium perchlorate of increasing salt concentration and decreasing pH with the purple monomer being eluted first, the blue-green dimer second, and the green trimer third.

Identification and Characterization of the Purified Oligomer Solutions

The monomer, dimer, and trimer were identified from their UV absorption spectra (Stunzi, Thompson). The Cr(III) concentrations of the oligomer solutions were determined by oxidation of the Cr(III) to Cr(VI) with excess 30% H_2O_2 under alkaline (pH 11-12) conditions and measurement of the UV absorbance at 374 nm (Dona, 1993). $NaClO_4$ concentrations were determined from the oligomer solution densities and a standard curves of density versus $NaClO_4$ concentration.

The oligomer solution purities were established by oligomer separation on an analytical liquid chromatography column, followed by conversion of the HPLC oligomer peak heights to oligomer concentrations. A Wescan cation-exchange column (Cat. No. 269-004) and a Wescan Cation guard column (Cat. No. 269081) in series with a Waters Chromatograph pump (Model 6000A), an in-line Waters 490 Programmable Multiwavelength UV detector (3 mm path length and a 2.7 μl volume), and a Cole-Parmer chart recorder (Model No. 8373-20) were used with a Rheodyne 100 μl injection loop (Model 7125) (Figure 6.5).

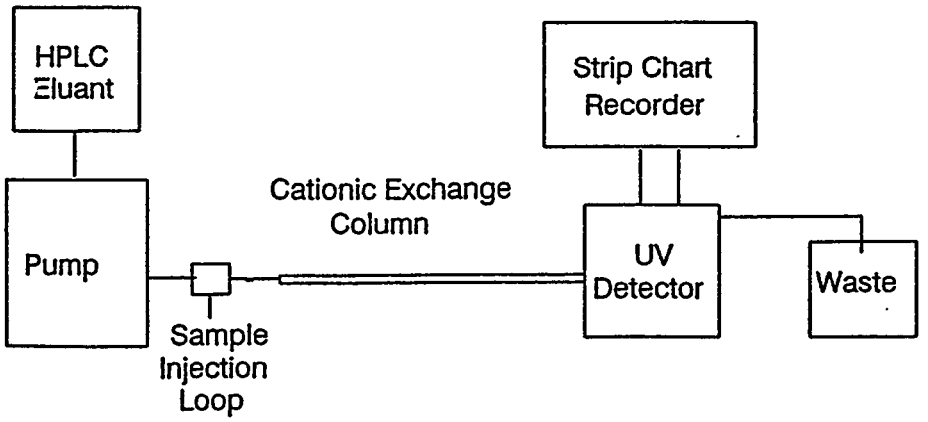

Figure 6.5 Schematic of the oligomer separation and measurement apparatus.

Eluant solutions of 0.4 M $Mg(NO_3)_2$ or 1 M $Mg(NO_3)_2$ were used with 8 ppm methanol added for pump maintenance and 2 ppm Na_3N added for column bacterial protection. The pH values of the eluant solutions were adjusted to pH 2.5 with 6 N HNO_3. The monomer and dimer solutions were separated with 0.4 M $Mg(NO_3)_2$ eluant solutions at an eluant flow rate of 1 ml/min and elution times of 0.45 minutes for the solvent, 0.63 minutes for the monomer, and 0.89 minutes for the dimer. Using 0.4 M $Mg(NO_3)_2$, the trimer solutions were separated from the monomer and dimer at a flow rate of 2 ml/min and elution times of 0.27 minutes for the solvent, 0.3 minutes for the monomer, 0.54 minutes for the dimer, and 2.4 minutes for the trimer. Because of the broad trimer peaks with the 0.4 M $Mg(NO_3)_2$, the eluant concentration was increased to 1 M $Mg(NO_3)_2$ for more accurate measurement of the trimer peak heights. At 1 M $Mg(NO_3)_2$, the trimer was separated from the monomer and dimer at a flow rate of 2 ml/min with elution times of 0.25 min for the solvent, 0.26 min for the monomer, 0.36 min for the dimer, and 0.43 min for the trimer.

For determination of the relative amounts of oligomers in the oligomer solutions obtained from the Sephadex ion-exchange column, the oligomer HPLC peak heights at the wavelengths characteristic of each species (monomer; 408, 576 nm; dimer; 418, 582 nm, trimer: 426,584 nm) were measured at their characteristic HPLC elution times. The peak heights were converted to oligomer concentrations through standard curves based on HPLC peak height. The standard curves were established by taking essentially pure stock solutions of monomer, dimer, and trimer at approximately pH 2, adjusting the brine concentration to 1 M $NaClO_4$, and diluting with 1 M $NaClO_4$ to several different concentrations. Stock oligomer solution concentrations were determined by conversion of the Cr(III) to Cr(VI) with H_2O_2 and base, followed by measurement of the UV absorbances at 374 nm.

The purities of the monomer, dimer, and trimer solutions were then determined by taking the ratios of the primary oligomer concentrations over the total oligomer concentrations. The dimer and trimer solutions used in the gelation experiments contained less than 10% of the next smaller oligomers (monomer and dimer, respectively) whereas the monomer solutions contained less than 1% dimer and no detectable trimer.

Preparation and characterization of the PAAm solutions

Stock PAAm solutions with nominal concentrations of 20,000-30,000 ppm were prepared from Aldrich PAAm (Cat. 18,127-7. Lot 9; nominal MW 5-6,000,000). The PAAm was added to 1 M $NaClO_4$ brine solutions, stirred for three days, and allowed to set for at least five days before use in preparation of the gelling solutions. The solutions were stored at 4°C between runs, with the PAAm solutions for each experiment being placed in a 25°C water bath twelve hours before runs.

The PAAm amide UV absorbances were measured at 236 nm and converted to PAAm concentrations through standard curves of UV absorbance versus PAAm concentration, constructed using purified PAAm solutions (Dona, 1993). PAAmcarboxyl concentrations were obtained by multiplying the PAAm concentrations by 0.023, the fraction of the PAAm side groups that were carboxyl groups (Tackett, 1990).

Preparation of the Cr(III) Oligomer-PAAm Gelling Solutions

Gelling solutions were prepared by adding the purified Cr(III) monomer, dimer, or trimer solutions to PAAm solutions while keeping the pH of the gelling solutions constant through the addition of 0.01 M NaOH using an automatic titrater (Figure 6.6). The pH values of the gelling solutions were measured by a Fisher pH and reference electrode pair connected to either a titrator electrometer (Fisher Model 380) or a Fisher Accumet pH meter (Model 910). An outer reference electrode fill solution of 1 M Na_2SO_4 was used instead of the saturated KCl solution supplied with the electrode to avoid the formation and precipitation of $KClO_4$ on the reference electrode junction. The gelling solution temperature was kept constant at 25°C with a circulating, constant temperature water bath.

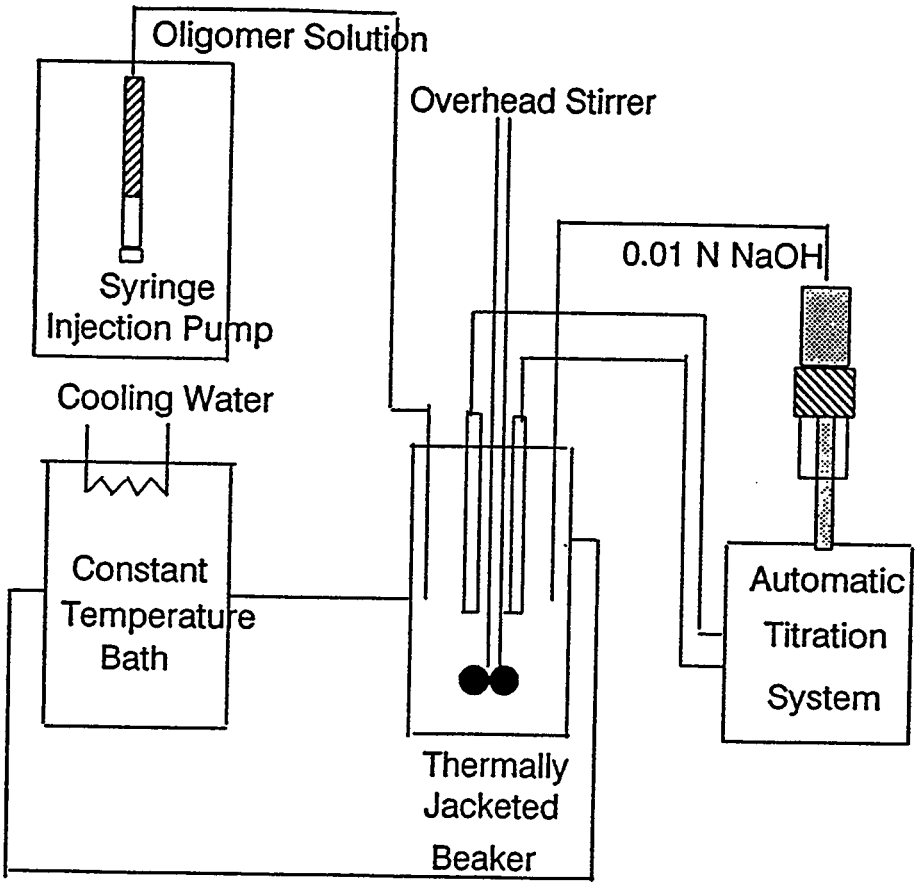

Figure 6.6 Schematic of the gelling and oligomerization solution preparation apparatus.

Measurement of the Oligomer-PAAm Rheological Data

Immediately after preparation, gelling solution volumes of 29 ml were placed in a Bohlin Rheologi controlled stress rheometer using a double gap geometry. The temperature was maintained at 25°C through a Neslab Instruments Inc. temperature control unit designed specifically for use with the Bohlin Rheoligi rheometer and controlled through a Bohlin CS rheometer interface. A 29 cp standard oil was applied to the exposed outer and inner fill surfaces of the gelling solutions to prevent evaporation. The gelling solutions were subjected to intermittent oscillation (5 sec duration every 180 sec) at a frequency of 1 Hz, with rheological measurements being taken every three minutes. The oscillatory stress was held constant, with the oscillatory strain (initially 0.28) decreasing as the gelations proceeded. The gelling solution rheological data were collected and converted to storage moduli (G') and loss moduli (G") values using software provided by Bohlin with a Compaq DESKPRO 386/20e personal computer connected to the Bohlin CS rheometer interface.

Equilibrium Dialysis of the Cr(III) Free in Solution and Attached to the PAAm

After removal of the portions of gelling solutions for rheological data collection, the remaining portions of the gelling solutions were held at 25° C in jacketed beakers. Gel samples were removed periodically and diluted in 1:10 or 1:20 gel/brine ratios with 1 M $NaClO_4$ brine. From each diluted gel sample, triplicate dialysis samples were prepared. For each sample, five ml of the diluted gel sample were placed on the retentate side of a dialysis cell with five ml of 1 M $NaClO_4$ brine of the initial gelling solution pH placed on the diffusate side of the dialysis cell (Figure 6.7). A 0.05 micron Micropore polycarbonate filter separated the retentate and diffusate chambers and allowed free movement of the unreacted oligomers and solvent while preventing the movement of the the PAAm and the Cr(III) attached to the PAAm. The dialysis cells consisted of circular, Teflon discs with a inner dialysis volume of approximately 7 cm^3 (Hunt, 1987). The filled dialysis cells were continuously rotated in a 25°C water bath for three hours (Hunt, 1987). In addition to the dialysis samples, triplicate samples of the same diluted gel sample (termed undialyzed samples) were set aside for separate Cr(III) concentration determination.

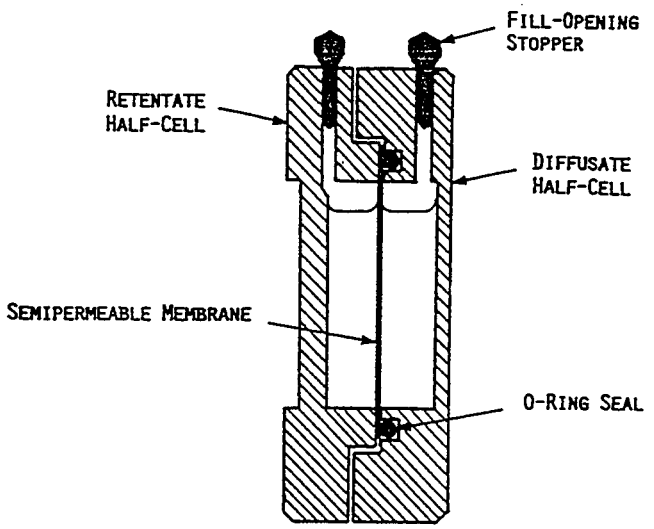

Figure 6.7 Schematic of the dialysis cell used for the equilibrium dialysis of the gelling solutions (from Hunt, 1987).

Determination of the Cr(III) Free in Solution and Attached to the PAAm

After equilibrium of the free-solution oligomers was obtained, a process which required three hours, the retentate and diffusate solutions were removed to polyethylene bottles containing 0.04 ml of 20 wt% NaOH. Immediately after retentate and/or diffusate solution removal to the bottles, 0.16 ml of 30% H_2O_2 were added. The undialyzed samples were treated with NaOH and H_2O_2 in a similar manner immediately after placement of the diluted gel samples in the polyethylene bottles. The H_2O_2 under basic conditions oxidized the Cr(III) to Cr(VI) and converted the PAAm to gasous by-products (Dona, 1993).

After four to eight days, the Cr(VI) concentrations of the retentate, diffusate, and undialyzed solutions were measured at 374 nm after degassing of the solutions in a sonic mixer for approximately five minutes. The UV measurements were taken in 1 cm quartz cells on a Perkins and Elmer Lambda 3

UV spectrophotometer against 1 M $NaClO_4$. Cr(VI) concentrations were determined from the UV absorbances and a standard Cr(VI) vs UV absorbance curve. The standard curves were constructed from a series of dilutions of a 1 mg/ml Cr(VI) standard solution obtained from EM Science. Final retentate, diffusate, and undialyzed Cr(VI) concentrations were corrected by subtracting the apparent Cr(VI) concentrations due to dialysis and gel impurities from the experimentally measured Cr(VI) concentrations (Dona, 1993). The concentrations of the undialyzed samples were used for material balance comparisons between the total Cr(III) concentrations in and outside of the dialysis cells. The fractional free Cr(III) concentrations were determined for each individual dialysis cell by dividing the sum of the retentate and diffusate free Cr(III) concentrations by the sum of the total diffusate and retentate Cr(III) concentrations.

Preparation of the pH-adjusted Oligomer Solutions

The pH-adjusted oligomer solutions were prepared with the same basic method as the oligomer-PAAm gelling solutions. Before use in the oligomerization experiments, the purified oligomer solutions were adjusted to brine concentrations of 1 M $NaClO_4$. In a selected number of oligomerization runs, proprionamide was added to the $NaClO_4$ solutions in a concentration equivalent to 15,000 ppm PAAm to test the effect of the amide groups on the oligomerization rates.

The pH adjustments of the oligomer solutions were performed in a procedure similar to the Cr(III)-PAAm gel solution preparation except that the Cr(III) solutions were added to 1 M $NaClO_4$ solutions instead of PAAm solutions. The $NaClO_4$ solutions were adjusted to the desired experimental pH before addition of the oligomer solutions. The purified monomer, dimer, or trimer solutions were added to the $NaClO_4$ solutions in ratios of 1:1 to 1:4 depending on the concentrations of the stock oligomer solutions and the desired concentrations of the final oligomer solutions. During addition of the oligomer solutions to the $NaClO_4$ solutions, the pH of the solution was kept constant at the designated experimental pH by the simultaneous addition of 0.01 N NaOH. The same equipment and experimental conditions used in the preparation of the oligomer-PAAm gels were used in the pH adjustment of the oligomer solutions except that stirring rates of 100-150 rpm were used. For selected runs, where the pH of the oligomer solutions naturally decreased with time, constant pH was maintained by the addition of 0.01 N NaOH after solution preparation. In another run, where the pH of the oligomer solution naturally increased with time, constant pH was maintained by the addition of 0.01 $HClO_4$ after solution preparation. In both cases, the pH was kept constant through the automatic titration system described in "Preparation of the Oligomer-PAAm Gelling Solutions".

Determination of the Oligomer Concentrations in the pH-adjusted Oligomer Solutions

After pH adjustment, the solutions were maintained at 25°C. The primary oligomer (monomer, dimer, or trimer) was separated from the oligomerization products using the same equipment and experimental conditions used in the analysis of the purities of the oligomer stock solutions ("Identification and Characterization of the Purified Oligomers"). The UV absorbances of the primary oligomers were measured with the in-line UV spectrophotometer and recorded as peak heights on the chart recorder. The HPLC peak heights were adjusted for the sample injection pH (Dona, 1993) and then converted to oligomer concentrations through the use of HPLC peak height vs oligomer concentration standard curves.

EXPERIMENTAL RESULTS AND DISCUSSION

Oligomer-PAAm Uptake Results

The effects of oligomer type, PAAm concentration, and gelling solution pH on the rates of monomer, dimer, and trimer uptake by PAAm were explored. The conditions for each run are summarized in Table 6.1. For each run, the zero-time was defined as the time of the first sample, which was taken immediately after the completion of gelling solution preparation. This gelling solution preparation process took approximately five minutes.

Table 6.1 Summary of the experimental conditions for the uptake runs

Run No.[1]	[Cr(III)] (ppm)	[Cr(III)] (mM)	[PAAm] (ppm)	Average pH
monupt1	27.3	0.558	8,782	3.97
monupt2	25.4	0.519	13,441	4.06
monupt3	30.6	0.625	14,857	3.98
monupt4	27.3	0.558	19,908	4.02
monupt5	10.9	0.225	15,000	4.99
dimupt1	25.3	0.258	8,427	3.95
dimupt2	24.3	0.248	14,415	3.96
dimupt3	17.3	0.177	19,274	3.97
dimupt4	8.3	0.085	15,050	5.05
triupt1	24.7	0.168	4,433	3.90
triupt2	24.1	0.164	8,633	3.92
triupt3	22.8	0.155	13,153	3.93
triupt4	19	0.130	14,667	3.94
triupt5	7.4	0.050	14,657	3.95
triupt6	7.6	0.051	14,923	3.94
triupt7	10.8	0.074	14,045	4.98

[1] Monomer, dimer, and trimer runs are designated by mon, dim, and tri, respectively.
[2] Concentrations are in mM oligomer

Effect of Oligomer Type on the Oligomer-PAAm Uptake Rates. The effect of oligomer type on the rate of reaction of free-solution oligomers with PAAm was examined for three series of [Cr(III)], [PAAm], and pH conditions. The first series was performed at pH 4, Cr(III) concentrations of 22.8-25.4 ppm, and PAAm concentrations of 8,427-8,782 ppm. The fractional free Cr(III) concentrations, which correspond to the uptake by the PAAmcarboxyl groups, are shown in Figure 6.8. The results of the second series of runs, performed at essentially the same experimental conditions but for the higher PAAm concentrations of 13,153-14,415 ppm, are shown in Figure 6.9. The results of the third series, performed at pH 5, Cr(III) concentrations of 25.4-27.3 ppm, and PAAm concentrations of 14,045-15,050 ppm are shown in Figure 6.10.

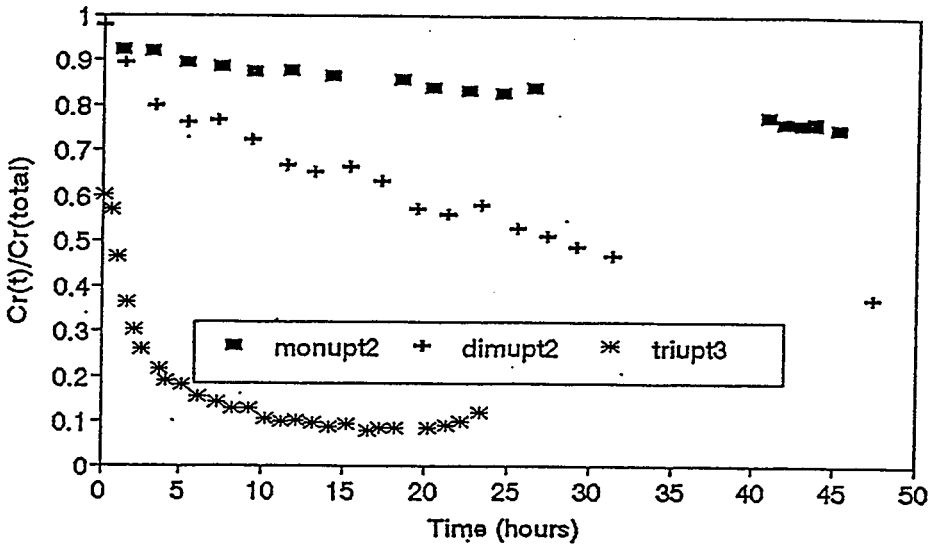

Figure 6.8 The effect of oligomer type on the fractional uptake for the pH 4 runs using 22.8-25.4 ppm Cr(III) and 13,153-14,415 ppm PAAm (monupt2, dimupt2, triupt3, Table 6.1).

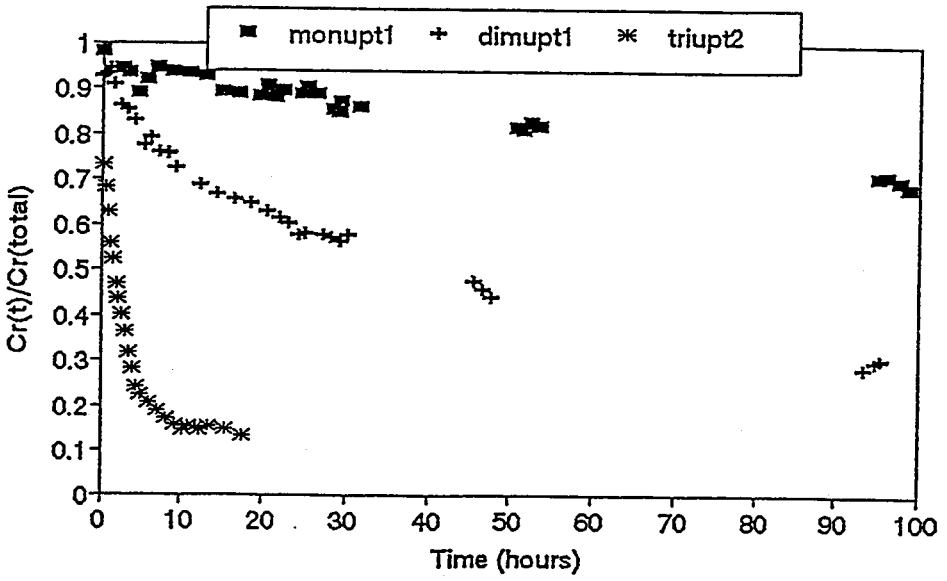

Figure 6.9 The effect of oligomer type on the fractional uptake for the pH 4 runs using 24.1-27.3 ppm Cr(III) and 8,427-8,782 ppm PAAm (monupt1, dimupt1, triupt3, Table 6.1).

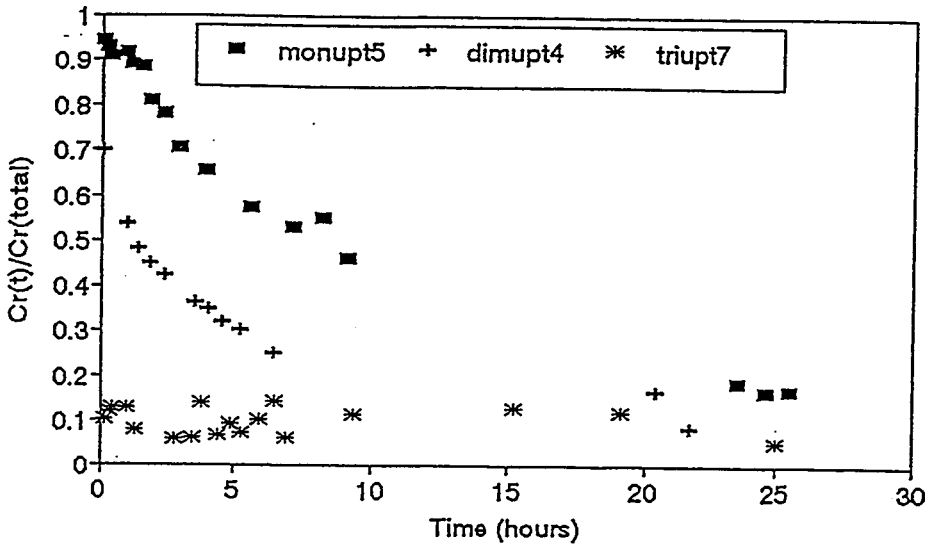

Figure 6.10 The effect of oligomer type on the fractional uptake for the pH 5 runs using 8.3-10.9 ppm Cr(III) and 14,045-15,050 ppm PAAm (monupt5, dimupt4, triupt7, Table 6.1).

The amounts of monomer, dimer, and trimer reacting with the PAAm at three hours (pH 4) and one hour (pH 5), summarized for the three series in Table 6.2, show that the uptake rates are fastest for the trimer and slowest for the monomer. The rates of dimer and trimer reaction are greater than those expected from assuming equal molar rates of reaction, where the amounts of dimer and trimer reacted would be expected to be two and three times more than the monomer because the dimer and trimer contain two and three atoms per oligomer, respectively. This suggested that dimer and trimer are more reactive on a molecular level with the PAAm than the monomer, with the trimer particularly exhibiting high reactivity with the PAAm.

Table 6.2 Comparison of experimental amounts of oligomers reacted with PAAm

[PAAm] (ppm)	pH	[Cr(III)] (ppm)	Uptake reaction time (hr)	% monomer reacted	% dimer reacted	% trimer reacted
4,433	4	24.7	3			57
8,427-8,782	4	24.1-25.3	3	6	15	65
13,153-14,415	4	22.8-25.4	3	7	20	78
19,274-19,908	4	17.3-27.3	3	8	30	
15,000-15,050	5	8.3-10.9	1	10	47	87
14,657-14,923	4	7.4-7.6	1			52

Effect of PAAm Concentration on the Oligomer-PAAm Uptake Rates. The effect of PAAm concentration on the oligomer-PAAm uptake rates was examined by performing a series of runs for each oligomer at pH 4 with three different gelling solution PAAm concentrations. The decreases in fractional free Cr(III) for the monomer, dimer, and trimer runs for the PAAm concentration ranges of 8,782-19,908, 8,427-19,908, and 4,433-13,153 ppm, respectively, are shown in Figures 6.11-6.13. A lower PAAm concentration range was used for the trimer runs because rapid increases in the trimer gelling solution viscosities made uniform mixing difficult at the higher PAAm concentrations.

Figures 6.11-6.13 and Table 6.1 show that the uptake rates for the oligomer increase with PAAm concentration. This is consistent with the trends found by Hunt (1987) and Lockhart (1991) who investigated the behavior of Cr(III) monomeric salt solutions with PAAm.

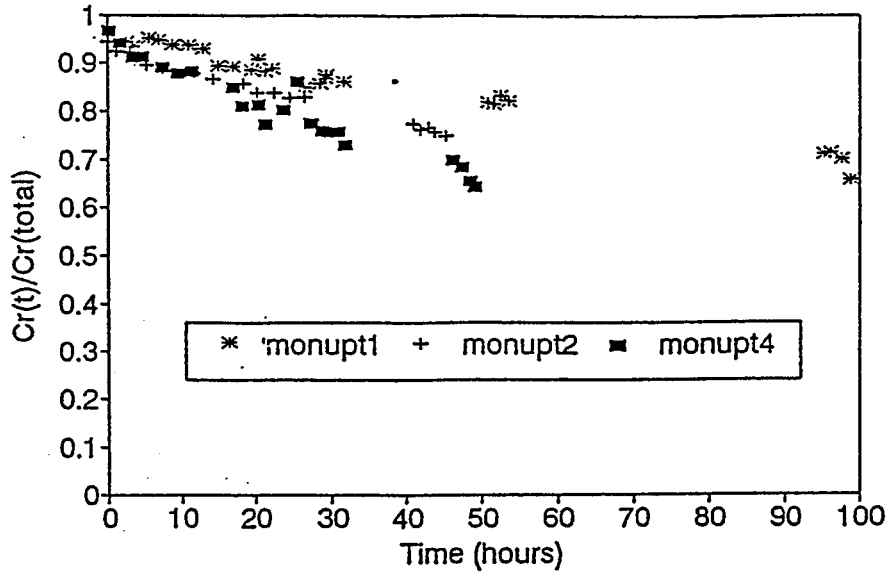

Figure 6.11 The effect of PAAm concentration on the fractional uptake for the pH 4 monomer runs using 25.4-27.3 ppm Cr(III) and 8,782 ppm (monupt1), 13,441 ppm (monupt2) and 19,908 ppm (monupt4) PAAm (Table 6.1).

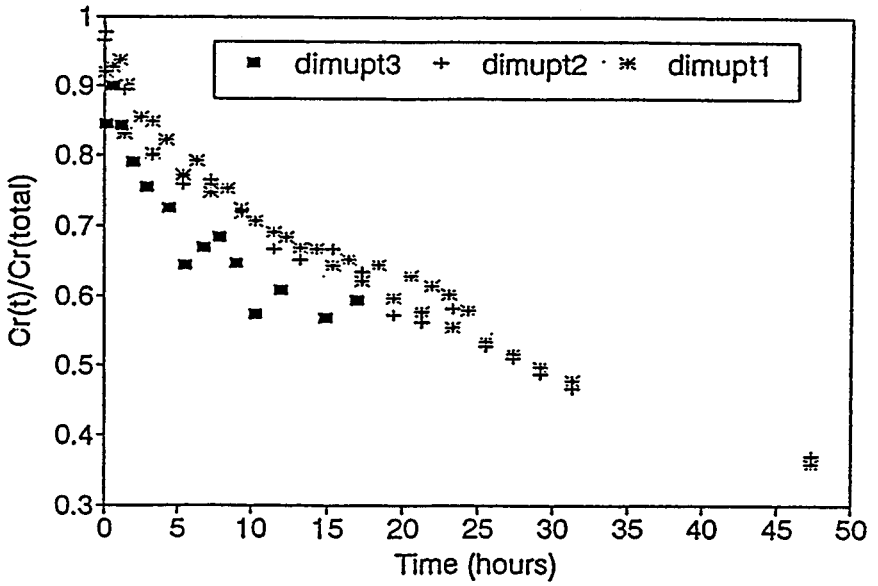

Figure 6.12 The effect of PAAm concentration on the fractional uptake for the pH 4 dimer runs using 17.3-25.3 ppm Cr(III) and 8,427 ppm (dimupt1), 14,415 ppm (dimupt2) and 19,274 ppm (dimupt3) PAAm (Table 6.1).

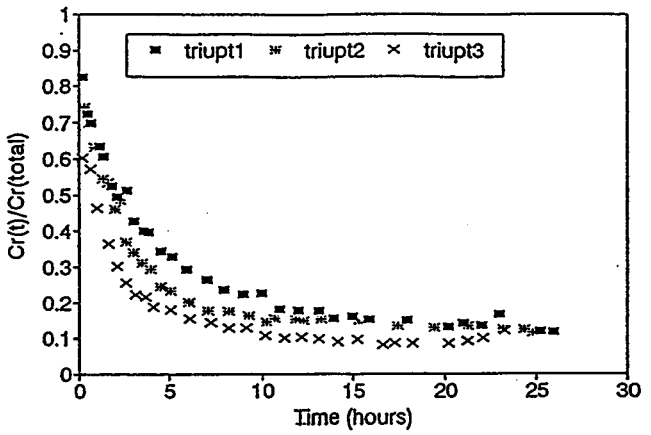

Figure 6.13 The effect of PAAm concentration on the fractional uptake for the pH 4 trimer runs using 22.8-24.7 ppm Cr(III) and 4,433 ppm (triupt1), 8,633 ppm (triupt2), and 13,153 ppm (triupt3) PAAm (Table 6.1).

Effect of Gelling Solution pH on the Oligomer-PAAm Uptake Rates. The effect of gelling solution pH on the trimer uptake rates is shown in Figure 6.10 for the trimer runs with Cr(III) concentrations of 8.3-10.8 ppm, PAAm concentrations of 14,045-14,923 ppm, and initial gelling solution pH values of 4 and 5. The results in Figure 6.14 and Table 6.1 indicate that the trimer uptake rates increase with increasing pH. The trimer-PAAm uptake is particularly rapid at pH 5 where 90% of the trimer has reacted with the PAAm at the time of the first uptake sample, taken approximately five minutes after the start of the addition of the stock trimer solution to the PAAm solution. Similar comparisons for the monomer and dimer were not possible because data was not available at comparable Cr(III) concentrations at different pH values. Data was not collected on the slow-reacting pH 4, 8-11 ppm monomer and dimer gelling solutions because it was not possible to accurately measure the changes in the free-solution Cr(III) concentrations in these gelling solutions with the measurement technique used. Comparison experiments at the higher Cr(III) concentration (25 ppm) were not performed because relatively high oligomerization-to-uptake rate ratios were expected at pH 5 with the higher Cr(III) concentrations. (Dona, 1993).

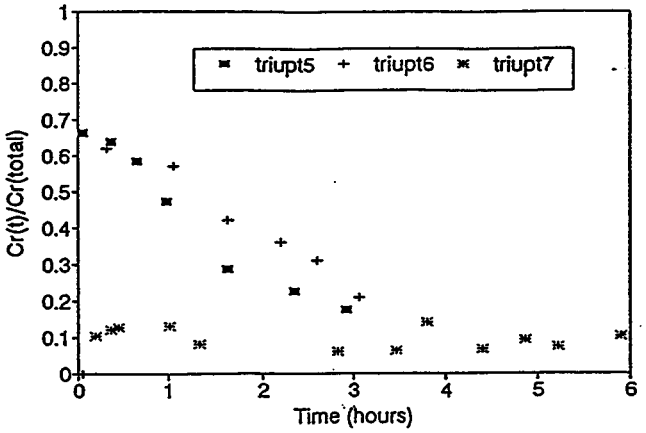

Figure 6.14 The effect of gelling solution pH on the fractional uptake for the trimer runs using 7.1-10.8 ppm Cr(III), 14,045-14,923 ppm PAAm, and pH values of 4 (triupt5 and triupt6) and 5 (triupt7) (Table 6.1).

Gelation Results

Oligomer-PAAm gelation experiments were performed on gelling solutions prepared under similar conditions to those used in the uptake experiments to allow comparison of the relative rates of gelation and oligomer-PAAm uptake. In these experiments, the effects of oligomer type, concentration, and solution pH were examined by following the storage (G') and loss (G") moduli as functions of time. For all the gelation comparisons, the zero time was taken as the time where the first G' measurement on the gelling solution was taken (5-10 minutes after gelling solution preparation).

Two relative measures of the rates of gelation were used. The first was the initial slopes of the storage moduli (G') versus time. This method assumed that the G' values represented the solid or elastic properties of the gelling solutions, with the G' values being measures of the solution gel strengths (Ferry, 1980; Prudhomme, 1984; Bhaskar, 1988). In the second method, gelation time was defined as the time where the G' value had increased to the value of the loss modulus (G") (Winter, 1987; Tung and Dynes, 1982; Lockhart, 1991). At times beyond this point, it was assumed that the gelling solution had more solid or elastic-like properties, as represented by G', than liquid or viscous properties, as represented by G".

All the gelling solutions that were used for gelation comparisons were designed to have PAAm concentrations of approximately 15,000 ppm. Final PAAm concentrations ranging between 13,000 and 16,000 ppm were obtained because the gelling solutions were prepared from PAAm and oligomer stock solutions with different concentrations and varying amounts of base were added during gelling solution preparation. It was found that the G' values were very sensitive to the gelling solution PAAm concentrations with the G' values of the gelling solutions immediately after preparation (G'(int)) decreasing by approximately 20% for a 7% decrease in PAAm concentration (Figure 6.15). In order to account for these initial differences, the increases in G' relative to the initial values (G'(t)-G'(int)) were used for direct graphical comparisons.

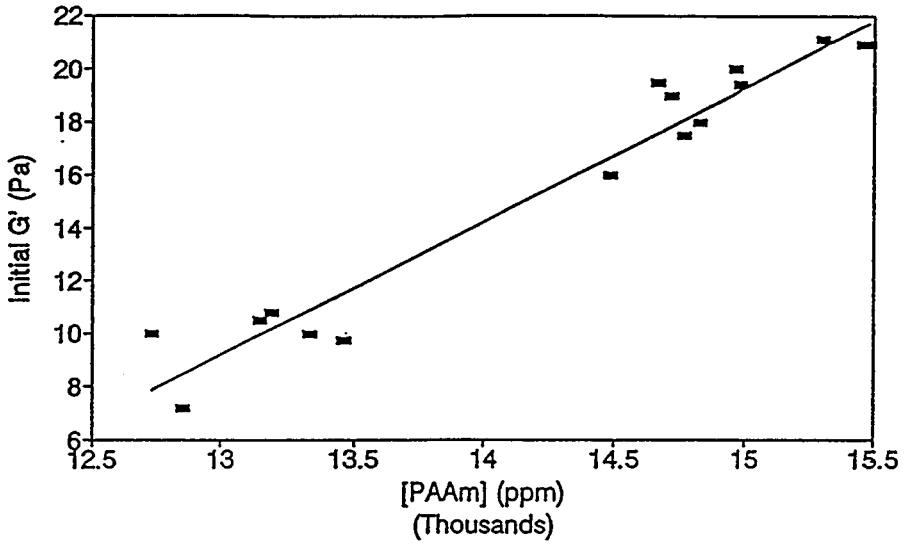

Figure 6.15 The effect of PAAm concentration on the initial storage modulus (G') values.

Effect of Oligomer Type on the Rate of Gelation. The effect of oligomer type on the rate of gelation was examined for three series of [Cr(III)], [PAAm], and pH conditions. The results for the first series, performed at pH 4, Cr(III) concentrations of 7.4-11.7 ppm, and PAAm concentration of 14,657-14,965 ppm are shown in Figure 6.16. The G' results for the second series, performed at essentially the same conditions as the first series but with Cr(III) concentrations of 19-24.6 ppm, are shown in Figure 6.17. The results of the third series, performed at pH 5, 8.3-10.9 ppm Cr(III), and 14,045-15,050 ppm PAAm, are shown in Figure 6.18.

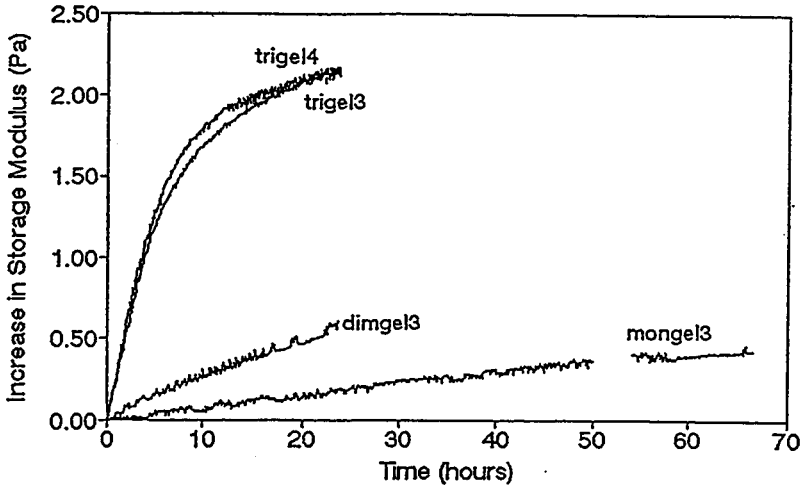

Figure 6.16 The effect of oligomer type on the increases in G' for the pH 4 gelation runs using 7.4-11.7 ppm Cr(III) and 14,657-14,965 ppm PAAm (mongel3, dimgel3, trigel3, trigel4, Table 6.3).

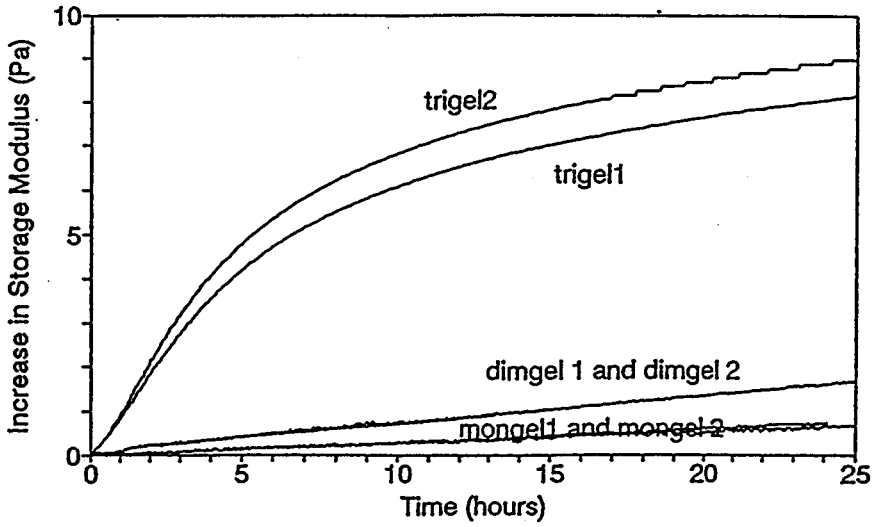

Figure 6.17 The effect of oligomer type on the increases in G' for the pH 4 gelation runs using 19-24.6 ppm Cr(III) and 14,666-15,462 ppm PAAm (mongel1, mongel2, dimgel1, dimgel2, trigel1, trigel2, Table 6.3).

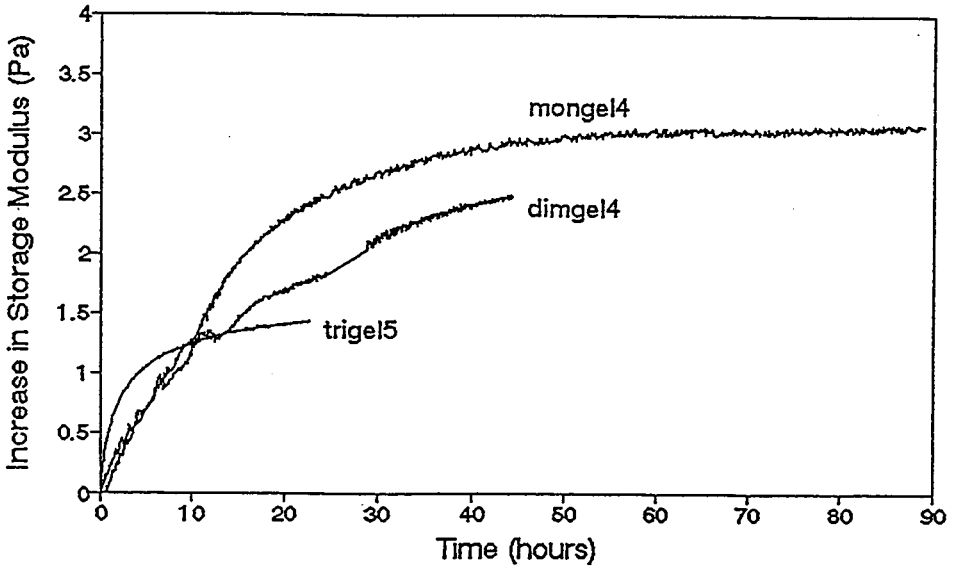

Figure 6.18 The effect of oligomer type on the increases in G' for the pH 4 gelation runs using 8.3-10.9 ppm Cr(III) and 14,045-15,050 ppm PAAm (mongel4, dimgel4, trigel5, Table 6.3).

The calculated initial G' versus time slopes and G'-G" crossing times for the runs in Figures 6.12-6.14, listed in Table 6.3, indicate that at comparable total oligomer concentrations (similar ppm), the rates of gelation are slowest with the monomer, more rapid with the dimer, and significantly faster with the trimer. The increase in gelation rate with increasing oligomer size is even more apparent when the molar oligomer concentrations are compared. Since the trimer and dimer concentrations are 1/3 and 1/2 of the monomer concentrations on a molar basis, the large trimer G' slopes indicate that the trimer was as much as 100 times more reactive on a molecular basis than the dimer or monomer. The rapid rates of gelation which occur with the trimer confirm the more qualititive results of Fei and Mertes (1991) who found instant gelation with the trimer in systems using 80 ppm trimer, 5000 ppm PAAm, and a gelling solution pH of 4.5. The differences in gelation rate with the different oligomers at comparable total Cr(III) concentrations are more pronounced at pH 4 than at pH 5. At pH 4, the initial rates of gelation of the trimer solutions are 36-37 times faster than the rates of the monomer solution, as compared to approximately 6 times faster at pH 5. The gelation times, as measured by the G'-G" crossing times, generally show corresponding trends, with the gel times decreasing with oligomer size at similar total Cr(III) concentrations. The comparison of the monomer, dimer, and trimer gelation runs at pH 5 (Figure 6.14) indicate that the maximum values of G' reached are largest with the monomer and smallest with the trimer. This phenomenon potentially indicated that the total gel strength in the pH 5 gelling solutions may be a function of the molar concentrations of the oligomers. However, definite conclusions were difficult because the results of oligomerization experiments predicted that significant amounts of oligomer products were present in the pH 5 gelling solutions (Dona, 1993), indicating the potential of uptake of a mixture of oligomers during the experiments. Similar comparisons of the maximum G' values were not made with the pH 4 gelling solutions because the monomer and dimer systems did not reach G' plateaus over the times where data was collected. However, long-time tests in which the gelling solutions were held in bottles indicated that the pH 4 trimer gels remained considerably thicker than the pH 4 monomer and dimer gels prepared under comparable conditions. Therefore, although the initial relative rates of gelation

increased with increasing oligomer size at comparable total and molar concentrations, the final gel strengths appeared to be functions of the oligomer type, molar oligomer concentration, and/or the initial gelling solution pH values.

Table 6.3 Comparison of the initial G' versus time slopes and the G'-G" crossing times for the oligomer-PAAm gelation runs.

Gelation run	pH	[Cr(III)] (ppm)	[Cr(III)] (mM)[1]	[PAAm] (ppm)	Initial slope (Pa/hr)	G'-G" Crossing Time (hr)
mongel1	4	21.9	0.447	15,309	0.0255	47
mongel2	4	24.6	0.502	15,462	0.0313	no crossing up to 24 hr
dimgel1	4	21	0.215	14,766	0.0631	25
dimgel2	4	21	0.215	14,828	0.0644	no crossing up to 14 hr
trigel1	4	19	0.129	14,666	0.951	1.6
trigel2	4	21	0.143	14,980	1.10	1.9
mongel3	4	11.7	0.238	14,965	0.0080	no crossing up to 67 hr
dimgel3	4	10.9	0.111	14,980	0.024	no crossing up to 25 hr
trigel3	4	7.4	0.050	14,715	0.295	11.3
trigel4	4	7.6	0.051	14,963	0.299	8.4
mongel4	5	10.9	0.225	15,000	0.19	15
dimgel4	5	8.3	0.085	15,050	0.19	24.3
trigel5	5	10.8	0.074	14,045	1.10	2.6

[1] Cr(III) concentrations are in mM oligomer.

Effect of Oligomer Concentration on the Gelation Rate. The effect of oligomer concentration on the gelation rate was examined by running gelation experiments for each oligomer at two sets of Cr(III) concentrations. The results for the monomer runs are shown in Figure 6.19 for the Cr(III) concentrations of 21.9-24.6 ppm and 11.7 ppm. Similarly, the results for the dimer and trimer runs are shown in Figures 6.20 and 6.21 for dimer concentrations of 21 and 11 ppm and trimer concentrations of 7.4-7.6 and 19-21 ppm.

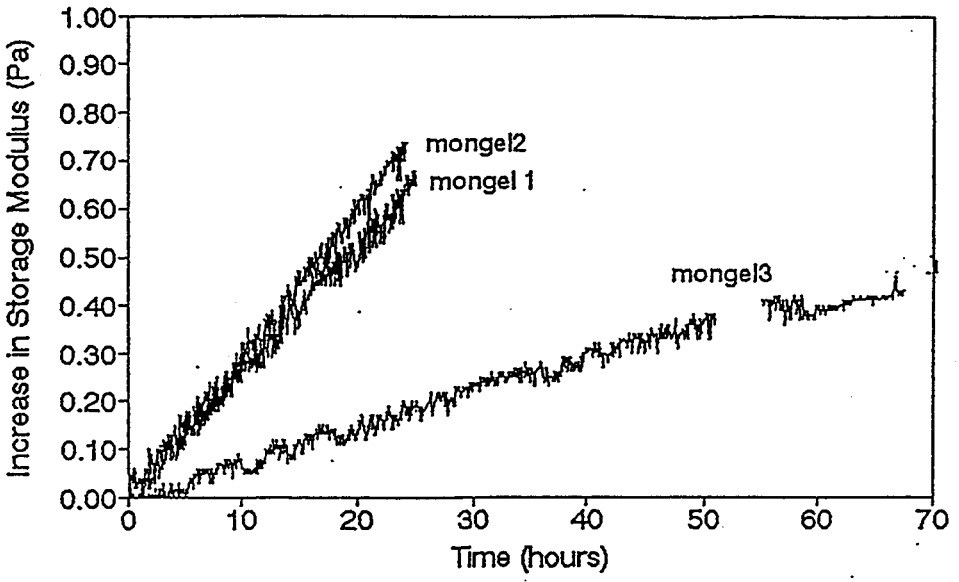

Figure 6.19 The effect of monomer concentration on the increases in G' for the pH 4 gelation runs using 14,965-15,462 ppm PAAm and 11.7 ppm Cr(III) (mongel3), 21.9 ppm Cr(III) (mongel2), and 24.6 ppm Cr(III) (mongel1, Table 3)

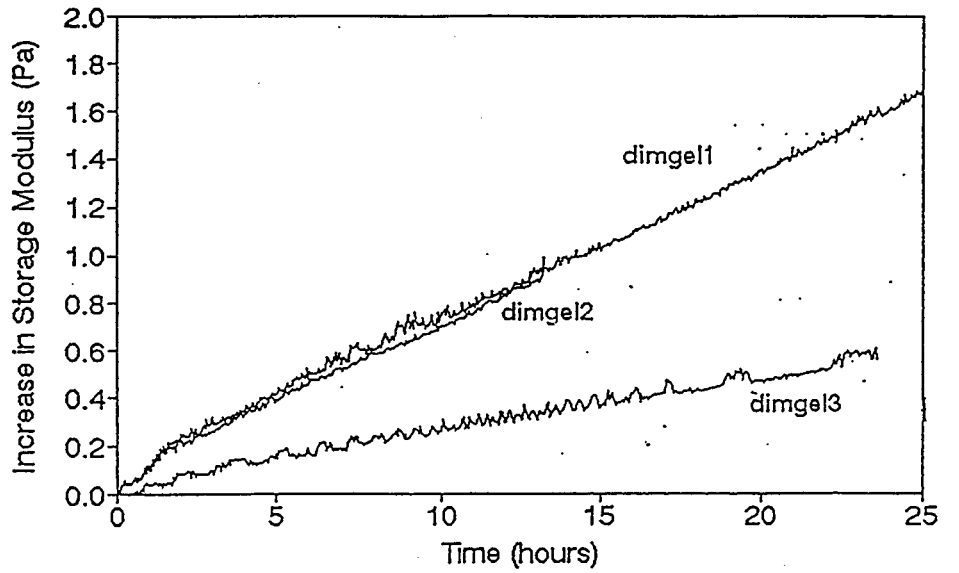

Figure 6.20 The effect of dimer concentration on the increases in G' for the pH 4 gelation runs using 14,766-14,960 ppm PAAm (dimgel3) and 21 ppm Cr(III) (dimgel1 and dimgel2) (Table 6.3).

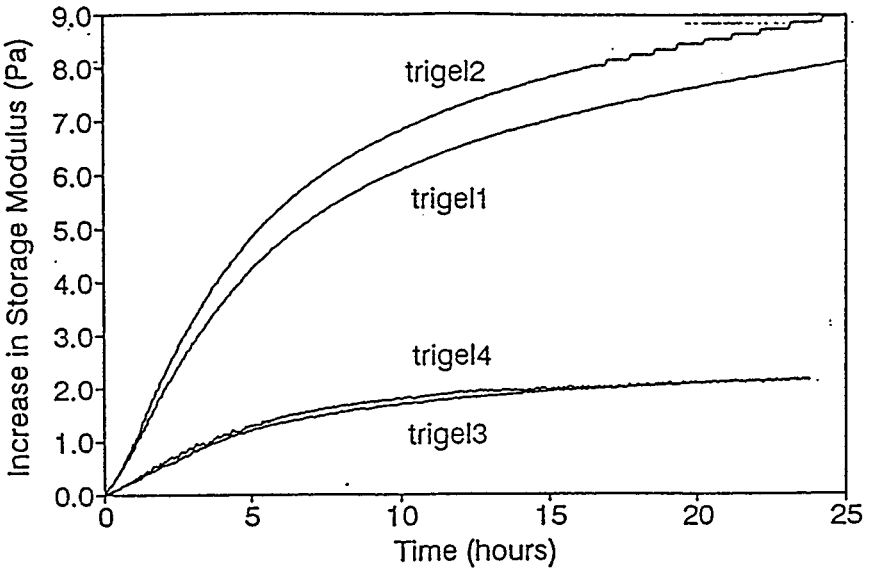

Figure 6.21 The effect of trimer concentration on the increases in G' for the pH 4 gelation runs using 14,666-14,960 ppm PAAm and 21 ppm Cr(III) (trigel1), 19 ppm Cr(III) (trigel2), 7.6 ppm Cr(III) (trigel4), and 7.4 ppm (trigel3) (Table 6.3).

For comparison purposes, the G' slope and G'-G" crossing times from the replicate runs at the higher Cr(III) concentrations were averaged and then compared against the values from the runs at the lower Cr(III) concentration in Table 6.4. For each oligomer, the initial slopes of the G' versus time curves are higher for the higher oligomer concentration. The slope ratios are 30-80% higher than the oligomer molar ratios, indicating that the relative gelation rates increase above that expected from a linear dependence of gelation rate on oligomer concentration. For the monomer and dimer pH 4 gelation runs, the G' values did not cross the G" values during the times of data collection. However, the trimer gelation times decrease with increasing trimer concentration, again indicating that the relative rates of gelation increase with oligomer concentration.

Table 6.4 Effect of oligomer concentration on the rates of gelation

Gelation run(s)	Average [Cr(III)] (ppm)	Ratio, $[Cr]_1/[Cr]_2$[1]	Average initial slope (Pa/hr)	Ratio, $slope_1/slope_2$[1]	G'-G" crossing time (hr)
mongel1 and mongel2	23.3	2.0	0.0285	3.56	47
mongel3	11.7		0.008		no crossing
dimgel1 and dimgel2	21	1.91	0.0638	2.66	25
dimgel3	10.9		0.024		no crossing
trigel1 and trigel2	20	2.67	1.02	3.43	1.7
trigel3 and trigel4	7.5		0.297		10.6

[1] $[Cr]_1$ is the higher Cr(III) concentration, $[Cr]_2$ is the lower concentration.

Effect of pH on the Gelation Rate. The effect of gelling solution pH on the rate of gelation was examined by performing gelation experiments with each oligomer type at gelling solution pH values of 4 and 5. The results for the monomer, dimer, and trimer comparative runs are shown in Figures 6.22-6.24 with the G' slopes and G'-G" crossing times listed in Table 6.5. With each oligomer, the slopes of the G' versus time curves increase with pH, with the largest increase (2,400%) occuring between the monomer solutions and the smallest increase (370%) occurring between the trimer solutions. There was no crossing of G'-G" in the monomer and dimer data. However, for the trimer runs, the gelation times decrease with pH, again indicating that the rates of gelation increase with pH.

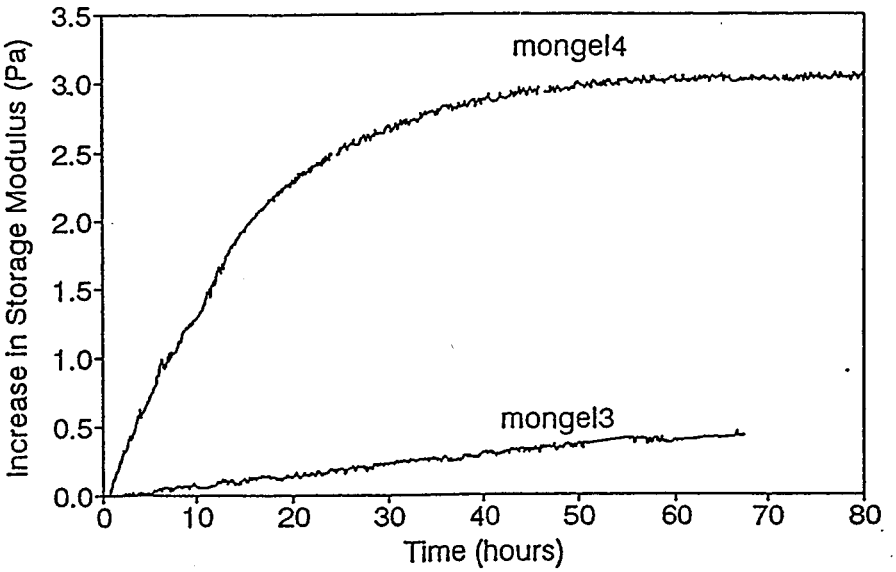

Figure 6.22 The effect of pH on the increases in G' for the monomer gelation runs using 10.9-11.7 ppm Cr(III), 14,965-15,000 ppm PAAm, and pH values of 4 (mongel3) and 5 (mongel4) Table 6.3).

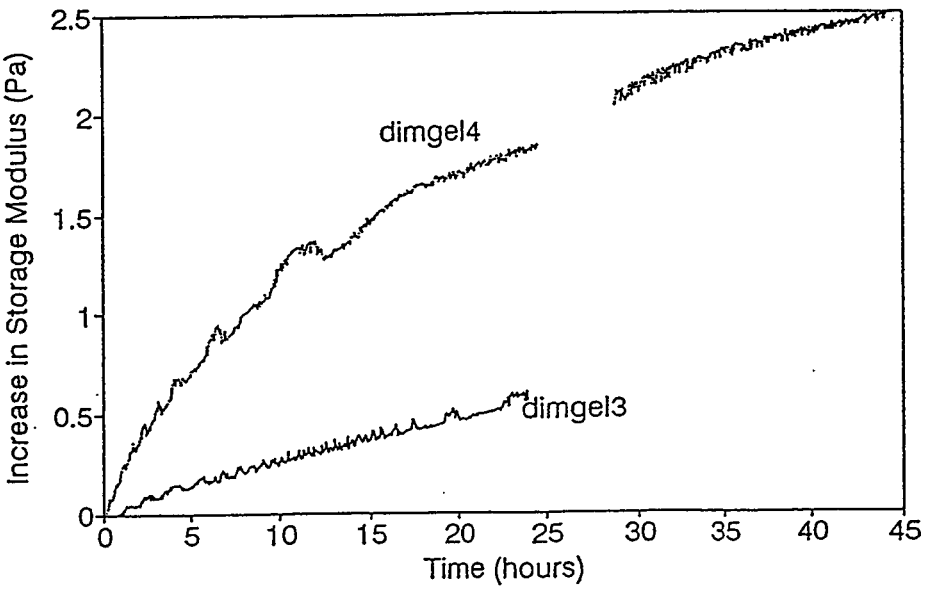

Figure 6.23 The effect of pH on the increases in G' for the dimer gelation runs using 8.3-11 ppm Cr(III), 14,980-15,050 ppm PAAm, and pH values of 4 (dimgel3) and 5 (digmel4) (Table 6.3).

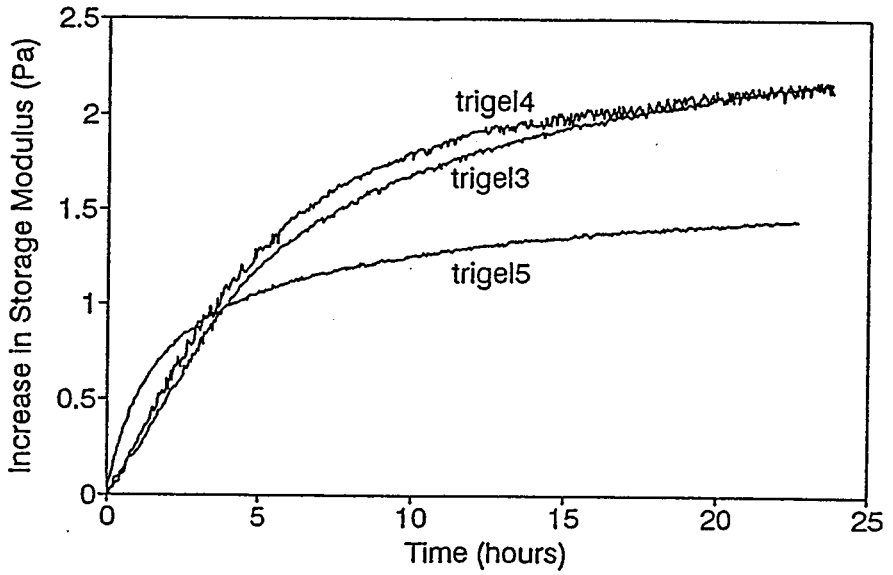

FIgure 6.24 The effect of pH in the increases in G' for the trimer gelation runs using 7.4-11 ppm Cr(III), 14,045-14,963 ppm PAAm, and pH values of 4 (trigel3) and 5 (trigel5) (Table 6.3).

For the monomer and dimer gelling solutions, the G' values of the pH 5 solutions increased more rapidly and obtained significantly higher G' values than the pH 4 solutions. For the trimer comparison, the initial slope of the G' values versus time for the pH 5 gelling solution is higher than the corresponding slope of the pH 4 solution. However, the G' values at pH 5 level off at lower values than those at pH 4. This indicates that the pH 4 trimer gelling solutions had higher long-term gel strengths than the pH 5 gelling solution.

Table 6.5 Effects of the gelling solution pH on the rates of gelation

Gelation run(s)	pH	Average [Cr(III)] (ppm)	Average initial slope (Pa/hr)	Ratio, $slope_{pH5}$/ $slope_{pH4}$	G'-G" crossing time (hr)
mongel3	4	11.7	0.008		no crossing
mongel4	5	11	0.19	24	15
dimgel3	4	10.9	0.024		no crossing
dimgel4	5	8.3	0.19	7.9	24
trigel3 and trigel4	4	7.4	0.295		10.6
trigel5	5	11	1.1	3.7	2.6

Comparison of the Relative Rates of Uptake and Gelation

A number of uptake and gelation runs performed under similar oligomer type, [Cr(III)], [PAAm], and pH conditions were directly compared to determine the relative rates between the uptake and gelation reactions. Knowledge of the relative lag between the uptake and gelation processes along with an uptake model was useful because it could potentially be used with an predictive uptake model to predict the rates of gelation.

The rates of oligomer-PAAm uptake and gelation were compared by plotting on the same graph the fractional Cr(III) reacted with the PAAm and the increase in G' as a function of time. Comparisons were performed for each oligomer for gelling solution pH values of 4 and 5. Figures 6.25 and 6.26 show the comparison for the pH 4 and pH 5 monomer runs. Similar comparisons for the dimer and trimer runs are shown in Figures 6.27-6.30.

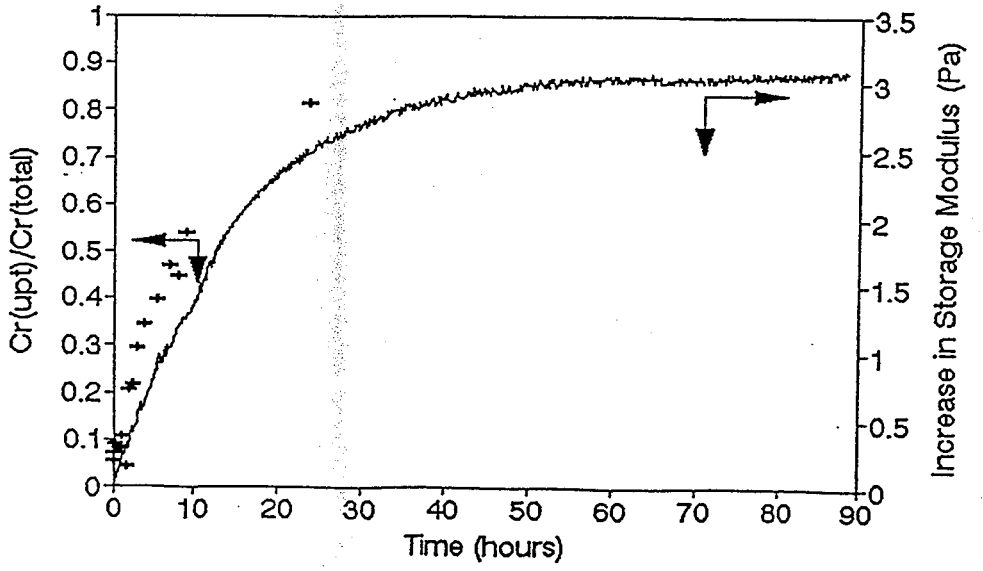

Figure 6.25 : Comparison of the fractional uptake and increases in G' from the pH 4, 21.9-25.4 ppm monomer, 13,411-15,462 ppm PAAm uptake and gelation runs (monupt2, Table 6.1; mongel1, mongel2, Table 6.3.)

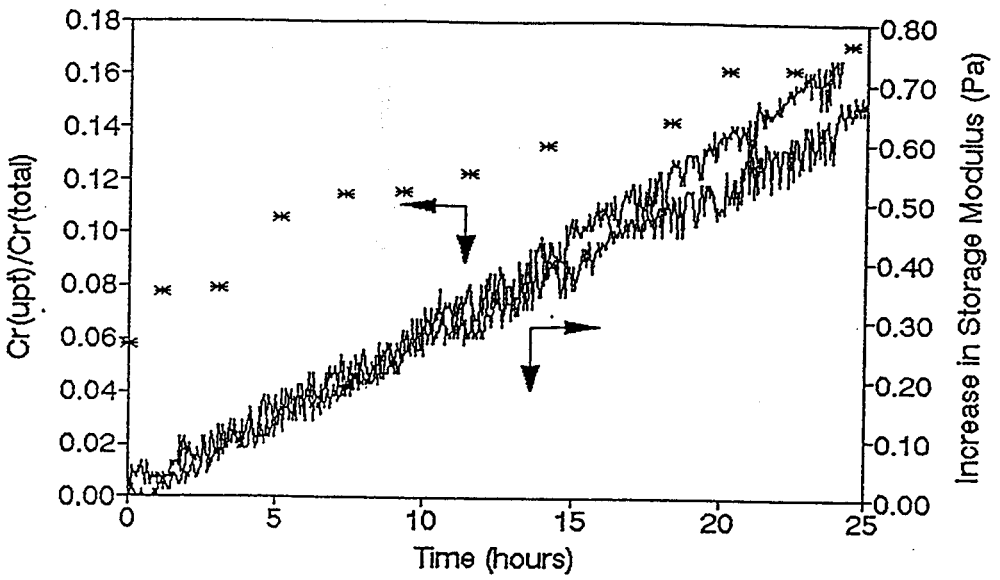

Figure 6.26 : Comparison of the fractional uptake and increases in G' from the pH 5, 10.9 ppm monomer, 15,000 ppm PAAm uptake and gelation runs (monupt5, Table 6.1 and mongel4, Table 6.3).

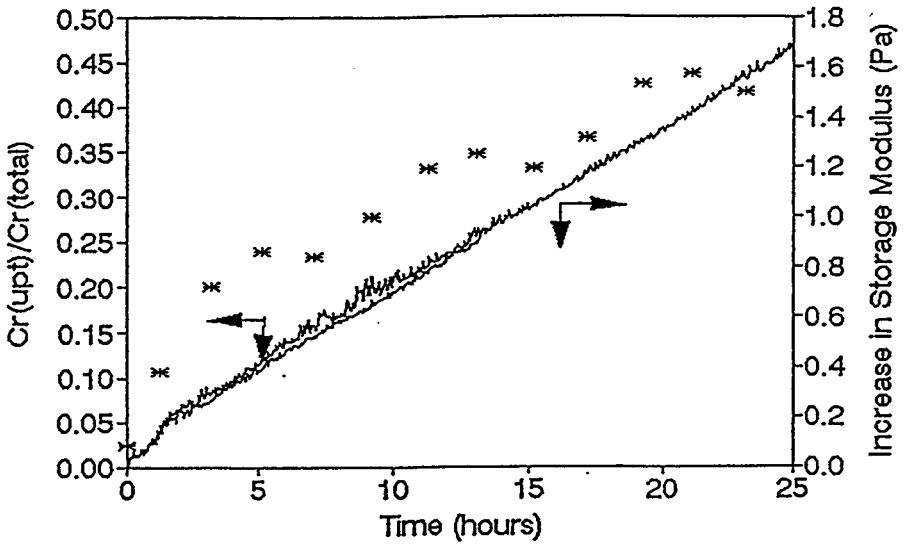

Figure 6.27 : Comparison of the fractional uptake and increases in G' from the pH 4, 21-24.3 ppm dimer, 14,415-14,879 ppm PAAm uptake and gelation runs (dimupt2, Table 6.1; dimgel1, dimgel2, Table 6.3).

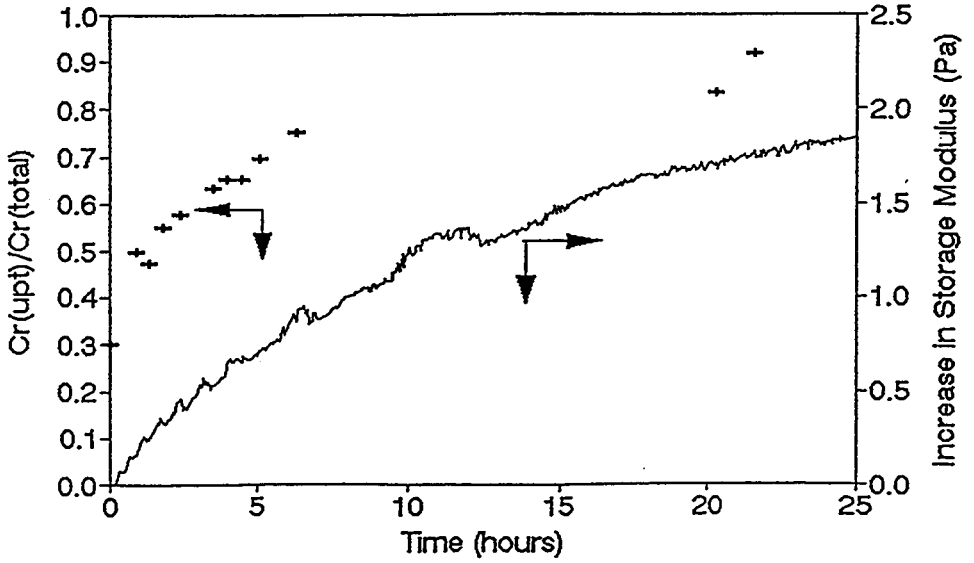

Figure 6.28 : Comparison of the fractional uptake and increases in G' from the pH 5, 8.3 ppm dimer, 15,050 ppm PAAm uptake and gelation run (dimupt4, Table 6.1; dimgel4, Table 6.3).

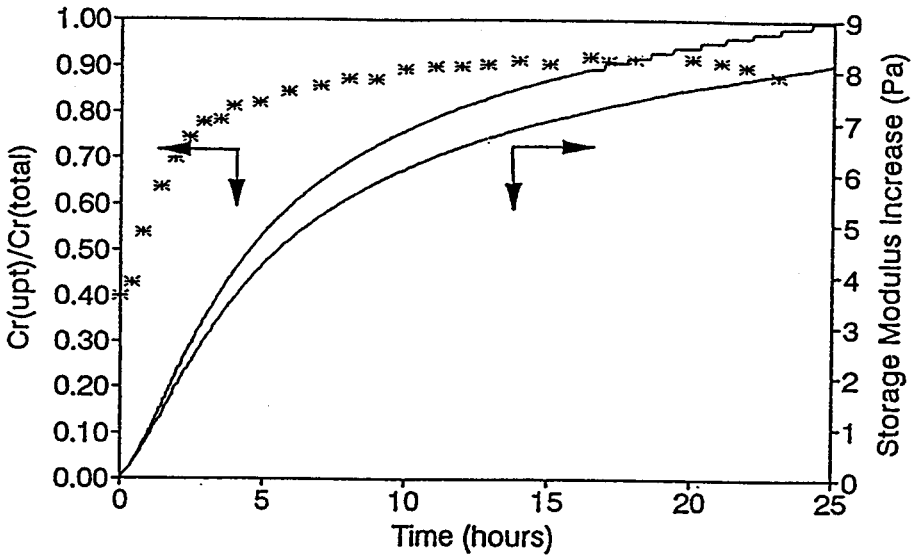

Figure 6.29 : Comparison of the fractional uptake and the increases in G' from the pH 4, 19-22.8 ppm trimer, 13,153-14,980 PAAm uptake and gelation runs (triupt3, Table 6.1; trigel1, trigel2, Table 6.3).

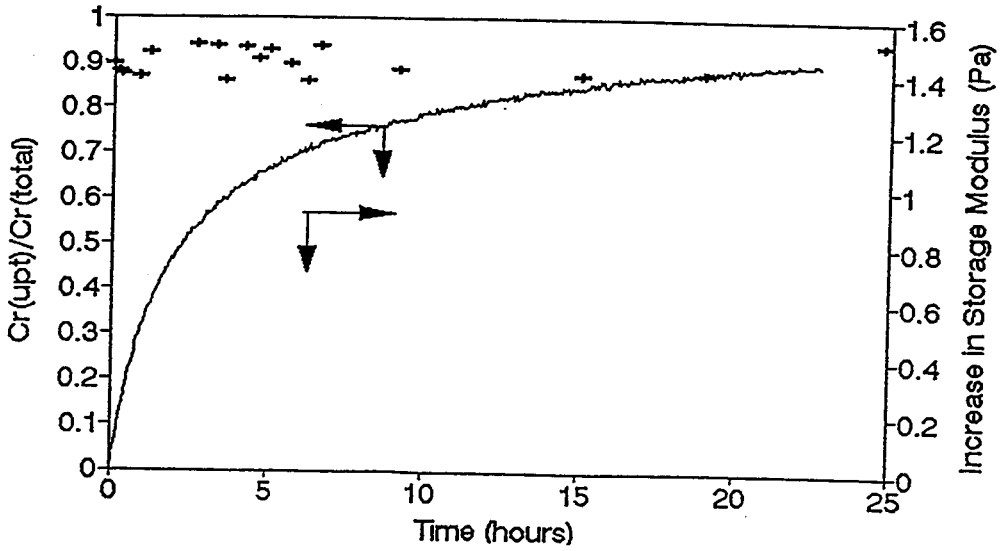

Figure 6.30 : Comparison of the fractional uptake and the increases in G' from the pH 5, 10.8 ppm trimer, 14,045 ppm PAAm uptake and gelation run (triupt8, Table 6.1; trigel5, Table 6.3).

The comparisons in the monomer and dimer runs show that the increases in G' closely follow the increases in Cr(III) reacted with the PAAm. This behavior is specifically shown in the monomer and dimer pH 5 runs where relative plateaus in the G' values occur when the majority of the uptake has occurred. Although concentration plateaus did not occur in the pH 4 monomer and dimer runs, the comparisons show that increases in G' are occuring at the same relative rates as the increases in the oligomer-PAAm uptake. For the trimer runs, initial rapid increases in the G' values occur along with the uptake of the trimer by the PAAm. The G' values of the trimer solutions continue to rise after the majority of the trimer uptake has occured, although at slower rates than those occuring in or immediately following the time of rapid trimer uptake. The comparisons of the uptake and gelation data suggest that the gelation step occurs a short but finite time after PAAm uptake of the oligomers. For the monomer and dimer runs, where relatively slower uptake rates occur, the gelation closely followed the uptake. For the trimer runs, where relatively fast uptake occurs, the gelation continued after the majority of the trimer had reacted with the PAAm. The delay in increase of G' in the trimer runs was more pronounced at higher pH. In all the oligomer-PAAm systems, however, the relative gelation rates, as indicated by the increases in G' and the G'-G" crossing times, correlated with the uptake rates and, in general, closely followed the uptake of the oligomers by the PAAm.

Oligomerization Results

The uptake and gelation gelling solutions were prepared with pure monomer, dimer, or trimer oligomer stock solutions. Assuming minimal oligomer product formation during gel preparation, the oligomer-PAAm gelling solutions initially contained only one oligomer. However, if the rates of oligomerization were significant compared to the rates of oligomer-PAAm uptake, the formation and uptake of oligomer products over the data collection time periods could occur. The uptake rates would then represent a mixture of different sized oligomers with the PAAm. In order to estimate the amounts of oligomer products, oligomerization runs were performed where essentially pure monomer, dimer, or trimer solutions were adjusted to pH 4 or pH 5 in the absence of PAAm.

A higher overall oligomer concentration range (20-61 ppm) was used for the oligomerization experiments as compared to the concentration range used in the uptake experiments (8-30 ppm) because accurate oligomer concentration measurement was difficult at the uptake oligomer concentration ranges (Dona, 1993). Because of the different concentration ranges, it was necessary to formulate rate expressions and determine oligomerization rate constants to calculate the amounts of oligomer products expected at the uptake experimental conditions. For this purpose, the general second order Cr(III) dependence found by Rotzinger et al. (1986) and Besso (1983) was assumed. An inverse $[H^+]^2$ dependence was assumed after finding that dividing the observed Besso (1983) and Rotzinger et al. (1986) rate constants by $[H^+]^2$ resulted in reasonably constant rate constants over the pH ranges of 3.9 to 5 for the monomer and 4 to 4.5 for the dimer (Dona, 1993). This resulted in the general oligomerization equation, Eqn. 6.8.

$$\frac{d[Cr_i]}{dt} = -\frac{k_i(ol)\ [Cr_i]^2}{[H^+]^2} \qquad (6.8$$

where for the monomer, i=1, for the dimer, i=2, and for the trimer, i=3.

For the runs where pH changes of less than ±0.1 pH units occured in data used for the regressions, the H^+ concentration was assusmed constant at the average H^+ concentration. The solution to Eqn. 6.8 was then Eqn. 6.9. Linear regressions of the $([Cr_i(0)]/[Cr_i(t)]-1)/[Cr_i(0),]$ values versus $t/[H^+]^2$ were then performed, with the slope of the regression line being equal to $k_i(ol)$.

$$\frac{\frac{Cr_i(0)}{Cr_i(t)} - 1}{Cr_i(0)} = \frac{k_i(ol)t}{[H^+]^2} \qquad (6.9$$

If the pH variation over which the regression was performed was greater than ± 0.1 pH units, the $[H^+]$ versus time curve was fit with a power-law polynomial to obtain an expression for $[H^+]$ as a function of t (denoted as $[H^+](t)$). $[H^+](t)$ was then substituted into Eqn. 6.8, the resulting equation was integrated, and $k_i(ol)$ obtained from plotting the integrated function of time, g(t), against $([Cr_i(0)]/[Cr_i(t)]-1)/[Cr_i(0)]$.

Linear regressions of the $([Cr_i(0)]/[Cr_i(t)]-1)/[Cr_i(0)]$ values versus time or the adjusted functions of time were performed with the statistical program, JMP-IN. Since positive or negative deviations of the Cr(III) concentrations from the regressed Cr(III) concentrations generally occurred with increasing reaction times, sequential linear regressions were performed with JMP-IN with the reaction times being reduced until no consistent positive or negative direction deviations of the residuals from the regression lines occurred. For the monomer and dimer runs, positive deviations or rate acceleration occurred with increasing time whereas with the trimer runs, the negative deviations or rate decceleration occurred.

The resulting oligomerization rate constant and regression time ranges are listed in Table 6.6.

Table 6.6 Oligomerization rate constants and regression times

Oligomer	[Cr(III)] range (ppm)	pH	$k_i(ol)$ (M/hr) (X 10^8)	Regression time range (hr)
monomer	30-56	4	0.59-0.69	100-193
monomer	49-56	5	0.93-0.96	3-5
dimer	25-62	4	5.3-27	4-29
dimer	37	5	3.1	1.4
trimer	26-54	4	32-171	6-30
trimer	37-53	5	42-69	3-4

The pH 4 monomer rate constants in Table 6.6 agreed well with each other and with the rate constant obtained by Rotzinger et al. (1986) after adjustment for an inverse $[H^+]^2$ dependency (5.8 X 10^{-9} M/hr). The rate constants for the pH 5 runs also show good agreement with each other, although the average value was approximately 50% higher than that expected from the inverse $[H^+]^2$ dependency shown by the Rotzinger et al. rate constants. The relatively larger variability in the dimer and trimer rate constants was attributed to the generally larger and more variable amounts of base used for pH adjustment

(Rotzinger et al., 1986), the relatively low stability of the dimer (Stunzi et al., 1989), and the relatively large and variable changes in pH after initial pH adjustment in the dimer and trimer runs.

The ranges of rate constants in Table 6.6 were used with Eqn. 6.8 to estimate the amounts of immediate oligomer product (dimer, tetramer, or hexamer) in the oligomer gelling solutions at the conclusion of the data collection time periods (T_f) (Table 6.7). In the calculations, initial gelling solution Cr(III) concentrations and average H^+ concentrations were used. This assumed that the oligomerization of the oligomer was independent of the uptake, i.e. once an oligomer attached to a PAAmcarboxyl group it remained available for further reaction with other solution oligomers. The amount of oligomer products in the pH 5 trimer run were estimated at one hour since the majority of the uptake occurred during the five-minute gelling solution preparation time period.

Table 6.7 Estimated Amounts of Oligomer Products at the End of Uptake Data Collection

Species	Solution pH	% Oligomer Products
monomer	4	1-5
monomer	5	34-35
dimer	4	6-66
dimer	5	57
trimer	4	10-40
trimer	5	1-3 (1 hr)

The low estimates of dimer in the pH 4 monomer runs over the uptake data collection time ranges indicate that the rates of oligomerization in the monomer uptake gelling solutions were expected to be low compared to the monomer-PAAm uptake rates. For the remainder of the uptake and gelation runs, the oligomerization results indicated the potential of significant oligomerization occurring during the uptake data collection time periods. The effects of the oligomerization products on the oligomer-PAAm uptake are discussed further with the modelling of the oligomer-PAAm uptake data.

In order to assess the effect of the amide group on the rates of oligomerization in the gelling solutions, two comparison monomer runs at pH 4 and pH 5 were performed with an amount of proprionamide equivalent to 15,000 ppm PAAm added to the oligomer solutions. Direct comparison of the fractional Cr(III) concentrations from the solutions with and without proprionamide indicated that the rates of oligomerization were essentially unaffected by the presence of the amide group (Dona, 1993).

MODELLING OF THE OLIGOMER-PAAm UPTAKE DATA

As discussed in the Results section, the gelation of the oligomer-PAAm solutions closely follwed the uptake of the oligomers by the PAAm. This suggested that if a predictive model of the oligomer-PAAm uptake model could be developed, it could be used to predict both the rates of uptake and gelation in permeability modification applications. An additional advantage of developing a kinetic uptake model

to predict the rates of uptake and gelation was the concentrations of the Cr(III) and PAAm species involved in the oligomer-PAAm uptake reactions were more easily measured than the Cr(III) and PAAm species involved in the gelation reactions (Dona, 1993).

Model Assuming Low Oligomerization Rates and Elementary Reactions

The uptake differential rate equation corresponding to Eqns. 6.2-6.4 is Eqn. 6.10. In order to simplify the model development, it was assumed that the rates of oligomerization were low compared to the rates of oligomer-PAAm uptake rates.

$$\frac{d[Cr_i]}{dt} = \frac{-k_i(op)\ [Cr_i]^{l_i}[PAAmcarboxyl]^{m_i}}{fn([H^+])} + \frac{-k_i(oap)\ [Cr_i]^{l_i'}[Cr_iPAAmcarboxyl]^{m_i'}}{fn'([H^+])} + \frac{-k_i(opp)\ [Cr_{2i}]^{l_i''}[PAAmcarboxyl]^{m_i''}}{fn''([H^+])} \qquad \text{(6.10}$$

With low oligomerization to uptake rate ratios, the second and third right-hand terms in Eqn. 6.8 are small compared to the first right-hand term, resulting in the simplified Equation 6.11.

$$\frac{d[Cr_i]}{dt} = \frac{-k_i(op)[Cr_i]^{l_i}[PAAmcarboxyl]^{m_i}}{fn([H^+])} \qquad \text{(6.11}$$

Previous studies indicate that the reaction between monomeric Cr(III) and the carboxyl group is generally first order in Cr(III) and carboxyl, with an inverse $[H^+]$ dependence (Table 6.8). Assuming that the first order Cr(III) and carboxyl dependencies and inverse $[H^+]$ dependencies apply to the oligomer-PAAmcarboxyl reactions here, Eqn. 6.11 then becomes Eqn. 6.12.

$$\frac{d[Cr_i]}{dt} = \frac{-k_i(op)[Cr_i][PAAmcarboxyl]}{[H^+]} \qquad \text{(6.12}$$

Table 6.8 Cr(III), carboxyl and H^+ reaction orders from previous studies

Study	Cr(III) reaction order	Carboxyl reaction order	H^+ reaction order
Hamm, et al.	+1	0	-1
Banergea and Chaudhuri	+1	1	-1
Khan and Ud-din	Cr(III) held constant	1	-1
Hartley	+1	+1	not determined
Hunt	+1.32	0.8	-1
Montanari et al.	+1	+0.8	-0.8

Using the experimental conditions of relatively constant H^+ and PAAmcarboxyl concentrations, a pseudo rate constant, $k_i'(op)$, was defined with Eqn. 6.12 becoming Eqn. 6.13 whose solution is then Eqn. 6.14.

$$\frac{d[Cr_i]}{dt} = -k_i'(op)[Cr_i] \qquad (6.13$$

$$where\ k_i'(op) = \frac{k_i(op)[PAAmcarboxyl]}{[H^+]}$$

$$\ln\left(\frac{[Cr_i(t)]}{[Cr_i(0)]}\right) = -k_i'(op)t \qquad (6.14$$

If this model, referred to here as the elementary reaction model with assumed low rates of oligomerization (ERLO), correctly described the experimental uptake data, a plot of the $\ln(Cr_i(t)/Cr_i(0))$ values versus time would be linear with the slopes equal to $k_i'(op)$. In addition, the values of $k_i'(op)[H^+]$ would be linear with PAAmcarboxyl concentration with slopes of $k_i(op)$.

The model was first tested on the pH 4 monomer uptake data where relatively low rates of oligomerization were expected (Table 6.7). The first order Cr(III) dependence was checked by performing regressions on the triplicate ln([Cr(t)]/[Cr(0)]) values versus time. The regressions were performed with JMP-IN, a SAS-equivalent McIntosh statistics software program. The JMP-IN analysis provided three types of sums of squares with associated mean square values; the sum of squares and mean square values for the linear ln([Cr(t)]/[Cr(0)]) versus time model, the sum of squares and mean square value for the total error (the deviation of the experimental points from the regression line), and the sum of squares and mean square value for the pure error (the deviation of the experimental points from the regression line expected

from random error). From the three types of sums of squares and/or mean square values, goodness of fit values, effect F ratios, and lack of fit F ratios for the ln([Cr(t)]/[Cr(0)]) versus time regressions were calculated by JMP-IN. From the effect and lack of fit F ratios and the number of experimental data points, significance probabilities were also calculated by JMP-IN.

The results of the statistical analysis for the pH 4 monomer uptake runs are summarized in Table 6.9 and the regressed and experimental ln([Cr(t)]/[Cr(total)]) versus time plots are shown in Figures 6.31 and 6.32. The goodness of fit values (Table 6.9) and the experimental and model comparative plots indicate good agreement between the first order Cr(III) model predicted values and the experimental data. In addition, the significance probabilities of the effect F ratios are all less than 0.1%, indicating highly significant correlations between the ln([Cr(t)]/[Cr(0)]) values and time. The significance probabilites of the lack of fit F ratios were all non-significant at a 10% significance probability, implying that the total errors from the individual regressions were not statistically different than the random errors.

Table 6.9 Statistics for the [Cr(III)] fits of the monomer-PAAm data

pH	[PAAm] (ppm)	Goodness of fit (r^2)[1]	F ratio, effect	Effect significance probability (%)	F ratio, lack of fit	Lack of fit significance probability (%)
4	19,908	0.949	>999	<0.01	1.08	41
4	14,857	0.960	>999	< 0.01	1.40	19
4	13,441	0.949	>999	< 0.01	0.87	61
4	8,782	0.940	>999	< 0.01	1.22	29

[1] r^2 ≡ the square of the correlation coefficient

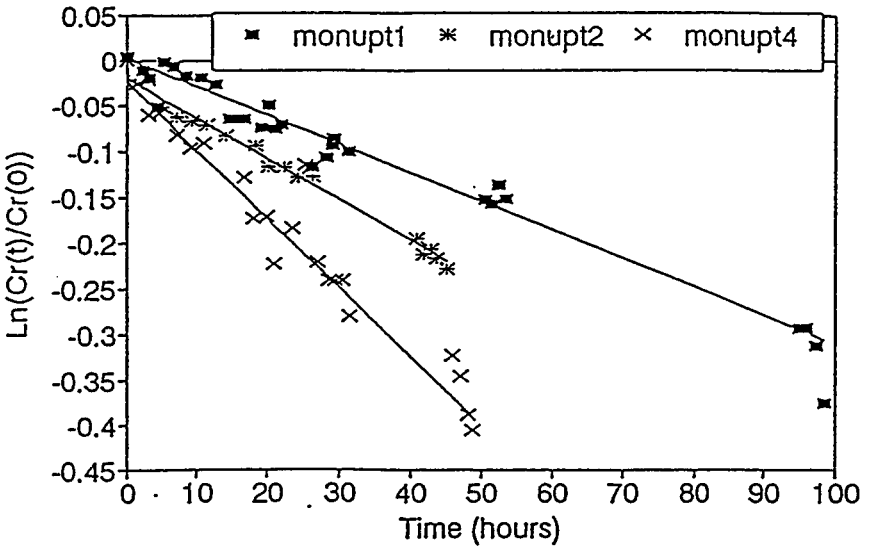

Figure 6.31 : Plots of the experimental and ERLO-model ln(Cr(t)/(Cr(0)) values for the pH 4 monomer uptake runs at different PAAm concentrations (see Table 6.1 for descriptions of the experimental conditions for the individual runs).

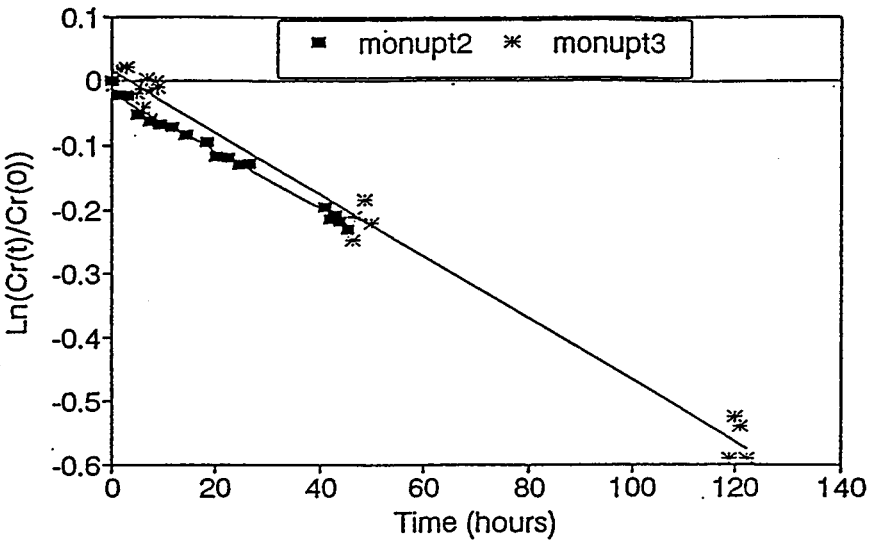

Figure 6.32 : Plots of the experimental and ERLO-model ln(Cr(t)/(Cr(0)) values for the pH 4 monomer uptake replicate runs (see Table 6.1 for descriptions of the experimental conditions for the individual runs).

The second step in assessing the fit of the pH 4 monomer uptake data to the ERLO model was to determine the goodness of fit of the linear regression of the $k_i'(op)[H^+]$ values versus the PAAmcarboxyl concentrations. The pseudo-rate constants ($k_i'(op)$'s) were obtained from the values of the slopes of the linear regressions of the ln([Cr(t)]/[Cr(0)] values versus time. The $k_1'(op)$ values were then

multiplied by the average $[H^+]$ values of the gelling solutions over the data collection time periods to obtain $k_1'(op)[H^+]$ values. The PAAm concentrations of the gelling solutions were determined as described in "Preparation and Characterization of the PAAm Solutions". The molar PAAmcarboxyl concentrations were determined from the gelling solution PAAm ppm concentrations by assuming that the molecular weight of the functional repeat groups on the PAAm molecules was 72 g/mole, the density of the 1 M $NaClO_4$ PAAm solutions was 1.072 g/ml, and the fraction of PAAm side groups that were carboxyl groups was 2.3% of the total amide and carboxyl PAAm side groups.

The regression of the experimental $k_1'(op)[H^+]$ values versus the PAAmcarboxyl concentrations yielded a regression line slope ($k_1(op)$) of 1.07 X 10^{-4} hr^{-1}. The close fit of the regressed line to the $k_1'(op)[H^+]$ values (Figure 6.33), along with the goodness of fit (r^2) value of 0.944 from the linear regression, indicated a good linear fit between the $k_1'(op)[H^+]$ and the PAAmcarboxyl concentrations. The combination of the linearity of the ln([Cr(t)]/[Cr(0)] values with time and the linearity of the $k_1'(op)[H^+]$ values with PAAmcarboxyl concentration indicated that the first order Cr(III), first order PAAm dependencies found by researchers for other Cr(III)-carboxyl systems could be applied to the oligomer-PAAm systems here under the conditions where relatively low rates of oligomerization were expected.

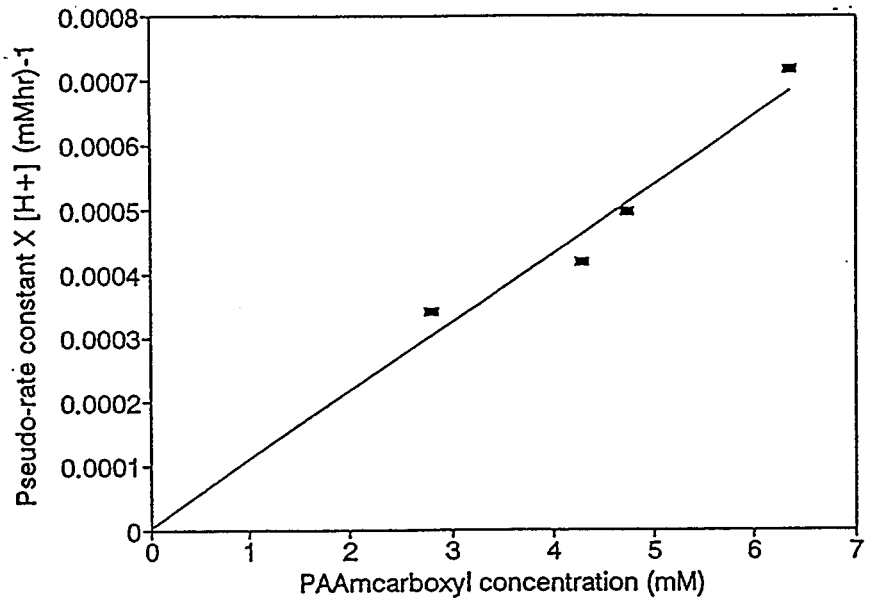

Figure 6.33 : Plot of the first order pseudo-rate constant values PAAmcarboxyl concentration.

The first order Cr(III) dependency of the pH 5 monomer data was also assessed by performing a regression on the ln(Cr(t)/Cr(0)) versus time data. Although a significant lack of fit significance probability (5.2%) was obtained for the first order regression, the excellent goodness of fit value (0.987) and the good graphical match between the experimental and regressed ln(Cr(t)/Cr()) values (Figure 6.34) indicated that the first order Cr(III) dependence fit the monomer pH 5 data well. Direct assessment of the first order PAAmcarboxyl dependence of the ERLO model was not possible for the monomer pH 5 uptake results because runs were not performed where the PAAm concentrations were varied. However, the pH 5 rate constant, $k_1(op)$, was calculated and compared against the pH 4 $k_1(op)$ by assuming first order [Cr(III)] and [PAAmcarboxyl] dependencies with the inverse $[H^+]$ dependency generally found by other researchers (Table 8). The resulting pH 5 $k_1(op)$ value, 1.55 X 10^{-4} hr^{-1}, was approximately 45% higher than the $k_1(op)$ value obtained at pH 4.

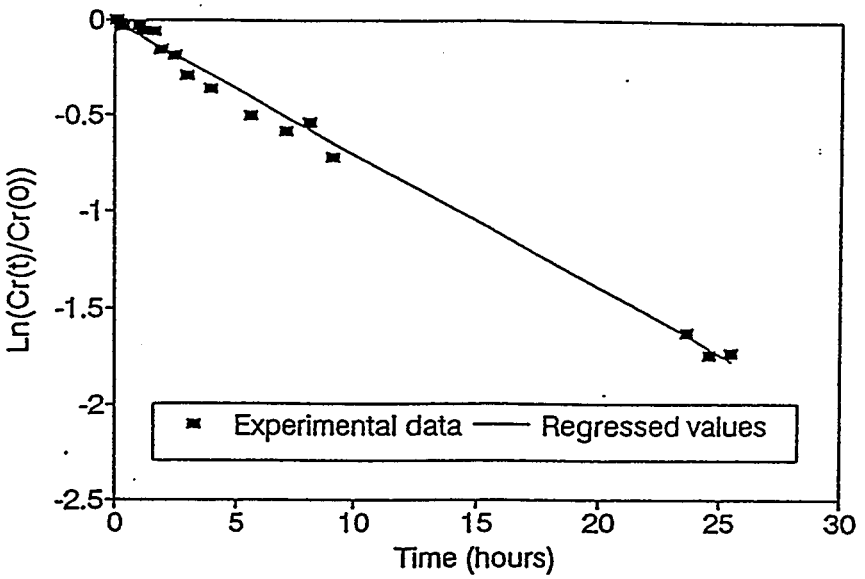

Figure 6.34 : Plots of the experimental and ERLO-model ln(Cr(t)/Cr(0)) values for the pH 4 monomer uptake run (monupt5, Table 6.1).

The ERLO model was then applied to the dimer and trimer pH 4 runs where several different PAAm concentrations were used. The ln((Cr(t)/Cr(0)) versus time plots for the 8,427, 14,415, and 19,274 ppm PAAm, pH 4 dimer uptake runs are shown in Figures 6.35-6.37 with similar plots for the 4,433, 8,633, and 13,153 ppm trimer uptake runs shown in Figures 6.38-6.40. Both sets of data show model deviations from the experimental data, with deviations occuring primarily in the initial time periods for the dimer runs and for both the initial and late reaction time periods for the trimer runs. For the set of dimer runs, where relatively long intermediate time ranges existed where the ln(Cr(t)/Cr(0)) values were linear with time, the initial data was excluded and regressions performed on the remaining data up to 50 hours. Although reasonable matches between the regressed and experimental data were obtained for the intermediate time periods (Figures 6.41-6.43), a plot of the $k'_2(op)[H^+]$ values versus PAAmcarboxyl concentration showed that the pseudo-rate constants were nearly indendent of PAAmcarboxyl concentrations (Figure 6.44). This indicated that the first order PAAmcarboxyl dependence of the ERLO model was not satisfied for the pH 4 dimer data. Comparison of the experimental and regressed ln(Cr(t)/Cr(0)) versus time values for the pH 5 dimer run (Figure 6.45) also indicated that a good match was not obtained between the model and the experimental data.

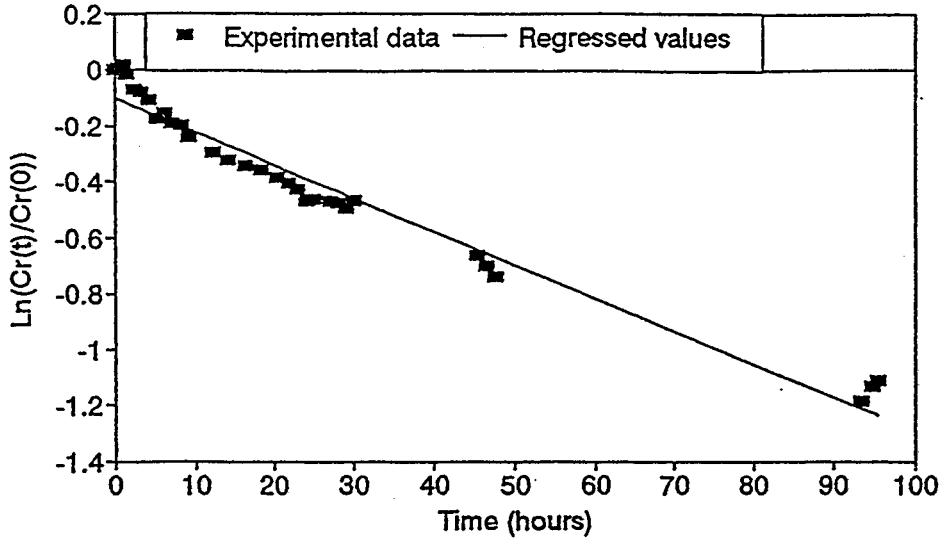

Figure 6.35 : Comparison of the experimental and regressed 1st order ln(Cr(T)/Cr(O)) values for the pH 4, 8,427 ppm PAAm, 25.3 ppm dimer uptake run (dimupt1, Table 6.1).

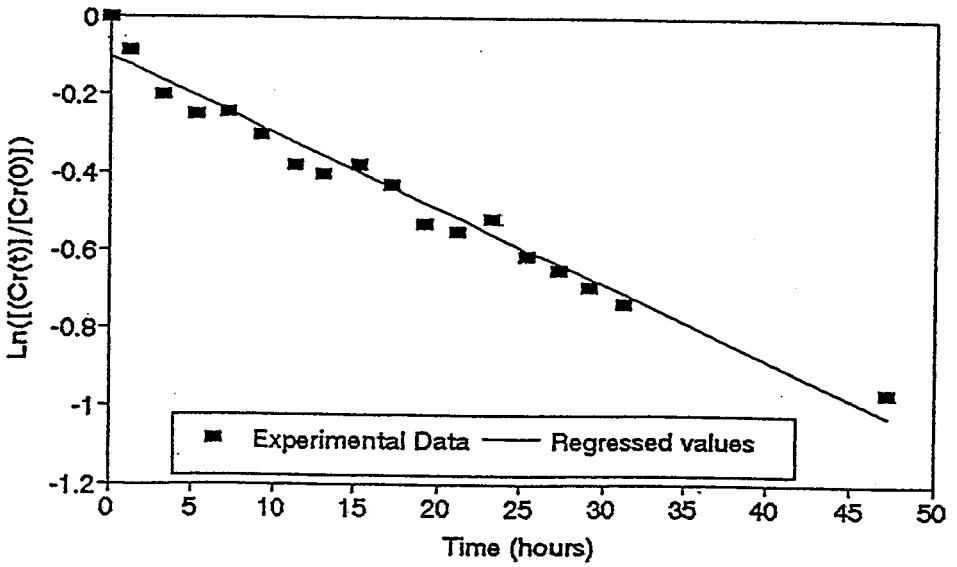

Figure 6.36 : Comparison of the experimental and regressed 1st order ln(Cr(t)/Cr(O)) values for the pH 4, 14,415 ppm PAAm, 24.3 ppm dimer uptake run (dimupt2, Table 6.1).

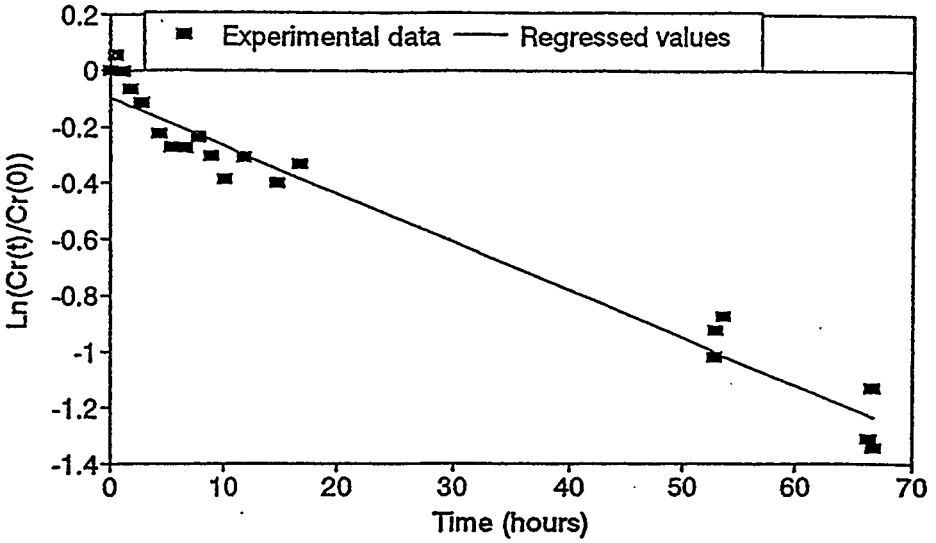

Figure 6.37 : Comparison of the experimental and regressed 1st order ln(Cr(t)/Cr(O)) values for the pH 4, 19,274 ppm PAAm, 17.3 ppm dimer uptake run (dimupt3, Table 6.1).

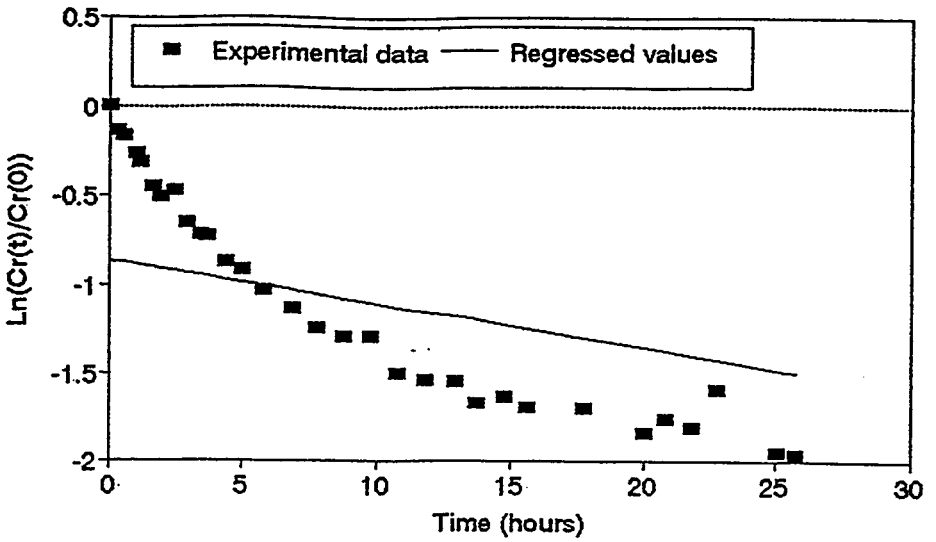

Figure 6.38 : Comparison of the experimental and regressed 1st order ln(Cr(t)/Cr(O)) values for the pH 4, 4,433 ppm PAAm, 24.7 ppm trimer uptake run (triupt1, Table 6.1).

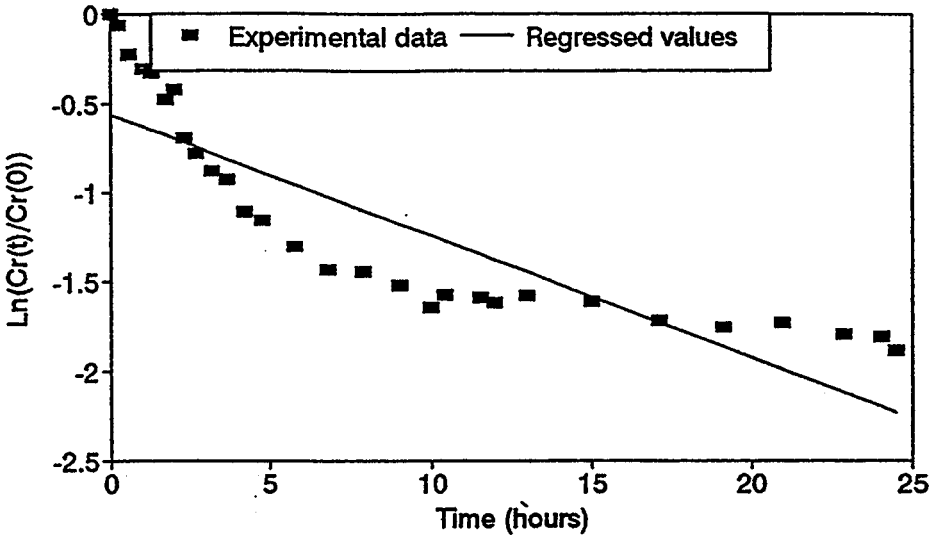

Figure 6.39 : Comparison of the experimental and regressed 1st order ln(Cr(t)/Cr(O)) values for the pH 4, 8,633 ppm PAAm, 24.1 ppm trimer uptake run (triupt2, Table 6.1).

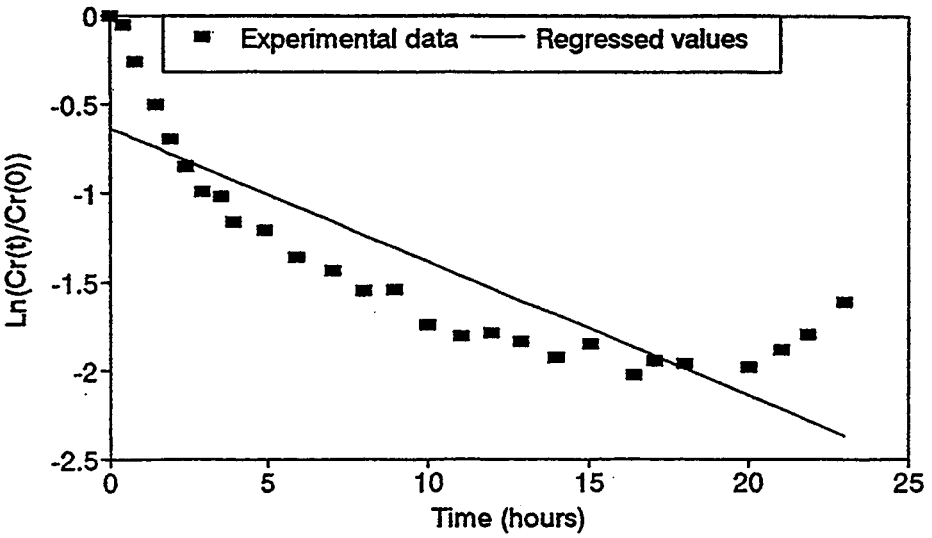

Figure 6.40 : Comparison of the experimental and regressed 1st order ln(Cr(t)/Cr(O)) values for the pH 4, 13,153 ppm PAAm, 22.8 ppm trimer uptake run (triupt3, Table 6.1).

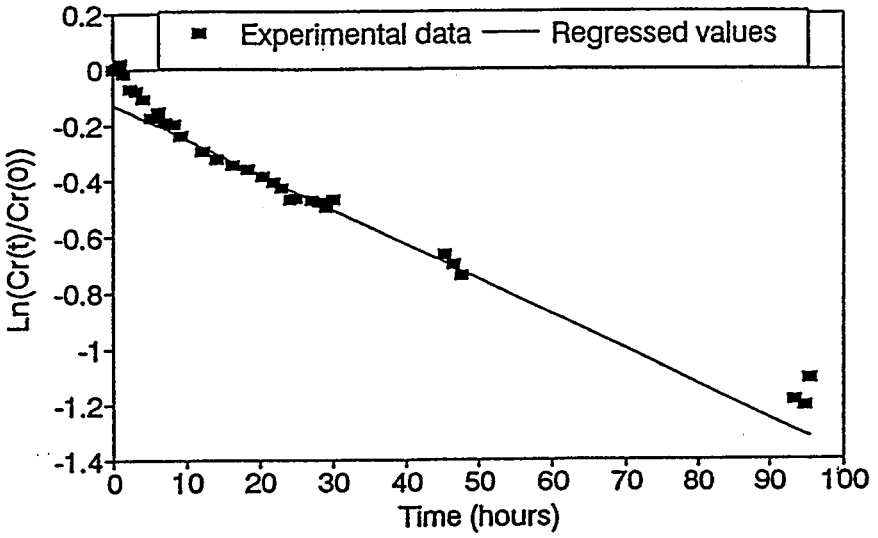

Figure 6.41 : Comparison of the experimental and regressed 1st order ln(Cr(t)/Cr(O)) values for the pH 4, 8,427 ppm PAAm, 25.3 ppm dimer uptake run (dimupt1, Table 6.1) with the initial time data excluded.

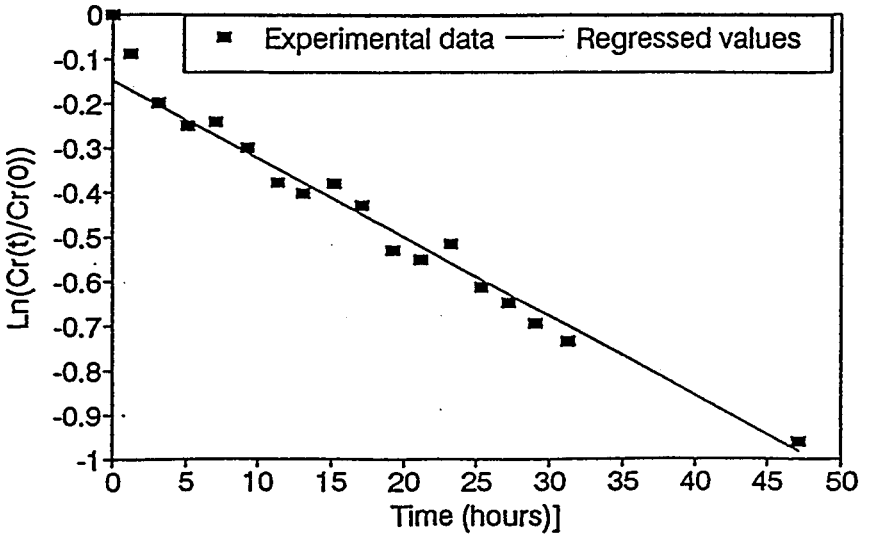

Figure 6.42 : Comparison of the experimental and regressed 1st order ln(Cr(t)/Cr(O)) values for the pH 4, 14,415 ppm PAAm, 24.3 ppm dimer uptake run (dimupt2, Table 6.1) with the initial data excluded.

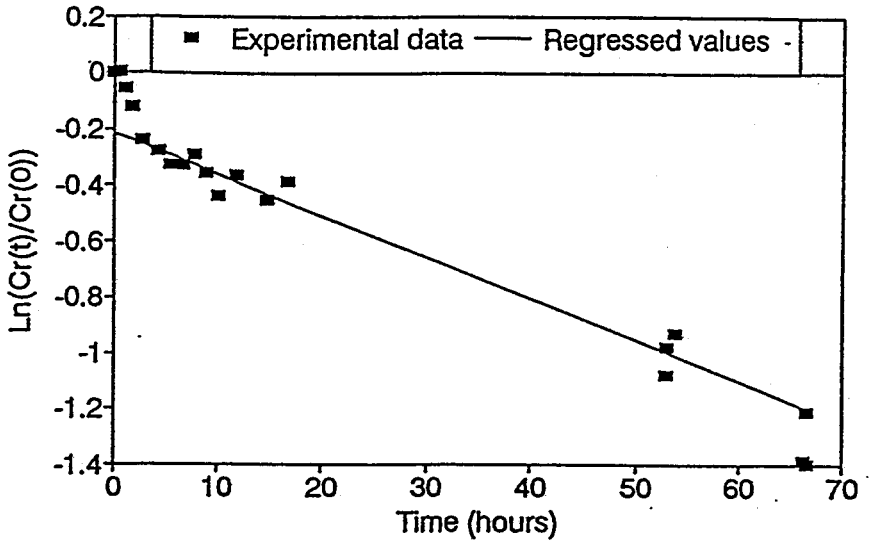

Figure 6.43 : Comparison of the experimental and regressed 1st order ln(Cr(t)/Cr(O)) values for the pH 4, 19,274 ppm PAAm, 17.3 ppm dimer uptake run (dimupt3, Table 6.1) with the initial time data excluded.

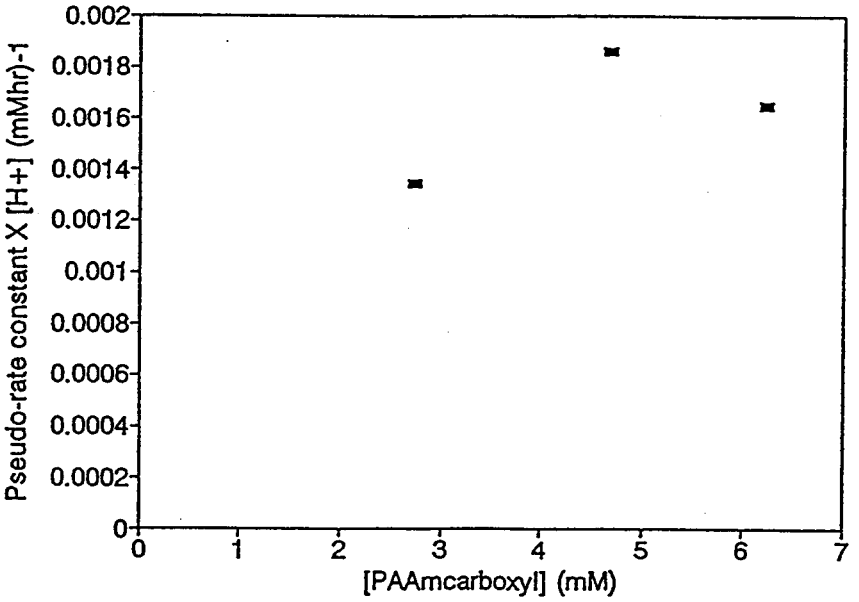

Figure 6.44 : Plot of the products of $[H^+]$ and the 1st order Cr(III) pseudo-rate constant values versus PAAmcarboxyl concentration for the pH 4 dimer regressions with the exclusion of the initial data.

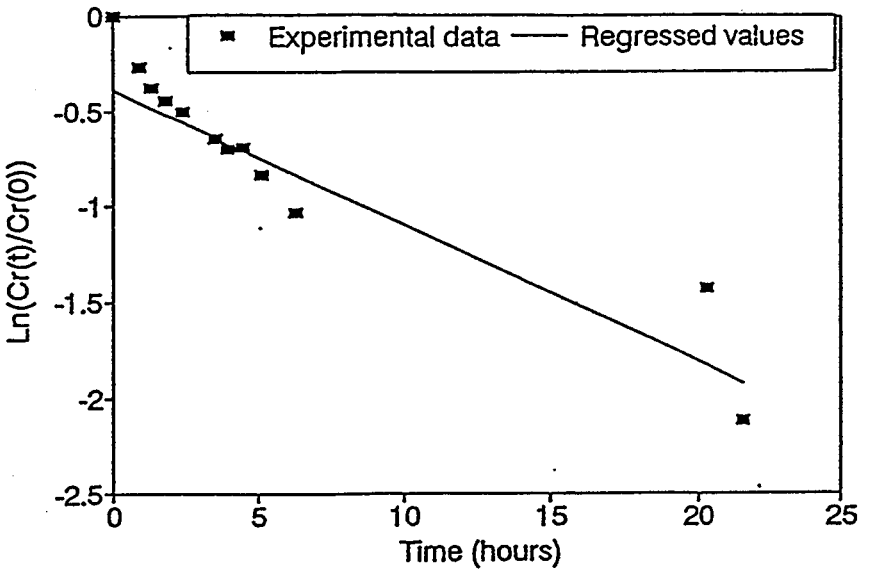

Figure 6.45 : Comparison of the experimental and regressed 1st order ln(Cr(t)/Cr(O)) values for the pH 5, 15,050 ppm dimer uptake run (dimupt4, Table 6.1).

Consideration of Other Factors of Potential Importance in the Modelling of the Uptake Data

The lack of fit of the ERLO model to the dimer and trimer data indicated that a more sophisticated model was necessary to describe the oligomer-PAAm uptake processes in these systems. Several situations were possible contributors to the deviations of the experimental data from the model. The first was the possibility of significant oligomerization to uptake rate ratios. The amounts of oligomer products predicted from the oligomerization experiments in the absence of PAAm (Table 6.7) indicated the possibility that the uptake was occurring from a mixture of different size oligomers reacting with the PAAm, particularly in the pH 5 monomer run and the dimer and trimer runs.

In order to assess the effect of oligomerization on the uptake reactions, a second order Cr(III) dependence was assumed. This is the Cr(III) order expected in the limiting case where the oligomerization reaction is rapid compared to the uptake reaction (Dona, 1993). Assuming constant PAAmcarboxyl and H^+ concentrations, and elementary reactions between the oligomer product, the dimer, and the PAAmcarboxyl groups, the uptake is described by Eqn. 6.15.

$$\frac{\frac{Cr_i(0)}{Cr_i(t)}-1}{Cr_i(0)} = k''_{2i}t \qquad (6.15$$

Although the monomer pH 4 data was fit well by the ERLO model, linear regressions were performed on the pH 4 monomer $(Cr_i(0)/Cr_i(t)-1)/Cr_i(0)$ values versus time to assess the sensitivity of the data to the Cr(III) rate order. As seen from Figures 6.46 and 6.47 and Table 6.10, the second-order Cr(III) fits resulted in goodness of fit values that were comparable to the first order Cr(III) fits. In addition, the plots of $k'_2[H^+]$ versus PAAmcarboxyl concentration were linear with a goodness of fit (0.946) comparable to the first order goodness of fit (0.944) (Figure 6.48). This indicated that modelling of the data was fairly insensitive to the Cr(III) order over the 0-50% uptake range modelled in the pH 4 monomer runs. However, even with the improved early time fits, the lack of fit significance probabilities with the second order Cr(III) fits are generally worse, with the 14,597 ppm PAam run having a significant lack of fit at 6.5% significance probability. Combined with the low amounts of dimer predicted in the pH 4 monomer uptake gelling solutions (Table 6.7), the lower lack of fit significance probabilities suggested that the more likely reason for the ERLO model underprediction of the initial data was a temporary continuation of the rapid uptake during gelling solution preparation. This hypothesis is supported by the relatively large amounts of oligomers reacted with the PAAm during gelling solutions preparation (Table 6.11) and the small but consistent ERLO model underprediction of the experimental data for the initial uptake measurements (Figures 6.31 and 6.32).

Table 6.10 Comparison of the statistics for the first order and second order Cr(III) fits to the pH 4 monomer uptake data

Run no.	First order zero-time Cr(t)/ Cr(0) inter-cept	Second order zero-time Cr(t)/ Cr(0) inter-cept	r^2, first order	r^2, second order	First order, lack of fit signifi-cance probability (%)	Second order lack of fit signifi-cance proba-bility (%)
monupt1	1.002	1.007	0.945	0.932	29	10
monupt2	0.981	0.988	0.960	0.962	61	73
monupt3	1.014	1.027	0.961	0.961	19	6.5
monupt4	0.977	0.991	0.956	0.956	41	33

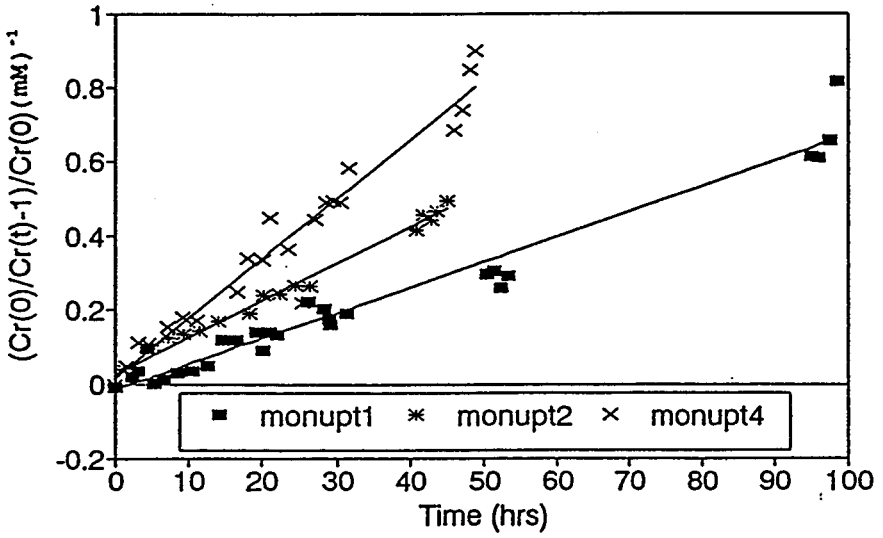

Figure 6.46 : Plots of the experimental and second order (Cr(0)/Cr(t)-1/Cr(0)) values for the pH 4 monomer uptake runs at different PAAm concentrations (see Table 6.1 for descriptions of the experimental conditions for the individual runs).

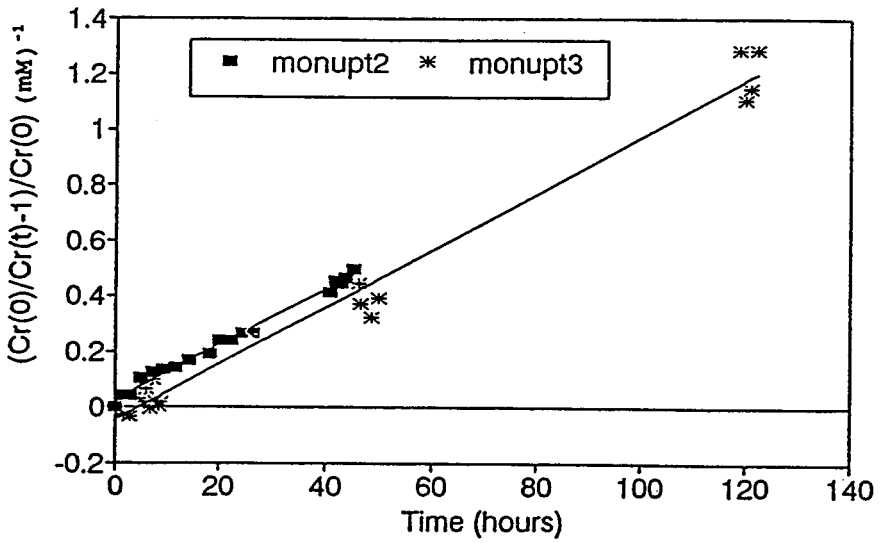

Figure 6.47 : Plots of the experimental and second order (Cr(0)/Cr(t)-1/Cr(0)) values for the pH 4 monomer uptake replicate runs (see Table 6.1 for descriptions of the experimental conditions for the individual runs).

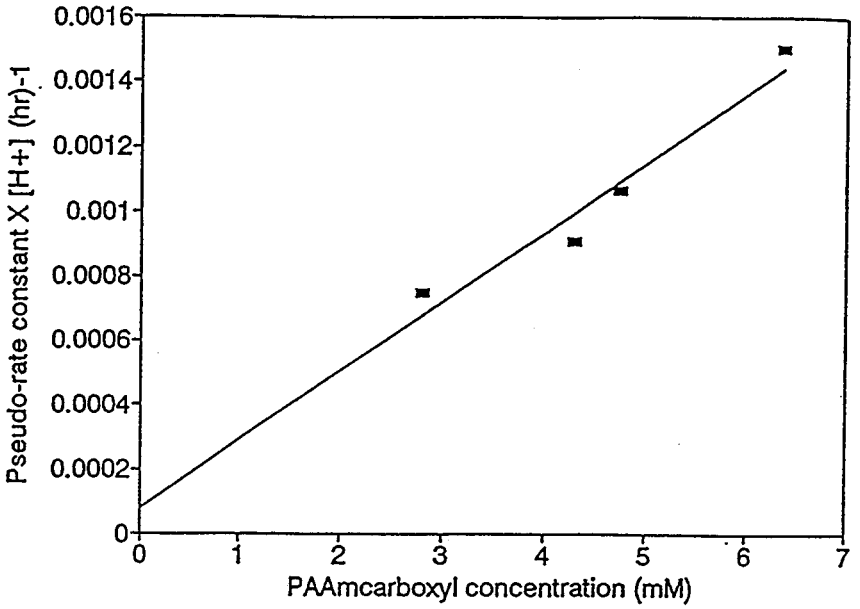

Figure 6.48 : Plot of the second order Cr(III) pseudo-rate constant values versus PAAmcarboxyl concentration.

Table 6.11 Comparison of the amounts of oligomers reacted during gelling solution preparation

[PAAm] (ppm)	pH	% monomer reacted immediately after gel preparation	% dimer reacted immediately after gel preparation	% trimer reacted immediately after gel preparation
4,433	4			18
8,427-8,782	4	2%	8%	26
13,153-14,415	4	6	4	40
19,274-19,908	4	6	10	
14,045-15,050	5	5	30	90

Although relatively low amounts of oligomerization products were predicted in the pH 4 monomer gelling solutions, the oligomerization results predicted that in the pH 5 monomer solution, approximately 33% of the solution and/or attached monomer was dimer at the end of the uptake data collection time period (Table 6.7). The presence and the relatively rapid uptake rates of the dimer are possible explanations for the higher ERLO k'(op) value in the pH 5 monomer run (previous section).

As with the monomer runs, the effects of oligomerization were assessed for the dimer runs by assuming a second order Cr(III) dependence. Eqn. 6.15 was then used to perform linear regressions of the (Cr(0)/Cr(t)-1)/Cr(0) values versus time. The statistical results in Table 6.12 and the comparison of the experimental and regressed (Cr(0)/Cr(t)-1)/Cr(0) values in Figures 6.49-6.51 show significantly better fits of the Cr(III) data than the first order Cr(III) fits. In addition, the good linear fit of the $k^{*}_{2}[H^{+}]$ values with PAAmcarboxyl concentration (goodness of fit of 0.940) (Figure 6.52) indicates that the elementary reaction model with rapid oligomerization gave significantly better fits to the dimer pH 4 data than the ERLO model.

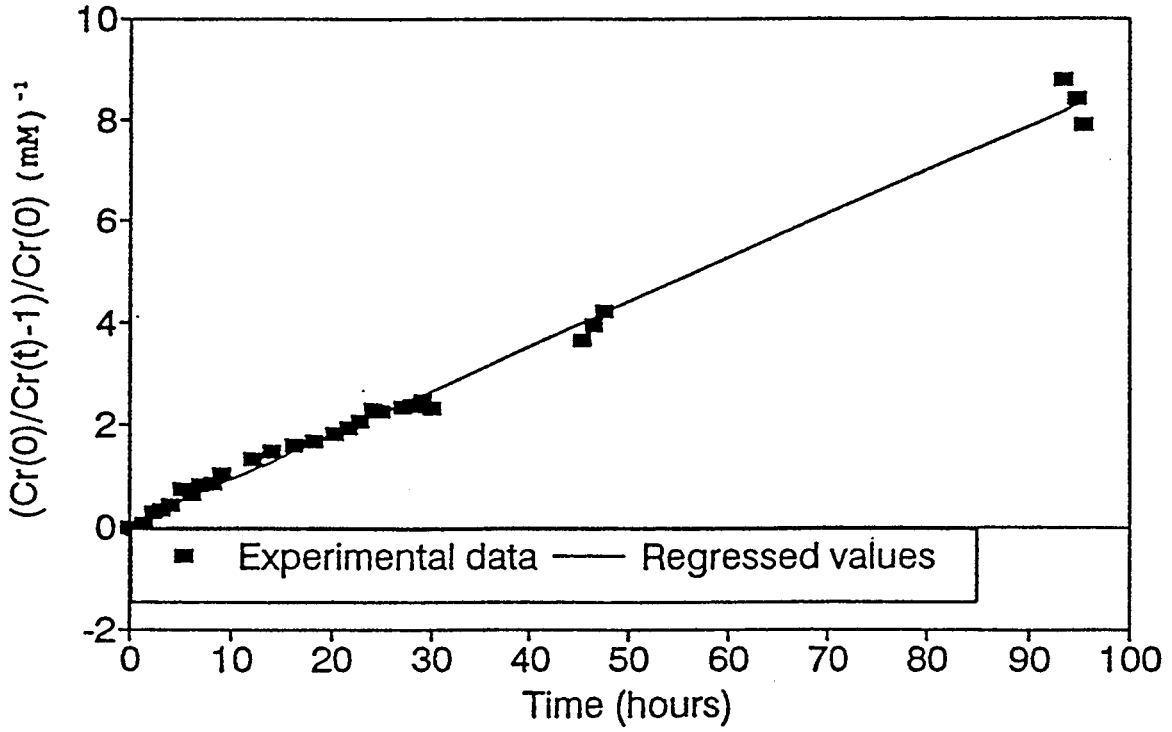

Figure 6.49 : Comparison of the experimental and regressed 2nd order (Cr(0)/Cr(t)-1)/Cr(0) values for the pH 4, 8,427 ppm PAAm, 25.3 ppm dimer uptake run (dimupt1, Table 6.1).

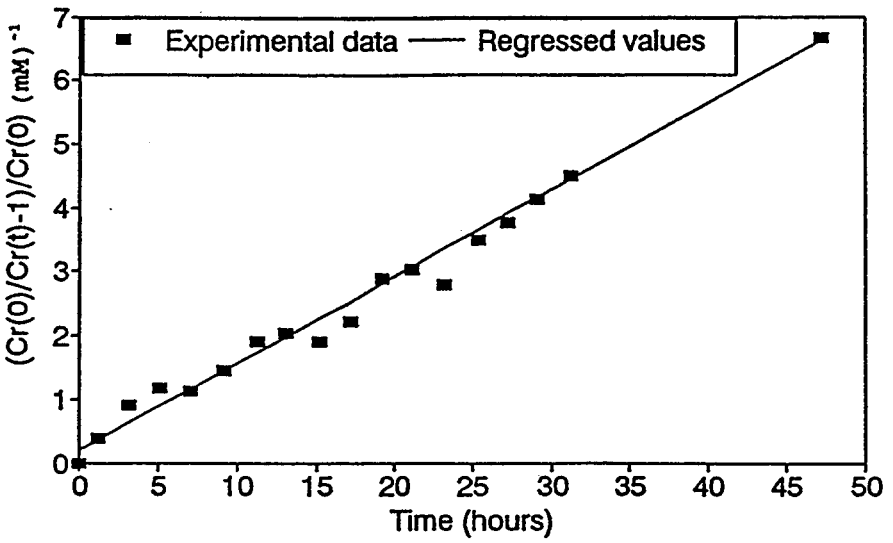

Figure 6.50 : Comparison of the experimental and regressed 2nd order (Cr(0)/Cr(t)-1)/Cr(0) values for the pH 4, 14,415 ppm PAAm, 24.3 ppm dimer uptake run (dimupt2, Table 6.1).

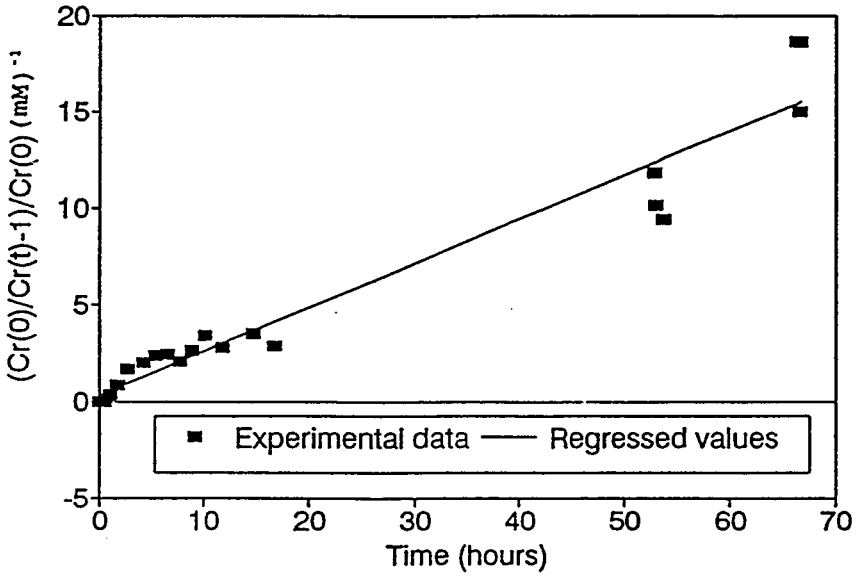

Figure 6.51 : Comparison of the experimental and regressed 2nd order (Cr(0)/Cr(t)-1)/Cr(0) values for the pH 4, 19,274 ppm PAAm, 17.3 ppm dimer uptake run (dimupt3, Table 6.1).

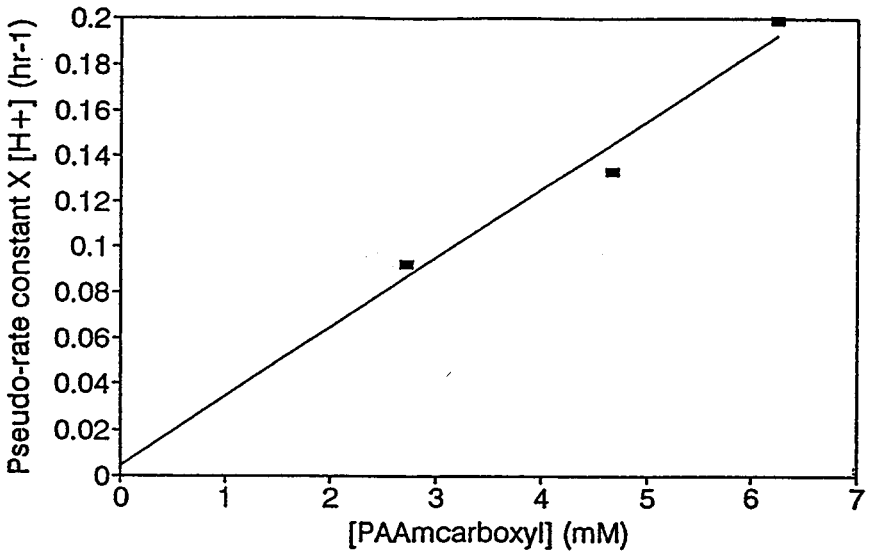

Figure 6.52 : Plot of the products of $[H^+]$ and the second order Cr(III) pseudo-rate constant values versus PAAmcarboxyl concentration for the pH 4 dimer regressions.

Table 6.12 Statistical results for the second order Cr(III) fit to the pH 4 dimer uptake data

Run No.	[PAAm] (ppm)	r^2	$k^{\cdot}_4$ $(mMhr)^{-1}$	Second order Cr(III) lack of fit F ratio	Lack of fit significance probability (%)
dimupt1	8,427	0.960	0.0919	0.767	79
dimupt2	14,415	0.940	0.133	0.688	77
dimupt3	19,274	0.82	0.198	3.5	1

Although the fit of the second order Cr(III), elementary reaction model gave reasonable fits to the dimer pH 4 data, two other situations could also explain the deviation of the experimental data from the ERLO model. The first is continuation of the relatively rapid uptake occuring during gelling solution preparation into the initial uptake time periods. The second situation is potential differences between the stabilities of the dimer and the immediate oligomer product, the tetramer. The equilibrium oligomer concentration curve for 50 ppm Cr(III) (0.001 M) (Figure 6.53) calculated by Stunzi et al. (1989) indicates that at pH 4, the tetramer is expected to be the most stable oligomer form, with the dimer being the least stable. Assuming the uptake rates of the dimer are significantly faster than those of the tetramer, the relatively fast uptake rates at early time could be due primarily to dimer uptake, whereas the slower rates at relatively long times could be due to the potentially slower tetramer uptake rates.

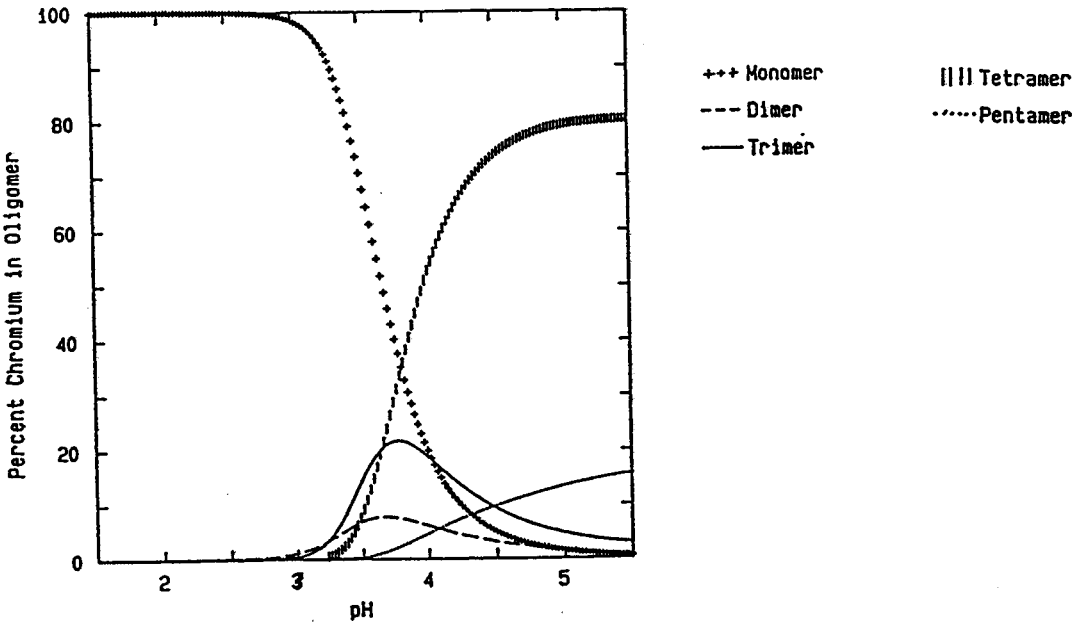

Figure 6.53 : Calculated equilibrium distribution of the different oligomers as a function of equilibrium pH for a solution with $[Cr_{total}$ = 0.001 M
(from Stunzi et al., 1989)

The possibility of significant oligomerization occuring for the conditions used in the pH 4 trimer runs was also indicated by the oligomerization results (Table 6.7) and was explored by performing regressions on the pH 4 trimer (Cr(0)/Cr(t)-1)/Cr(0) values versus time. The plots of the experimental and regressed (Cr(0)/Cr(t)-1)/Cr(0) values (Figures 6.54-6.56) and the statistical results (Table 6.13) indicate that although the model fits are better with the second order Cr(III) dependence, significant deviations still existed.

Table 6.13 Lack of fit significance probablities for the second order Cr(III) fit to trimer uptake data.

Run no.	[PAAm] (ppm)	r^2	Second order Cr(III) lack of fit F ratio	Lack of fit significance probability (%)
triupt1	4,433	0.915	10.95	≤.01
triupt2	8,633	0.87	5.34	≤.01
triupt3	13,153	0.81	7.39	≤.01

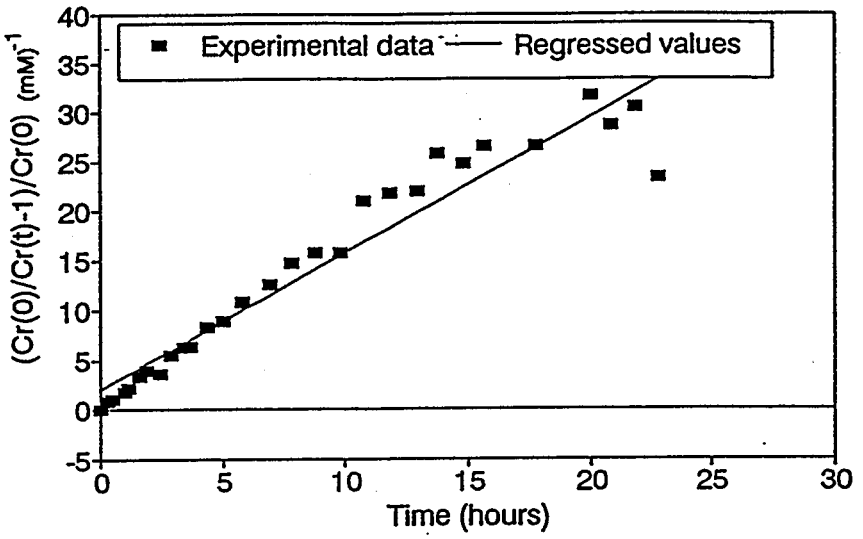

Figure 6.54 : Comparison of the experimental and regressed 2nd order (Cr(0)/Cr(t)-1/Cr(0) values for the pH 4, 4,433 ppm PAAm, 24.7 ppm trimer uptake run (triupt1, Table 6.1).

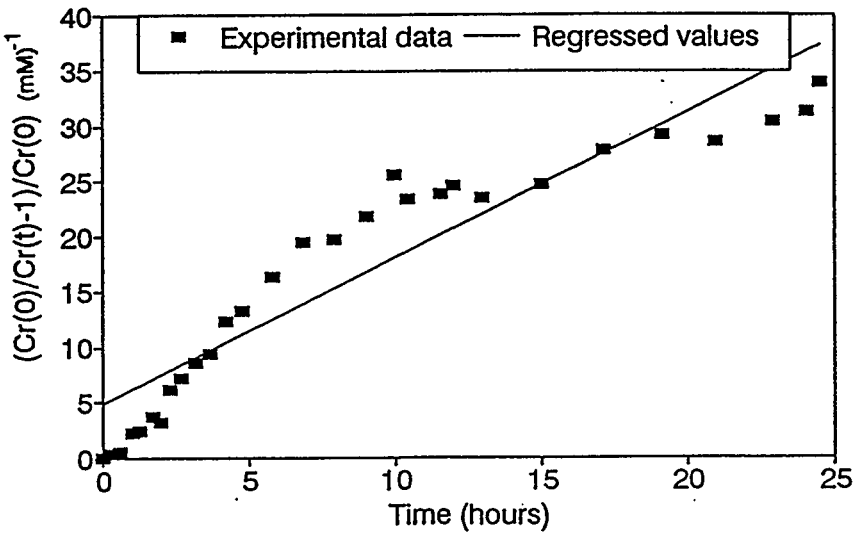

Figure 6.55 : Comparison of the experimental and regressed 2nd order (Cr(0)/Cr(t))-1 values for the pH 4, 8,633 ppm PAAm, 24.1 ppm trimer uptake run (triupt2, Table 6.1).

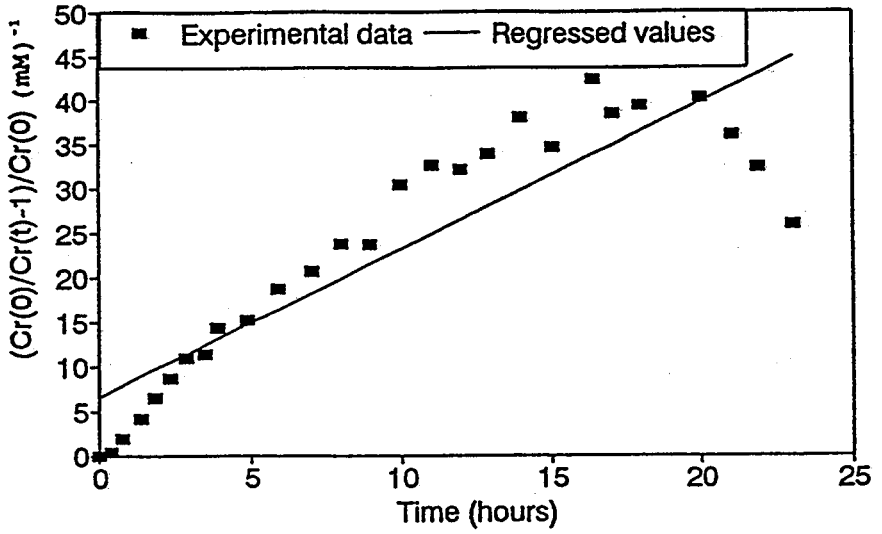

Figure 6.56 : Comparison of the experimental and regressed second order (Cr(0)/Cr(t)-1)/Cr(0) values for the pH 4, 13,153 ppm PAAm, 22.8 ppm trimer uptake run (triupt3, Table 6.1).

As with the monomer and dimer uptake runs, the possibility existed that the initial high uptake rates were due to a temporary continuation of the rapid uptake occuring during gelling solution preparation. The potential for this possibility is reinforced by the relatively high amounts of trimer reacted during gelling solution preparation (Table 6.11).

Two additional situations were possible explanations for the lack of fit of the trimer uptake data to the ERLO model. The calculations of Stunzi et al (1989) for a 50 ppm Cr(III) in the absence of PAAm (Figure 6.52) indicate that residual amounts of the trimer as well as the tetramer remain in equilibrium at pH 4. The relatively high stabilities of the trimer and tetramer indicate the possibility that free-solution trimer and tetramer concentrations could exist in equilibrium with the oligomers bound to the PAAm. This hypothesis is supported by the long-term uptake studies on a series of monomer and dimer gelling solutions (Dona, 1993). As seen in Table 6.14, between 6 and 8% of the original Cr(III) in the gelling solutions was found to remain free in solution for reaction times up to 331 days (Dona, 1993).

Table 6.14 Long-term fractional free Cr(III) concentrations of selected gelling solutions (from Dona, 1993).

Species	pH	[Cr(III)] (ppm)	[PAAm] (ppm)	Reaction time (days)	Final [Cr(t)]/ [Cr(total)]
monomer	4	25	13,320	76	0.089
monomer	4	23	15,200	331	0.061
monomeric salt	5	100	18,000	8	0.079
monomeric salt	5	100	18,000	484	0.071
dimer	4	24	14,415	111	0.067
trimer	4	23	13,153	13	0.069

A second situation which could contribute to the lack of fit of the trimer data to the ERLO model was mass transfer limitations on the trimer uptake reactions. This potentially could occur because the viscosities of the gelling solutions increased with time, raising the possibility that the uptake rates could be limited by the speed at which the oligomer molecules could diffuse to the PAAmcarboxyl groups. The quantitative effect of the gelling solution viscosity changes on the uptake rates was not assessed because of the time required to determine gelling solution viscosities as functions of time and the lack of knowledge concerning the diffusion coefficient of the trimer as a function of the gelling solution viscosities. However, the work of Brown and Chitumbo (1975), where the diffusion coefficients of small salt molecules in PAAm gels were approximately an order of magnitude less than the comparable diffusion coefficients in water, indicates the possibility that mass transfer limitations on the uptake reaction could exist, particularly for the trimer gelling solutions where the changes in viscosity were relatively rapid.

Effects of Brine Type and/or Concentration on the Uptake Rates

Hunt (1987) performed experiments using the same basic Cr(III)-PAAm system used here but with a 0.1 M KNO_3 brine. Preliminary uptake experiments using the Hunt basic system of 5,000 ppm, 50 ppm Cr(III), 0.1 M KNO_3, and pH 5 indicated that significantly lower uptake rates occured in runs using 1 M $NaClO_4$ brine (Dona, 1993). In order to further investigate the effect of brine anion type and/or concentration on the uptake rates, the $k_1(ol)$ value for the pH 4, 5,000 ppm PAAm, 50 ppm Cr(III) system of Hunt was calculated and compared against the $k_1(ol)$ obtained from the pH 4 monomer runs.

The pH 4, 5,000 ppm PAAm, 50 ppm Cr(III) system of Hunt was chosen for comparison purposes since it was the most likely to have low oligomerization to uptake rate ratios. Hunt used the same type and lot of PAAm used here (cat. 18,127-7, Lot 9; nominal MW 5-6,000,000, carboxyl content of 2.3%) and initially monomeric $Cr(NO_3)_3$ solutions. The pH of the gelling solution was maintained at pH 4 by the addition of small amounts of base. Hunt followed the Cr(III) uptake up to a fractional free Cr(III) concentration of 0.81. Assuming that the pH 4 oligomerization to uptake rate ratio in 0.1 M KNO_3 was the same as the rate ratio in 1 M $NaClO_4$, it was estimated that 26% of the Cr(III) was dimer at the end of Hunt's data collection time period. Using the PAAm carboxyl content of 2.3%, assuming that all

PAAm-attached oligomer was monomeric, and each Cr(III) molecule was attached to one PAAmcarboxyl group, 89% of the PAAmcarboxyl sites remained at the end of data collection.

Assuming first order Cr(III) and PAAmcarboxyl dependencies and constant PAAmcarboxyl concentrations, Eqn. 6.14 was used to perform a linear regression on the ln([Cr(t)]/[Cr(0]) values versus time. The experimental and regressed ln([Cr(t)]/[Cr(0)]) values are shown in Figure 6.57. Using a $[H^+]$ value of 10^{-4} M and a PAAmcarboxyl concentration of 1.62 mM, a $k_1(ol)$ of 1.43 X 10^{-3} hr^{-1} was obtained. This value was approximately 13 times larger than the $k_1(ol)$ of 1.07 X 10^{-4} hr^{-1} obtained from the pH 4 monomer runs performed here with 1 M $NaClO_4$. The higher Hunt rate constant could partially be attributed to the presence of dimer in the gelling solution. However, the increase due to dimer uptake was expected to be relatively small since a 55% increase in $k_1(op)$ was found in the pH 5 uptake run where approximately 33% of the monomer was dimer at the end of the data collection time period (previous section). This implied that the majority of the increase in the Hunt $k_1(ol)$ rate constant was due to the differences in brine anion type and/or concentration. The trend of faster Cr(III)-PAAm uptake reactions in 0.1 M nitrate brines as compared to 1 M perchlorate brine is consistent with the recent data of McGuire (1993) who has found that the gelation times in 0.1 M $NaNO_3$ are approximately 10 times faster than those in 1 M $NaClO_4$.

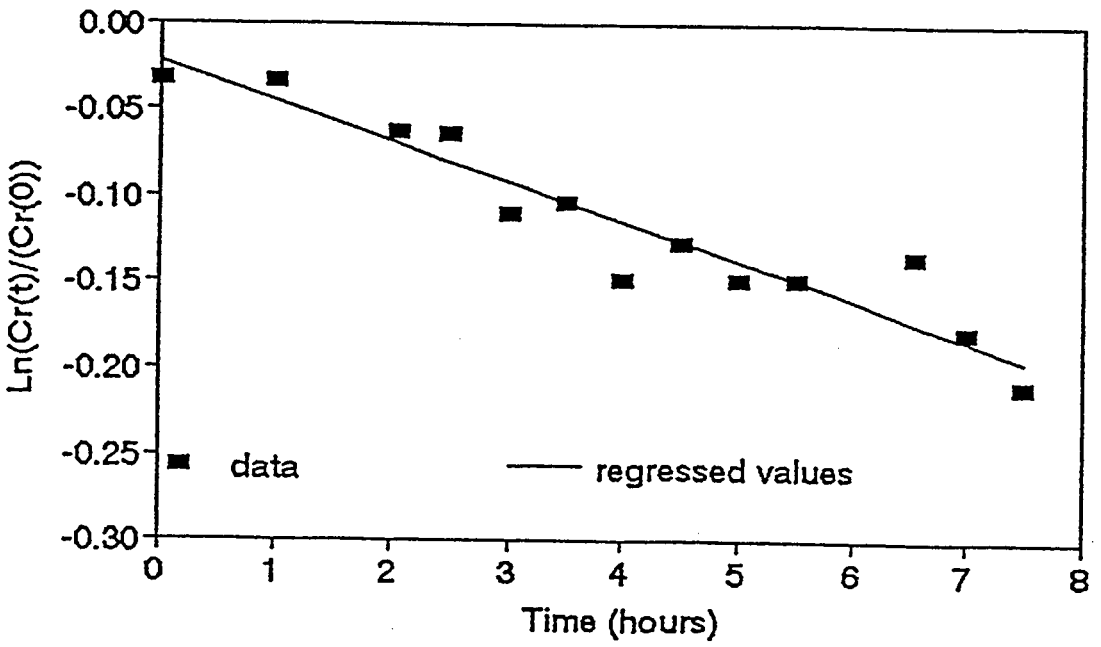

Figure 6.57 : Experimental and regressed ln(Cr(t)/Cr(0)) values for the Hunt pH 4, 50 ppm Cr(III), 5,000 ppm PAAm uptake run (1987).

REFERENCES

Besso, C., "Etude Cinetique et Mecanistique de la Dimerisation du Dimer Du Cr(III), Doctural Dissertation, University of Neuchatel, 1983.

Bhaskar, R. "Transient Rheological Properties of Chromium/Polyacrylamide Solutions under Superposed Steady and Oscillatory Shear Strains", Doctoral Dissertation, 1988, Univ. of Kansas.

Billheimer, J.S. and Parrette, R. "Apparatus for Automatic Determination of Gel Time", Analytical Chemistry, 1956, 28, 272-278.

Dolan, D.M. "An Experimental Study of the Effect of pH and Shear on the Gelation of a Xanthan-Chromium(III) Solution", Master's Thesis, University of Kansas, 1989.

Dona, C.L.G. "An Experimental Study of the Uptake and Gelation Reactions of Cr(III) Oligomers with Polyacrylamide", Doctoral Dissertation, University of Kansas, September 1993.

Dona, C.L.G. "Chapter 4 Kinetics of Cr(III) Species Formation and Uptake by Polyacrylamide (PAAm)" in Gelled Polymer Systems for Permeability Modification in Petroleum Reservoirs by Willhite, G.P, Green, D.W., Thiele, J.T., McCool, C.S., and Mertes, K.B., DOE/ID/12846-6, 1991.

Dona, C.L.G. "An Experimental Study of the Uptake and Gelation Reactions of Cr(III) Oligomers with Polyacrylamide", Doctoral Dissertation, University of Kansas, 1993.

Fei, R. and Mertes, K.B. "Chapter 2 Chemical Structure of Polymer/Metal Ion Complexes" in Gelled Polymer Systems for Permeability Modification in Petroleum Reservoirs by Willhite, G.P, Green, D.W., Thiele, J.T., McCool, C.S., and Mertes, K.B., DOE/ID/12846-6, 1991.

Fei, R. and Mertes, K.B. Unpublished data, University of Kansas, 1989.

Ferry, J.D. Viscoelastic Properties of Polymers, 3rd edition, 1980, John Wiley and Sons, N.Y., pp 234-5.

Githens, C.J. and Burnham, J.W. "Chemically Modified Natural Gum for Use in Well Simulation" SPEJ, February 1977, pp 5-10.

Green, D.W., Willhite, G.P., and Huang, C.G. "An Experimental Study of the In-Situ Gelation of Chromium (+3)/Polyacrylamide Polymer in Porous Media" SPE Reservoir Eng., 1986, pp 583-592.

Huey. J.E. Inorganic Chemistry: Principles of structure and reactivity, 3rd edition, 1983, Harper and Row, N.Y., Chapter 7.

Hunt, J.A., "An Experimental Study of the Kinetics of the Crosslinking Reaction Between Chromium (III) and Polyacrylamide", Doctoral Dissertation, University of Kansas, 1987.

Jordan, D.S., Green, D.W., Terry, R.E., and Willhite, G.P.,"The Effect of Temperature on Gelation Time for Polyacrylamide-Chromium(III) Systems", SPE 10059, presented at the 56th Technical Conference of SPE of AIME, San Antonio, Texas, October, 1981.

Kansas Department of Health and Environment, "Hazardous Waste Generator Handbook: A Guide to Complying with Kansas Hazardous Waste Generator Regulations", June 1992.

Kolnes, J., Stavland, A., and Thorsen, S. "The Effect of Temperature on the Gelation Time of Xanthan/Cr(III) Systems, SPE paper 21001, presented at the SPE International Symposium on Oilfield Chemistry , Anaheim, California, February 1991.

Lockhart, T.P. "Chemical and Structural Studies on Cr+3/Polyacrylamide Gels", SPE Paper 20998, presented at the SPE International Symposium on Oilfield Chemistry, Anaheim, Claiformia, February 1991.

McGuire, M. Unpublished data, University of Kansas, 1993.

Montanari, M., Gallino, G. and Lockhart, T.E. "Rheological Kinetic Studies of the Gelation of Cr(+3)/Polyacrylamide Solutions", Polymeric Materials Science Proceedings, ACS Division of Polymeric Materials Science Engineering, ACS Spring Meeting, 1992, San Francisco, 66, pp. 58-59.

Prudhomme, R.K. and Uhl, J.T. "Kinetics of Polymer/Metal-Ion Gelation", SPE/DOE Paper 12640, presented at the SPE/DOE Fourth Symposium on Enhanced Oil Recovery, Tulsa, OK, April 1984.

Rotzinger, F.P., Stunzi, H., and Werner, M., "Early Stages of the Hydrolysis of Chromium(III) in Aqueous Solutions. 3. Kinetics of Dimerization of the Deprotenated Aqua Ion", Inorg. Chem. 1986, 25, 489-495.

Shu, P., "The Gelation Mechanism of Chromium(III)", paper presented at the Symposium of Advances in Oil Field Chemistry, Division of Petroleum Chemistry, ACS, June 1988, Toronto, Ont.

Stunzi, H., Spiccia, L. Rotzinger, F.P., and Marty,W., "Early Stages of the Hydrolysis of Chromium(III) in Aqueous Solutions. 4. Stability Constants of the Hydrolytic Dimer, Trimer, and Tetramer at 25 °C and I= 1.0 M", Inorg. Chem. 1989, 28, 66-71.

Sydansk, R.D., "A New Conformance-Improvement-Treatment Chromium(III) Gel Technology", SPE/DOE 17329, presented at the SPE/DOE Enhanced Oil Recovery Symposium, Tulsa, Oklahoma, April, 1988.

Tackett, J.E., "Characterization of Chromium(III) Acetate in Aqueous Solution", Applied Spectroscopy, 1989, 43(3), 490-499.

Terry, R.E., Huang, C.G., Green D.W., Willhite, G.P., and Michnick, M.J. "Correlation of Gelation Times for Polymer Solutions Used as Sweep Improvement Agents", SPEJ, April 1981, pp. 229-235.

Winter, H.H., Polym. Eng. Sci., 1987, 27, pp 1698-1704.

Chapter 7

Bulk Gelation of the KUSP1 Polysaccharide by Ester Hydrolysis

Principal Investigators: Don Green, Paul Willhite, Stan McCool

Graduate Research Assistant: Medie Youogo

INTRODUCTION

KUSP1 is a microbial polysaccharide that dissolves in 1 N NaOH solution and forms a gel as the pH of the solution is lowered below 11. This change of physical state from a solution to a gel is the basis for potential use in permeability modification treatments applied to oil reservoirs.

In situ gelation of KUSP1 in an oil reservoir might be accomplished by adding an ester to the solution. The ester reacts with water to produce acid thus lowering the pH. The objective of the work described in this chapter was to determine the applicability of using an ester to reduce the pH of bulk KUSP1 solutions to cause gelation. Also included in this report is a rheological characterization study of KUSP1 solutions.

BACKGROUND

Two criteria for the selection of an ester to be used to gel KUSP1 solutions are 1) the reaction rate must be relatively slow such that the gelation time is on the order of days, and 2) the ester must be soluble in the KUSP1 solution. Slow reaction rates are required for application of this system to *in-depth* permeability treatments. A commercially-available ester that meet these criteria was not found. However, the ester *ethylbenzoate-2-sulfonic acid* (EBSA) met these criteria and is easily prepared. The chemical structure of EBSA is:

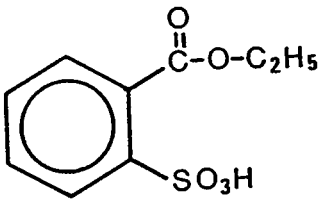

Two acid groups are made available when EBSA is added to NaOH solutions. During mixing, the sulfonic acid group ionizes and lowers the pH of the solution. This reaction is described by an equilibrium acid-base reaction but essentially goes to completion due to the high pH of the solution. The second acid group is made available by the ester hydrolysis reaction according to the following equation:

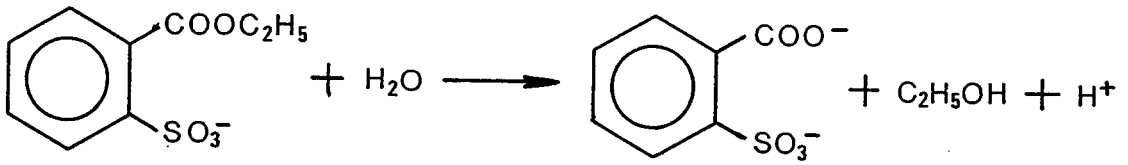

This reaction is relatively slow and provides the means to control the rate of acid production and, thus, gelation of KUSP1.

EXPERIMENTAL APPROACH

Samples of KUSP1 polymer were received as a hydrogel. Concentrations of the polymer in the hydrogel were determined by a standard colorimetric method[1] using glucose standards.

The EBSA ester was prepared by dissolving 2-sulfobenzoic acid cyclic anhydride in ethanol by heating the solution to approximately 50 °C.[2] The mole ratio of anhydride to ethanol was 1:2. The product was a thick yellow-orange syrup that contained the EBSA ester in ethanol. It was assumed that all of the anhydride was converted to EBSA.

Polymer solutions were prepared by mixing the appropriate amounts of polymer (dried or hydrogel), NaCl, 1.00 N NaOH solution and water. Gel samples were prepared by the following procedure. The polymer solution and the EBSA solution were maintained at 25° C. The polymer solution was stirred with a magnetic stir bar to form a deep vortex. The EBSA solution was added dropwise from a syringe on the shoulder of the vortex. Gel would form around the drops EBSA due to localized acidity of the drop. These gel-drops dissolved within 30 minutes.

All samples were kept in a 25° C water bath and were monitored periodically. The pH was measured with a Fisher Accumet pH meter equipped with a combination electrode. One-half milliliter aliquots of the sample were removed for viscosity measurements on a Brookfield micro-viscometer equipped with a cone-and-plate geometry. Viscosities were determined at a shear rate of 11.25 /sec. The viscosity increased rapidly when the samples gelled. A *gel time* was defined as the time when the viscosity reached 100 cp during the rapid increase.

The rheological characterization study was conducted on samples containing selected KUSP1 and NaOH concentrations and 2.0 percent NaCl. Dried polymer was used to prepare theses samples. The samples were maintained at 25° C and viscosities and pH values were measured every two or three days. Viscosity was measured as function of shear stress on a Bohlin CS rheometer using a cone-and-plate geometry (4 degrees, 40 mm diameter).

RESULTS AND DISCUSSION

Rheological Characterization

Eighteen samples were prepared at selected concentrations of polymer and NaOH. All samples contained 2.0 wt. % NaCl. Viscosity as a function shear *stress* were determined with a controlled-stress rheometer. These data are summarized in Table 7.1.

Table 7.1: Viscosity, pH and Color Changes of KUSP1 solutions

NaOH Conc. (wt. %)	KUSP1 concentration (wt %)		
	0.5	1.0	2.0
0.012	insoluble	insoluble	insoluble
0.037	pH_0 = 11.85 pH_{10} = 11.69 μ_0 = 1.826 μ_{10} = 1.252	pH_0 = 11.60 pH_{10} = 11.26 shear-thinning see Figure 7.3	pH_0 = 11.64 pH_{10} = 11.40 shear-thinning see Figure 7.2
0.12	pH_0 = 12.45 pH_{10} = 12.25 μ_0 = 2.609 μ_{10} = 1.686	pH_0 = 12.35 pH_{10} =12.04 μ_0 = 8.292 μ_{10} = 4.183	pH_0 = 12.10 pH_{10} = 11.9 shear-thinning see Figure 7.1
0.37	pH_0 = 13.04 pH_{10} = 12.91 μ_0 = 1.422 μ_{10} = 1.192	pH_0 = 12.92 pH_{10} = 12.86 μ_0 = 2.209 μ_{10} = 1.405 change to yellow after 10 days	pH_0 = 12.95 pH_{10} = 12.85 μ_0 = 6.665 μ_{10} = 3.967 change to yellow after 2 days, then to brown
1.2	pH_0 = 13.35 pH_{10} = 13.11 μ_0 = 1.246 μ_{10} = 1.119	pH_0 = 13.21 pH_{10} = 13.06 μ_0 = 1.677 μ_{10} = 1.255 change to yellow after 2 days, then to brown	pH_0 =13.29 pH_{10} = 13.25 μ_0 = 3.414 μ_{10} = 1.780 change to yellow after 2 days,then to brown
3.7	pH_0 = 13.67 pH_{10} = 13.41 μ_0 = 1.352 μ_{10} = 1.206	pH_0 = 13.62 pH_{10} = 13.53 μ_0 = 2.168 μ_{10} = 1.722 change to yellow after 2 days,then to brown	pH_0 = 13.55 pH_{10} = 13.52 μ_0 = 4.000 μ_{10} = 2.141 change to yellow after 2 days, then to brown

pH_0 = initial pH; pH_{10} = pH at 10 days

μ_0 = initial viscosity (cp); μ_{10} = viscosity at 10 days (cp)

Viscosity measured at shear stress of 0.12 Pa.

The initial pH and the pH at 10 days are listed in Table 7.1 as pH_0 and pH_{10}, respectively. In all cases, the pH decreased with time. Part of the pH drop could be caused by dissolution of atmospheric CO_2 when the containers were opened.

The viscosity of samples that were weak functions of shear rate (shear rates between approximately 10 to 200 /sec) are listed in Table 7.1. μ_0 and μ_{10} are the viscosities (@ shear stress of 0.12 Pa) of these samples at 0 and 10 days, respectively. The viscosities of most of these samples were still decreasing with time at the end of 10 days.

Samples prepared in 0.012 wt.% NaOH did not dissolve. Samples prepared with 1.0 and 2.0 percent polymer and at NaOH concentrations of 0.37 wt.% and greater changed color over the 10 day period. The cause of this color change is unknown.

Viscosity measurements on samples containing 2.0 percent polymer in 0.037 and 0.12 wt.% NaOH exhibited shear-thinning behavior as shown in Figures 7.1 and 7.2. The data are presented in the usual manner of viscosity as a function of shear rate although the data were obtained as a function of shear stress. Viscosity of the 0.12 wt.% NaOH sample sustained shear-thinning characteristic but the value of viscosity at a given shear rate decreased with time (Figure 7.1). The shear-thinning behavior increased with time for the 2.0 percent polymer sample in 0.037 wt.% NaOH as shown in Figure 7.2. Similar increases in shear-thinning behavior were observed for the sample containing 1.0 percent polymer and 0.037 wt.% NaOH (Figure 7.3). No shear thinning behavior was observed for the samples containing 0.5 percent polymer.

The viscosity behavior of KUSP1 solutions is shown in Figure 7.4 where viscosity is plotted as a function of pH. These data were obtained at a shear stress of 0.12 Pa on two-day old samples. The viscosity was less than 7 cp and exhibited near-Newtonian behavior for the 1.0 and 2.0 percent polymer samples that had pH values greater than 12.5. Similar behavior was observed for all samples containing 0.5 percent polymer. As pH was reduced in the 1.0 and 2.0 percent polymer samples, the solutions exhibited increasing shear-thinning behavior that indicated aggregation or structure build-up of the polymer. This aggregation appears to increase until a bulk gel is formed at a pH of 10.8. This aggregation phenomenon could be important to the injection and transport of these solutions through porous media.

The reduction in viscosity of KUSP1 solutions with time might be caused by slow dissolution process whereby the polymer molecules are approaching an equilibrium physical state. If this is the case, preparation of gel solutions from hydrogel stock, rather than dried polymer, might exhibit different time-dependent behavior. It is also possible that chemical changes or that bio-degradation had occurred. Further work is needed to determine the cause of this time-dependent viscosity behavior.

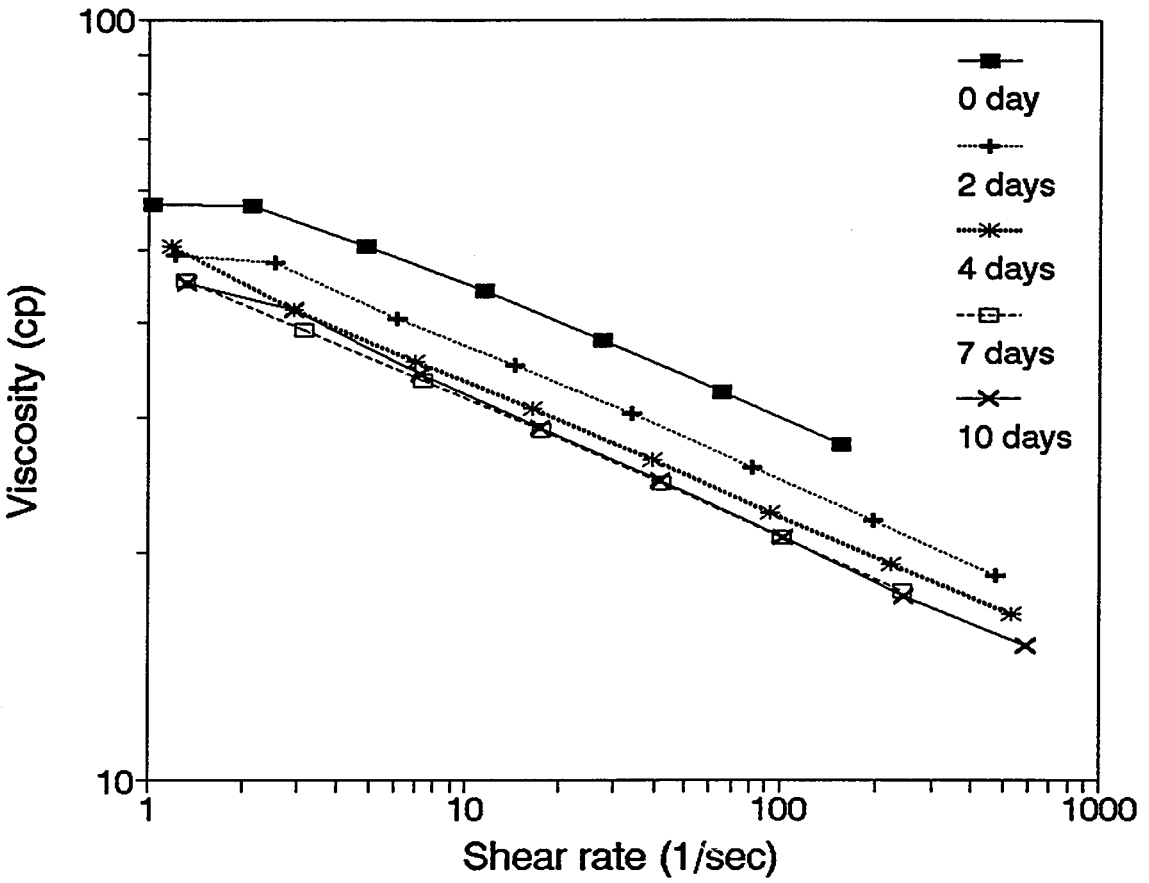

Figure 7.1 : Viscosity as a Function of Shear Rate and Time for Solutions Containing 2.0 % KUSP1 and 0.12 % NaOH.

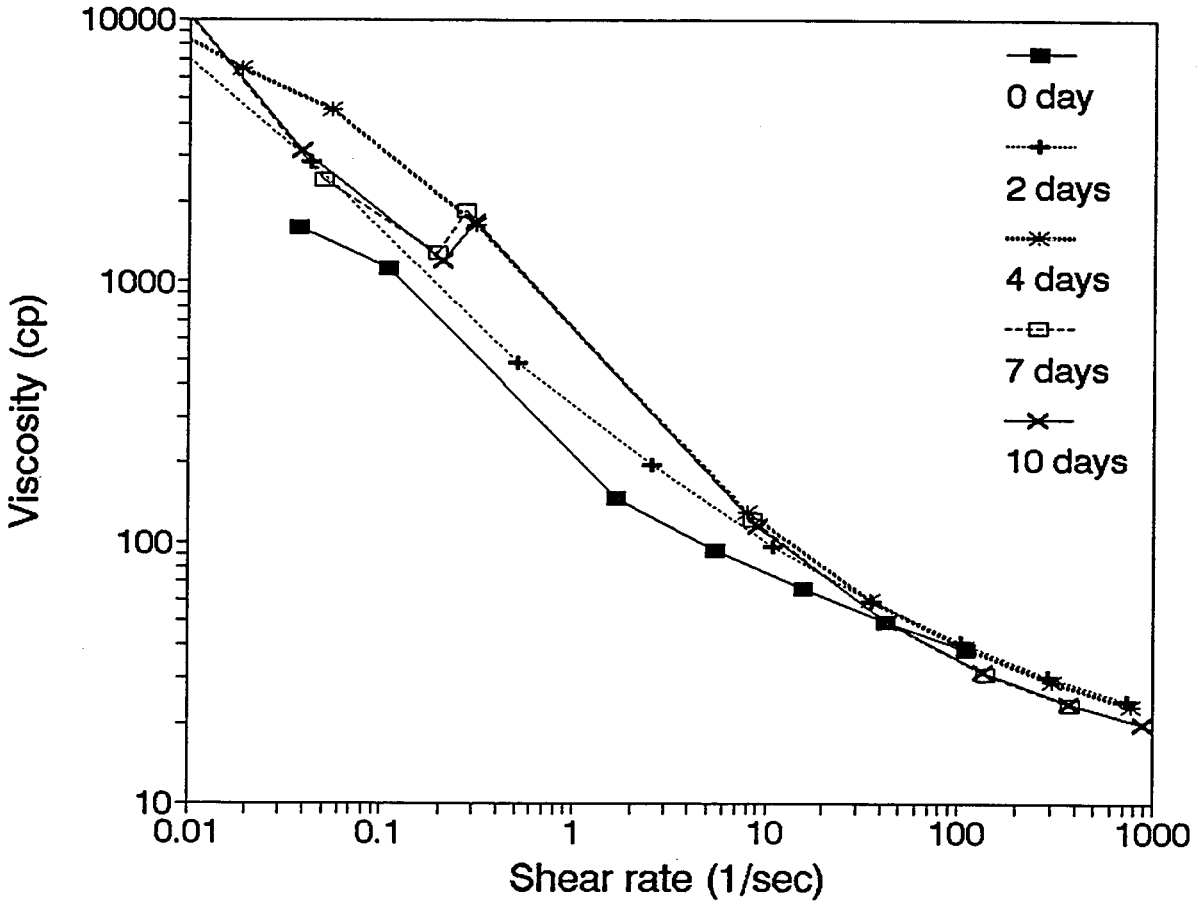

Figure 7.2 : Viscosity as a Function of Shear Rate and Time for Solutions Containing 2.0 % KUSP1 and 0.037 % NaOH.

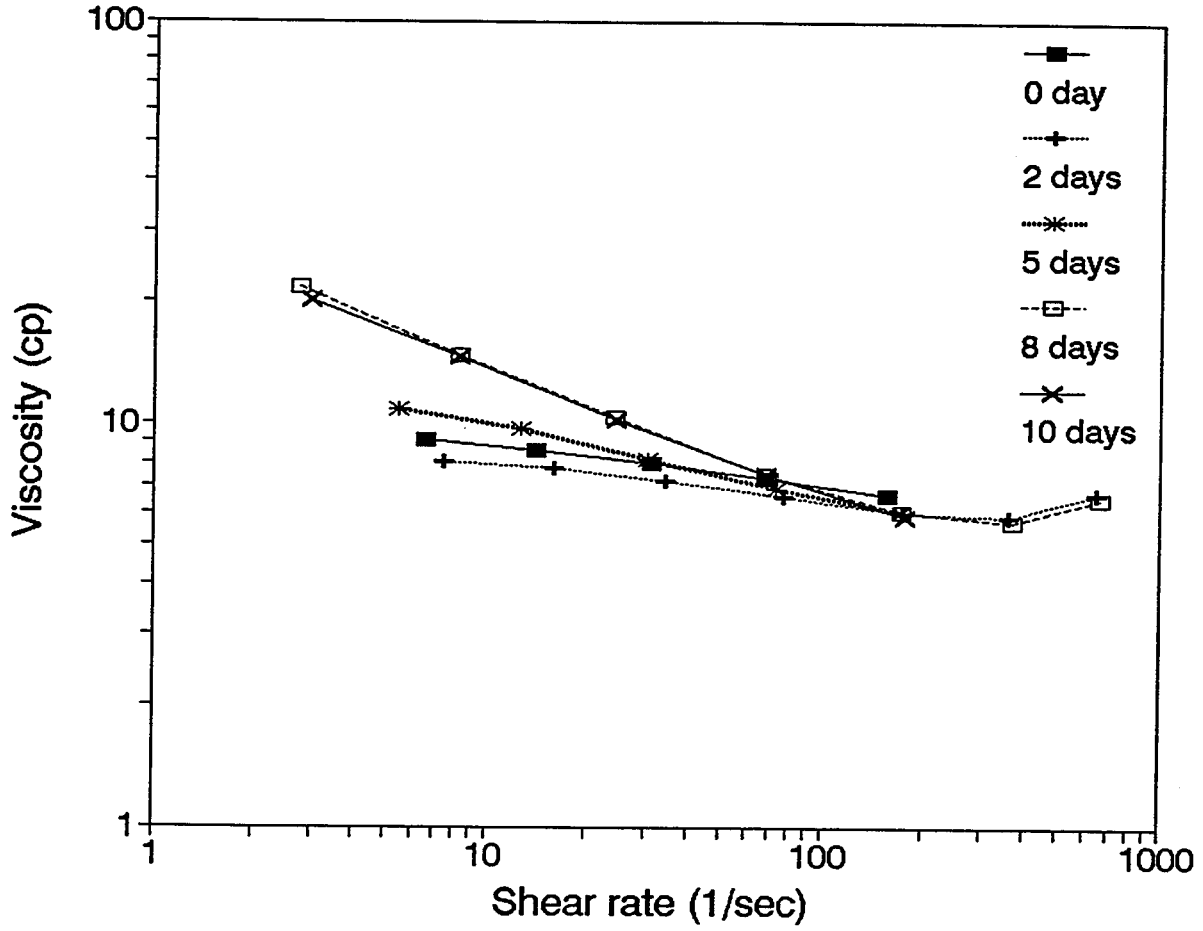

Figure 7.3 : Viscosity as a Function of Shear Rate and Time for Solutions Containing 1.0 % KUSP1 and 0.037 % NaOH.

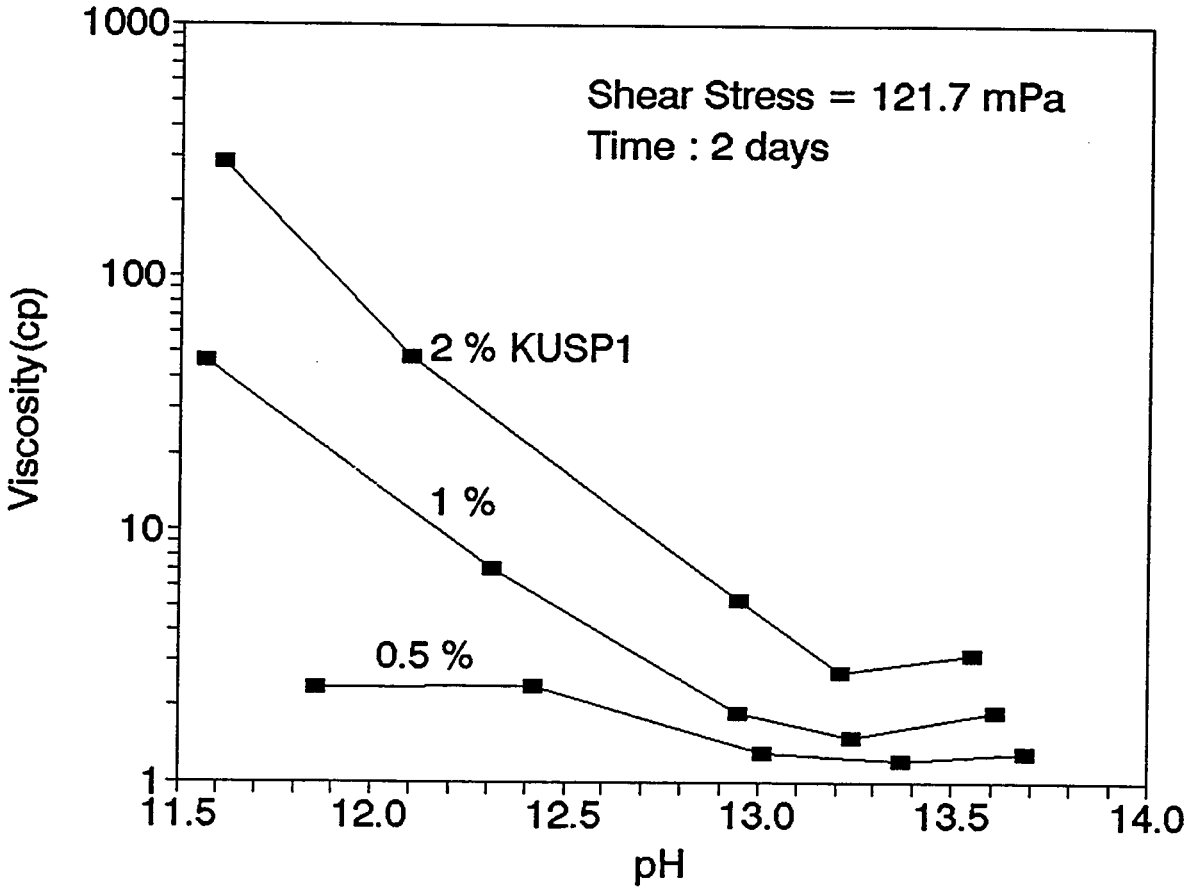

Figure 7.4 : Viscosity as a Function of pH and KUSP1 Concentration for Solutions at an Age of 2 Days.

Bulk Gelation by Ester Hydrolysis

Gelation of an alkali KUSP1 solutions requires the pH of the solution be lowered below the value of approximately 10.8. This reduction in pH was accomplished by the hydrolysis of EBSA. The mole ratio of EBSA to NaOH must be greater than approximately 0.5 to produce gelation since EBSA contributes two hydrogen ions per molecule. Also, the mole ratio of EBSA to NaOH must be lower than approximately 1.0 so that the ionization of the sulfonic acid group does not induce immediate gelation.

Preliminary experiments were conducted to determine the amount of EBSA that is required to achieve a pH value of 10.8 over a time period on the order of days. Selected amounts of EBSA were added to solutions containing 2.0 percent NaCl and 0.384 wt percent NaOH (approximately 0.1 N NaOH). The time to reach a pH value of 10.8 for these solutions are given in Table 7.2.

Table 7.2 : pH Behavior of Ester-NaOH-NaCl Solutions

Mole Ratio ester/NaOH	pH Before Ester Addition	pH After Ester Addition	Time to pH = 10.8 (days)
0.524	12.73	12.44	29
0.786	12.72	11.58	6
1.07	12.72	2.32	immediate
1.30	12.73	1.67	immediate

These data showed that the range of mole ratios of EBSA/NaOH to produce a timed-delayed gelation were between 0.5 and 1.0. The pH of the solutions before and after addition of EBSA are also given in Table 7.2. The pH drop by addition of EBSA was caused by the ionization of the sulfonic acid group. This initial ionization reaction requires a higher concentration of NaOH in the polymer solution.

Gelation of KUSP1 by the hydrolysis of EBSA was investigated. During the preparation of the samples, gel formed around the drops of ester solution as it was added to the polymer solution. This was caused by the localized low pH of the ester solution. Experimental time was started when the gel drops dissolve in the solution which took 30 minutes or less. This mixing procedure could prove difficult under field conditions.

The effects of polymer, NaOH and ester concentrations on the gelation of KUSP1 were investigated. The initial concentrations and gel times are presented in Table 7.3. Gel times ranged from 2 to 11 days for samples containing 0.38 wt % NaOH (approximately 0.1 N NaOH) depending on the polymer and EBSA concentrations. Samples containing 0.12 wt. % NaOH (approx. 0.03 N NaOH) gelled during mixing with EBSA. Viscosity and pH data as a function of time are given in Figures 7.5 through 7.9 for the first 12 runs listed in Table 7.3.

Table 7.3 : Gel Times for Gelation of KUSP1 by Ester Hydrolysis

Run #	Concentrations weight percent			Mole ratio EBSA:NaOH	pH		Gel time (days)
	KUSP1 polymer	NaOH	EBSA ester		Before EBSA addition	After EBSA addition	
53	2.82	0.377	1.70	0.784	12.52	11.16	2
83	2.82	0.376	1.71	0.790	12.55	11.23	2
93	2.82	0.378	1.74	0.800	12.56	11.29	2
52	2.00	0.377	1.73	0.797	12.58	11.49	5
82	2.00	0.376	1.72	0.795	12.60	11.47	5
51	1.00	0.377	1.72	0.793	12.64	11.75	9*
11	0.0	0.374	1.68	0.781	12.70	12.03	5**
23	2.82	0.378	1.35	0.621	12.55	11.92	7
33	2.82	0.381	1.37	0.625	12.53	11.90	8
03	2.82	0.378	1.34	0.616	12.54	11.93	7
02	2.00	0.378	1.34	0.616	12.60	12.09	10
32	2.00	0.381	1.36	0.620	12.59	12.03	11
63	2.82	0.121	0.55	0.79	11.74	10.66	0
62	2.00	0.121	0.55	0.79	11.92	10.71	0
61	1.00	0.121	0.59	0.85	12.09	10.74	0

* 60 cp after 9 days
** Time to reach pH = 10.8

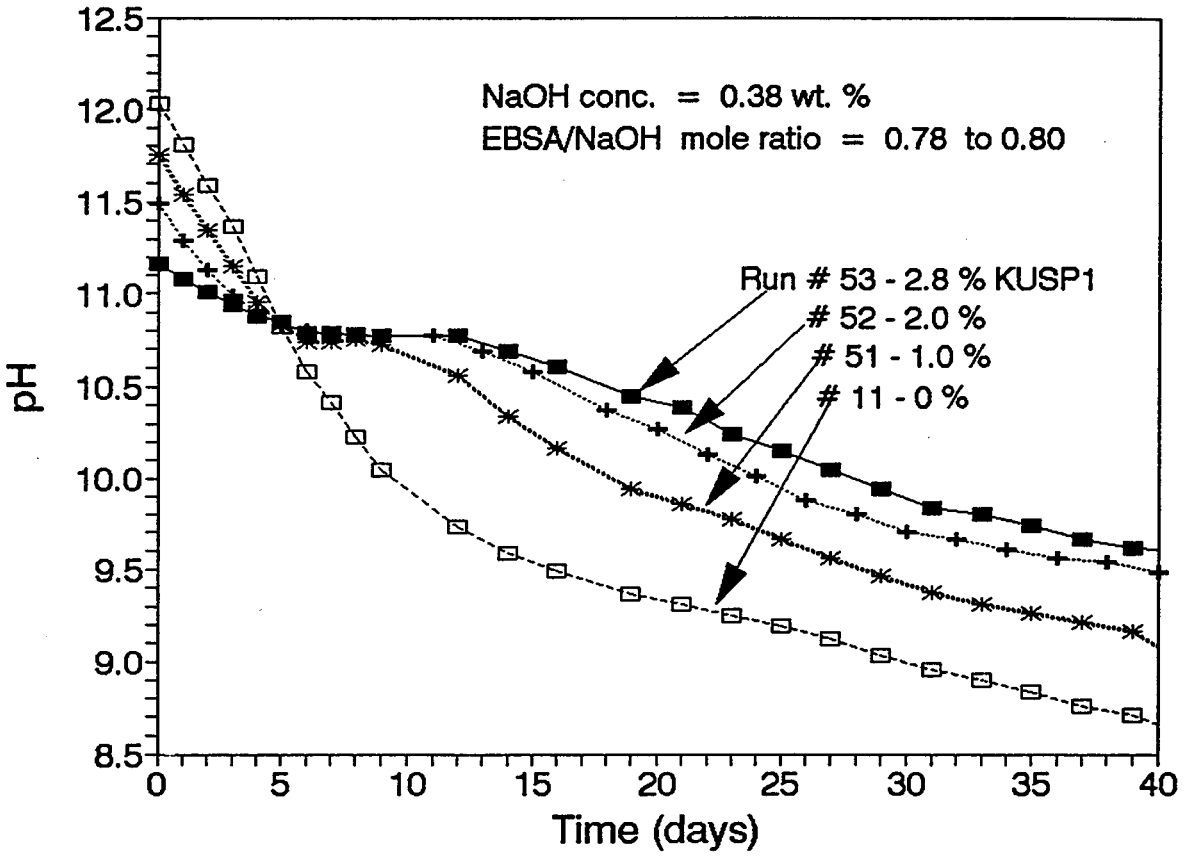

Figure 7.5 : pH-Time Data for KUSP1 Solutions at a Mole Ratio of EBSA/NaOH between 0.78 and 0.80 - Part 1.

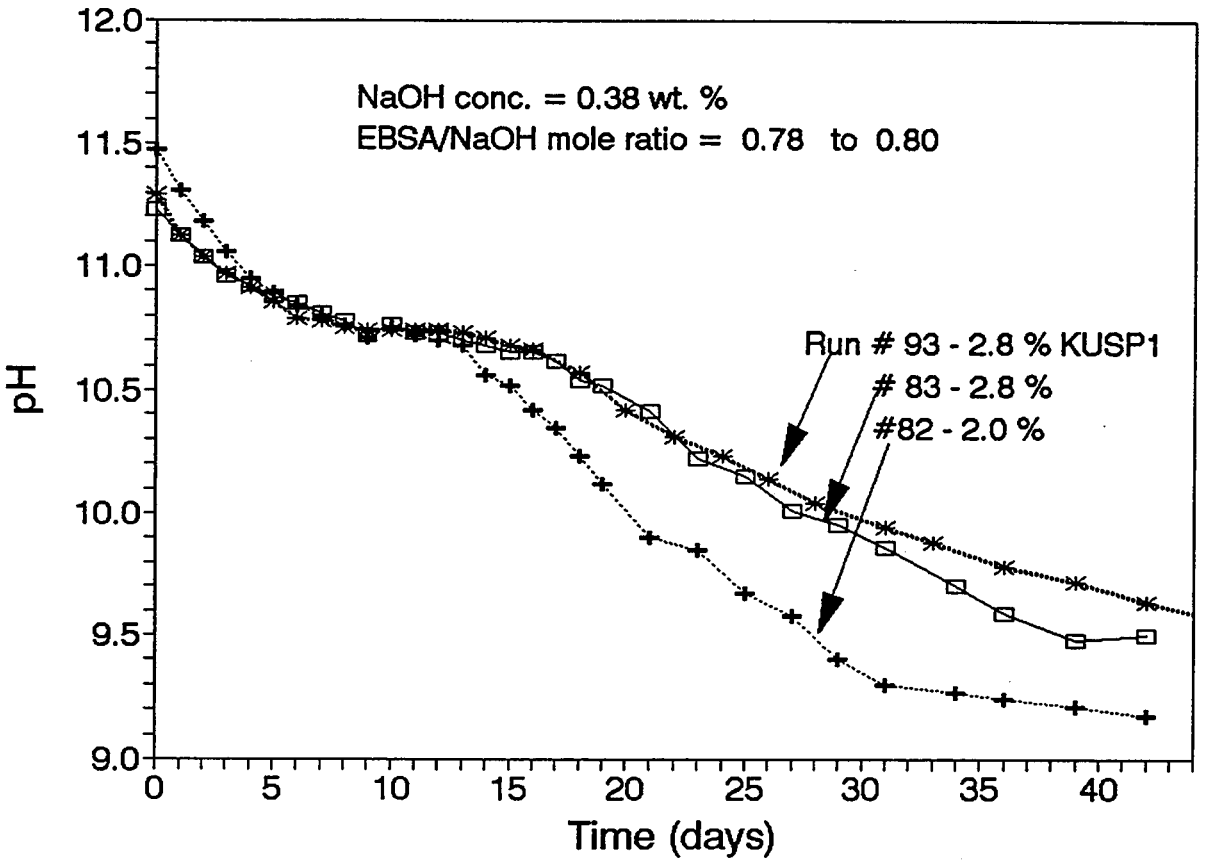

Figure 7.6 : pH-Time Data for KUSP1 Solutions at a Mole Ratio of EBSA/NaOH between 0.78 and 0.80 - Part 2.

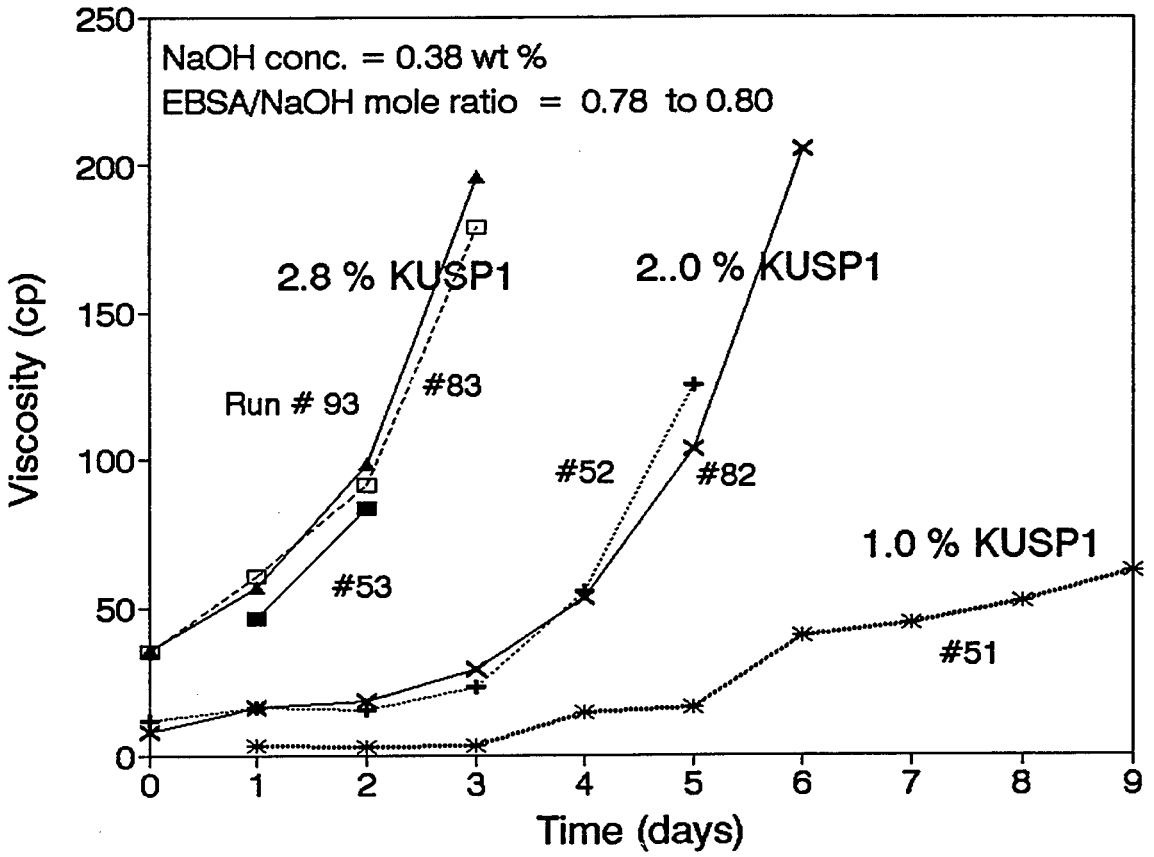

Figure 7.7 : Viscosity-Time Data for KUSP1 Solutions at a Mole Ratio of EBSA/NaOH between 0.78 and 0.80.

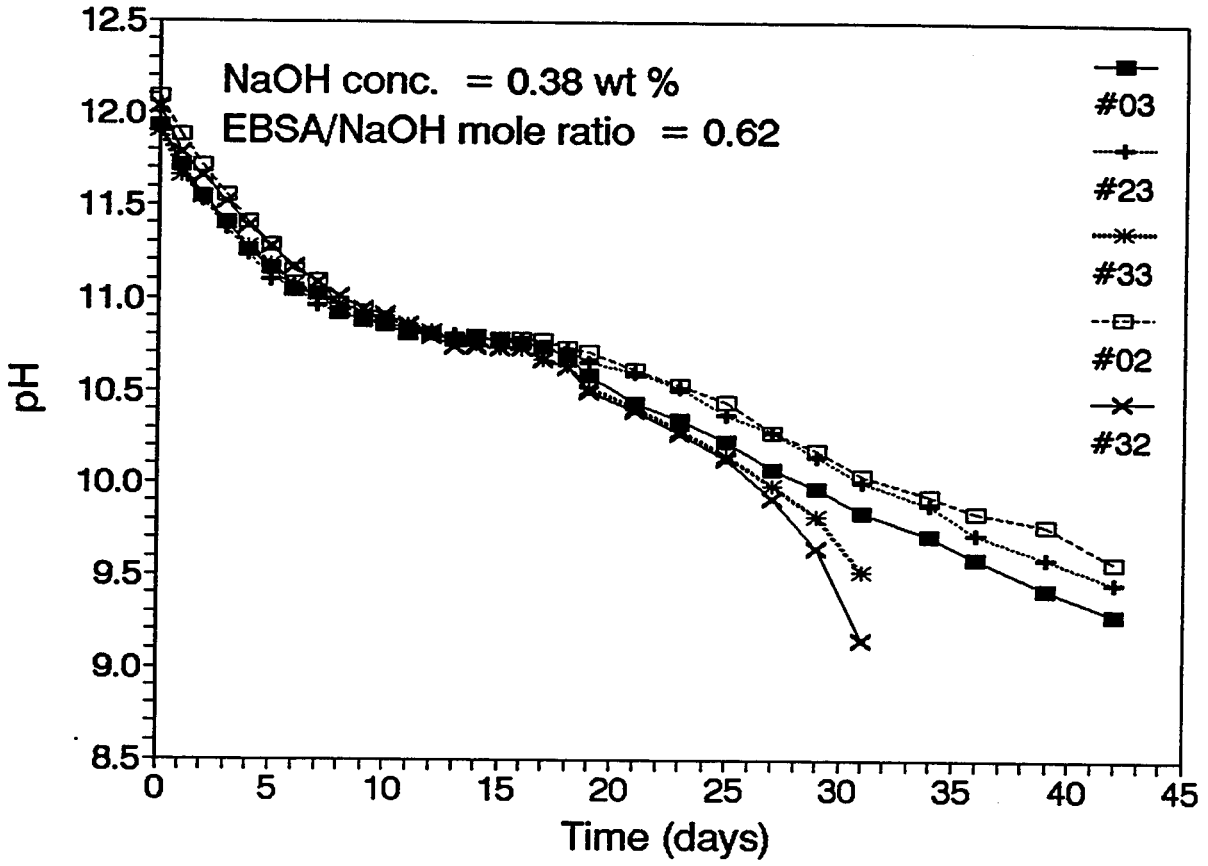

Figure 7.8 : pH-Time Data for KUSP1 Solutions at a Mole Ratio of EBSA/NaOH of 0.62.

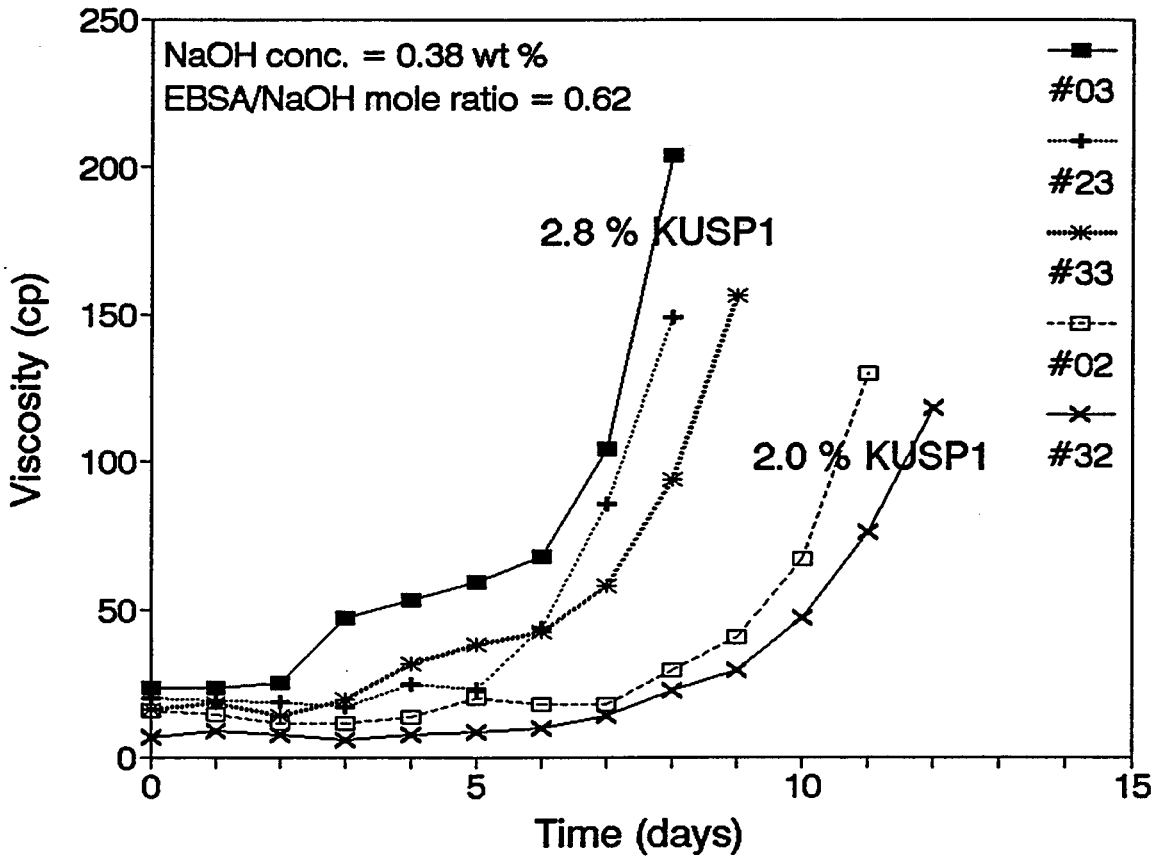

Figure 7.9 : Viscosity-Time Data for KUSP1 Solutions at a Mole Ratio of EBSA/NaOH of 0.62.

Gel times were a function of polymer concentration for given initial NaOH and EBSA concentrations. Solutions at higher polymer concentrations gelled earlier as shown in Table 7.3 and in Figures 7.7 and 7.9. This relationship was related to the lower initial pH values before and after EBSA addition for higher concentrations of polymer (see Table 7.3).

pH-time data for different concentrations of polymer (similar NaOH and EBSA conc.) are shown in Figure 7.5. The pH value decreased slower for higher polymer concentrations which indicated the polymer was consuming hydrogen ions. A continuous drop in pH was observed for the sample containing 0 % polymer while the pH of samples containing polymer was constant for a period of time when the pH value was approximately 10.8. Samples containing sufficient polymer gelled during the constant-pH period.

CONCLUSIONS

This investigation has shown that the gelation of KUSP1 can be accomplished by a chemical method, namely ester hydrolysis. Gel times on the order of days can be obtained and controlled by the selection of component concentrations.

Insights into the gelation process of KUSP1 were made. The polymer consumed hydrogen ions and developed structure and/or aggregates as the pH of a solution was lowered from high values to approximately 10.8. At the pH value of 10.8, the consumption of hydrogen ions was greatest and gelation occurred.

The cost of EBSA is probably prohibitive for use in field treatments. A search for a less-expensive alternative is being conducted.

An investigation of the gelation of KUSP1 by ester hydrolysis in porous media will be conducted. Subjects that will be addressed are the injectability of the polymer solution, the transport of the polymer and polymer aggregates, and the transport of the ester.

REFERENCES

1. Whistler, R.L. and Wolfrom, M.L., *Methods in Carbohydrate Chemistry*, Vol. 1, Academic Press, (1962), p 388.

2. Sohon, *American Chemistry Journal*, **20**, p 260.

Chapter 8

Gelation of KUSP1 by CO_2 in Sandpacks at Low Pressure

Principal Investigators: Shapour Vossoughi, Don Green and Paul Willhite

Graduate Research Assistant: Milind Raje

INTRODUCTION

Enhanced oil recovery techniques are used to recover additional oil trapped in the reservoirs which have already been exploited under primary and secondary recovery processes. Carbon dioxide flooding is one of the various EOR techniques employed in reservoirs where the temperature and pressure are at or near the critical values for CO_2. Supercritical CO_2 is an excellent solvent and miscibility with the oil results in efficient displacement of oil where the oil is contacted by CO_2.

Although the microscopic displacement efficiency of the miscible CO_2 displacement is high, the macroscopic sweep efficiency is low due to channelling in the reservoir. Channelling is the result of a poor mobility ratio of the crude oil/CO_2 system and gravity override.

The scope of the research is to increase sweep efficiency of CO_2. The objective is to determine the applicability of using the KUSP1 polymer to block CO_2 channels that develop during CO_2 flooding. It is realized that early breakthrough of CO_2 occurs because of its channeling through the oil zone. Plugging these channels with gelled KUSP1 polymer should increase the sweep efficiency and recover additional oil.

The KUSP1 polymer dissolves in alkaline solution and forms a gel upon reduction of the pH below 11. Reduction of pH can be achieved by several chemicals including CO_2. Bubbling CO_2 in bulk KUSP1 solutions produces gelation. CO_2 dissolves in the aqueous solution and reacts with water to form acidic species which lower the pH.

In situ gelation experiments have been performed with sandpacks saturated with the KUSP1 polymer. Significant permeability reduction was observed when a dilute strong acid was injected to reduce the pH of the polymer solution. It was also demonstrated that uniform permeability reduction along the length of a sandpack was achieved when alternate slugs of acid and polymer solutions were injected[2]. Initial permeability of the sandpack was restored by injecting NaOH solution. Using CO_2 to gel KSUP1 solutions during flow experiments in porous media have not been conducted.

This report describes experiments that were conducted to determine if CO_2 would gel the KUSP1 polymer under flow conditions in sandpacks. These experiments were conducted at low pressures and 25 °C in preparation for experiments conducted at supercritical CO_2 conditions.

EXPERIMENTAL APPROACH

The sandpack container was 30.2 cm in length and had a diameter of 1.90 cm. It was packed with Waldron fine Silica having a porosity of 34%. The sandpack was divided in two equal-length sections by a pressure port. The pack was saturated with water and dispersion runs were conducted by displacing 2.0 % brine solution by 2.2 % brine. Effluent concentrations were determined by an in-line differential refractometer. Permeabilities were determined for the two sections and for the total core length.

Polymer solutions were prepared by dissolving 2.00 grams of dry polymer in 100 ml of 1.0 N NaOH by stirring the solution. The clear solution was then filtered through a 5-micron nylon filter.

RESULTS AND DISCUSSION

Two flow experiments were conducted with CO_2 at low-pressure conditions.

Continuous CO_2 Injection

The objective of this experiment was to determine the permeability reduction achieved by continuously flowing CO_2 through a sandpack saturated with KUSP1 solution. The sandpack was saturated with polymer solution that had a pH of pH 13.5. CO_2 was then flowed through the sandpack at a flow rate of 0.5 ml/min (approximately 6 ft/day) until gas breakthrough was observed in the effluent. Water was then flowed through the sandpack to remove gaseous CO_2. The gas was removed by immiscible displacement and by dissolution of the gas into the water. Gas removal was verified by determining the compressibility of the sandpack. Post-treatment permeabilities were then determined.

Initial and post-treatment permeabilities are presented in Table 8.1. The permeability of the sandpack was reduced by a factor of approximately 80 and the reduction was uniform between the front and rear sections of the sandpack.

Table 8.1 Permeability Data; Continuous CO_2 Injection

	Initial Permeability (md)	Post-Treatment Permeability (md)
Total Sandpack	3,600	44
Front Section	3,500	43
Rear Section	3,600	45

Alternating Slug Injection

The objective of this experiment was determine the permeability reduction achieved in a sandpack by the injection of alternating slugs of KUSP1 polymer solutions and CO_2. The sandpack used in the previously described experiment was used. 1.0 N NaOH solution was flowed through the sandpack to remove gelled polymer. The sandpack was then saturated with water and initial permeabilities for this experiment were determined. The permeability was not restored to original values which indicated that not all of the gelled polymer was removed.

A 6-ml slug of polymer solution was injected into the sandpack followed by the injection of a CO_2 slug. The volume of the CO_2 slug was approximately 55 ml which was calculated to be the approximate amount required for the neutralization and gelation of 6 ml of polymer solution. The flow rate for both slugs was 0.5 ml/min. Injection of alternate slugs of CO_2 and polymer solution was continued for 17 cycles. Water was then flowed through the sandpack to displace the gaseous CO_2. Removal of the gas was verified by determining the compressibility of the sandpack system. After removal of gas, the post-treatment permeabilities were determined.

The permeabilities determined before and after the alternating-slugs treatment are given in Table 8.2. The permeability was reduced but most of the reduction occurred in the front section of the sandpack.

Table 8.2 Permeability Data; Alternating Slug Injection of CO_2

	Initial Permeability (md)	Post-Treatment Permeability (md)
Total Sandpack	1,610	60
Front Section	1,680	30
Rear Section	1,550	450

CONCLUSION

These preliminary flow experiments have demonstrated that the KUSP1 polymer system can reduce the permeability of a porous media by using low-pressure CO_2 to induce gelation. These results raise the possibility of using a low-pressure CO_2-KUSP1 polymer system for permeability modification treatments in reservoirs under waterflooding.

Equipment is being assembled to conduct flow experiments in Berea cores with CO_2 at super-critical conditions. The objective will be to determine the applicability of KUSP1 gel system for permeability modification treatments during miscible-CO_2 floods.

REFERENCES

1. S. Vossoughi, C.S.Buller, "Permeability Modification by In-Situ Gelation With a Newly Discovered Biopolymer," *SPE Reservoir Engineering* (Nov. 1991) 485-489.

2. S. Vossoughi, A. Putz "Reversible Insitu Gelation by Change of pH Within the Rock," SPE Paper No. 20977, SPE International Symposium of Oilfield Chemistry, Anaheim, CA (Feb. 20-22, 1991).

Chapter 9

Simulation of Interactions Between Fluids and Rocks

Principal Investigators: Paul Willhite, Don. W. Green, C. S. McCool

Graduate Research Assistant: Vikas Midha

OBJECTIVE

The efficacy of a gelled-polymer treatment typically depends on the penetration of the injected polymer solution before the onset of gelation. The gelation of commonly used polymers is a strong function of the solution pH. Fluid-rock interactions play an important role in determining the pH behavior of solutions injected into reservoirs.

The overall objective of this project is to study the important forms of fluid-rock interactions in reservoir sands and mathematically model their effects on the solution pH. When a solution is injected into a reservoir core, a myriad of fluid-rock interactions are possible depending on the rock mineralogy, nature of the injected solution and physical parameters such as flow rate, core length, etc. The scope of this work is limited to a simplified system consisting of the injection of high pH NaCl solutions in sandstone cores.

FLUID-ROCK INTERACTIONS

Previous alkaline flooding experiments in sandstone cores show the presence of two forms of fluid-rock interactions[1]:

1) The first reaction consists of an ion exchange between the sodium ions in the injected solution and the hydrogen ions on the rock surface. This reaction is typically a fast, reversible process and results in a delay of the breakthrough of the injected pH levels. Like other forms of ion-exchange, this reaction may be attributed to the various clay minerals present in the core.

2) The second reaction consists of a slow, kinetically-controlled dissolution of the silica-rich minerals in the core. This reaction results in the continuous production of silica and a simultaneous reduction in the effluent pH. Since quartz is predominant in most types of sands, quartz dissolution is a useful prototype for this reaction.

MATHEMATICAL MODELING

Simple mathematical models have been used in this work to study the effects of sodium/hydrogen ion exchange and silica dissolution in core flood experiments. The first phase consists of numerical simulations using an existing model, UTCHEM.

The UTCHEM Model

UTCHEM is a powerful compositional simulator developed at the University of Texas at Austin for modeling displacement processes. It incorporates fluid-rock, fluid-fluid reaction chemistry with extensive physical and flow property models. A detailed description of the complete UTCHEM model is available elsewhere[2,3,4]. A major limitation in the UTCHEM model arises from the assumption of local equilibrium. This assumption forces the concentrations of all the chemical species in the fluid-phase to instantaneously attain equilibrium with the rock. Most fluid-fluid reactions and ion-exchange reactions are fast enough to justify this assumption. In the case of slow, kinetically-controlled reactions like silica dissolution, however, the assumption of local equilibrium is not warranted.

The UTCHEM model calculates the solution pH and silica concentration in the effluent of a core-flood based on equilibrium considerations only. These equilibrium concentrations will, therefore, be independent of parameters like the flow rate and core length. The experimental results of Bunge and Radke[1] and Sydansk[5] show otherwise. As the residence time of the flood is increased, more dissolution of the rock is observed. This trend suggests that the reaction does not reach equilibrium within the residence times of the experiments. Bottle tests conducted by Southwick[6] show that high pH NaOH solutions at 50°C require contact times of the order of 300 days to equilibrate with sand particles. Such large residence times are not anticipated in typical laboratory-scale core-flood experiments.

Based on the experimental evidence, it is possible to conclude that the assumption of local equilibrium is valid for cases involving extremely long residence times only. The UTCHEM model will not be able to describe silica dissolution in experiments involving "short times". Clearly, a new model is required which will be valid for all time frames in general. Such a model would have important applications in scaling the effects of silica dissolution from laboratory experiments to field-scale conditions.

Development of a New Mathematical Model

In order to overcome some of the limitations in UTCHEM, a new model including the reaction kinetics for the slow dissolution reactions is proposed. In this section, the governing equations describing both the sodium/hydrogen ion-exchange and the silica dissolution reactions in core flood experiments have been formulated. The details of the model derivation and the complete program listing are available in reference [7].

The ion-exchange reaction. The proposed model is based on a coupled mechanism proposed by Bunge and Radke[8] which describes sodium-hydrogen ion-exchange equilibria. The ion-exchange on the surface of the matrix is represented by the following reaction mechanism:

$$MOH + Na^+ + OH^- \rightleftarrows MONa + H_2O,$$

where M denotes a mineral exchange site. This reaction states that each sodium-occupied site consumes one hydroxide ion. Hence, sodium ion adsorption onto the rock is equivalent to an hydroxide ion consumption from the fluid-phase. Using the reaction mechanism shown above, the fraction of sites occupied by sodium ions is given by the following relationship:

$$\frac{n_{Na^+}}{n_T} = \frac{K_I C_{Na^+} C_{OH^-}}{(1+K_I C_{Na^+} C_{OH^-})} \qquad (9.1$$

A complete description of all the symbols is provided in the nomenclature section. Eqn.[9.1] shows that the overall uptake of sodium (or hydroxide) is a function of both sodium ion concentration and hydroxide ion concentration in the fluid phase. It is clear from Eqn. [9.1] that the sodium uptake increases as either the solution pH or the salt concentration is increased. The relation also predicts a Langmuir-type isotherm if the sodium ion concentration is held constant.

It is important to recognize an inherent limitation in this simplified approach. The active site MO^- denotes a hydrolyzable acid site on oxides (such as silica) and a negative lattice exchange site for clay minerals like kaolinite and montomorillonite. Eqn. [9.1] is therefore highly simplified in that a single average equilibrium value K_I characterizes the complex mineral mixture in rock. Even for a single, pure mineral, all exchange sites probably will not be described by a single value of K_I.

The silica-dissolution reaction. Unlike ion-exchange reactions, dissolution reactions in reservoir sands are slow, kinetically controlled reactions. The next step, therefore, in developing a complete model describing pH behavior consists of determining the appropriate form of kinetics governing silica dissolution. Thornton and Radke[9] have concluded that silicic acid adsorbs onto the silica surface and serves as an intermediate for the formation of other silicate species. Although the adsorption step does not directly contribute to a consumption of hydroxide ions, it acts as the rate-determining step in the series of reactions leading to pH change. The kinetic model developed by Thornton and Radke must therefore be expanded to include the formation of all the silicate species in the fluid-phase and the simultaneous change in solution pH.

Previous work[10,11,12] on the speciation equilibria of silica in alkaline solutions shows that at low silicate concentrations monomers of silicic acid predominate. At higher silicate concentrations near solubility limit, however, oligomers and possibly polymers exist. Here, a definitive description of the dissolution chemistry is not available. For pH values less than 13, the tetrahedral monomers H_4SiO_4, $H_3SiO_4^-$, and $H_2SiO_4^{2-}$ govern solution behavior. Within this range, the following overall reaction sequence for the dissolution/condensation of silica is proposed:

1) $SiO_2 + 2H_2O \rightleftarrows H_4SiO_4$ ....r_1

2) $H_4SiO_4 + OH^- \rightleftarrows H_3SiO_4^- + H_2O$ ....r_2

3) $H_3SiO_4^- + OH^- \rightleftarrows H_2SiO_4^{2-} + H_2O$ ....r_3

The first step consists of the following elementary reactions:

1a) $SiO_2 + 2H_2O + S^* \rightleftarrows H_4SiO_4^*$ (rate limiting)

1b) $H_4SiO_4^* \rightleftarrows H_4SiO_4 + S^*$

where S^* represents an active site on the silica lattice and $H_4SiO_4^*$ represents the adsorbed silicic acid molecule. By assuming that reaction 1b) is at pseudo-steady state relative to 1a) and an overall

conservation of sites, the following rate expression may be derived:

$$r_1 = k_1 \frac{(1 - \frac{[H_4SiO_4]}{[H_4SiO_4]^{sat}})}{(1 + \frac{[H_4SiO_4]}{F_x[H_4SiO_4]^{sat}})} \qquad (9.2$$

Typically, fluid-phase reactions are much faster than reactions taking place at the fluid-solid interface. It is proposed that reactions 2 and 3 are also in pseudo-steady state with respect to reaction 1. The corresponding rate expressions for these reactions are given by relations of the form:

$$r_2 = F_{eq} k_1 (Q_2[H_4SiO_4][OH^-] - [H_3SiO_4]) \qquad (9.3$$

$$r_3 = F_{eq} k_1 (Q_3[H_3SiO_4^-][OH^-] - [H_2SiO_4^{2-}]) \qquad (9.4$$

where F_{eq} is a factor which ensures that the rate of reaction of steps 2 and 3 is much faster than that of step 1. This procedure ensures that the forward and backward reactions in reactions (2) and (3) are assumed fast enough that these reactions are in "pseudo-equilibrium" with reaction (1). It is important to note that reactions (2) and (3) are not in "absolute" equilibrium as this would force $r_2 = r_3 = 0$.

Some of the typical values of the equilibrium quotients Q_1, Q_2 and Q_3 documented in the literature are shown in Table [9.1]. Since there is considerable variation in the values of Q_2 and Q_3, depending on background electrolyte concentration and temperature, representative values have been used for simulation purposes.

Temperature (°C)	$Q_1=[H_4SiO_4]^{sat}$ (mol/liter)	Reference
23	$5.18*10^{-5}$	13
25	$1.0*10^{-4}$	6
70	$3.43*10^{-4}$	13

Background Electrolyte	T (°C)	Q_2 $(mol/liter)^{-1}$	Q_3 $(moles/liter)^{-1}$	Reference
1.0 M NaCl	23	25,500	3.2	10
0.5 M NaCl	25	19,500	9.8	10
not reported	25	25,118	10	6
0.5 M $NaClO_4$	25	18,600	15	12
0.5 M $NaClO_4$	50	6,920	12	12
1.0 M NaCl	70	4,940	2.4	10

Table 9.1: Typical values of equilibrium quotients Q_1, Q_2 and Q_3

The rate constant k_1 is determined experimentally from the initial rate of dissolution. This initial rate is reported to be a complicated function of solution pH, temperature and ionic density[9]. The following model proposed by House and Orr[14] describing the dependance of k_1 on pH, specifically for a 0.1N solution at 25°C has been used to describe the functionality of k_1 in general:

$$\log k_1 = -14.55 + 0.361 pH \qquad (9.5$$

where k_1 is in moles/m^2.sec. A more detailed discussion on the validity of this assumption is presented in a later section.

Using the above expressions, the rates of reaction of all the species may derived in terms of r_1, r_2 and r_3:

$$r_{OH^-} = -(r_2 + r_3) \qquad (9.6$$

$$r_{H_4SiO_4} = r_1 - r_2 \tag{9.7}$$

$$r_{H_3SiO_4^-} = r_2 - r_3 \tag{9.8}$$

$$r_{H_2SiO_4^{2-}} = r_3 \tag{9.9}$$

The above expressions ensure that the rate of consumption of hydroxide ions is determined by the rate of formation of the silicate species. This rate, in turn is dictated by the rate of reaction of silicic acid k_1 and the overall change in pH is a slow, kinetically-controlled process.

Assumptions in the flow model. Some of the major assumptions in the generalized model equations are :

1) A simple one dimensional, incompressible flow is assumed with no axial gradients.
2) The core is assumed to be homogenous with a constant porosity.
3) Change in the physical properties of the core (*i.e.* the porosity, bulk density *etc.*) due to chemical interactions have not been taken into account.
3) The core is isothermal.
4) Mass transfer limitations at the solid-fluid interface are negligible.

The generalized continuity equations. The equation of continuity for the i^{th} species accounting for adsorption, convection, dispersion, and chemical reaction in the aqueous phase yields:

$$\frac{\partial C_i}{\partial \tau} + \sum_{i=1}^{i=N} \alpha_i \frac{\partial C_i}{\partial \tau} = -\frac{\partial C_i}{\partial \zeta} + \frac{1}{Pe}\frac{\partial^2 C_i}{\partial \zeta^2} + Da f_i(C) \tag{9.10}$$

with the boundary conditions:

$$1)\ \tau = 0 \qquad C_i = C_{initial} \qquad for\ all\ \zeta \tag{9.11}$$

$$2)\ \zeta = 0 \qquad C_i = C_{inj} \qquad for\ all\ \tau > 0 \tag{9.12}$$

$$3)\ \zeta = 1 \qquad \frac{\partial C_i}{\partial \zeta} = 0 \qquad for\ all\ \tau > 0 \tag{9.13}$$

where:

τ and ξ are dimensionless time and distance defined by:

$$\tau = t\frac{v}{\phi L} \qquad \zeta = \frac{x}{L} \tag{9.14}$$

and the Pe (Peclet Number), Da (Damkohler Group) and α_i (dimensionless retardation factor) are groups of parameters defined by the following relations:

$$Pe = \frac{K\phi}{Lv} \tag{9.15}$$

$$Da_i = \frac{k_i a_s \rho_s (1-\phi)}{\phi} \cdot \frac{L\phi}{v} \tag{9.16}$$

$$\alpha_i = \frac{a_s \rho_s (1-\phi)}{\phi} \frac{\partial n_i}{\partial C_i} \tag{9.17}$$

The physical significance of each of these groups will be discussed in detail in the following sections.

The final step in formulating the model equations consists of incorporating the ion-exchange equilibria and silica-dissolution kinetics into the flow model. Firstly, the assumption of local equilibrium between the fluid phase and the adsorbed phase is invoked which enables one to determine the α_i groups for the ion-exchange reaction:

$$\alpha_{Na^+} = \left(\frac{a_s \rho_s (1-\phi)}{\phi}\right) \frac{\partial n_{Na^+}}{\partial C_{Na^+}} = \left(\frac{a_s \rho_s (1-\phi)}{\phi}\right) \frac{n_T K_I C_{OH^-}}{(1 + K_I C_{Na^+} \cdot C_{OH^-})^2} \tag{9.18}$$

$$\alpha_{OH^-} = \left(\frac{a_s \rho_s (1-\phi)}{\phi}\right) \frac{\partial n_{Na^+}}{\partial C_{OH^-}} = \left(\frac{a_s \rho_s (1-\phi)}{\phi}\right) \frac{n_T K_I C_{Na^+}}{(1 + K_I C_{Na^+} \cdot C_{OH^-})^2} \tag{9.19}$$

The overall kinetics of silica dissolution are dictated by only one rate constant, namely k_1. Thus, the model equations are characterized by one Da group:

$$Da = \frac{k_1 a_s \rho_s (1-\phi)}{\phi} \frac{L\phi}{v} \tag{9.20}$$

The general model, therefore, consists of the set of continuity equations with the appropriate reaction terms for the Na^+, OH^-, H_4SiO_4, $H_3SiO_4^-$ and $H_2SiO_4^{2-}$ species. The hydrogen ion concentration species is calculated by the following equilibrium relation:

$$C_{H^+}=\frac{K_w}{C_{OH^-}} \tag{9.21}$$

and the Cl^- is found by an overall charge balance in the fluid phase:

$$C_{Cl^-}=C_{Na}+C_{H^+}-C_{OH^-}-C_{H_3SiO_4^-}-2C_{H_2SiO_4^{2-}} \tag{9.22}$$

The model equations for static bottle experiments. Static bottle tests provide an effective method for studying the kinetics of silica dissolution without all the complications of a complete flooding process. These simple experiments consist of contacting quartz sand with high pH brine solutions and monitoring the change in solution pH and silica concentration as a function of time. The equation of continuity for the i^{th} species is given by:

$$\frac{dC_i}{dt}=(k_i S_L a_s) f_i(C) \tag{9.23}$$

with the initial condition:

$$C_i=C_{initial} \qquad at\ t=0 \tag{9.24}$$

This equation is analogous to the generalized continuity equation in the flow model given by Eqn. [9.10], with the initial concentrations corresponding to the injected concentrations in the core-flood.

The complete model consists of the set of continuity equations given by Eqn. [9.23] for all the independent chemical species, the equilibrium relation for H^+ in Eqn. [9.21] and the overall constraint of electrical neutrality given by Eqn. [9.22].

Numerical solution of the model equations. A numerical solution to a coupled set of partial differential equations (PDEs) describing the displacement poses a formidable problem. The classical approach to solving such equations in the literature is to use finite-difference approximations in both space and time. Due to the complicated nature of the chemical reaction and the coupled adsorption terms, this approach would require the use of either an iterative solution or a non-linear solution technique. Such solutions typically involve a large amount of computational effort to achieve adequate convergence. In order to avoid these problems, the familiar method of lines (MOL)[15] has been employed in this work. In this method, only the spatial terms are discretized to yield a set of ordinary differential equations (ODEs) with time as the independent variable. This system may then be solved using any one of the many robust and well-developed ODE solution algorithms.

The governing equations of the flow problem form a set of second order, hyperbolic, "advection

equations." In the case of highly convective systems, two spurious effects are observed:

i) numerical oscillations,
ii) numerical dispersion.

These effects arise due to the presence of a sharp front in the concentration profiles. In the vicinity of this front, large errors in the finite difference approximations are induced. Centered-finite differences lead to large oscillations in the concentration profiles. These oscillations may be reduced by using upstream-finite differences for the convection term. Upstream differences however introduce numerical dispersion into the solution. The magnitude of the dispersion is dictated by the total number of grid points in the discretization. Although using a large number of grid points will produce less dispersion, it would also result in a considerable amount of computational workload. The problem is compounded further by the high degree of accuracy required in the concentrations values. At low pH values, the logarithmic nature of the pH function tends to magnify minute changes in the hydroxide species concentration.

Due to the factors mentioned above, numerical dispersion has been used to approximate the physical dispersion term in the model equations. A detailed account for the justification of this assumption is presented in a later section. DSS/2 software[16] has been used to discretize the spatial derivatives. Single-point, upstream-finite differencing has been selected for the convection term in the model equations. Due the stiff nature of the resulting ODEs, an implicit integrator LSODE[17] has been used to solve the system of equations.

The model equations for the static beaker tests are much simpler to solve. These equations consist of a set ODE's and are solved by the same LSODE routine used in solving the flow problem.

RESULTS AND DISCUSSION

In the following sections, the mathematical models are employed to examine of the nature of the different types of fluid-rock interactions and study the effects of various parameters which govern their behavior. The first set of results consist of a series of simulations with the UTCHEM simulator.

Results from the UTCHEM Model

As mentioned earlier, silica dissolution is one of the dominant forms of fluid-rock interactions in reservoir sands. Under typical laboratory conditions, this dissolution is a slow chemical reaction governed by reaction kinetics rather than reaction equilibria. In the following set of preliminary results, some of the important effects of silica dissolution in core-flood experiments have been modeled using the UTCHEM simulator. The UTCHEM model is based on the assumption of local equilibrium. The results from these simulations, therefore, should provide valuable insights into the limitations of the local equilibrium assumption in rate-limited processes. For simplification purposes, the core is considered to consist of pure quartz sand particles only, which enables one to neglect all forms of ion-exchange on the matrix surface.

In this particular set of simulations, a complex equilibrium model has been used to describe the silica dissolution reaction which accounts for the formation of H_4SiO_4, $H_3SiO_4^-$, $H_2SiO_4^{2-}$, $HSiO_4^{3-}$ and $Si_2O_5^{2-}$ species. A summary of the reaction chemistry and equilibrium relations has been provided in Table [9.2]. The equilibrium constants shown in this table correspond to those used by Bhuyan[2].

1. ELEMENTS
Hydrogen, Sodium, Silicon, Oxygen, Chlorine.

2. REACTIVE CHEMICAL SPECIES
Fluid Species:
H^+, Na^+, Cl^-, H_4SiO_4, H_2O (Independent Species)
OH^-, $H_3SiO_4^-$, H_2SiO4^{2-},$HSi_2O_6^{3-}$, $Si_2O_5^{2-}$ (Dependant Species)

Solid Species:
SiO_2 (quartz)

3. REACTION EQUILIBRIA

Solid Phase Dissolution:
$SiO_2 + 2H_2O = H_4SiO_4$ $\quad K_{sp} = [H_4SiO_4]$ $\quad K_{sp} = 1E\text{-}04$

Fluid Phase Equilibria for the Dependant Species:

Equilibrium Reaction	definition of K	K
$H^+ + OH^- = H_2O$	$1/[H^+][OH^-]$	1.01E-14
$H_4SiO_4+OH^-=H_3SiO_4^-+H_2O$	$[H_3SiO4^-][H^+]/[H_4SiO_4]$	1.69E-09
$H_4SiO_4+2OH^-=H_2SiO4^{2-}+2H_2O$	$[H_2SiO_4^{2-}][H^+]^2/[H_4SiO_4]$	4.26E-21
$2H_4SiO_4+3OH^-=2HSi_2O_4^{3-}+3H_2O$	$[HSi_2O_6^{3-}][H^+]^3/[H_4SiO_4]^2$	1.15E-31
$2H_4SiO_4+2OH^-=Si_2O_5^{2-}+2H_2O$	$[H_2SiO_4^{2-}][H^+]^2/[H_4SiO_4]^2$	7.24E-19

Table 9.2: Summary of the reaction chemistry used in the simulations with the UTCHEM model.

An initial condition consisting of a sand-core saturated with a 1.7% NaCl solution has been considered. A brine solution containing 0.5% NaOH is injected into the core and displaces the initial brine solution. In the presence of the high pH solution, dissolution of the sand particles starts taking place which, in turn, causes a consumption of hydroxide ions. A complete summary of the initial conditions, injected concentrations and the physical parameters is presented in Table [9.3]. In the following sections, the concentration profiles along the length of the core have been studied as a function of pore volumes (PV) of injection.

1. SUMMARY OF CORE DATA

Core data	:	2 ft * 0.16 ft * 0.16 ft
Grid size	:	80 * 1 * 1
Time step	:	0.002 PV
Permeability	:	1,000 md
Porosity	:	0.20
Flow rate	:	0.00512 ft^3/day

2. INITIAL CONDITIONS (Concentrations in moles/liter PV)

fluid species:

H^+ 3.23E-06 Na^+ 0.2857 H_4SiO_4 0.1E-3 Cl^- 0.2857 OH^- 3.12E-8 $H_3SiO_4^-$ 5.24E-8 H_2SiO4^{2-} 4.07E-13 $HSi_2O_6^{3-}$ 3.39E-21 $Si_2O_5^{2-}$ 6.92E-15

solid species:

SiO_2 (quartz) 172.9

3. INJECTION CONDITIONS (Concentrations in moles/liter PV)

H^+ 0.127E-12 Na^+ 0.126 H_4SiO_4 0.1E-3 Cl^- 0.05 OH^- 0.079 $H_3SiO_4^-$ 0 H_2SiO4^{2-} 0 $HSi_2O_6^{3-}$ 0 $Si_2O_5^{2-}$ 0

Table 9.3: Summary of physical parameters, initial concentrations and injected concentrations used in the simulations with the UTCHEM model.

Figure [9.1] shows the concentration profiles of the silicate species and the total Si concentration in the fluid-phase after 0.25 PV injection. In the given time interval, the injected solution travels a distance of $\xi=0.25$ within the core. Dissolution of the matrix takes place in this region and results in high concentrations of silica in the solution. Due to the nature of the silicate speciation equilibria, it may be seen that the tetrahedral monomers $H_3SiO_4^-$ and $H_2SiO_4^{2-}$ predominate. In comparison, the contributions of H_4SiO_4, $HSiO_4^{3-}$ and $Si_2O_5^{2-}$ species are negligible.

Figure [9.2] shows the OH^- species concentration profile and the corresponding pH profile after 0.25 PV injection. A large consumption of hydroxide is produced by the silica dissolution reaction which reduces the solution pH from the injected value of 12.9 to an equilibrium value of 11.9. The concentration profile of the OH^- species is similar to the profiles of the silicate species in Figure [9.1] and shows a relatively sharp front centered at $\xi=0.25$. Due to the logarithmic nature of the pH function however, the pH profile shows a much broader front ranging from $\xi=0.2$ to $\xi=0.55$. Thus, dispersion is expected to play an important role in characterizing the pH profile within the core.

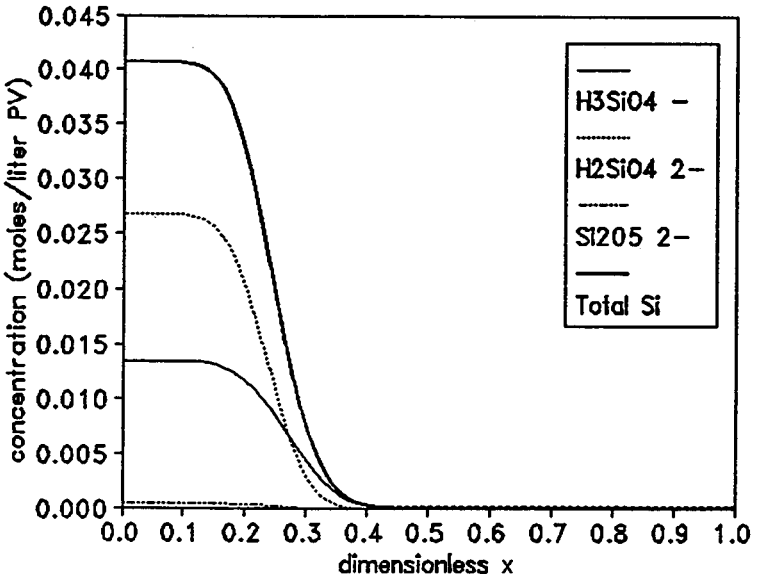

Figure 9.1: Concentration profiles of the silicate species after 0.25 PV injection predicted by the UTCHEM model.

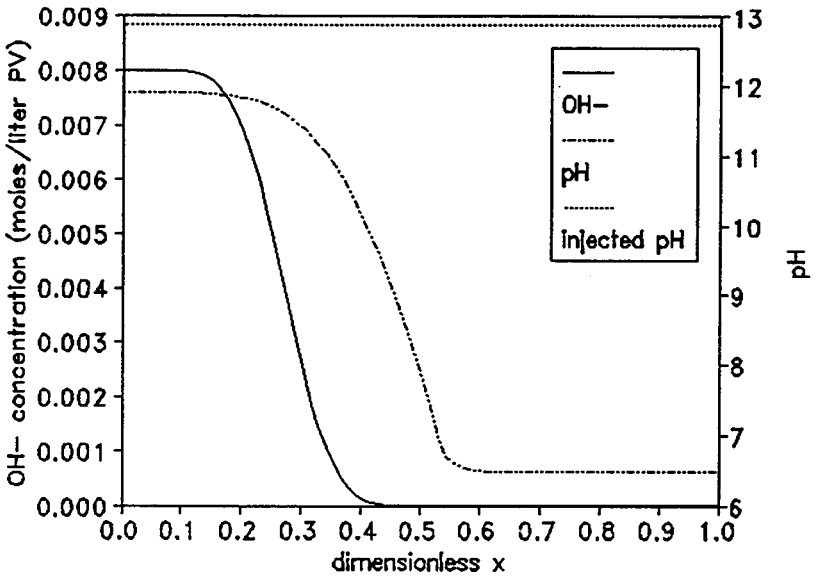

Figure 9.2: Concentration profiles of the OH^- species and the corresponding pH profile after 0.25 PV injection predicted by the UTCHEM model.

Before studying the effects of dispersion in detail, it is important to investigate the effect of residence time on the concentration profiles. Flooding experiments show a decrease in the total silica concentration and hydroxide consumption as the residence time is lowered. Figure [9.3] shows the profiles of the total silica concentration as a function of flow-rate. Despite a twenty-fold reduction in the residence time, the concentration of silica in the injected solution within the core remains unchanged. Similar trends may be seen in the pH profiles shown in Figure [9.4]. The only effect of flow-rate that the UTCHEM model does show is a small decrease in the dispersion of the concentration profiles as the flow-rate is increased.

The results shown in Figures [9.3] and [9.4] establish that UTCHEM is incapable of describing the kinetic nature of the silica-dissolution reaction. By assuming local equilibrium, the concentration profiles become independent of physical parameters like the flow-rate and core length. In a later section, it will be shown that the results from UTCHEM are valid only for the limiting case of extremely long residence times. In the case of the short time-scales considered here, the effects of silica dissolution are grossly overpredicted.

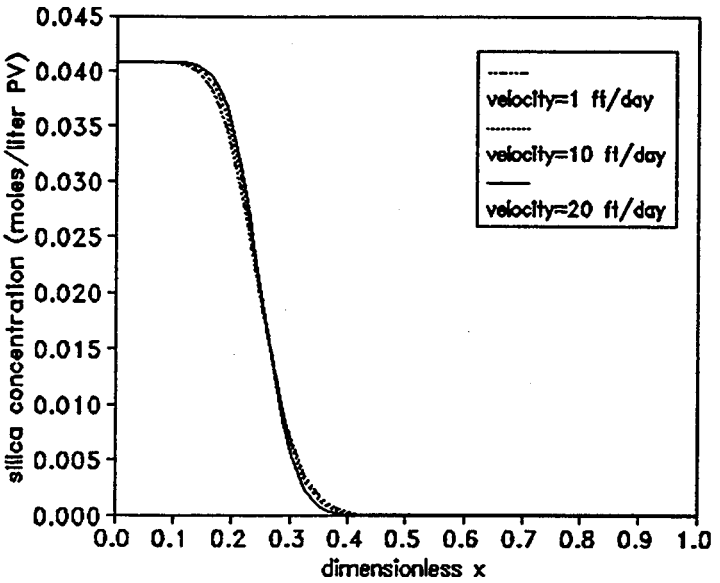

Figure 9.3: Silica concentration profiles after 0.25 PV injection predicted by the UTCHEM model as a function of flow rate.

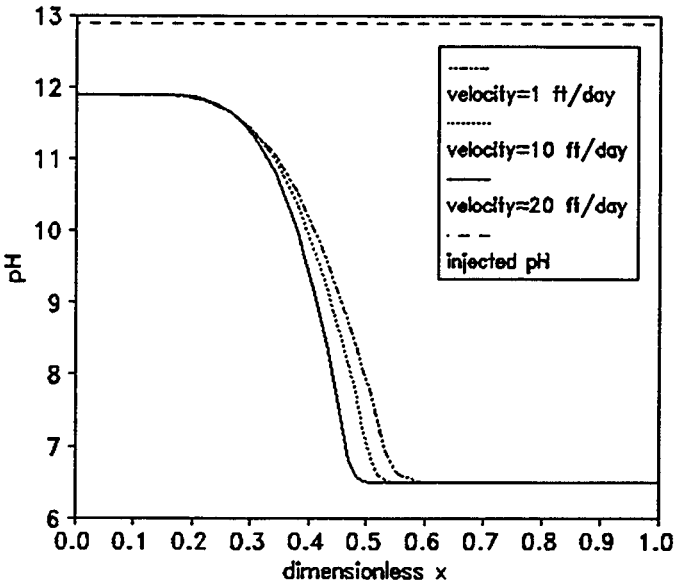

Figure 9.4: pH profiles after 0.25 PV injection predicted by the UTCHEM model as a function of flow rate.

Effect of numerical dispersion

Despite its limitations, UTCHEM provides an effective means to study the effects of dispersion on the concentration profiles within the core. This dispersion is largely dependant on the numerical technique used to solve the governing equations. In the simulations shown in Figures [9.1] through [9.4], a single-point, upstream finite-difference scheme has been used to evaluate the convection term in Eqn. [9.10]. In each case, the diffusivity of all the chemical species and the phase dispersivity was forced to zero. This implies that the dispersion in the concentration profiles is purely numerical in nature. An ideal solution to the governing equations after 0.25 PV of injection would consist of concentration profiles with a step change from the equilibrium concentration to the initial concentration exactly at the point $\xi=0.25$. In the following sections, two fundamental questions regarding dispersion will be addressed: First, will numerical dispersion show the same behavior as physical dispersion of the chemical species? If so, is it possible to quantify numerical dispersion and use it to approximate the physical dispersion term in the governing equations? The answers to these questions form the basis for the manner in which dispersion has been modeled in the new model proposed in this work.

As a first step, the simulations shown by Figures [9.1] and [9.2] have been repeated using no physical dispersion and various different numerical techniques to control the numerical dispersion. The corresponding results have been summarized in Figures [9.5] and [9.6]. The single-point, upstream method is a first order method and shows the maximum amount of numerical dispersion. Chaudhray's second-order method reduces the numerical dispersion but shows large oscillations in the concentration profiles. These oscillations are typical of centered finite-difference schemes. The third-order, upstream method reduces the numerical dispersion significantly and at the same time, does not show any oscillatory behavior. This solution is assumed to be reasonably close to ideal concentration profiles with no physical dispersion. The third-order method, therefore, may be used to model the effects of physical dispersion with negligible contribution from the numerical dispersion.

Next, a simulation is carried out with third-order dispersion control and a physical phase dispersivity of 0.00625 ft. This value compares favorably with the values of dispersivity observed in sand-cores which are typically in the range of 0.001-0.01 ft. The results from this simulation are shown by the solid lines in Figures [9.7] and [9.8]. The dotted lines correspond to the results from a simulation with single-point, upstream, finite differencing with purely numerical dispersion. The concentration profiles show good agreement suggesting that numerical dispersion shows the same behavior as physical dispersion. More importantly, the value of the dispersivity used in the figures is not an adjusted value and has been determined *a priori* as described in what follows.

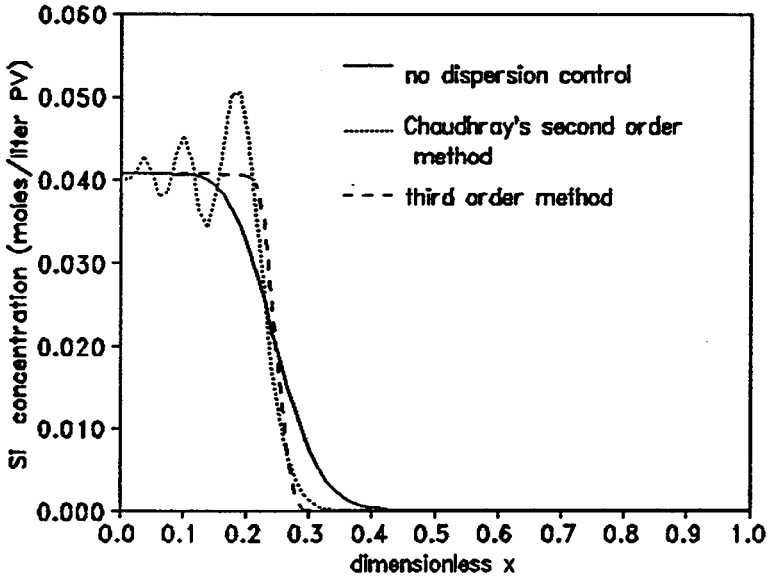

Figure 9.5: Silica concentration profiles after 0.25 PV injection and no physical dispersion predicted by the UTCHEM model with different numerical techniques for dispersion control.

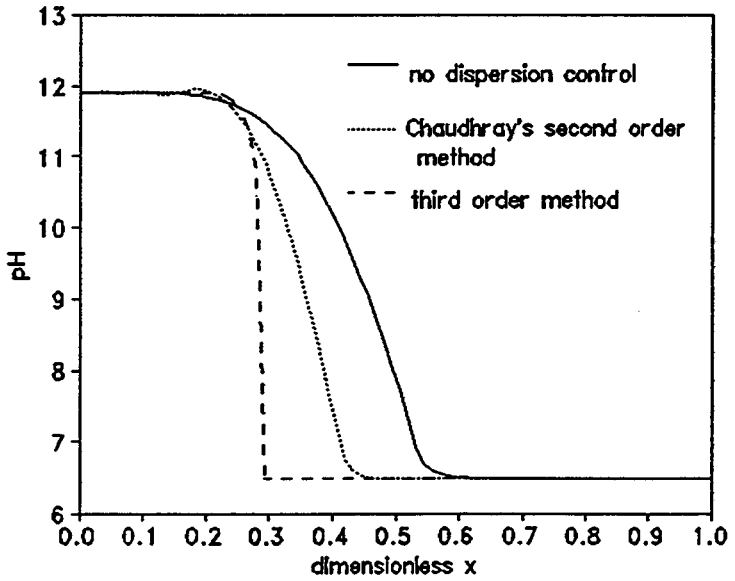

Figure 9.6: pH profiles after 0.25 PV injection and no physical dispersion predicted by the UTCHEM model with different numerical techniques for dispersion control.

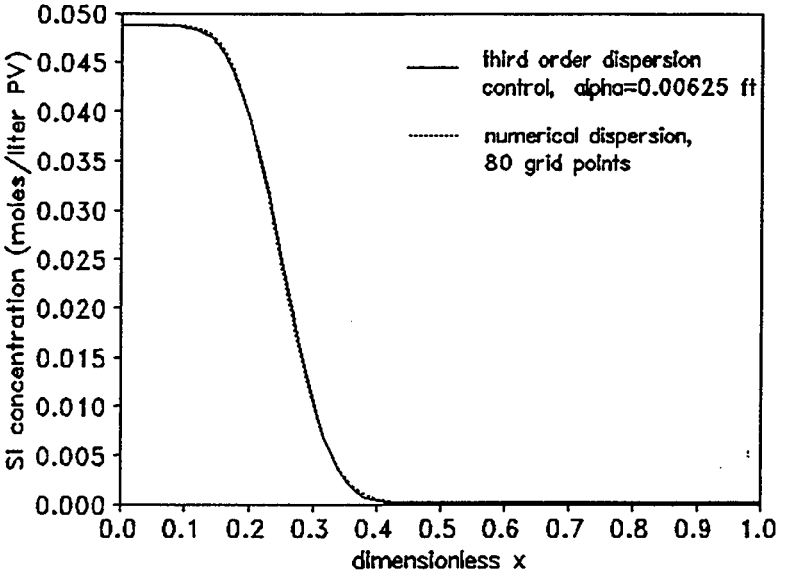

Figure 9.7: Comparison of physical dispersion and numerical dispersion in the silica concentration profiles after 0.25 PV injection predicted by the UTCHEM model.

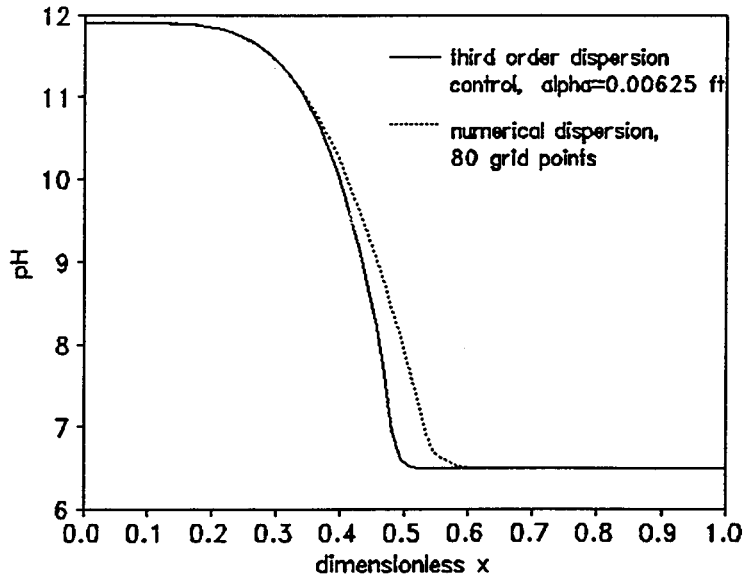

Figure 9.8: Comparison of physical dispersion and numerical dispersion in the pH profiles after 0.25 PV injection predicted by the UTCHEM model.

The UTCHEM model uses an explicit finite-difference scheme for approximating the time derivative and upstream finite differencing for the spatial derivative. Introducing these approximations into the governing equation results in a total dispersion coefficient given by[7]:

$$K_d+(\frac{v}{\phi})\frac{\Delta x}{2}-\frac{1}{2}(\frac{v}{\phi})^2\Delta t \qquad (9.25$$

where:

Δt is the time-step in the finite-difference approximations.
Δx is the grid block size in the finite-difference approximations.

This quantity is the sum of the contributions due to the physical-dispersion coefficient and numerical-dispersion coefficient. The coefficient characterizing the numerical dispersion is determined by the total number of grid blocks and time steps used in the integration of the model equations. The UTCHEM model relates the physical dispersion coefficient to the interstitial velocity by the following relation:

$$K_d=\frac{D}{\tau_T}+\frac{v}{\phi}\alpha_d \qquad (9.26$$

where:

D is the diffusivity of the species (ft^2/day).
τ_T is the tortuosity of the core (dimensionless).
α_d is the longitudinal dispersivity of the fluid-phase (ft^2/day).

Typically, the diffusivities of most species are negligible in comparison to the hydrodynamic dispersion in the fluid-phase. Based on this assumption, it is possible to directly relate the value of numerical dispersion coefficient to a physical dispersivity by the relation:

$$\alpha_d=\frac{\Delta x}{2}-(\frac{v}{\phi})\frac{\Delta t}{2} \qquad (9.27$$

The time step used in the simulations is typically very small such that $(v/\phi)\Delta t \ll \Delta x$. Thus, a total of 80 grid blocks discretizing a 1 ft core in the spatial direction yields a physical dispersivity of 0.00625 ft.

Despite the simplified nature of analysis presented above, the profiles shown in Figures [9.7] and [9.8] indicate that it is possible to assign a physical dispersivity which characterizes the amount of numerical dispersion. This dispersivity may then be controlled by simply varying the total number of grid blocks in the x-direction. Based on these conclusions, the new model proposed in this work uses numerical dispersion to model the physical dispersion term in the governing equations.

Results from the New Model

Due to the inherent assumptions in the UTCHEM model, its application is restricted to a limited set of conditions. The following sections show how some of the important limitations in the UTCHEM model were overcome in the new model.

Before simulating complete core-flood experiments with the proposed model, it is essential to verify the kinetics of silica dissolution. The kinetic equations ought to be able to describe the dissolution of silica for both "small" time scales and the approach to equilibrium in "long" time scales. For this purpose, static bottle tests corresponding to both time frames have been simulated and the results have been compared to experimental data in the literature.

Simulation of static beaker tests

Wirth and Gieskes[18] studied the initial kinetics of dissolution of silica. Their experiments consisted of dissolving exactly 5 g of vitreous silica powder in 500 ml of water at 25°C and monitoring the increase in the silica content in the solution as a function of time. Throughout the course of each experiment, the pH of the solution was maintained constant.

In order to simulate the experiments of Wirth and Gieskes, the model equations for static bottle tests described earlier were used. In addition, the time derivative of the hydroxide species was forced to zero to ensure a constant solution pH. An effective value of the rate constant k_1 on a unit volume basis was directly adjusted to fit the experimental data with the kinetic model. The parameter F_{eq} was determined such that any further increase in its value produced no noticeable change in the concentration profiles. This procedure forced all the reactions to a pseudo-steady state relative to the rate-limiting step. A summary of the values of the parameters used in the simulations is presented in Table [9.4].

Q_1 (mol/liter)	Q_2 (mole/liter)$^{-1}$	Q_3 (mole/liter)$^{-1}$	Q_W (mol/liter)^2	F_{eq} (moles/liter)
1.0 E-4	2.0 E4	1.0 E1	1.0 E-14	1 E4

Table 9.4: Summary of parameters used in simulation of static beaker tests for "short" time scales.

Figures [9.9] and [9.10] compare the "small time" response of the kinetic model to experimental data at pH values of 11 and 6 respectively. The pH values have been chosen to correspond to typical injected and initial conditions in flooding experiments. The model correctly shows a linear increase in the total silica concentration for small times. As the solution pH is lowered, there is an appreciable decrease in the rate of reaction which is also reflected in the value of k_1 used in the simulations. Although these results shed no light on the pH behavior, the excellent fit of the silica concentration profiles suggest the validity of kinetic expressions.

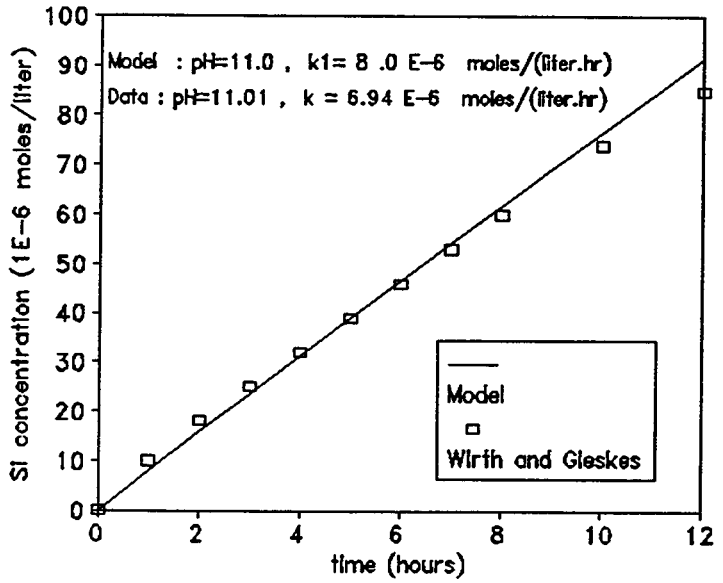

Figure 9.9: Silica concentration profiles in beaker tests for "short" time scales at pH=11. Experimental data obtained from Wirth and Gieskes[18].

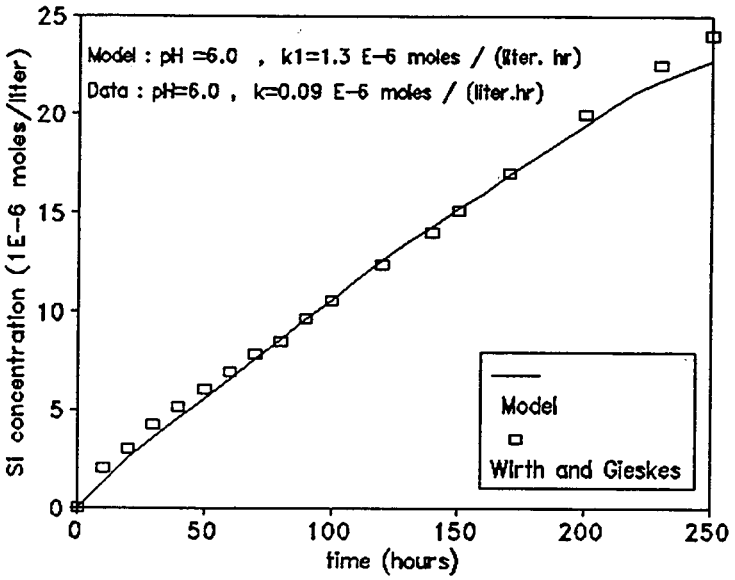

Figure 9.10: Silica concentration profiles in beaker tests for "short" time scales at pH=6. Experimental data obtained from Wirth and Gieskes[18].

Wirth and Gieskes fitted their experimental data with straight lines to determine zero-order rate constants. The values of these rate constants are included in the Figures [9.9] and [9.10] (shown by the symbol k). Although the kinetic model proposed is more complicated than simple zero-order kinetics, the values of the rate constant k_1 used in the simulations at two different pH values compare favorably with the rate constants reported by Wirth and Gieskes. Based on this observation, it may be concluded that the rate constant k_1 is a strong function of the solution pH.

In order to study the "long time" behavior of the kinetics, the bottle tests conducted by Southwick have been simulated using the proposed kinetic model. In this case, time scales of the order of hundreds of days are considered. Southwick's experiments consisted of dissolving 33g of quartz sand in 75g of 0.25N NaOH solutions at various different temperatures. Due to the lack of sufficient experimental and thermodynamic data, no attempt has been made to obtain a good fit to the experimental data. Rather, the main objective of the simulations was simply to reproduce some of the important features of the experimental results.

The model equations and kinetic expressions used in the simulation of short-time bottle tests were adopted for simulating long-time experiments. Again, k_1 is measured directly on a unit volume basis and is adjusted to match the experimental data. The equilibrium parameters are also adjusted to account for the elevated temperatures and are shown in Table [9.5].

Q_1 (mol/liter)	Q_2 $(mole/liter)^{-1}$	Q_3 $(mole/liter)^{-1}$	Q_w $(mol/liter)^2$	F_{eq} (moles/liter)
3.0 E-4	5.0 E3	1.0 E1	1.0 E-14	1 E4

Table 9.5: Summary of parameters used in simulation of static beaker tests for "long" time scales.

Figure [9.11] shows the variation in the solution pH with time at 50°C and 74°C due to silica dissolution. The simulated profiles with two values of k_1 have been superimposed on the experimental data. Figure [9.12] shows the corresponding increase in the silica concentration in the solution. An important feature of these figures is that the plots also show the simultaneous change in solution pH and silica concentration predicted by the kinetic model. At a given temperature, the pH profiles and the silica concentration profiles both correspond to the same value of k_1.

The model is able to predict the fast initial dissolution rate shown by the experiment, followed by a gradual decrease in the reaction rate till an equilibrium is attained. As the temperature is increased, there is an appreciable enhancement in the reaction rate which is produced without any significant change in the final equilibrium values. The same effect has been generated in the simulations by increasing the rate constant k_1 to eight times its original value and using the same equilibrium quotients.

From the above discussion, it may be concluded that the kinetic model is able to match the experimental results for all time frames. The accuracy of the results however hinges on the values of parameters characterizing the system, namely, the equilibrium quotients and rate constant k_1. The values of the equilibrium quotients Q_0, Q_1 and Q_2 used in the simulations are well within the range of typical values shown earlier in Table [9.1]. Resolution of the value of k_1, however, is a more complicated problem and deserves a detailed analysis.

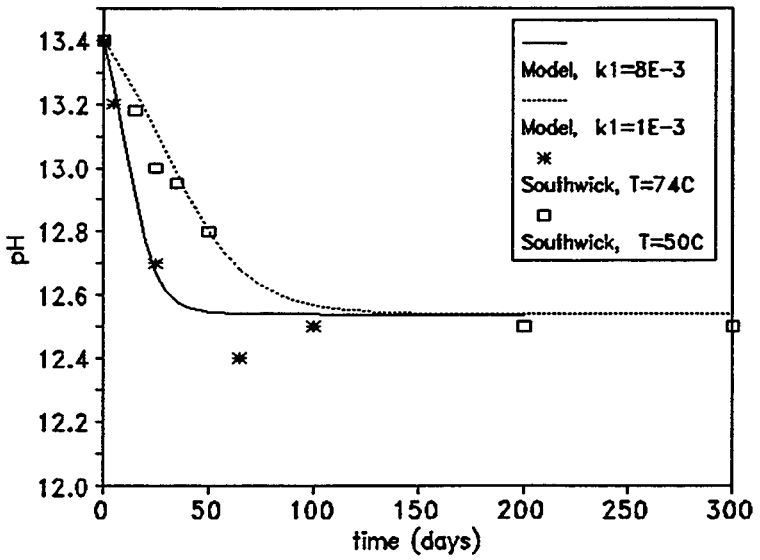

Figure 9.11: Variation of pH with time for "long times" in beaker tests. Experimental data from Southwick[6]. Values of k_1 are reported in moles/liter.day.

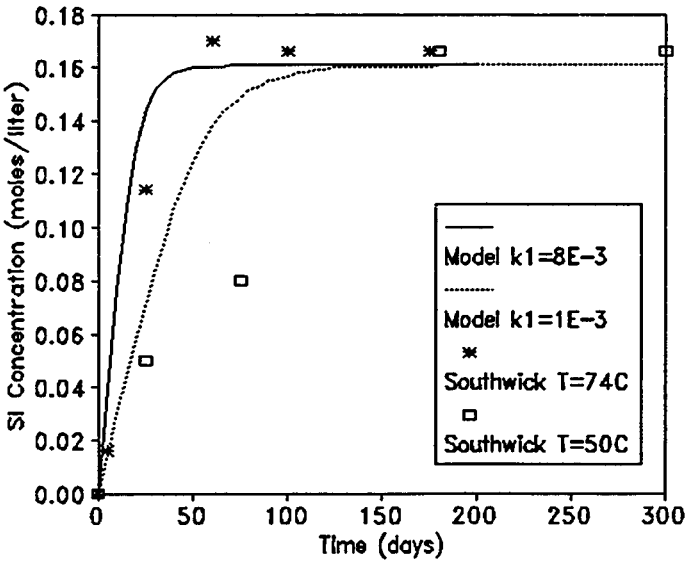

Figure 9.12: Variation of silica concentration with time for "long times" in beaker tests. Experimental data from Southwick[6]. Values of k_1 are reported in moles/liter.day.

The simulations shown in Figures [9.11] and [9.12] were performed using constant values of the rate constant k_1. Previous results from the short-time experiments indicate that the parameter k_1 is a strong function of the solution pH and will decrease as the pH is lowered. Nevertheless, it is useful to compare the value of k_1 used in the simulations to some of the typical values of the initial dissolution rate reported in the literature. For this purpose, Eqn. [9.5] is recalled and the value of k_1 is converted to a unit area basis by dividing with the term ($a_s.S_L$). By assuming a value of 1 m^2/g as a rough estimate for the specific area of the sand particles (a^s), the two values of k_1 used in the simulations are 2.2 E-6 moles/(m^2.hr) and 1.9 E-5 moles/(m^2.hr) corresponding to the two temperatures of 50°C and 70°C respectively. Although no direct comparisons can be drawn at the given temperatures, Figure [9.13] shows that these values compare favorably with experimental results at other temperatures. Figure [9.13] also correlates the experimental results of House and Orr and Thornton and Radke to the empirical fit by Eqn. [9.5]. The equation provides a good match to the experimental data at 23°C for the pH range of 4.5 to 11.0. Beyond this range, k_1 is expected to be relatively independent of pH and equal to the experimental value obtained by Thornton and Radke.

The overall change in solution pH during the course of the long-time beaker test is only of the order of 1 unit. In the case of flooding experiments, however, a much larger variation from the initial pH values to the injected pH values is expected. Here, a constant value of k_1 is not justified. Subsequently, in the following sections, the function described by the dashed line in Figure [9.13] has been adopted to model k_1.

Simulation of silica dissolution in core floods

The results from the static beaker tests provide valuable insight into the kinetic nature of the silica dissolution reaction. It is, however, difficult to extrapolate directly the effects of silica dissolution from static beaker tests to core-flood experiments. Firstly, there is no single time scale which will adequately represent a complete flooding experiment. Different points along the core are exposed to the injected solution for varying amounts of time depending on their position in the core. Secondly, the physical conditions governing the dissolution reaction in the two types of experiments are quite different. The solid-liquid ratios (S_L) used in the static beaker tests by Wirth and Gieskes in their short-time experiments and Southwick in his long-time experiments are 10 g/liter and 440 g/liter, respectively. The equivalent value of S_L in a core with a solid density of 2.5 g/cm^3 and a porosity of 0.2 is 10,000 g/liter. Evidently, the corresponding rates of dissolution encountered in sand cores will be much greater than those observed in the beaker tests. Thus, in order to study the effects of silica dissolution in flooding experiments, it is necessary to solve the complete set of governing equations of a flow model. This section deals with the simulation of a set of experiments similar to that previously described, but with the new flow model. This model is based on the same kinetic expressions used to describe silica dissolution in the static beaker tests.

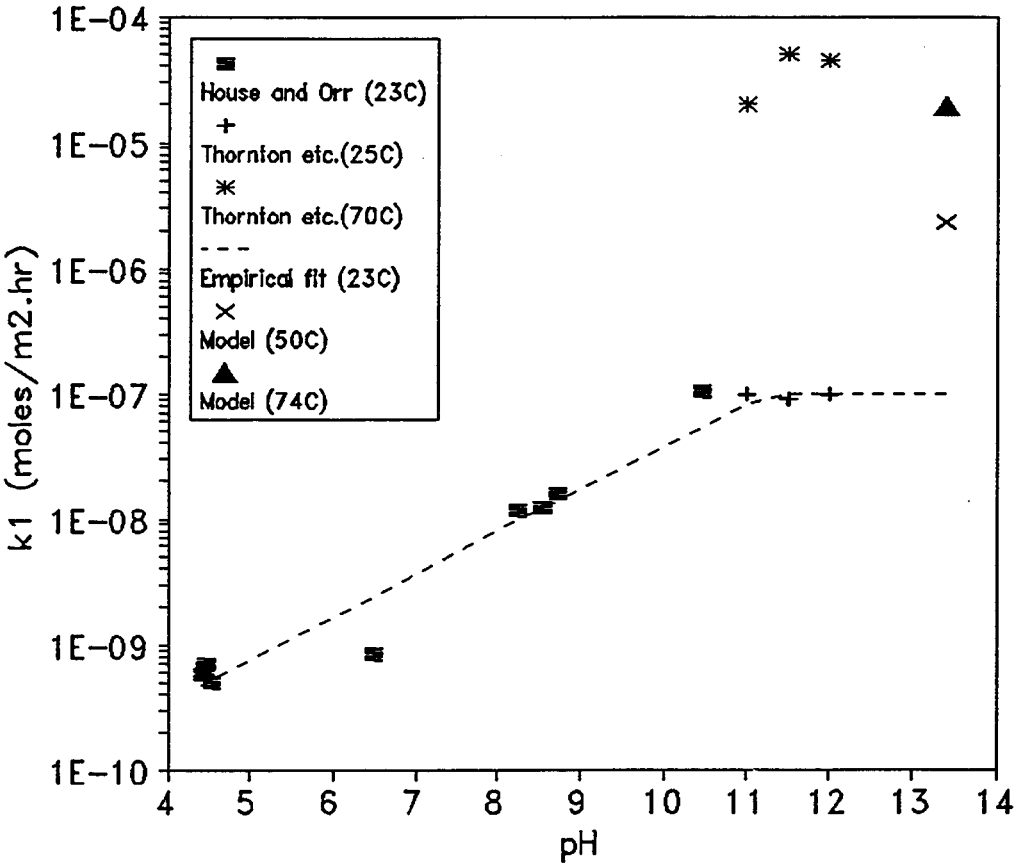

Figure 9.13: Variation of the initial rate of dissolution of quartz (k_1) as a function of solution pH.

The governing equations of the proposed model have been discussed earlier. Neglecting all contributions of ion-exchange on the surface of the matrix, the reaction term in the equations is characterized by the group of parameters given in Eqn. [9.19]. This group physically represents the ratio of the characteristic residence time to the characteristic reaction time of the system. Consequently, it is termed as the Damkohler Group (Da). A high value of Da signifies relatively more time is available for the reaction to occur which, in turn, implies greater dissolution of silica within the core. Rather than studying the effects of the rate of reaction, flow rate and core length individually, the Damkohler Group provides a single parameter for effectively analyzing the kinetic nature of the silica dissolution reaction in core-flood experiments.

It is important to realize that the Damkohler Group is not a simple dimensionless quantity. In its given form, Da has the units of concentration. In addition, since the reaction rate k_1 is a strong function of the solution pH, the value of Da also changes with pH. Thus, the Damkohler Group in this analysis is not a constant parameter, rather, it describes the set of physical conditions defining the system. A reference set of conditions (Da_0), corresponding to typical laboratory scales, has been adopted for simulation purposes. These conditions are summarized in Table [9.6] and are very similar to those used with the UTCHEM model.

Core length :	1 ft
Porosity :	0.20
Superficial velocity :	1 ft/day
specific surface area :	2 m^2/g
solid density :	2.5 g/cm^3
Equilibrium quotient Q_1 :	1 E4 moles/liter
Equilibrium quotient Q_2 :	2 E4 $(moles/liter)^{-1}$
Equilibrium quotient Q_3 :	10 $(moles/liter)^{-1}$
Rate constant k_1 : exp(-14.55+0.361pH) ($moles/m^2.sec.$)	

Table 9.6: Summary of the reference physical parameters corresponding to typical laboratory scale conditions (Da_0).

A change in the physical conditions is also manifested in the value of the Damkohler group of the system. For example, typical field-scale applications correspond to core lengths of the order of 1000 ft and flow rates of 10 ft/day. In this case, the Damkohler Group is of the order of $100*Da_0$. Thus, by simply varying the value of Da in the model, it is possible to scale the effects of silica dissolution from laboratory-scale conditions to field-scale conditions.

Once again, a silica core saturated with 1.7% NaCl brine solution is considered. A 0.5% NaOH brine solution is injected into the sand core and displaces the initial brine solution. The chemical compositions of the two solutions are shown in Table [9.7].

INITIAL CONDITIONS (Concentrations in moles/liter PV) OH^- 3.23E-06 Na^+ 0.2857 H_4SiO_4 0.1E-3 Cl^- 0.2857 H^+ 3.12E-8 $H_3SiO_4^-$ 5.24E-8 H_2SiO4^{2-} 4.07E-13
INJECTION CONDITIONS (Concentrations in moles/liter PV) OH^- 0.079 Na^+ 0.126 H_4SiO_4 0 Cl^- 0.05 H^+ 0.13E-8 $H_3SiO_4^-$ 0 H_2SiO4^{2-} 0

Table 9.7: Summary of the initial concentrations and injected concentrations used in the simulations shown in Figures [9.14] and [9.15].

Figures [9.14] and [9.15] show the silica concentration profiles and the corresponding pH profiles after 0.25 PV injection as a function of the Damkohler Group. These profiles are also compared to the results from a simulation with the UTCHEM model using the same equilibrium parameters and physical conditions. The figures demonstrate the following features:

1) Under conditions of extremely short residence times (Da=0), the concentration of silica in the solution is negligibly small. The pH profile shows a very broad front similar to the pH profiles produced by the UTCHEM model and shows a transition from the injected value of the pH to the initial value.

2) At the given reference conditions ($Da=Da_0$), an appreciable amount of silica dissolution takes place and causes the formation of a peak in the silica concentration profile. The dissolution reaction causes an increase the silica concentration with time whereas the dispersive and the convective mechanisms tend to equalize the concentrations in the fluid phase. The peak, therefore, corresponds to the point at which these opposing mechanisms balance each other out. In the absence of dispersion, this peak would lie exactly at the point $\xi=0.25$. The silica dissolution reaction is accompanied by a simultaneous decrease in the solution pH.

3) Although the maximum contact time at the given reference conditions is only 0.25 days, the silica concentrations observed here are much higher than the corresponding concentrations produced in the beaker tests. It may be concluded that the high S_L ratio of the porous core exposes a large surface area to the injected solution and causes a significant enhancement of the rate of reaction.

4) On increasing the Damkohler Group, more dissolution of the core takes place resulting in progressively higher silica concentrations in the injected solution and greater consumption of hydroxide. At a value of $Da=100*Da_0$, the results from the proposed model match the results predicted by the UTCHEM model. Under these conditions, the residence time of the system is long enough to ensure that the injected solution effectively attains equilibrium with the rock. The local equilibrium assumption in the UTCHEM model, therefore, is valid only for physical conditions corresponding to $Da \geq 100*Da_0$.

5) The dispersion of all the chemical species is characterized by the Peclet Number (Pe).

This dimensionless group is defined in Eqn. [9.15]. The Peclet Number physically represents the ratio of the characteristic convective velocity to the characteristic dispersion velocity of the system. It is possible to directly relate the Peclet Number to the coefficient characterizing the numerical dispersion in the model equations by the following relation:

$$Pe=\frac{2}{\Delta\xi}=2N \qquad (9.28$$

where N is the total number of grid points used in the finite difference approximations of the spatial derivatives. The results shown in Figures [9.14] and [9.15] were determined from simulations with 80 grid points. Hence, the Peclet Number characterizing all the profiles is 160. In addition, since the profiles from the proposed model match the results from UTCHEM, it is anticipated that the numerical dispersion produced by the two models is also equal. It is possible to prove this analytically by relating the Peclet Number in the proposed model to the physical dispersivity in the UTCHEM model by the relation:

$$Pe=\frac{L}{\alpha_d} \qquad (9.29$$

Thus, a Peclet Number of 160 in a 1 ft long core is equivalent to a physical dispersivity of 0.00625 ft. This is the same result derived previously for the UTCHEM model.

From the definition of the Peclet Number in Eqn. [9.15], it may be anticipated that it would be a function of both the velocity and the core length. Eqn. [9.29], however, shows that in a porous medium with a given dispersivity, the Peclet Number is independent of the flow rate. Figures [9.14] and [9.15], therefore, accurately depict the scaling of the effects of silica dissolution with respect to the flow rate. An increase in the core length, however, would cause a proportionate increase in the Peclet Number defining the system and the corresponding concentration profiles would tend to show a sharper fronts at $\xi=0.25$. Eqn. [9.28] shows that the Peclet Number generated by the numerical dispersion is incapable of describing this effect. One of the important limitations of the proposed model, therefore, is that it does not directly predict the change in dispersion in the concentration profiles as the length of the core is varied. This effect, however, may be simulated by simply increasing the total number of grid blocks in the spatial dimension.

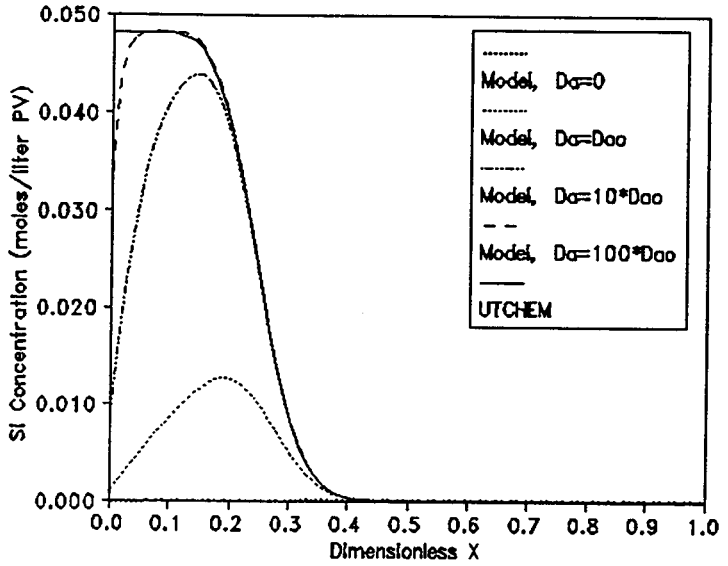

Figure 9.14: Silica concentration profiles along the length of the core after 0.25 PV injection as a function of the Damkohler Group.

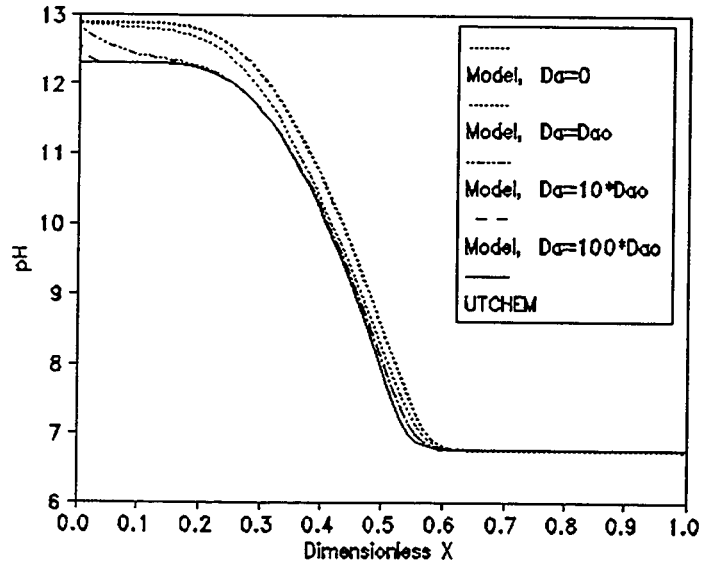

Figure 9.15: pH profiles along the length of the core after 0.25 PV injection as a function of the Damkohler Group.

Simulation of sodium/hydrogen ion-exchange in core floods

In this section the effects of sodium/hydrogen ion exchange in simple core flood experiments in the absence of silica dissolution are examined. A coupled mechanism describing the sodium/hydrogen ion-exchange reaction on the surface of the rock was given in Eqn. [9.1]. The flow model is based on the assumption of local equilibrium between the fluid-phase concentrations and the adsorbed-phase concentrations on the rock surface. Unlike the silica-dissolution reaction, ion-exchange reactions are typically fast enough to justify this assumption.

A sand core saturated with 1.7% NaCl is considered. A solution containing 0.1N NaOH is injected into the core and displaces the initial brine solution. Table [9.8] summarizes some of the system parameters used in the simulations.

CORE DATA	
Core length :	0.1 ft
Porosity :	0.20
Superficial velocity :	10 ft/day
specific surface area :	2 m^2/g
solid density :	2.5 g/cm^3
INITIAL CONDITIONS (Concentrations in moles/liter PV)	
OH^- 3.23E-06 Na^+ 0.2857 Cl^- 0.2857 H^+ 3.12E-8	
INJECTION CONDITIONS (Concentrations in moles/liter PV)	
OH^- 0.1 Na^+ 0.126 Cl^- 0.026 H^+ 0.1E-12	

Table 9.8: Summary of the initial concentrations and injected concentrations used in the simulations shown in Figures [9.16] and [9.17].

Figure [9.16] shows the concentration profiles of the Na^+ species as the injected solution advances along the length of the core for typical values of the equilibrium parameters K_I and n_T. Figure [9.17] shows the corresponding pH profiles. As expected, the ion-exchange reaction has a considerably different effect on the concentration profiles as compared to the silica dissolution reaction. The concentration profiles show the formation of two distinct fronts which move through the porous medium. For example, the profiles at 0.75 PV injection show the following features:

1) The first front is centered at $\xi=0.75$ and travels at the interstitial velocity with no retardation. This front simply entails the displacement of the initial solution and corresponds to concentration variations in the fluid phase only. These fronts are termed as *salinity waves*. The region after the salinity wave, therefore, comprises of the initial fluid-phase concentrations and solid-phase conditions.

2) The second front is centered at $\xi=0.42$ and involves a change in both the solid-phase composition and the fluid-phase concentrations. This wave front is termed the *ion-exchange wave*. Since the velocity of this wave front is slower than the interstitial velocity, the injected pH levels appear in the effluent after a delay. The region before the

ion exchange wave corresponds to fluid-phase concentrations at the injected level and solid phase concentrations in equilibrium with the injected concentrations.

3) The intermediate region between the salinity wave and the ion-exchange wave has a modified fluid-phase composition in equilibrium with the initial solid-phase composition. Since the velocities of the two waves are different, the intermediate region expands as the waves progress along the core. The breakthrough of this intermediate region will result in a plateau in the effluent concentration profiles.

4) The velocities of the salinity waves and the ion-exchange waves appear to be the same for both the Na^+ species and the OH^- species. This property has also been commonly observed for other ion exchange reactions such as Na^+/Ca^{2+} ion exchange. The condition in which the concentration velocities of all the species at any given point in time and space are equal is called *coherence*.

5) The salinity waves show a broad front governed solely by the dispersive mixing of the injected solution and the initial solution. The ion-exchange waves, however, show much sharper fronts in comparison to the salinity waves. These sharp changes in concentration are termed as *shock fronts*.

6) It is important to note that the overall shape of the shock fronts appears to be constant as the wave propagates through the core. Based exclusively on the Langmuir-like equilibrium describing the ion-exchange reactions, the ion-exchange wave is expected to continuously sharpen as it propagates through the core. These wave fronts are commonly observed in nature and are termed as *self-sharpening waves*. Lake and Helffrich have shown that physical dispersion has an important role in defining the shape of self-sharpening waves[19]. Dispersion, by nature, tends to smother all the sharp concentration gradients and therefore opposes the sharpening character of the wave fronts. These competing phenomena tend to balance each other and the resultant waves are indifferent with respect to sharpening behavior and maintain a constant shape as they progress through the core.

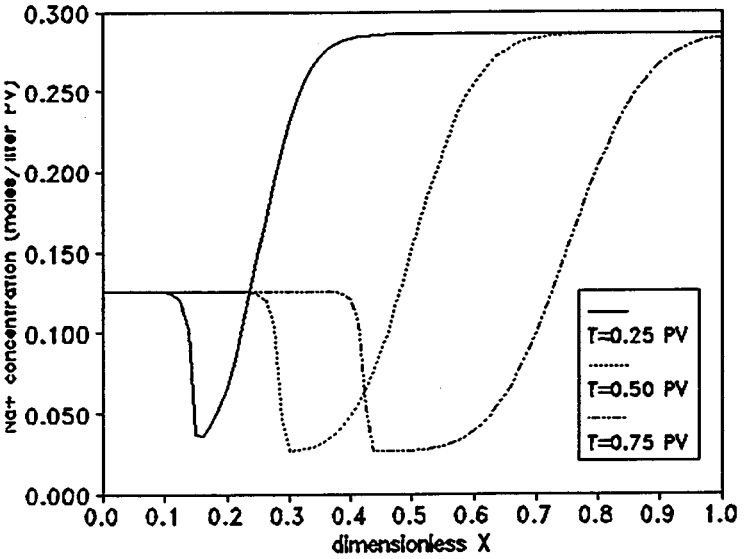

Figure 9.16: Na^+ concentration profiles along the length of the core as a function of pore volumes of injection (K_I=1E5 (moles/liter)$^{-2}$, n_T=0.85 meq/100g).

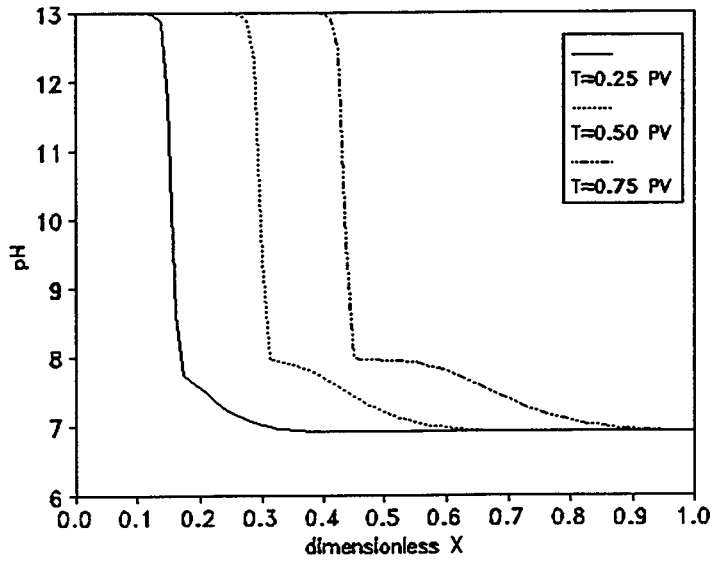

Figure 9.17: pH profiles along the length of the core as a function of pore volumes of injection (K_I=1E5 (moles/liter)$^{-2}$, n_T=0.85 meq/100g).

CONCLUSIONS

Simulation of flooding experiments with high pH brine solutions shows that the UTCHEM model does not describe the kinetic nature of the silica dissolution reaction. The concentrations profiles predicted by UTCHEM are independent of the physical conditions and are valid only in the limiting case of long residence times.

A kinetic model describing the silica dissolution reaction was developed which is generally valid for all time frames. Based on sodium/hydrogen equilibria and silica dissolution kinetics, a new mathematical model was developed for describing core flood experiments. This model describes the effects of flow rate and core length in terms of the Damkohler Group. By varying the value of the Damkohler Group it is possible to scale the effects of silica dissolution from laboratory-scale conditions to field-scale conditions. In addition, a mathematical criterion was developed for checking the validity of the local equilibrium assumption.

The proposed model was also used to study the sodium/hydrogen ion-exchange in simulated simple core floods. The model predicts a delay in the breakthrough of the injected pH levels and the formation of an intermediate plateau in the concentration profiles.

NOMENCLATURE

a_s specific surface area of the solid particles (ft^2/g).
C vector representing the concentrations of all the transported species (moles/liter PV).
C_i concentration of i^{th} species in the fluid phase (moles/liter PV).
D diffusivity of the species (ft^2/day).
Da Damkohler Group (moles/liter PV).
$f_i(C)$ reaction rate expression in terms of the species concentrations.
F_k ratio of the condensation and dissolution rate constants (dimensionless).
k_i surface reaction rate constant of the i^{th} reaction.
K_d dispersion coefficient (ft^2/day).
K_I equilibrium constant for sodium/hydrogen ion-exchange reaction (moles/liter)^2.
n_i concentration of the adsorbed form of the ith species on the rock (moles/ft^2).
n_T total cation exchange capacity of the rock (moles/m^2 solid).
Q_i equilibrium coefficient of the i^{th} reaction.
Q_0 equilibrium quotient for water.
$r_i(C)$ surface rate of reaction (moles/ft2.day).
$R_i(C)$ rate of generation of the i^{th} species per unit volume (moles/liter).
S_L solid-liquid ratio (g solid/liter liquid).
v velocity of injected brine (ft/day)
x spatial coordinate (ft).

Greek symbols

α_i retardation factor of the i^{th} chemical species (dimensionless).
α_d longitudinal dispersivity of the fluid-phase (ft^2/day).
ξ dimensionless distance in x direction.
ρ_s density of the rock (g solid/liter solid).
τ dimensionless time.
τ_T tortuosity of the core (dimensionless).
ϕ porosity of the core (dimensionless).

Other symbols

[] molar concentration (moles/liter).
$H_4SiO_4^*$ adsorbed silicic acid molecule.
$[H_4SiO_4]^{sat}$ equilibrium value of the silicic acid concentration.
S^* active site on the silica lattice.

REFERENCES

1. Bunge, A.L. and Radke, C.J., "Migration of Alkaline Pulses in Reservoir Sands," *SPEJ*, (Dec. 1982) 998-1012.
2. Bhuyan, D., "Development of an Alkaline-Surfactant-Polymer Compositional Reservoir Simulator," Ph.D. Dissertation, The University of Texas at Austin (Dec. 1988).
3. Bhuyan, D., Lake, L.W. and Pope, G.A., "Mathematical Modeling of High pH Chemical Flooding," *SPERE* (May 1990) 212-220.
4. Bryant, S.L., Schechter, R.S. and Lake, L.W., "Interactions of Precipitation/Dissolution Waves and Ion-exchange in Flow through Permeable Media," *AIChE J* (May 1986) vol. 32, no. 5, 751-764.
5. Sydansk, R.D., "Elevated-Temperature Caustic/Sandstone Interaction: Implications for Improving Oil Recovery," *SPEJ* (Aug. 1982) 453-462.
6. Southwick, J.G., "Solubility of Silica in Alkaline Solutions: Implications for Alkaline Flooding," *SPEJ* (Dec. 1985) 857-864.
7. Midha, V., "Mathematical Modeling of Fluid-Rock Interactions During the flow of Alkaline Solutions through Porous Media," M.S. Thesis, University of Kansas (1994).
8. Bunge, A.L. and Radke, C.J., "The Origin of Reversible Hydroxide Uptake on Reservoir Rock," *SPEJ* (Oct. 1985) 711-718.
9. Thornton, S.D. and Radke, C.J., "Dissolution and Condensation Kinetics of Silica in Alkaline Solutions," *SPERE* (May 1988) 743-752.
10. Busey, R.H. and Mesmer, R.E., "Ionisation Equilibria of Silicic Acid and Polysilicate Formation in Aqueous Sodium Chloride Solutions to 300°C," *Inorg. Chem.*, vol. 16, no. 10 (1977) 2444-50.
11. Ingri, N., "Equilibrium Studies of Polyanions, IV. Silicate Ions in NaCl Medium," *Acta Chem. Scand.*, vol. 13, no. 4 (1959) 758-75.
12. Lagerstrom, G., "Equilibrium Studies on Polyanions, III. Silicate Ions in $NaClO_4$ Medium," *Acta. Chem. Scand.*, vol. 21, no. 9 (1959) 722-36.
13. Fleming, B.A. and Crerar D.A., "Silicic Acid Ionisation and Calculation of Silica Solubility at Elevated Temperature and pH," *Geothermics*, vol. 11, no. 1 (1982) 15-29.
14. House, W.A. and Orr, D.R., "Investigation of the pH Dependance of the Kinetics of Quartz Dissolution at 25°C," *J. Chem. Soc. Faraday Trans.* (1992) vol. 88, no. 2, 233-241.
15. Byrne, G.D. and Hindmarsh, A.C., *J. Comput. Phys.*, vol. 70, no. 1 (1987).
16. Schiesser, W.E., Differential Systems Simulator, Version 2, Lehigh University, (1977).
17. Hindmarsh, A.C., "LSODE and LSODI, Two New Initial Value Ordinary Differential Equation Solvers," *ACM-SIGNUM Newsletter*, vol. 15, no.4 (1980) 10-11.
18. Wirth, G.S. and Gieskes, J.M., "The Initial Kinetics of the Dissolution of Vitreous Silica in Aqueous Media," *J. Colloid Interface Sci.* (1979) vol. 68, No.3, 492-500.
19. Lake, L.W. and Helfferich, F., "Cation Exchange in Chemical Flooding: Part 2—The Effect of Dispersion, Cation Exchange, Polymer/Surfactant Adsorption in Chemical Flood Environment," *SPEJ* (Dec. 1978) 435-444.

☆U.S. GOVERNMENT PRINTING OFFICE: 1994 - 560-030/00031